306132771U

THE PARTICLE SPECTRA OF CONFINING FIELD THEORIES

R. D. Kenway

Department of Theoretical Physics,
University of Oxford.

A thesis submitted for the degree of

Doctor of Philosophy

at Oxford University

BODLEIAN LIBRARY OXFORD
DEPOSITED
THE818
12.1.79

Jesus College

August 1978

ACKNOWLEDGEMENTS

I am sincerely grateful to my supervisor Don Sinclair for his guidance and to Chris Hamer who collaborated with me on some of the calculations reported in Chapters 2, 3 and 6.

Much of Chapter 4 is familiar to John Kogut and I thank him for his suggestions. My understanding of some aspects of Chapter 5 has benefited from correspondence with Paul Steinhardt.

I thank Professor Dalitz and everyone in the Theoretical Physics Department, especially Christine Hemming, Leo Marland and Tim Ziman.

Finally, I thank my parents for their love and support. This thesis is dedicated to them.

THE PARTICLE SPECTRA OF

CONFINING FIELD THEORIES

R. D. Kenway

Jesus College, Oxford

A thesis submitted for the degree of
Doctor of Philosophy,

Trinity Term 1978.

Abstract

Massive QED (Schwinger model) for one and two fermion species in 1+1 dimensions is studied using Hamiltonian lattice techniques. Bound-state masses are calculated as strong-coupling expansions in inverse powers of the dimensionless coupling constant. Various Padé approximant methods for extracting continuum predictions from these are compared.

The non-relativistic limit of both lattice theories is the lattice linear potential model. This can be solved exactly. It is used to test convergence of the sequence of Padé approximants. The investigation is continued for the ordinary Schwinger model. At all coupling strengths, the best continuum estimates for bound-state masses come from values of the Padé approximants at non-zero lattice spacing.

Two different lattice formulations of the two-species Schwinger model are studied. Both have a restoration of chiral SU(2) symmetry as the fermion mass vanishes. The corresponding symmetric vacuum is too complicated to do a perturbative calculation beyond second order, where the low-lying states are those of a Heisenberg antiferromagnetic chain, in qualitative agreement with the continuum theory.

Strong-coupling expansions are carried out to high orders about the unsymmetric vacua of the massive theories. Continuum estimates for bound-state masses are compared. For weak coupling their convergence is understood in terms of the linear potential model. But for strong coupling convergence is slow; neither lattice can account for the whole particle spectrum, though each treats part of it well.

Matrix methods are studied in an attempt to obtain better convergence from low-order calculations. Strong-coupling expansions for the Hamiltonian matrix in a non-degenerate subspace are extrapolated to zero lattice spacing using matrix Padé approximants. Improved continuum estimates are obtained from the scalar mass matrix of the ordinary Schwinger model, but not from the pseudoscalar mass matrix.

CONTENTS

	Page
Chapter 1: Introduction	1
Chapter 2: The Linear Potential Model	6
(a) The Continuum Theory	6
(b) The Lattice Theory	8
(c) An Exact Solution of the Lattice Theory	27
Chapter 3: The Ordinary Schwinger Model	32
(a) The Continuum Theory	32
(b) The Lattice Theory	42
(c) Estimates for the Particle Spectrum of the Continuum Model	54
(d) Half-Asymptotic Particles in the Lattice Theory	70
Chapter 4: Matrix Methods	75
(a) Matrix Padé Approximants	76
(b) Matrix Methods for the Linear Potential Model	80
(c) Matrix Methods for the Schwinger Model	92
Chapter 5: The SU(2) Flavour Schwinger Model	111
(a) The Continuum Theory	111
(b) The Lattice Theory	120

	Page
Chapter 6: Particle Spectrum Calculations for the SU(2) Schwinger Model	139
(a) The Unperturbed Particle States	140
(b) Mass Matrices for $(1,0)^-$ and 0^+ Mesons of Lattice II	147
(c) The Strong-Coupling Expansion to High Orders	159
(d) Continuum Estimates for Particle Masses	174
Chapter 7: Results and Conclusions	183
Appendix A: Rayleigh-Schrödinger Perturbation Theory	187
Appendix B: Quasi-Degenerate Perturbation Theory	193
References	
Tables	
Figures	

CHAPTER 1

INTRODUCTION

An old idea that the elementary constituents of matter are unobservable (Paul c.70) now receives wide support from physicists. The matter is hadronic and the constituents are quarks. Although their confinement remains a conjecture, it is embodied in a unique theoretical framework called quantum chromodynamics, or QCD (Marciano and Pagels 1978, and references therein).

Quarks have spin $\frac{1}{2}$ and fractional electric charge. All known baryons are made of three quarks; all mesons are quark-antiquark pairs. Each quark carries a non-abelian charge called colour, and transforms as the fundamental representation of the colour group $SU(3)_C$. The evidence for three colours is indirect. They are needed to put right the statistics of baryons, and to account for the observed $\pi^o \to 2\gamma$ decay rate and e^+e^- annihilation cross-section into hadrons. It is postulated that the world is invariant under local colour rotations. This requires that there exist an octet of coloured vector bosons, called gluons, which interact with themselves as well as quarks. The result is a non-abelian gauge field theory: QCD. If correct, it promises a 'grand unification' with similar gauge theories of weak and electromagnetic interactions, and possibly even gravity.

Apart from the local colour symmetry, the QCD Lagrangian, for massless quarks, possesses a global chiral $SU(N)_F \times SU(N)_F$ symmetry. Here $N \geq 4$ is the number of quark flavours, which include the familiar isospin, strangeness and charm degrees of freedom. In the real world the full chiral symmetry appears to be spontaneously broken to $SU(N)_F$, with the accompaniment of N^2-1 pseudoscalar Goldstone bosons, amongst them the pion. Even this symmetry is not exact. It is further broken by the quark masses, thought to originate in the domain of weak and electromagnetic interactions. The u and d quarks stay light, so isospin symmetry survives to a good approximation, and the pion becomes the lightest hadron (PCAC). There is also a $U(1)_B$ symmetry associated with baryon number conservation and an unwanted axial $U(1)_A$ symmetry. This last symmetry would lead to the prediction of an extra pseudoscalar meson with mass $\leq \sqrt{3}\, m_\pi$. Its removal, through the effects of instantons, encourages confidence in QCD. Then, with the additional postulate that all physical particles are colour singlets, QCD has just the symmetries observed in the hadronic world, and no more.

Colour confinement is presumed to be a dynamical effect synonymous with quark confinement. It remains a postulate, because QCD has no solution. Still, QCD is known to be renormalisable and is essentially unique in being asymptotically free (provided the number of flavours $N \leq 16$). This means that the effective quark-gluon coupling constant vanishes at large space-like momenta, or short distances. Convincing evidence for such behaviour comes from deep inelastic electroproduction experiments, in which the observed scaling, and corrections to scaling, agree well with predictions based on asymptotic freedom.

The situation appears paradoxical: When probed at short distances, quarks are seen as almost free point-like particles inside hadrons. Yet quarks do not escape. A popular suggestion is that the effective coupling constant, known to get small at small distances, becomes large at distances of order the hadron radius. If this is true, then conventional perturbation theory will be of little help in understanding whether or not bound states exist in QCD.

The assumption that the effective coupling grows huge in the infrared limit ('infrared slavery'), allows an approximate calculation of the low-energy bound-state spectrum to be attempted. Following an idea of Wilson (1974, 1975) a gauge-invariant momentum cut-off is introduced by replacing space with a cubic lattice (Susskind 1976). Time is left continuous, allowing a Hamiltonian formulation of QCD, suitable for the calculation of bound-state masses. The quarks live on the lattice sites and the gauge fields live on the links. In the limit of large lattice spacing (strong coupling) the quarks and gluons do not move. The vacuum spontaneously breaks chiral symmetry and the eigenstates of the static Hamiltonian are known exactly. Quarks are confined in the sense that an isolated quark has infinite energy. Local gauge invariance requires that any single quark be connected to a line of colour electric flux extending to infinity and, since the flux on each link is quantised, the energy of this state diverges with the linear dimension of the lattice.

The kinetic terms in the lattice Hamiltonian are down by powers of g relative to the static terms and can be treated as a perturbation. They permit the quarks and gluons to move about the lattice in a gauge invariant fashion. Consequently, confinement is maintained order-by-order

in perturbation theory. The formulation is designed to be simple enough to make possible systematic expansions of matrix elements of the Hamiltonian in inverse powers of the coupling constant (Banks et al. 1977).

The lattice is not meant to have any physical reality and must eventually be removed. The small-lattice-spacing (weak-coupling) limit is the limit of large expansion parameter. So high orders in the strong-coupling expansion are needed to make confident continuum predictions. In addition, it is implicitly assumed that the extrapolation from strong coupling to weak coupling is smooth. The approach makes no sense if the system undergoes a phase transition at non-zero coupling. Approximate renormalisation group calculations support the hope that four is the lower critical dimension for gauge systems (Midgal 1975, Kadanoff 1976). If this is true, then the critical coupling is zero and this is exactly what is required if global symmetries, lost in the lattice formulation, are to be restored in the continuum limit.

Using a Hamiltonian formulation of the lattice QCD of massless u and d quarks, the nucleon and various non-strange meson masses have been calculated to fourth order in $1/g^2$ (Banks et al. 1977). Padé approximants were used to obtain continuum estimates for the meson/nucleon mass ratios. The results obtained were reasonable, with one exception: the pion. It should have zero mass in such a formulation; but was found to be nearly degenerate with the ρ. The situation is expected to improve at higher orders, where spin-spin forces should lead to a lowering of the π mass relative to the ρ. However, higher order calculations are extremely complicated.

This thesis is a discussion of several attempts to improve convergence of the calculational scheme. As a specific confining field theory we consider 1+1 dimensional QED (the Schwinger model).

In Chapter 2 we investigate the convergence of Padé approximants for a particularly simple lattice theory: the one-dimensional, non-relativistic linear potential model. This investigation is continued in Chapter 3, where the one-species Schwinger model is introduced. The outcome is a revised method for obtaining continuum estimates, which is applied later to the two-species model.

In Chapter 4 we develop matrix methods in an attempt to obtain more accurate continuum predictions from low-order lattice calculations.

Finally, in Chapters 5 and 6, we discuss two distinct lattice formulations of the two-species Schwinger model and compare their predictions for the low-energy bound-states of the continuum theory.

CHAPTER 2

THE LINEAR POTENTIAL MODEL

An elementary picture of confined quarks supposes that the interaction energy of a quark-antiquark pair grows linearly with their separation. Futhermore, if the quarks are heavy,so that particle production is suppressed, we can treat the problem non-relativistically, and we are led to the linear potential model.

A linearly rising potential is characteristic of the Coulomb interaction in one spatial dimension. So this model gains extra significance in 1+1 dimensions by describing the low-lying bound states of the massive Schwinger model (QED) in the non-relativistic limit.

(a) The Continuum Theory.

Suppose a quark has mass m and charge g. Then the wavefunction for a quark-antiquark bound state obeys the Schrödinger equation

$$\left(\frac{p^2}{m} + \frac{g^2}{2}|x|\right)\psi(x) = E\,\psi(x) \qquad (2.1)$$

where x and p are the relative coordinate and momentum. The non-relativistic limit of the massive Schwinger model corresponds to $m >> g$.

Equation (2.1) may be rewritten in terms of dimensionless variables (Hamer 1977)

$$z = \left(\frac{mg^2}{2}\right)^{1/3} x \quad , \qquad \lambda = \left(\frac{4m}{g^4}\right)^{1/3} E \, , \tag{2.2}$$

thus:

$$\left(\frac{d^2}{dz^2} - |z|\right)\psi(z) = -\lambda\psi(z). \tag{2.3}$$

The eigenfunctions are Airy functions (Abramowitz and Stegun 1965, p. 446 and 478):

$$\psi_n(z) = Ai\left(|z| - \lambda_n\right)(\operatorname{sgn} z)^n \, , \tag{2.4}$$

n = 0, 1, 2,...., and are alternately symmetric and antisymmetric; the ground state being symmetric. The symmetric-state eigenvalues are determined by the boundary condition at the origin,

$$Ai'(-\lambda_n) = 0 \tag{2.5}$$

and the ground-state energy is

$$E_0 = 0{\cdot}642 \, \frac{g^{4/3}}{m^{1/3}} \, . \tag{2.6}$$

Similarly, the antisymmetric-state eigenvalues are given by

$$Ai(-\lambda_n) = 0 \tag{2.7}$$

and so the energy of the first excited state is

$$E_1 = 1.473 \frac{g^{4/3}}{m^{1/3}}. \tag{2.8}$$

We restrict ourselves to the low-lying bound states of the linear potential, because only these are relevant to the discussion of the Schwinger model. A quantity we will refer to frequently is the energy ratio

$$\frac{E_1}{E_0} = 2.295. \tag{2.9}$$

(b) The Lattice Theory.

Our approach is to forget about the exact solution given above, and attempt to calculate the energies of the low-lying bound states of the Hamiltonian

$$H = \frac{p^2}{m} + \frac{g^2}{2}|x| \tag{2.10}$$

from scratch. The only tool at our disposal is perturbation theory. We notice that the potential is confining, so that the eigenstates will be localised around the origin in configuration space, fig. 2.1. So momentum eigenstates are an absurd starting point for perturbation theory. A better choice is to perturb in the kinetic energy about

position eigenstates. A momentum cut-off is needed to render this perturbation finite. Its introduction is rather like traditional "box normalisation", but with the roles of coordinate and momentum reversed. Its effect is to make the set of position eigenstates discrete i.e. a linear lattice with spacing a, and sites labelled by an integer n. The Hamiltonian

$$H = \frac{g^2}{2}|x| - \frac{1}{m}\frac{d^2}{dx^2}$$

$$\longrightarrow \frac{1}{2}g^2 a|n| - \frac{1}{m}\frac{\Delta^2}{(2a)^2} \qquad (2.11)$$

where the derivative is replaced by the symmetric difference operator Δ, defined by

$$\begin{aligned}\Delta^2\psi(n) &= \Delta\left[\psi(n+1) - \psi(n-1)\right] \\ &= \psi(n+2) + \psi(n-2) - 2\psi(n) \\ &\equiv \left(d^+ + d^- - 2\right)\psi(n)\end{aligned} \qquad (2.12)$$

and $d^{\pm}$ shifts n by ± 2. It is convenient to rescale H so that the static terms are independent of the lattice spacing:

$$W \equiv \frac{2}{ag^2}H = |n| + \frac{1}{2mg^2a^3}\left(2 - d^+ - d^-\right) \qquad (2.13)$$

Define

$$u \equiv \frac{1}{2mg^2a^3}. \qquad (2.14)$$

Then, since mg^2 is a finite constant in the non-relativistic limit of the massive Schwinger model, for large lattice spacing a, u is small and is a suitable expansion parameter. Thus, we apply Rayleigh-Schrödinger perturbation theory to the rescaled Hamiltonian:

$$\begin{aligned} W &= W_o + uV \\ W_o &= |n| \\ V &= 2 - d^+ - d^- \end{aligned} \qquad (2.15)$$

Because of the finite-difference approximation to the kinetic part of H, there are two distinct formulations of the lattice theory. V connects only all odd sites, or all even sites. So in one version the relative coordinate takes odd integral values and in the other even integral values. (This distinction becomes important for the lattice II formulation of the two-flavour Schwinger model, developed in Chapter 5, where there are some states for which the relative separation of the quark-antiquark pair, comprising the bound state, is an odd multiple of the lattice spacing and other states for which it is an even multiple). Both versions must have the same continuum limit, although the perturbation series on each lattice may be quite different (see Jurkiewicz and Wosiek 1978 for a similar treatment of the lattice harmonic oscillator).

We are interested in just the low-lying states. Because the potential in (2.15) (now it is the kinetic term) is symmetric, the states are alternately symmetric and antisymmetric. On the odd lattice, the lowest state has quarks one link apart. It is the symmetric combination

$$|0,\text{odd}\rangle \equiv \frac{1}{\sqrt{2}}\left(|n=1\rangle + |n=-1\rangle\right). \qquad (2.16)$$

(Recall that our spatial variable is the relative separation of the quarks). The first excited state is the antisymmetric combination

$$|1,\text{odd}\rangle \equiv \frac{1}{\sqrt{2}}\left(|n=1\rangle - |n=-1\rangle\right). \qquad (2.17)$$

On the even lattice, the ground state is the symmetric state

$$|0,\text{even}\rangle \equiv |n=0\rangle, \qquad (2.18)$$

whereas the first excited state has quarks two links apart:

$$|1,\text{even}\rangle \equiv \frac{1}{\sqrt{2}}\left(|n=2\rangle - |n=-2\rangle\right). \qquad (2.19)$$

We seek an expansion of the rescaled energy eigenvalues (c.f. (2.13)) in powers of u:

$$\frac{2\sqrt{x}}{g}E_i = \omega_i^{(0)} + a_i u + b_i u^2 + c_i u^3 + \cdots \qquad (2.20)$$

where

$$i = \begin{Bmatrix} 0 \\ 1 \end{Bmatrix} \begin{Bmatrix} \text{odd} \\ \text{even} \end{Bmatrix} \quad \text{and} \quad x = \frac{1}{a^2 g^2}\,. \qquad (2.21)$$

The coefficients in the expansion (2.20) are given by Rayleigh-Schrödinger perturbation theory (see Appendix A)

$$\omega_i^{(0)} = \langle i | W_0 | i \rangle ,$$

$$a_i = \langle i | V | i \rangle ,$$

$$b_i = \langle i | V \frac{1-P_i}{\omega_i^{(0)} - W_0} V | i \rangle ,$$

$$c_i = \langle i | V \frac{1-P_i}{\omega_i^{(0)} - W_0} V \frac{1-P_i}{\omega_i^{(0)} - W_0} V | i \rangle$$
$$- \langle i | V | i \rangle \langle i | V \left(\frac{1-P_i}{\omega_i^{(0)} - W_0} \right)^2 V | i \rangle ,$$

(2.22)

etc.

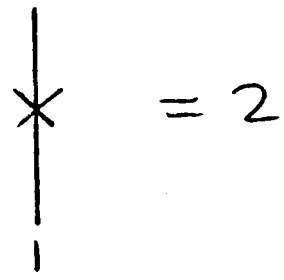
where P_i is the projection operator onto the state $|i\rangle$. Using simple diagrammatic techniques this expansion is easily carried out by hand to 6th order in u. The calculation to 19th order in u has been carried out by computer for the odd lattice formulation (Kenway and Hamer 1978). As an illustration of the method we will consider the low-lying states of the odd lattice to 3rd order in u. The results are surprising.

We do the calculation for the ground and first excited states, (2.16) and (2.17), simultaneously, because the graphs contributing to each are the same. Where the contribution of a given graph differs for the two states, we note the result for the first excited state in parentheses after the result for the ground state. At zeroth order,

the unperturbed energies are equal

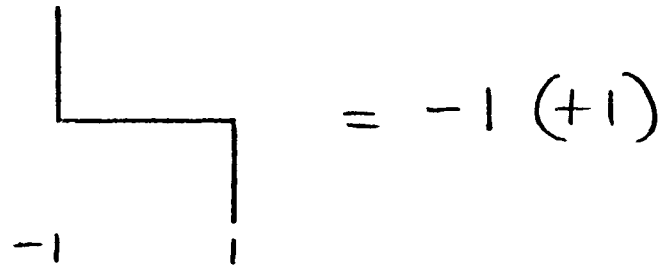
$$\omega^{(0)} = 1. \tag{2.23}$$

Nevertheless, degenerate perturbation theory is not required because the states have different parity. The degeneracy is lifted at first order when two graphs contribute



(2.24)

which is just the insertion of the factor 2 in (2.15) and

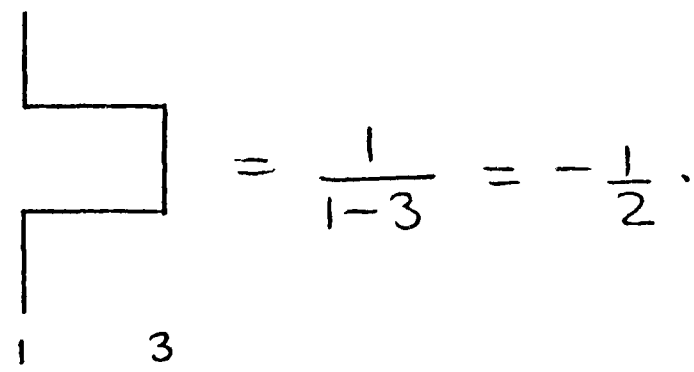


(2.25)

when $-d^{\pm}$ act once to shift the quark between sites 1 and -1. (2.25) is understood to be the sum of two equal matrix elements, one with the 'incoming' quark on site 1 and the other with it on site -1. Thus, adding (2.24) and (2.25),

$$a = 1(3). \tag{2.26}$$

The only allowed second order graph has the quark 'hopping' from site 1 out to site 3 and back again:

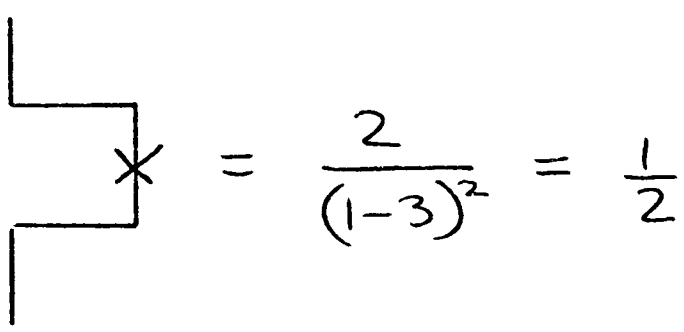


(2.27)

Thus,

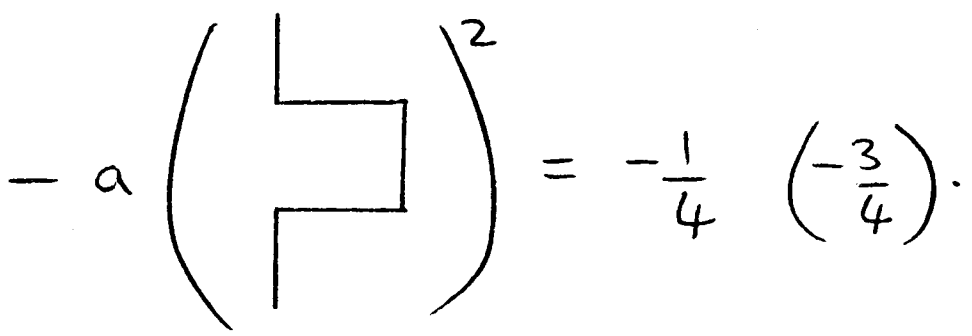
$$b = -\tfrac{1}{2}. \tag{2.28}$$

The effect of the projection operators in (2.22) is to forbid intermediate states in which the quark occupies sites ±1. This means that no graph higher than first order connects the states $|n = 1\rangle$ and $|n = -1\rangle$ and can distinguish between the two parity eigenstates. Third order corresponds to the graph (2.27) with the insertion of a factor 2:



(2.29)

together with the subtraction term:



(2.30)

Adding (2.29) and (2.30) gives

$$c = \tfrac{1}{4}(-\tfrac{1}{4}) \tag{2.31}$$

Hence, our results for the rescaled energy eigenvalues on the odd lattice are:

$$\frac{2\sqrt{x}}{g} E_0^{odd} = 1 + u - \frac{u^2}{2} + \frac{u^3}{4} + O(u^4) \tag{2.32}$$

and

$$\frac{2\sqrt{x}}{g} E_1^{odd} = 1 + 3u - \frac{u^2}{2} - \frac{u^3}{4} + O(u^4). \tag{2.33}$$

These constitute the solution, in inverse powers of the lattice spacing, for the low-energy bound states of the linear potential.

Continuum physics lies at the limit $a \to 0$, which, from (2.14), is equivalent to $u \to \infty$. Our results (2.32), (2.33) take the form of series expansions valid only near $u = 0$. So they will be useless unless we find a technique for extending their validity to all values of u. The most practical method turns out to be Padé approximants (Baker 1975, Zinn-Justin 1971).

Let f(z) be an analytic function defined by its Taylor series

$$f(z) = \sum_{n=0}^{\infty} a_n z^n. \tag{2.34}$$

The [N,M] Padé approximant, f[N,M](z) of f(z) is the rational function

$$f[N,M](z) = \frac{P_N(z)}{Q_M(z)} = f(z) + O(z^{N+M+1}) \tag{2.35}$$

where $P_N(z)$ and $Q_M(z)$ are polynomials in z of degree N and M respectively. The Padé approximant is constructed simply by multiplying up by $Q_M(z)$ in (2.35) and equating coefficients to order z^{N+M}. f[N,N] is called a diagonal Padé approximant, the others are off-diagonal.

The class of functions which can be approximated by rational functions is larger than the class which can be approximated by

polynomials, since rational functions are capable of describing behaviour near poles and singularities. However, there is a dearth of useful theorems on the convergence of sequences of Padé approximants. Those that exist require knowledge of the analytic structure of f(z). Although, uniform convergence can be proved if f(z) satisfies relatively weak regularity conditions, usually in applications nothing is known about the function f apart from the first few terms of its Taylor series. Then convergence can only be demonstrated in practice by going to higher and higher orders. When only low orders are available, application of Padé approximants can become a blind 'act of faith'. The main reason why Padé approximants enjoy their popularity is that at low orders they are often much better approximations to the function of interest than one has any right to expect.

In the specific application we are considering, quantities (like mass ratios) which should behave as bounded functions of the inverse lattice spacing are expressed as diagonal Padé approximants. Then our estimate of the continuum limit of the function is taken to be

$$\lim_{u\to\infty} f[N,N](u). \qquad (2.36)$$

From the point of view of convergence of the sequence of Padé approximants, the point $u = \infty$ is not distinguished from any other. This is because diagonal Padé approximants are invariant under origin-preserving homographic transformations

$$v = \frac{Au}{1+Bu} \qquad (2.37)$$

This means that if $P_N(u)/Q_N(u)$ is the [N,N] Padé approximant to f(u), then $P_N(v)/Q_N(v)$ is the [N,N] Padé approximant to f(v). In certain cases the point $u = \infty$ will be mapped to a point within the radius of convergence of the Taylor series for f(v). Then the success of the Padé approximant to extrapolate from v = 0 to v = A/B is not mysterious at all.

Consider the continuum estimates that can be obtained from the results (2.32) and (2.33) of our simple calculation. We note that, from (2.21) and (2.14),

$$\frac{2\sqrt{x}}{g} = \left(\frac{16mu}{g^4}\right)^{1/3} \tag{2.38}$$

Since E_o^{odd} should be a bounded function of u, the L.H.S. of (2.32) behaves like $u^{1/3}$ as $u \to \infty$. To approximate this behaviour by a rational function, we must first cube the series (2.32):

$$\frac{16mu}{g^4}\left(E_o^{odd}\right)^3 = 1 + 3u + \frac{3}{2}u^2 - \frac{5}{4}u^3 + O(u^4) \tag{2.39}$$

and then take the [N,N-1] Padé approximants. Even the most trivial one,

$$\frac{16mu}{g^4}\left(E_o^{odd}\right)^3 [1,0] = 1 + 3u \tag{2.40}$$

leads to a continuum estimate

$$E_o^{odd} \xrightarrow[u\to\infty]{[1,0]} 0.572\, \frac{g^{4/3}}{m^{1/3}} \tag{2.41}$$

which is within 11% of the exact result (2.6). The next Padé approximant

$$\frac{16mu}{g^4}\left(E_0^{odd}\right)^3[2,1] = \frac{1+\frac{23}{6}u+4u^2}{1+\frac{5}{6}u} \qquad (2.42)$$

gives an improved estimate

$$E_0^{odd} \xrightarrow[u\to\infty]{[2,1]} 0\cdot 669\, \frac{g^{4/3}}{m^{1/3}} \qquad (2.43)$$

which is within 5% of (2.6). Higher order estimates confirm the convergence of the sequence of Padé approximants to the ground state energy. Such an accurate result from so simple a calculation demonstrates the power of the method when the function we are approximating is well-behaved. In marked contrast to this success are the results for the companion series (2.33). The continuum estimates for the energy of the first excited state oscillate wildly, and warn us early on of the dangers involved in naively extrapolating to the continuum limit.

In order to understand these convergence problems for Padé approximants, we need to consider the results of high-order calculations. The results to 6th order are:

$$\frac{2\sqrt{x}}{g}E_0^{odd} = 1+u-\frac{u^2}{2}+\frac{u^3}{4}-\frac{u^4}{16}-\frac{3u^5}{64} + \frac{55u^6}{768}+O(u^7) \qquad (2.44)$$

$$\frac{2\sqrt{x}}{g}E_1^{odd} = 1 + 3u - \frac{u^2}{2} - \frac{u^3}{4} - \frac{u^4}{16} + \frac{3u^5}{64} + \frac{55u^6}{768} + O(u^7) \qquad (2.45)$$

$$\frac{2\sqrt{x}}{g}E_0^{even} = 2u - u^2 + \frac{3u^4}{8} - \frac{29u^6}{96} + O(u^7) \qquad (2.46)$$

$$\frac{2\sqrt{x}}{g}E_1^{even} = 2 + 2u - \frac{u^2}{2} + \frac{u^4}{16} - \frac{7u^6}{384} + O(u^7). \qquad (2.47)$$

The result (2.44) enables us to extend our simple calculation to form the [3,2] Padé approximant,

$$\frac{16mu}{g^4}\left(E_0^{odd}\right)^3[3,2] = \frac{1 + \frac{411}{92}u + \frac{621}{92}u^2 + \frac{643}{184}u^3}{1 + \frac{135}{92}u + \frac{39}{46}u^2} \qquad (2.48)$$

$$\Rightarrow \quad E_0^{odd}\ [3,2] \xrightarrow[u\to\infty]{} 0.636\ \frac{g^{4/3}}{m^{1/3}} \qquad (2.49)$$

which agrees with the exact result to within 1%. The higher order estimates are given in table 2.1 and rapidly become exact. In fig. 2.2 we plot, as functions of u, the diagonal Padé approximants to

$$\frac{d}{du}\ \frac{4mu}{g^4}\ (E_0^{odd})^3, \qquad (2.50)$$

which is an equally valid way of treating functions which are linear

in u as $u \to \infty$. This displays the rapid uniform convergence of the sequence of Padé approximants in the ideal case. The pole in the [3,3] Padé approximant is not unusual and is obviously irrelevant, since its effect is cancelled outside a small neighbourhood by a nearby zero.

The Padé approximants to the energy of the first excited state behave quite differently. As can be seen from table 2.1, there is not convergence of the $u \to \infty$ estimates from the off-diagonal Padé approximants. Gaps in the table mean the Padé approximant does not exist. Fig. 2.3 shows the diagonal Padé approximants to

$$\frac{d}{du} \quad \frac{4mu}{g^4} \quad (E_1^{odd})^3 \tag{2.51}$$

as functions of u. The function (2.51) appears to be trying to take a sharp corner at around $u = 1$, and is throwing off Padé approximants in all directions. This is a clear example of non-uniform convergence of the sequence of Padé approximants. It is a problem which must be resolved if the method is to be applied with any confidence to field theories.

Carroll, Baker and Gammel (1977) have come up with one answer. They suggest that the binding energy, as a function of u, may have an essential singularity at $u = \infty$ like e^{-u}. Convergence of the sequence of Padé approximants to such a function is non-uniform and, in particular, the convergence of their values at $u = \infty$ is likely to be poor. Then the error in our extrapolation procedure is an invalid assumption of the interchangeability of limits. We consider a sequence of Padé approximants to a function f(u). Assuming the

sequence converges, the number sought is

$$\lim_{u\to\infty} \lim_{N\to\infty} f[N + k,N](u) = \lim_{u\to\infty} f(u) \qquad (2.52)$$

Since only a few approximants are known, this limit is estimated by looking at the sequence

$$\lim_{N\to\infty} \lim_{u\to\infty} f[N + k,N](u), \qquad (2.53)$$

a procedure which is obviously unjustified in cases like the present one. Carroll et al. (1977) suggest that much better estimates can be obtained by considering the sequence

$$\lim_{N\to\infty} f[N + k,N](u_N) \qquad (2.54)$$

where $u_N \to \infty$ as $N \to \infty$. There is some arbitrariness in the choice of the sequence $\{u_N\}$. They suggest taking u_N to be the distance of the furthest pole in the $[N + k,N]$ Padé approximant from the origin, and trusting the Padé approximant only out to that distance. This method gives a considerable improvement in the estimates from the low-order Padé approximants, as we shall see.

We can understand the success of finite-u estimates intuitively: at any given order of perturbation theory, the lattice wavefunction extends over a finite number of sites, and so best represents the continuum wavefunction when the lattice spacing is such that they both have similar widths. This optimum lattice spacing obviously decreases (so that u_N increases) as we go to higher orders in perturbation theory.

In cases like the ground state energy E_o^{odd}, where the Padé

approximants are known to converge uniformly, the finite-u estimate is somewhat superfluous, but, nonetheless, gives quicker convergence at low orders e.g.

$$\left[\frac{d}{du}\ \frac{4mu}{g^4}\ (E_o^{odd})^3\right][1,1](u = 0.8) = 1.050 \qquad (2.55)$$

compared with the exact result 1.058. In the case of the first excited state there is a dramatic improvement in the low-order estimates e.g.

$$\left[\frac{d}{du}\ \frac{4mu}{g^4}\ (E_1^{odd})^3\right][2,2](u = 1.012) = 15.220 \qquad (2.56)$$

giving

$$E_1^{odd} = 1.561\ \frac{g^{4/3}}{m^{1/3}} \quad \text{(Carroll et al.)} \qquad (2.57)$$

compared with the exact result (2.8).

Having recognised the importance of finite-u estimates when the sequence of Padé approximants does not converge uniformly, a striking fact becomes apparent in fig. 2.3. The best continuum estimate comes from the peak value of the [7,7] Padé approximant:

$$E_1^{odd} = 1.466\ \frac{g^{4/3}}{m^{1/3}} \quad \text{(peak value)} \qquad (2.58)$$

which is correct to within 0.5%. This was noticed in the present context (Kenway and Hamer 1978) and independently in the context of the lattice harmonic oscillator (Jurkiewicz and Wosiek 1978). It motivates a slight modification of the estimation method proposed by

Carroll et al. (1978), which is important, because it is simpler to apply at high orders and draws directly on the essential ingredient of Carroll et al.'s argument.

Suppose we are seeking to approximate a function f(u) by the sequence of [N + k,N] Padé approximants. If f is singular at u = ∞, we cannot expect the sequence {f[N + k,N](∞)} to converge, but it should converge at any point u ≠ ∞. More precisely, for each N there exists a domain $D_N(\varepsilon)$ in the complex u plane, containing a neighbourhood of the origin, in which the given function is approximated with accuracy ε by f[N' + k,N'](u) with N' ≥ N, i.e.

$$|f(u) - f[N' + k,N'](u)| < \varepsilon \quad \forall\, u \in D_N(\varepsilon),\ N' \geq N. \qquad (2.59)$$

We assume that for N' > N,

$$D_{N'} \supset D_N. \qquad (2.60)$$

The singular point u = ∞ is not included in any domain $D_N(\varepsilon)$ with finite N; however, with N going to infinity, we hope to get closer and closer to this point.

Usually, f(u) is only known by the first few terms in its Taylor series around u = 0. In addition, there must be some justification for believing that

$$\frac{1}{u^k} f(u) \xrightarrow[u \to \infty]{} \text{constant} \qquad (2.61)$$

for some integer k (e.g. energies should become independent of u as u → ∞). Then we seek estimates for the asymptotic value, (2.61), based on the first few terms in the sequence {f[N + k,N]}.

Now we cannot construct the domains $D_N(\varepsilon)$ and so have to make do with some approximation, $\tilde{D}_N(\varepsilon)$, to them. One practical alternative is to take $\tilde{D}_N(\varepsilon)$ to be the domain on which $f[N + k,N]$ is within ε of $f[N + k + 1, N + 1]$ and any other higher-order Padé approximants which might be known. We assume that in this domain the original function is approximated with the same accuracy, and that (2.60) applies also to the $\tilde{D}_N$'s. Then, since from (2.61), f is monotonic for large u, our best estimate for (2.61) comes from evaluating $u^{-k}f[N + k,N](u)$ at

$$u_N(\varepsilon) \equiv \max_{u\varepsilon\tilde{D}_N(\varepsilon)} (u).$$

Thus, roughly speaking, u_N is the largest value of u for which the sequence $\{f[N' + k,N'](u)\}$ has already converged by the time $N' \geq N$. In practice, it is the point at which the Nth and subsequent Padé approximants start to diverge, e.g. in fig. 2.3 u_7 is the position of the peak in the [7,7] Padé approximant.

The final quantity of interest is the energy ratio which can be obtained from (2.44) and (2.45), or (2.46) and (2.47). In the odd-lattice formulation it is

$$\frac{E_1^{odd}}{E_0^{odd}} = 1 + 2u - 2u^2 + \frac{5}{2}u^3 - 4u^4 + \frac{191}{32}u^5 - \frac{69}{8}u^6 + O(u^7) \qquad (2.62)$$

The LHS is a bounded function of u which can be approximated by a sequence of diagonal Padé approximants. The first few terms in this sequence, together with their ($u \to \infty$) continuum limits are

$$\frac{E_1^{odd}}{E_0^{odd}}[1,1](u) = \frac{1+3u}{1+u} \xrightarrow[u\to\infty]{} 3 \qquad (2.63)$$

$$\frac{E_1^{odd}}{E_0^{odd}}[2,2](u) = \frac{1+5u+\frac{23}{4}u^2}{1+3u+\frac{7}{4}u^2} \xrightarrow[u\to\infty]{} 3.286 \qquad (2.64)$$

$$\frac{E_1^{odd}}{E_0^{odd}}[3,3](u) = \frac{1+\frac{179}{53}u+\frac{805}{848}u^2+\frac{515}{848}u^3}{1+\frac{73}{53}u+\frac{165}{848}u^2+\frac{401}{848}u^3} \xrightarrow[u\to\infty]{} 1.284 \qquad (2.65)$$

The [1,1] to [8,8] Padé approximants for the odd-lattice energy ratio as functions of u are plotted in fig. 2.4. Their values at $u \to \infty$ are shown in table 2.1. If there is any convergence at all to the exact result (2.9) it is extremely slow. Clearly this sequence is dominated by the non-uniform behaviour of the first excited state. Consequently it is amenable to the same finite-u techniques. Using the method of Carroll et al. (1978), we obtain for the low-order approximants:

$$\frac{E_1^{odd}}{E_0^{odd}}[1,1](u = 1) = 2 \qquad \text{(Carroll et al.)} \qquad (2.66)$$

$$\frac{E_1^{odd}}{E_0^{odd}}[2,2](u = 1.261) = 2.174.$$

The best estimate we can obtain from the [8,8] Padé approximant is its peak value,

$$\frac{E_1^{odd}}{E_o^{odd}}\ [8,8] = 2.120 \text{ (peak value)} \qquad (2.67)$$

and this occurs at approximately the largest value of u for which it and subsequent Padé approximants have all converged.

The even-lattice formulation has only been studied at low orders, because these are relevant for the discussion of the two-flavour Schwinger model. The behaviour is similar to that for the odd lattice, e.g. the energy ratio is

$$u\frac{E_1^{even}}{E_o^{even}} = 1 + \frac{3}{2}u + \frac{1}{2}u^2 + \frac{1}{16}u^3 - \frac{7}{32}u^4 - \frac{5}{96}u^5 + O(u^6) \qquad (2.68)$$

and

$$\frac{2}{3}\left(\frac{d}{du}\,u\,\frac{E_1^{even}}{E_o^{even}}\right)[2,2](u) = \frac{1 + \frac{392}{699}u + \frac{15925}{16776}u^2}{1 - \frac{74}{699}u + \frac{417}{466}u^2} \qquad (2.69)$$

giving

$$\frac{E_1^{even}}{E_o^{even}} \xrightarrow[u \to \infty]{} 1.591 \qquad (2.70)$$

to be compared with the value obtained by Carroll et al.'s method:

$$\left(\frac{d}{du}\,u\,\frac{E_1^{even}}{E_o^{even}}\right)[2,2](u = 1.118) = 2.110. \qquad (2.71)$$

(c) An Exact Solution of the Lattice Theory.

The lattice theories of both the harmonic oscillator and linear potentials can be solved exactly (Jurkiewicz and Wosiek 1978; Sinclair and Kenway, unpublished). The latter result is important, because it shows that in the non-relativistic limit the low-energy states of the lattice Schwinger model have the correct continuum limit.

We return to the rescaled Hamiltonian (2.15) and seek the eigenfunctions, $|\psi\rangle$, and corresponding eigenvalues, ω, of

$$W|\psi\rangle = \omega|\psi\rangle \qquad (2.72)$$

where

$$\omega \equiv \left(\frac{16mu}{g^4}\right)^{1/3} E. \qquad (2.73)$$

If $$\psi(n) = \langle n|\psi\rangle \qquad (2.74)$$

is the wavefunction at site n, the eigenvalue equation (2.72) becomes

$$\psi(n+2) + \psi(n-2) = \frac{1}{u}(|n| + 2u - \omega)\psi(n), \qquad (2.75)$$

together with the normalisation condition

$$\sum_n |\psi(n)|^2 = 1. \qquad (2.76)$$

Equation (2.75) is simply related to the recurrence relation for Bessel functions (Abramowitz and Stegun 1965, p. 361, 9.1.27). The correct choice of asymptotic behaviour for large n (Abramowitz and Stegun 1965, p. 365, 9.3.1.) leads to the symmetric solution:

$$\psi_s(n) = J_{\frac{|n|+2u-\omega}{2}}(u), \quad |n| \geq 2$$

$$J_{1+u-\frac{\omega}{2}}(u) = \frac{2u-\omega}{2u}\psi_s(0) \qquad (2.77)$$

$$J_{\frac{3+2u-\omega}{2}}(u) = \frac{1+u-\omega}{u}\psi_s(1)$$

and antisymmetric solution:

$$\psi_A(n) = (\operatorname{sgn} n) J_{\frac{|n|+2u-\omega}{2}}(u), \quad |n| \geq 2$$

$$\psi_A(0) = 0$$

$$\psi_A(1) = -\psi_A(-1) = \frac{u}{1+3u-\omega} J_{\frac{3+2u-\omega}{2}}(u). \qquad (2.78)$$

Here again we have two choices of lattice, because W connects only odd sites, or only even sites. On the odd lattice the condition for a symmetric solution is

$$\psi_s(1) = \psi_s(-1) \qquad (2.79)$$

and this is sufficient to determine the spectrum of ω as a function of u. Combining (2.75), (2.77) and (2.79) gives the condition on the eigenvalue:

$$J_{\frac{5+2u-\omega}{2}}(u) = \left(\frac{3+2u-\omega}{u} - \frac{u}{1+u-\omega}\right) J_{\frac{3+2u-\omega}{2}}(u). \qquad (2.80)$$

This may be expanded to give ω as a power series in u. Using standard recurrence relations (Abramowitz and Stegun 1965, p. 361, 9.1.27) we can

write (2,80) as

$$J'_{\frac{3+2u-\omega}{2}}(u) = \left(\frac{u}{1+u-\omega} - \frac{3+2u-\omega}{2u}\right) J_{\frac{3+2u-\omega}{2}}(u) \tag{2.81}$$

The continuum limit is $u \to \infty$. For $\nu \gg 1$,

$$J_\nu\left(\nu + \xi \nu^{1/3}\right) \underset{\nu \gg 1}{\sim} \frac{2^{1/3}}{\nu^{1/3}} Ai\left(-2^{1/3}\xi\right) + O\left(\frac{1}{\nu}\right)$$

$$J'_\nu\left(\nu + \xi \nu^{1/3}\right) \underset{\nu \gg 1}{\sim} -\frac{2^{2/3}}{\nu^{2/3}} Ai'\left(-2^{1/3}\xi\right) + O\left(\frac{1}{\nu^{4/3}}\right) \tag{2.82}$$

(Abramowitz and Stegun 1965, p. 367, 9.3.23 and 9.3.27). In our case,

$$\nu \equiv \frac{3}{2} + u - \frac{\omega}{2} \tag{2.83}$$

where $\omega = 2^{2/3}\lambda u^{1/3}$ (2.84)

and $\lambda = \lambda(u) \underset{u\to\infty}{\longrightarrow}$ constant (2.85)

Inverting (2.83) gives

$$u = \nu + \frac{\lambda}{2^{1/3}} \nu^{1/3} + O(1). \tag{2.86}$$

In the continuum limit ($u, \nu \to \infty$) the eigenvalue equation (2.81) becomes

$$J'_{\frac{3+2u-\omega}{2}}(u) \underset{u\to\infty}{\sim} \frac{3u^{4/3}2^{2/3}\lambda}{2u^2} J_{\frac{3+2u-\omega}{2}}(u) \tag{2.87}$$

and, using (2.82), this reduces to

$$Ai'(-\lambda) \xrightarrow[\nu\to\infty]{} \frac{\lambda\, Ai(-\lambda)}{\nu^{1/3}} + O\left(\frac{1}{\nu^{2/3}}\right). \qquad (2.88)$$

So the continuum limit eigenvalues for symmetric states are given by

$$A_i'(-\lambda) = 0 \qquad (2.89)$$

which is just (2.5).

In the same way the condition for an antisymmetric solution on the odd lattice

$$\psi_A(1) = -\psi_A(-1) \qquad (2.90)$$

may be translated into the eigenvalue condition

$$J'_{\frac{3+2u-\omega}{2}}(u) = \left(\frac{u}{1+3u-\omega} - \frac{3+2u-\omega}{2u}\right) J_{\frac{3+2u-\omega}{2}}(u). \qquad (2.91)$$

Then a similar argument to the one used above shows that the continuum ($u \to \infty$) limit of (2.91) is

$$Ai(-\lambda) \xrightarrow[\nu\to\infty]{} \frac{3}{2^{2/3}\nu^{1/3}} Ai'(-\lambda) + O\left(\frac{1}{\nu^{2/3}}\right) \qquad (2.92)$$

which is just (2.7).

The proof that the eigenvalues of the even lattice have continuum limits given by (2.5) and (2.7) follows in the same way.

Summary

The non-relativistic linear potential model provides a concrete introduction to the use of lattice methods. It contains the essence of a confining theory and is simple enough to enable high-order calculations to be performed. But it is not so simple that it misses an important weakness of the Padé approximant continuation method. In fact, it displays the problem so clearly that it is the ideal context in which to invent a remedy. Also in its favour are the existence of an exact solution of the lattice theory and its close relationship with the massive Schwinger model. All in all, it is a valuable trial theory.

CHAPTER 3

THE ORDINARY SCHWINGER MODEL

The massive Schwinger model (Schwinger 1962) is quantum electrodynamics in two-dimensional space-time. It is the theory of a Dirac particle ψ, with mass m and charge g, interacting with an abelian gauge field A_μ. The model is interesting because it displays most of the expected dynamical properties of 3+1 dimensional QCD in a tractable form. The theory for massless fermions has an exact solution (Schwinger 1962; Lowenstein and Swieca 1971) while the massive theory is well understood (Casher, Kogut and Susskind 1974; Coleman, Jackiw and Susskind 1975; Coleman 1976) if lacking a rigorous definition. It is both asymptotically free and confines electric charge. So, if, rather pretentiously, we call the fundamental fermions 'quarks' and the abelian charge 'colour' the Schwinger model is like a 1+1 dimensional version of QCD for one colour and one flavour. Later we shall make the extension to a more realistic model with two flavours.

(a) The Continuum Theory.

The massive Schwinger model is defined by the Lagrangian density[†]

[†]Notation: Lorentz indices $\mu,\nu = 0,1$,

$x = (x^0,x^1)$, $g^{00} = -g^{11} = 1$, $g^{01} = g^{10} = 0$,
$\varepsilon^{01} = -\varepsilon^{10} = 1$, $\varepsilon^{00} = \varepsilon^{11} = 0$,

$\{\gamma^\mu,\gamma^\nu\} = 2g^{\mu\nu}$, $\psi = \begin{pmatrix}\psi^{(1)}\\ \psi^{(2)}\end{pmatrix}$, $\bar{\psi} = \psi^+\gamma_0$, $\gamma_5 = \gamma_0\gamma_1$.

$$\mathcal{L} = -\frac{1}{4} F_{\mu\nu} F^{\mu\nu} + \bar{\psi}(i\not{\partial} - g\not{A} - m)\psi \qquad (3.1)$$

where

$$F_{\mu\nu} = \partial_\mu A_\nu - \partial_\nu A_\mu. \qquad (3.2)$$

A dimensional analysis of (3.1) shows that the coupling constant g has positive mass dimension,

$$[g] = [m] = (\text{length})^{-1}, \qquad (3.3)$$

so the theory is super-renormalisable. This means that no infinite renormalisations are required, other than a trivial renormalisation of the zero-point energy; in particular, g and m are finite (though bare) parameters. Asymptotic freedom follows directly from (3.3).

A Hamiltonian form of the theory is available in the Coulomb gauge,

$$A_1 = 0. \qquad (3.4)$$

Then the equation of motion for A_o,

$$\partial_1^2 A_o = -gN_m[\psi^+\psi] = -gj_o \qquad (3.5)$$

becomes an equation of constraint i.e. there are no photons in one spatial dimension, because of the absence of transverse directions. Here N_m denotes normal ordering with respect to the mass m. Equation (3.5) may be integrated to give the electric field for a given charge distribution. We restrict ourselves to the charge-zero subspace,

$$g\int_{-\infty}^{\infty} dx\, j_o(x) = 0. \qquad (3.6)$$

In doing so we lose no information, because if the theory contains charged particles, they can be discovered by searching the charge-zero subspace for widely separated particle-antiparticle pairs. Then

$$F_{o1}(x) = F + \frac{g}{2}\int_{-\infty}^{\infty} dx'\ \mathrm{sgn}\,(x - x')\ j_o(x') \qquad (3.7)$$

where F is a constant background electric field (Coleman 1976). The Hamiltonian in this gauge,

$$H = \int_{-\infty}^{\infty} dx\ [\bar{\psi}(i\gamma_1\partial_1 + m)\psi + \tfrac{1}{2}(F_{o1})^2] \qquad (3.8)$$

can now be written entirely in terms of fermions:

$$\begin{aligned} H = & \int_{-\infty}^{\infty} dx\ \bar{\psi}(i\gamma_1\partial_1 + m)\psi \\ & - \frac{g^2}{4}\int_{-\infty}^{\infty} dx \int_{-\infty}^{\infty} dy\ j_o(x)\,|x-y|\,j_o(y) \\ & - gF\int_{-\infty}^{\infty} dx\ x\, j_o(x) \\ & + \tfrac{1}{2}F^2\int_{-\infty}^{\infty} dx \end{aligned} \qquad (3.9)$$

The background field F is a physically significant parameter, because of the linear Coulomb potential. In 3+1 dimensional QED, such a field would quickly be neutralised by dielectric breakdown of the vacuum. But in 1+1 dimensions, it is not energetically favourable for the vacuum to produce a particle-antiparticle pair if $|F| \leq \frac{1}{2}g$. Should a state with $|F| > \frac{1}{2}g$ be created, pairs are produced until the system is returned to $|F| \leq \frac{1}{2}g$. Physics is periodic in F with period g.

From (3.3), the dimensionless parameter which measures the interaction strength is m/g. This indicates that the fermi form of the theory, (3.9), is ideal for discussing weak coupling, $m >> g$, because it displays the theory as that of heavy quarks with weak (linear) Coulomb interactions. Thus, a non-relativistic reduction of (3.9) is justified for the low-energy states. In the centre-of-mass system for a quark-antiquark pair with relative separation x and momentum p, the resulting Hamiltonian is

$$H = \frac{p^2}{m} + \frac{g^2}{2}|x| - gFx. \qquad (3.10)$$

Hence, if $|F| \neq \frac{1}{2}g$, this potential increases linearly with x, and there are an infinite number of bound states.

In contrast, the strong-coupling limit, $g >> m$, should be described well by the massless theory. This can be solved exactly (Schwinger 1962, Lowenstein and Swieca 1971). The solution exhibits what is believed to be a realistic mechanism for quark confinement via charge screening, which results from the strong polarisability of the vacuum. ψ and all its excitations are absent from the physical space of states. All that remains is a free neutral pseudoscalar meson ϕ with mass $g/\sqrt{\pi}$. This is an example of a dynamical Higgs phenomenon. It is signalled by the appearance of a pole at $g/\sqrt{\pi}$ in the 'photon' propagator. Local electric charge conservation is spontaneously broken, but no Goldstone boson appears, because the Goldstone mode may be gauged away. The solution also demonstrates a spontaneous breakdown of global chiral symmetry. This is announced by the appearance of an infinite family of degenerate vacuum states,

labelled by an angle $\theta \in [-\pi,\pi]$. Here again no Goldstone boson occurs, but for a different reason: the axial current is not conserved because of an anomaly (Jackiw 1973).

The correspondence between fermion and boson fields in 1+1 dimensions is:

$$j^{\mu} \equiv N_m[\bar{\psi}\gamma^{\mu}\psi] = \frac{1}{\sqrt{\pi}}\epsilon^{\mu\nu}\partial_{\nu}\phi \qquad (3.11)$$

and

$$N_m[\bar{\psi}\psi] \equiv -cm N_m[\cos(2\sqrt{\pi}\phi)] \qquad (3.12)$$

where

$$c \equiv \frac{e^{\gamma}}{2\pi} \qquad (3.13)$$

and γ is Euler's constant. The correspondence for the dynamics is

$$N_m[\bar{\psi}i\gamma_1\partial_1\psi] \longrightarrow \tfrac{1}{2}N_m[\dot{\phi}^2 + (\partial_1\phi)^2]. \qquad (3.14)$$

In the charge-zero subspace (3.6), using (3.11) in (3.7) gives for the electric field (Kogut and Susskind 1975a, Coleman 1976)

$$F_{01}(x) = \frac{g}{\sqrt{\pi}}\phi(x) + \frac{g\theta}{2\pi} \qquad (3.15)$$

where

$$\theta \equiv \frac{2\pi F}{g} . \qquad (3.16)$$

Through (3.16), θ receives a physical interpretation as the background electric field. Different values of this field give rise to

different vacuum states. Looked at this way, the breaking of C and P which occurs for $\theta \neq 0$ is not surprising, because this corresponds to $F \neq 0$ and a constant background electric field will certainly break these symmetries. The boson version of Hamiltonian (3.8) which results from (3.14), (3.15) and (3.12) is

$$\mathcal{H} = N_m\left[\tfrac{1}{2}\dot{\phi}^2 + \tfrac{1}{2}(\partial_1\phi)^2 - cm^2\cos(2\sqrt{\pi}\phi) + \frac{g^2}{2\pi}\left(\phi + \frac{\theta}{2\sqrt{\pi}}\right)^2\right] \tag{3.17}$$

We are free to shift the field

$$\phi \to \phi - \frac{\theta}{2\sqrt{\pi}} \tag{3.18}$$

and to change the normal-ordering mass to[†]

$$\mu \equiv g/\sqrt{\pi} \tag{3.19}$$

Then,

$$\mathcal{H} = N_\mu\left[\tfrac{1}{2}\dot{\phi}^2 + \tfrac{1}{2}(\partial_1\phi)^2 + \frac{\mu^2}{2}\phi^2 - cm\mu\cos(2\sqrt{\pi}\phi - \theta)\right]. \tag{3.20}$$

[†](Coleman 1975) Normal ordering with respect to a mass m is defined by Wick's theorem, with the contraction function that of a free field of mass m. Any theory of a scalar field with non-derivative interactions in 1+1 dimensions is free of divergences in every order of perturbation theory if the Hamiltonian is normal-ordered with respect to any mass m, although graphs involving contractions of two fields at the same vertex are cancelled completely only if m is the mass in the free Hamiltonian. As a result,

$$N_m[\dot{\phi}^2 + (\partial_1\phi)^2] = N_\mu[\dot{\phi}^2 + (\partial_1\phi)^2]$$

plus an irrelevant constant, and

$$N_m[\cos\beta\phi] = \left(\frac{\mu}{m}\right)^{\beta^2/4\pi} N_\mu[\cos\beta\phi].$$

This expression unites the massless and massive theories. It leads naturally to the construction of a perturbation series in m. However, the massive theory has not been solved exactly, and so it is not known whether (3.20) defines a physically sensible theory for any value of m or θ.

It might be supposed that, having written the massive Schwinger model in terms of canonical Bose fields alone, this immediately implies that the theory contains no fermions. This is false. Both weakly-coupled ϕ^4 and sine-Gordon theories are counter examples (Coleman 1975). A more careful argument is required (Coleman, Jackiw and Susskind 1975, Kogut and Susskind 1975b). Widely separated external charges, $\pm e$, are introduced and the long-range force between them is calculated. In the ground state of this system, neglecting "edge-effects" near the external charges, the energy density only differs from that of the θ-vacuum in the region between the charges, and there it is given by (3.20) but with the background field shifted by e. So, if $\varepsilon(\theta)$ is the energy density of the θ-vacuum, the interaction energy of external charges distance L apart is

$$E = \left[\varepsilon\left(\theta \pm \frac{2\pi e}{g}\right) - \varepsilon(\theta)\right] L + \cdots \qquad (3.21)$$

where the extra terms become constant as $L \to \infty$. Because of the periodicity in θ, there is no long-range force if e is an integral multiple of g. This result is independent of mass perturbation theory. On the other hand, for arbitrary e, the long-range force is present, at least in mass perturbation theory, where to first order

$$\varepsilon(\theta) = -cm\mu \cos\theta, \qquad (3.22)$$

from which we deduce that the Higgs phenomenon does not occur.

The mechanism for this charge screening is vacuum polarisation. If the two external charges are separated quasi-statically, the naive Coulomb energy grows linearly with their separation until it becomes energetically favourable for the vacuum to produce a pair of charges to shield the external sources. If e is an integer multiple of g, the long-range force will be exactly screened by the same integer number of pairs. However, if e/g is not an integer, there is no good reason for the screening to be exact., Likewise, if we try to separate a quark-antiquark pair, as the separation increases it is soon energetically favourable for a new pair to materialise from the vacuum. The new quark is attracted to the original antiquark and the new antiquark is attracted to the original quark. This both shields the long-range force and ensures that what we are separating is not a quark and an antiquark, but two quark-antiquark bound states.

The transformation from the fermion representation, (3.9), to the equivalent boson representation, (3.20), is a kind of duality transformation in that the roles of mass and coupling constant are interchanged. This makes (3.20) ideal for discussing the particle spectrum of the strongly-coupled massive Schwinger model. For $m \ll g$ it describes a heavy pseudoscalar meson with weak self-interactions. Thus, the theory always contains at least one particle: the original meson of mass $g/\sqrt{\pi}$. If it contains other particles they will be weakly-bound n-meson states, of mass $ng/\sqrt{\pi}$ (plus small corrections). These can be found by non-relativistic reasoning. We only consider the case $\theta = 0$. The terms in the expansion of $\cos(2\sqrt{\pi}\phi)$ lead to a string

of many-body δ-function potentials. In the two-meson subspace, only the ϕ^4 term is effective, and so

$$H \simeq \frac{1}{2}\int_{-\infty}^{\infty} dx \left[\dot{\phi}^2 + (\partial_1\phi)^2 + \left(\frac{g}{\sqrt{\pi}} + me^{\gamma}\right)^2\phi^2 - \frac{2}{3}\sqrt{\pi}\, mg e^{\gamma}\phi^4\right] \tag{3.23}$$

giving the pseudoscalar meson mass

$$M^- = g/\sqrt{\pi} + me^{\gamma} + O(m^2). \tag{3.24}$$

Next we perform a non-relativistic reduction of the scattering amplitude due to the ϕ^4 interaction in the two-meson subspace. Relating this to potential scattering via the Born approximation, gives an interaction potential between pseudoscalar mesons which is an attractive δ-function:

$$V(x) = \left(-\frac{2}{3}\sqrt{\pi}\, mg e^{\gamma}\right)\frac{12}{(2M^-)^2}\,\delta(x) \tag{3.25}$$

This potential has a single bound state. It is a scalar particle of mass

$$M^+ = 2M^- - \pi^2 e^{2\gamma}\frac{m^2}{M^-} + O(m^3). \tag{3.26}$$

The mass ratio resulting from (3.26) and (3.24) is

$$\frac{M^+}{M^-} = 2 - \pi^3 e^{2\gamma}\left(\frac{m}{g}\right)^2 + O\left(\frac{m}{g}\right)^4. \tag{3.27}$$

Since the background field $\theta = 0$, the cosine in (3.20) is an even function of ϕ, and so, in the strong-coupling limit the 3-meson bound state is also stable. All higher bound states are unstable, because

the ϕ^4 term enables an n-meson bound state to decay into n - 2 free mesons.

As a consistency check, we consider the transition from weak to strong coupling when $\theta = 0$ and the stable particles are eigenstates of C and P. For weak coupling, the potential in (3.10) is symmetric, so the ground-state wavefunction is spatially symmetric and successive excited-state wavefunctions are alternately antisymmetric and symmetric. Since the particles being bound are a fermion and an antifermion, this means the ground state is parity odd, and the first excited state is parity even, etc. All the bound states are CP even. This is the same pattern as in strong coupling where the meson is pseudoscalar, the two-meson bound state is scalar etc., and all states are CP even.

Lastly, we mention a peculiarity which occurs for $|\theta| = \pi$ (Coleman 1976). Then, for weak coupling, the potential in (3.10) becomes

$$V(x,\pi) = 0, \quad x > 0$$
$$= -g^2 x, \quad x < 0. \qquad (3.28)$$

So, if the quark is to the left of the antiquark there is an attractive linear potential between them, but if the quark is to the right, there is no long-range force at all. In the latter case, the electric field, F_{01}, changes sign between the particles, but the electrostatic energy $(F_{01})^2$ is unchanged. The system is in a category somewhere intermediate between confining theories and theories which contain asymptotic particle states. Here widely separated quarks and antiquarks can appear in asymptotic states, but only in a certain order. For this reason Coleman calls the

resulting "free" quark states "half-asymptotic particles". Coleman (1976) finds no trace of these half-asymptotic particles in the strong coupling limit, and so conjectures that the theory undergoes a phase transition on its passage to strong coupling.

(b) The Lattice Theory.

The massive Schwinger model has much in common with QCD, so methods devised to investigate its bound-state spectrum might be profitably applied to hadrons in 3+1 dimensions. Our technique is to convert the continuum field theory into a lattice theory, and thereby reduce the problem to one with a countable number of degrees of freedom. Space is replaced by a linear chain of sites (a cubic lattice in realistic theories; finite in practice), while time remains continuous. This trick enables us to define a Hamiltonian, and calculate the low-lying bound states by perturbing around the large-lattice-spacing limit. In this way the massive Schwinger model becomes a non-trivial test of lattice methods. If the approach is to be applied with any confidence to QCD, the lattice Schwinger model had better be understood and give accurate results. The continuum limit can be expected to present similar difficulties to those encountered in the linear potential model, at least for large fermion mass. Methods devised to handle these difficulties in 1+1 dimensions may be of significance in 3+1 dimensions. Our aim throughout will be to develop an accurate and practical way of extrapolating to the zero-lattice-spacing limit.

One subtlety of the lattice approach emerges early on and is of major significance. It concerns the way in which fermion fields are

defined on a spatial lattice. There is general agreement on how to define lattice gauge fields, but differing views exist on the best way to treat fermions (Susskind 1977; Drell, Weinstein and Yankielowicz 1976; Wilson 1975). We follow Susskind who has in mind the symmetries of the continuum theory and calculability. When a continuum theory is converted into a lattice theory some of the original continuous symmetries have to be replaced by discrete ones. We try to do this in the most 'natural' way. Ambiguities can arise in higher dimensions, or with more than one species of fermion. Then the choice we make can have profound consequences for convergence of our approximations (see Chapter 5).

First consider discrete forms of the free, massless, 1+1 dimensional Dirac equation:

$$\dot{\psi} = \alpha \partial_1 \psi \tag{3.29}$$

where the Dirac field is a two-component spinor

$$\psi = \begin{pmatrix} \psi(1) \\ \psi(2) \end{pmatrix} \tag{3.30}$$

and we use the representation

$$\gamma_0 = \begin{pmatrix} 1 & 0 \\ 0 & -1 \end{pmatrix}, \quad \gamma_1 = \begin{pmatrix} 0 & 1 \\ -1 & 0 \end{pmatrix}, \quad \alpha = \gamma_5 = \begin{pmatrix} 0 & 1 \\ 1 & 0 \end{pmatrix} \tag{3.31}$$

for the Dirac algebra. An obvious attempt at a lattice version of (3.29) is to place a two-component fermion field on each site n, and interpret $\partial_1\psi$ as the symmetric difference $\frac{1}{2a}[\psi((n+1)a)-\psi((n-1)a)]$, where a is the lattice spacing. However, this attempt fails: in the continuum limit ($a \to 0$) two massless Dirac particles result from such a

scheme. This can be understood by comparing the dispersion laws for (3.29) and its proposed discrete version

$$\dot{\psi}(na) = \frac{\alpha}{2a}\left[\psi((n+1)a) - \psi((n-1)a)\right]. \qquad (3.32)$$

Substituting plane waves, we obtain for the former,

$$\omega = \pm k \quad (-\infty < k < \infty) \qquad (3.33)$$

and for the latter,

$$\omega = \pm \frac{\sin ka}{a} \quad (-\pi < ka \leqslant \pi) \qquad (3.34)$$

(3.33) describes right- and left-moving fermions and antifermions, as shown in fig. 3.1. On the lattice, fig. 3.2, we are interested in those modes which have finite frequency as $a \to 0$. These occur in the neighbourhood of the origin, $ka \to 0$, and the edges of the Brillouin zone, $ka \to \pm\pi$. The finite-energy excitations around the origin account for the degrees of freedom we would normally expect to survive in the continuum limit. Those near the edges of the Brillouin zone correspond to an extra unwanted fermion species.

Our method of avoiding this problem (Susskind 1977) is to recognise that the naive approach has too many degrees of freedom in the unit cell. By halving the number we can give a lattice description of a single fermion species. To do this we place a single-component fermion field $\phi(n)$ on each lattice site and let the 'hopping' Hamiltonian be

$$H_{K.E.} = \frac{i}{2a}\sum_n \left[\phi^+(n)\phi(n+1) - \phi^+(n+1)\phi(n)\right]. \qquad (3.35)$$

$\phi(n)$ obeys canonical anticommutation relations

$$\{\phi(n),\ \phi(m)\} = 0,\ \{\phi^{+}(n),\ \phi(m)\} = \delta_{nm} \tag{3.36}$$

and the resulting Heisenberg equation of motion is

$$\begin{aligned}\dot{\phi}(n) &= i\left[H_{K.E.},\ \phi(n)\right] \\ &= \frac{1}{2a}\left[\phi(n+1) - \phi(n-1)\right]\end{aligned} \tag{3.37}$$

Now the dispersion law is

$$\omega = \frac{\sin ka}{a} \quad (-\pi \leq ka < \pi) \tag{3.38}$$

shown in fig. 3.3 and left- and right-moving waves are identified with the neighbourhoods of $ka = 0$ and $ka = \pm\pi$ respectively. That equation (3.37) describes a two-component field in the continuum limit can be seen by identifying $\phi(n)$ on even (odd) sites with the upper (lower) component of a conventional Dirac spinor:

$$\frac{1}{\sqrt{a}}\,\phi(n) \equiv \psi^{(n+1 \bmod 2)}(na) \tag{3.39}$$

Then (3.37) can be written as

$$\dot{\psi}(na) = \begin{pmatrix} 0 & 1 \\ 1 & 0 \end{pmatrix} \frac{1}{2a}\left[\psi((n+1)a) - \psi((n-1)a)\right] \tag{3.40}$$

and the Dirac equation (3.29), is regained as $a \to 0$.

Placing the fermion and antifermion parts of ψ on adjacent lattice sites has unusual consequences. For example, a translation of the lattice by an even number of sites is clearly a symmetry of

$H_{K.E.}$, (3.35), and corresponds to conventional translational invariance. However, a shift by an odd number of sites, which is also a symmetry of $H_{K.E.}$, interchanges even and odd sites. According to (3.39) this is the product of a conventional translation and the discrete U(1) chiral rotation:

$$\psi \longmapsto \gamma_5 \psi. \tag{3.41}$$

This takes on new significance when gauge interactions are incorporated into the Hamiltonian. The point is that the Hamiltonian of the massless lattice Schwinger model also has the discrete γ_5 symmetry observed here and that this symmetry is sufficient to preclude the dynamical generation of a fermion mass. Furthermore, this odd-shift invariance is spontaneously broken by the vacuum of the lattice theory. The symmetry is explicitly broken when a mass term is added to the Hamiltonian (3.35). Using the correspondence between lattice and continuum fields given in (3.39) this is

$$m\int dx\, \bar{\psi}\psi \longrightarrow m\sum_n (-1)^n \phi^\dagger(n)\phi(n) \tag{3.42}$$

and is clearly only invariant under translations by an even number of lattice sites.

The general formulation of gauge fields on a spatial lattice has been extensively reviewed elsewhere (Susskind 1976). Here we concentrate on the abelian theory in one spatial dimension. All work is carried out in the class of gauges

$$A_o = 0 \tag{3.43}$$

for which a simple Hamiltonian form of the theory exists. The spatial component of the gauge field enters the theory through the unitary

connection

$$U(n,n+1) \equiv \exp[iagA(na)] = U^{+}(n+1,n) \qquad (3.44)$$

which occupies the links of the lattice. Because of this, the meaningful range of variation of the vector potential is compact, $agA(na) \in [0,2\pi)$. The variable conjugate to this angle is

$$L(n) \equiv \frac{1}{g}\dot{A}(na) \qquad (3.45)$$

and obeys the quantisation condition

$$[agA(na), L(m)] = i\delta_{nm}. \qquad (3.46)$$

It follows that L(m) is an angular momentum operator whose spectrum is the integers. In the gauge (3.43) the electric field is

$$E(na) = \dot{A}(na) + F = gL(n) + F \qquad (3.47)$$

where F is the constant background field. So physics is periodic in F with period g, just as in the continuum theory. Also (3.47) shows that the electric field is quantised in units of g. This quantisation of electric flux is not an artefact of the lattice formulation. It also occurs in the continuum Schwinger model as a result of Gauss' Law and the lack of transverse spatial dimensions. This fact suggests that a smooth continuum limit of the lattice theory may exist.

Following Coleman (1976), we define

$$\theta \equiv \frac{2\pi F}{g} \in [-\pi,\pi] \qquad (3.48)$$

Then the energy stored in the electric field is

$$H_G = \tfrac{1}{2}\int dx\,[E(x)]^2 \longrightarrow \tfrac{1}{2}\sum_n a\left[gL(n) + \frac{g\theta}{2\pi}\right]^2$$

$$= \frac{ag^2}{2}\sum_n \left[L(n) + \frac{\theta}{2\pi}\right]^2. \qquad (3.49)$$

Usually we set $\theta = 0$, then the static gauge field energy is just a sum of squares of integers. The ground state of H_G is the state $|0\rangle$ with

$$L(n)|0\rangle = 0 \quad (|\theta| \neq \pi). \qquad (3.50)$$

From it states of definite L^2 are obtained by applying the raising and lowering operators U and U^+, (3.44), since from (3.46)

$$[L(n),\ U(n,n+1)] = U(n,n+1) \qquad (3.51a)$$

and

$$[L(n),\ U^+(n,n+1)] = -U^+(n,n+1). \qquad (3.51b)$$

The fermion and gauge field degrees of freedom are coupled together through the requirement of local gauge invariance. This demands that the Hamiltonian be invariant under

$$\phi(n) \longmapsto e^{ig\Lambda(n)}\phi(n) \qquad (3.52a)$$

$$U(n,n+1) \longmapsto e^{ig\Lambda(n)}U(n,n+1)e^{-ig\Lambda(n+1)} \qquad (3.52b)$$

corresponding to the discrete gauge transformation

$$A(na) \longmapsto A(na) + \frac{1}{a}\left[\Lambda(n) - \Lambda(n+1)\right]. \qquad (3.53)$$

H_G is automatically invariant and so is the mass term (3.42), being the product of fermion fields at the same site. But point-separated operators like $H_{K.E.}$ (3.35) have to be rendered locally gauge invariant by introducing the connection (3.44):

$$H_{K.E.} = \frac{i}{2a}\sum_n \left[\phi^+(n)\,U(n,n+1)\,\phi(n+1) + \phi(n)\,U^+(n,n+1)\,\phi^+(n+1)\right] \qquad (3.54)$$

Thus we arrive at the Hamiltonian for the massive lattice Schwinger model as the sum of (3.42), (3.49) and (3.54) (Banks, Susskind and Kogut 1976, Kogut 1976):

$$H = \frac{ag^2}{2\theta}\sum_n \left[L(n) + \frac{\theta}{2\pi}\right]^2 + m\sum_n (-1)^n \phi^+(n)\phi(n) + \frac{i}{2a}\sum_n \left[\phi^+(n)\,U(n,n+1)\,\phi(n+1) - h.c.\right] \qquad (3.55)$$

It is straightforward to verify that this reduces to the (classical) continuum Hamiltonian in the limit $a \to 0$.

For the rest of this chapter we will be concerned with the particle spectrum of (3.55). In order to make clear the relative sizes of the three terms in (3.55) it is convenient to scale out a factor $\frac{ag^2}{2}$ and work with the dimensionless Hamiltonian ($\theta = 0$):

$$W \equiv \frac{2}{ag^2} H = W_o + xV \qquad (3.56)$$

where

$$W_o = \sum_n [L(n)]^2 + \mu \sum_n (-1)^n \phi^+(n) \phi(n) \qquad (3.57)$$

$$V = i \sum_n [\phi^+(n) U(n,n+1) \phi(n+1) + \phi(n) U^+(n,n+1) \phi^+(n+1)] \qquad (3.58)$$

and the dimensionless parameters x and μ are

$$x \equiv \frac{1}{a^2 g^2} \, , \quad \mu \equiv \frac{2m}{ag^2} = 2\sqrt{x}\,\frac{m}{g} \qquad (3.59)$$

We have separated W into two terms. The first, W_o, is a static term involving operators all at single sites. The second term, V, allows quarks to hop about the lattice in a gauge-invariant fashion. It is multiplied by the dimensionless inverse coupling constant x. According to our general method of analysing lattice theories, we shall perform a strong-coupling expansion in the variable x using conventional perturbation theory (m/g is an independently variable parameter). The real challenge lies in a proper interpretation of this expansion, since in the continuum limit $x \to \infty$. Before discussing this issue, we should understand some of the properties of the cut-off theory. In particular, before seeking the particle spectrum, we must find the theory's vacuum.

Consider the massless theory. The vacuum minimises W_o so it must be fluxless (3.50). However, the fermion content of the ground state is not determined by W_o. All states $|0\Psi\rangle$ which are fluxless

and have arbitrary fermion content are degenerate in zeroth order. This degeneracy is lifted in perturbation theory. Using degenerate Rayleigh-Schrodinger perturbation theory (see appendix A) to second order in xV, the shift in the vacuum energy is

$$\delta W = x\langle 0,\Psi|V|0,\Psi\rangle + x^2\langle 0,\Psi|V\frac{Q}{-W_0}V|0,\Psi\rangle + \cdots \tag{3.60}$$

Here Q forbids fluxless intermediate states, and we have used the fact that the unperturbed energy is zero. The first order term vanishes, because $V|0,\Psi\rangle$ is a state with flux and does not project back onto $|0,\Psi\rangle$. (All odd orders vanish for the same reason). The second order matrix element is non-zero only if the piece of flux created by the first V is destroyed by the second V. So, eliminating the gauge fields,

$$\delta W = \frac{x^2}{2}\langle 0,\Psi|\sum_n\left[\rho(n)\rho(n+1)-1\right]|0,\Psi\rangle \tag{3.61}$$

where

$$\rho(n) \equiv \left[\phi^+(n),\phi(n)\right] \tag{3.62}$$

is the local fermion number operator, taking the values ±1 depending on whether the site n is occupied or not. Hence we seek the ground state of the effective Hamiltonian

$$W_{eff} = \frac{x^2}{2}\sum_n \rho(n)\rho(n+1). \tag{3.63}$$

This is an Ising antiferromagnetic chain whose ground state

$$\langle 0|\rho(n)|0\rangle = -\langle 0|\rho(n+1)|0\rangle \quad \forall n \qquad (3.64)$$

is doubly degenerate; even sites may be occupied and odd sites unoccupied, or vice versa. It is important to realise that this remaining two-fold degeneracy is a real property of the theory and is not lifted at higher orders in perturbation theory. The two vacua are related by a lattice translation through one link i.e. the discrete chiral transformation $\psi \to \gamma_5\psi$. Thus, in choosing one vacuum on which to base the lattice Shwinger model, we spontaneously break the symmetry under discrete chiral transformations. Since chiral symmetry is known to be broken by the vacuum structure of the continuum model, the strongly-coupled lattice theory shares an important qualitative feature with the theory we eventually wish to make contact with.

Since we are primarily interested in the massive Schwinger model, we should choose the vacuum of the massless model which changes smoothly as the fermion mass is increased from zero. For $\mu > 0$ the mass term in (3.57) picks out the vacuum in which odd sites are occupied

$$\langle 0|\rho(n)|0\rangle = \begin{cases} 1 & n \text{ odd} \\ -1 & n \text{ even} \end{cases} \qquad (3.65)$$

This is the zeroth order ground state on which we base our strong-coupling perturbation theory.

Particle states on the lattice are gauge invariant combinations of quarks and antiquarks joined together with flux lines. We are interested in the static energies i.e. masses of the low-lying bound states. These meson states may be constructed by allowing spatial integrals of various currents to operate on the vacuum. Since the only "spatial rotations" are inversions, the spatial component of a vector is a pseudoscalar and of an axial vector is a scalar. So the only meson states are scalars and pseudoscalars (there is no spin in 1+1 dimensions).

Thus, we generate a pseudoscalar meson out of the vacuum by applying the lattice version of $\int dx \bar{\psi} \gamma_1 \psi$. Using the prescription (3.39) and taking care of gauge invariance by inserting the appropriate connection, gives

$$|1-\rangle = \frac{1}{\sqrt{N}} \sum_n \left[\phi^\dagger(n)\, U(n,n+1)\, \phi(n+1) - \phi(n)\, U^\dagger(n,n+1)\, \phi^\dagger(n+1) \right] |0\rangle. \quad (3.66)$$

(All states are normalised to unity on a finite periodic lattice of N(even) sites). The scalar particle is generated by the kinetic energy term in H:

$$|1+\rangle = \frac{1}{\sqrt{N}} \sum_n \left[\phi^\dagger(n)\, U(n,n+1)\, \phi(n+1) + \phi(n)\, U^\dagger(n,n+1)\, \phi^\dagger(n+1) \right] |0\rangle. \quad (3.67)$$

Both of these are 1-link states at rest relative to the fixed lattice sites. They are the lowest-lying eigenstates of W_o, corresponding to the eigenvalue

$$w_{\pm}^{(o)} = 1 + 2\mu. \quad (3.68)$$

There are also non-zero momentum states, e.g. the scalar particle at momentum k is

$$|1+,k\rangle = \frac{1}{\sqrt{N}} \sum_n \left[e^{ikna} \phi^+(n) U(n,n+1) \phi(n+1) \right.$$
$$\left. + e^{-ikna} \phi(n) U^+(n,n+1) \phi^+(n+1) \right] |0\rangle \qquad (3.69)$$

but they will not concern us much. Other eigenstates of W_o, composed of two quarks and two antiquarks, or a quark-antiquark pair more than one link apart, become relevant when we try to extrapolate away from the strongly coupled lattice theory. They are discussed in detail in Chapter 4.

(c) Estimates for the Particle Spectrum of the Continuum Model.

Next we consider the effect of the perturbation V, given in (3.58) We use ordinary, non-degenerate Rayleigh-Schrödinger perturbation theory to expand the vacuum energy density and low-lying meson masses as power series in x (3.59). Our hope is that,by working to high orders in perturbation theory, we can obtain sufficiently accurate representations of these quantities as functions of the lattice spacing to extrapolate them reliably via Padé approximants to the continuum limit. These calculations are lengthy and tedious. Nevertheless, several independent groups have carried out the calculation to sixth order in V by hand. To date the eighth order calculation remains accessible only to a computer But recent advances suggest that hand calculations on finite lattices

could be pushed higher. After taking the precautions which proved necessary for the linear potential, it is possible to make confident predictions, based on these results, about the particle spectrum of the continuum model for all values of the interaction strength m/g.

As a specific illustration of the method we consider the mass of the pseudoscalar particle (3.66). Where the calculation for the scalar particle (3.67) differs from it, we record the corresponding result in parentheses. Only even orders in V contribute, so the formula for the perturbation expansion, given in appendix A, reduces to

$$\frac{2\sqrt{x}}{g} M^- = \langle 1^- | W_0 | 1^- \rangle + x^2 \langle 1^- | V \frac{Q}{\omega_-^{(0)} - W_0} V | 1^- \rangle + x^4 \left[\langle 1^- | V \left(\frac{Q}{\omega_-^{(0)} - W_0} \right)^3 V | 1^- \rangle - \langle 1^- | V \frac{Q}{\omega_-^{(0)} - W_0} V | 1^- \rangle \langle 1^- | V \frac{Q}{(\omega_-^{(0)} - W_0)^2} V | 1^- \rangle \right] + O(x^6). \tag{3.70}$$

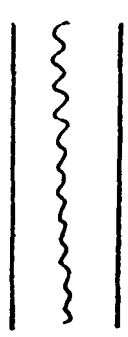
Here Q ensures that intermediate states are orthogonal to the incoming state, and the zeroth order energy is

$$\omega_-^{(0)} = \langle 1^- | W_0 | 1^- \rangle = 1 + 2\mu \tag{3.71}$$

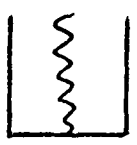
Note that this is not strictly-speaking "zeroth order" because μ is proportional to $\sqrt{x}$. However, the mass term in (3.57) is a static operator and so can be included in the unperturbed Hamiltonian, provided we ultimately expand the energy denominators as power series

in $\sqrt{x}$ to the same order as our perturbation series.

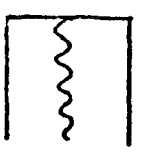
The diagram rules simply catalogue the allowed configurations of quark-antiquark pairs and electric flux as the initial state develops under the action of the perturbation. The spatial lattice is represented across the page, while "time" increases vertically. Thus, in zeroth order, the pseudoscalar meson is represented by



which is just a quark-antiquark pair on neighbouring sites, joined by a unit of electric flux. The action of the perturbation V is to create and destroy similar quark-antiquark pairs, denoted by the vertices.



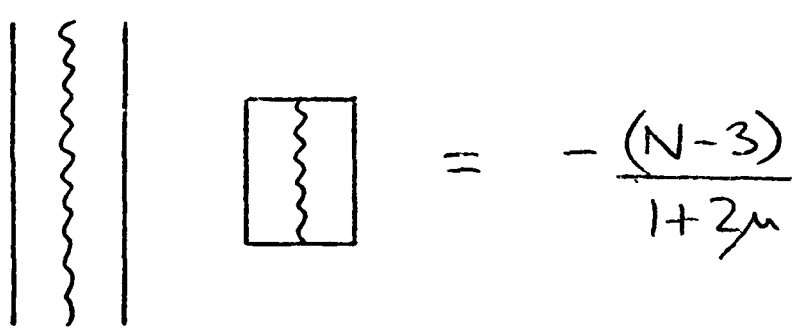
and



respectively. Fermi statistics forbid more than one fermion on any site, but there can be any integral unit of flux on the links consistent with Gauss' law. The intermediate states are horizontal slices bounded above and below by vertices. The corresponding energy denominator is

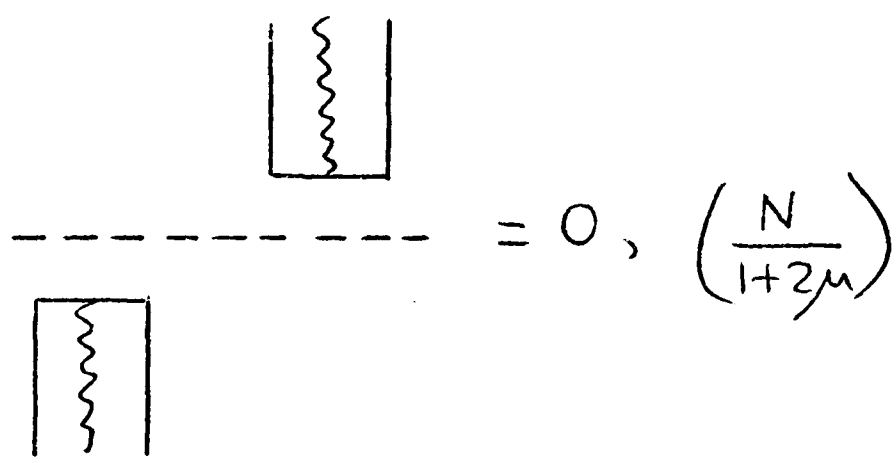
obtained by subtracting the sum of the squares of the fluxes on each link and μ times the number of fermion lines from (3.71).

At second order there are two distinct types of graph. In the first, the perturbation acts to create a vacuum fluctuation on any link except the one occupied by the through-going particle and the two adjacent to it (N-3 possibilities):



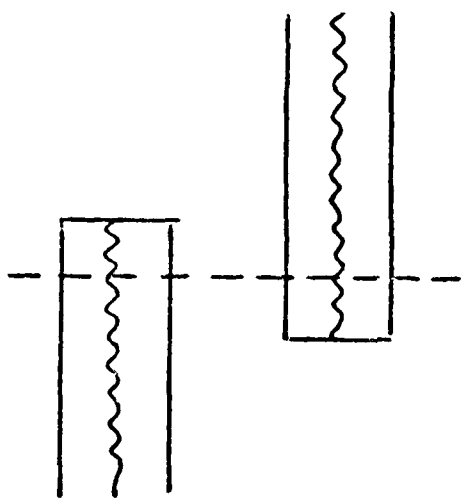
(3.72)

The second type allows the particle to move by destroying the incoming particle and recreating it on another link. The intermediate state (denoted in the diagrams by a horizontal dashed line) may be the vacuum, in which case the outgoing particle may emerge on any one of the N links:



(3.73)

or the two particle state, in which case the outgoing particle is excluded from the three links occupied by and adjacent to the incoming particle:

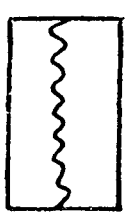


$$= -\frac{1}{1+2\mu}\cdot\left(-\frac{(N-3)}{1+2\mu}\right) \qquad (3.74)$$

Notice that the counting is different for scalars and pseudoscalars. For scalars, each graph is counted with a + sign regardless of the relative separation of the incoming and outgoing particles, whereas for pseudoscalars there is an extra - sign when they are adjacent or separated by an even number of links (compare (3.66) and (3.67)). The second order matrix element is obtained by adding the contributions (3.72), (3.73) and (3.74):

$$\langle i|V\frac{Q}{\omega_-^{(0)}-W_0}V|i\rangle = -\frac{(N-2)}{1+2\mu}\cdot\left(-\frac{(N-6)}{1+2\mu}\right) \qquad (3.75)$$

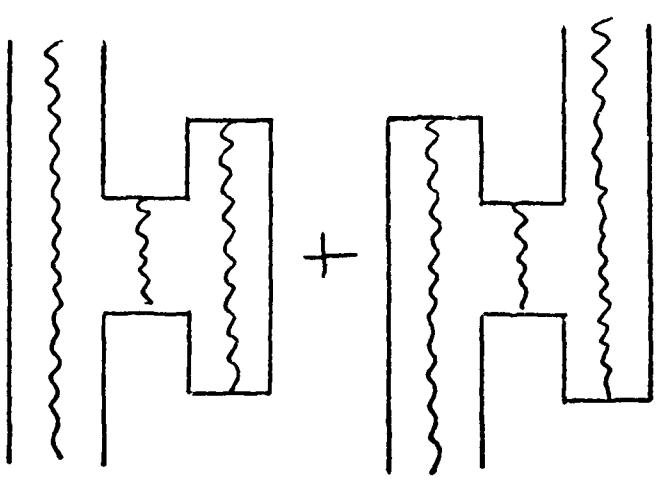
Of course the mass of the state must be measured relative to the vacuum energy which also shifts at second order. The graph responsible is



$$= -\frac{N}{1+2\mu} \qquad (3.76)$$

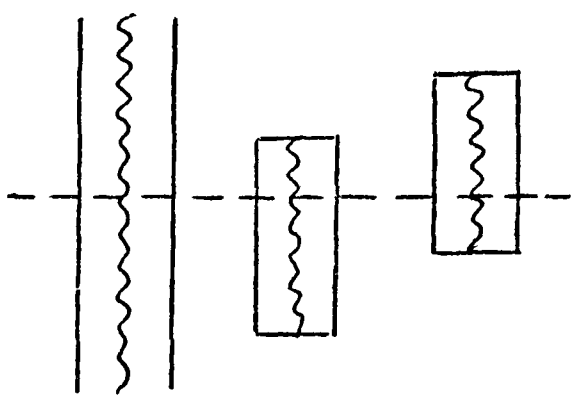
When this is subtracted from (3.75), the intensive character of the particle mass is re-established.

Returning to the formula (3.70), we see that the fourth order contribution comes in two parts. The first consists of the direct fourth-order graphs, while from these must be subtracted the product of contributions from lower-order graphs. The former can be further classified as connected or disconnected. The connected examples are



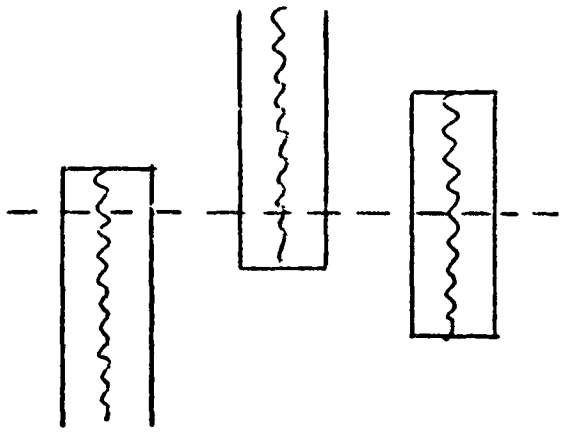
$$= \frac{2.2}{(-2)(1+2\mu)^2} \qquad (3.77)$$

where we have drawn one of two possible orientations for each graph. These allow one of the constituent quarks to propagate two links in the "linear confining potential". The disconnected graphs may either involve two vacuum fluctuations:



$$= -\frac{1}{2}(N-4)(N-5)\cdot\frac{4}{(1+2\mu)^2(2+4\mu)} \qquad (3.78)$$

or the destruction and recreation of the initial particle:



$$= -(N-4)\cdot\frac{4}{(1+2\mu)^2(2+4\mu)}\,, \qquad (3.79)$$

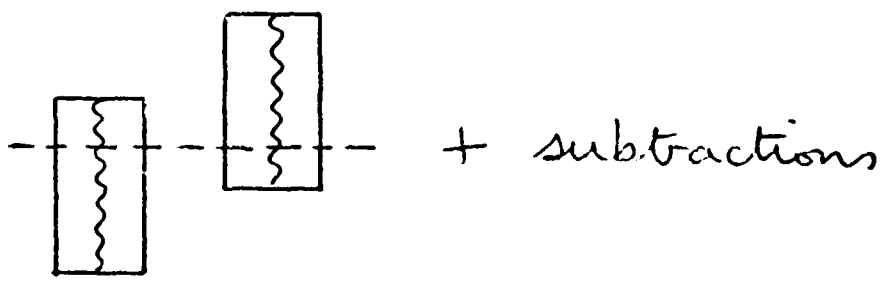
$$\left(-(N-4)(N-5)\cdot\frac{4}{(1+2\mu)^2(2+4\mu)}\right)$$

Here the horizontal dashed line fixes one intermediate state, but each of the remaining four relative time-orderings of the vertices are counted equally. Counting the number of graphs is less trivial. In (3.78) the through-going particle excludes the vacuum fluctuations from a few of the links surrounding it. This also happens in (3.79) where for the pseudoscalar particle it is best to count the number of excluded graphs. The subtraction term in (3.70) can be computed easily from (3.72), (3.73) and (3.74), by squaring the energy denominators in one case. The result for the fourth order matrix element is

$$\langle 1-|V\left(\frac{Q}{\omega_-^{(0)}-W_0}V\right)^3|1-\rangle - \langle 1-|V\frac{Q}{\omega_-^{(0)}-W_0}V|1-\rangle\langle 1-|V\frac{Q}{(\omega_-^{(0)}-W_0)^2}V|1-\rangle$$

$$= \frac{-2}{(1+2\mu)^2} + \frac{3N-8}{(1+2\mu)^3}\,, \left(\frac{-2}{(1+2\mu)^2} + \frac{3N-24}{(1+2\mu)^3}\right) \qquad (3.80)$$

Again, the fourth-order shift in the vacuum energy must be subtracted to obtain a finite result. This is



$$= -\frac{1}{2} N(N-3) \cdot \frac{4}{(1+2\mu)^2(2+4\mu)} + \frac{N^2}{(1+2\mu)^3}$$

$$= \frac{3N}{(1+2\mu)^3} . \qquad (3.81)$$

Hence, the pseudoscalar and scalar particle masses to fourth order in V are (Banks, Susskind and Kogut 1976)

$$\frac{2\sqrt{x}}{g} M_1^- = 1+2\mu + \frac{2x^2}{1+2\mu} + x^4 \left[\frac{-2}{(1+2\mu)^2} - \frac{8}{(1+2\mu)^3} \right] + O(x^6), \qquad (3.82)$$

and

$$\frac{2\sqrt{x}}{g} M_1^+ = 1+2\mu + \frac{6x^2}{1+2\mu} + x^4 \left[\frac{-2}{(1+2\mu)^2} - \frac{24}{(1+2\mu)^3} \right] + O(x^6). \qquad (3.83)$$

It is important to recognise that, due to the x-dependence of μ, (3.82) and (3.83) should be interpreted as series in $\sqrt{x}$ valid to order $(\sqrt{x})^{11}$. To this end, we define

$$z \equiv \sqrt{x}, \qquad f \equiv \frac{4m}{g} \qquad (3.84)$$

so that

$$2\mu \equiv fz. \tag{3.85}$$

and expand in z. The customary next step is to form Padé approximants to these series and their ratio, with the hope of then being able to estimate the $z \to \infty$ limit. The best estimate we can obtain for the mass ratio is

$$\frac{M_1^+}{M_1^-}[4,4](f) \xrightarrow[z\to\infty]{} 1.667 \tag{3.86}$$

independent of f! This is an encouraging result for the massless Schwinger model where the exact answer is 2, (3.27). But evidently the fourth order calculation cannot cope with a non-zero quark mass. Off-diagonal Padé approximants to the individual masses are no better:

$$\frac{1}{z}\left(z\frac{M_1^-}{g}\right)[5,4](f) \xrightarrow[z\to\infty]{} 0.66f \tag{3.87}$$

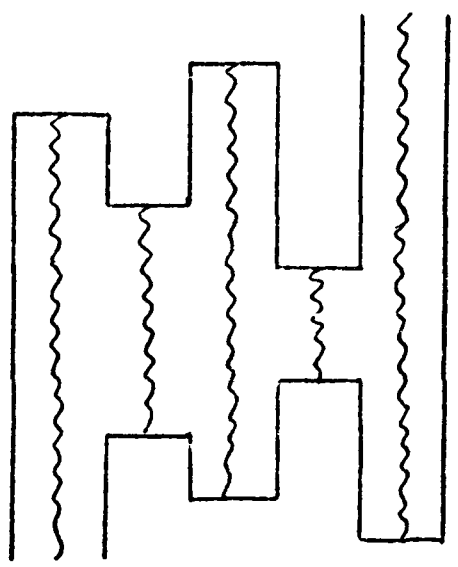
and

$$\frac{1}{z}\left(z\frac{M_1^+}{g}\right)[5,4](f) \xrightarrow[z\to\infty]{} 1.14f, \tag{3.88}$$

and stand little comparison with (3.24) and (3.26), or the non-relativistic results (2.6) and (2.8).

So we proceed with the high-order calculations. The formula for Rayleigh-Schrödinger perturbation theory to eighth order is derived in

appendix A. It simplifies considerably in the present case where only even orders are non-vanishing. A condensed version of the diagram rules is used to generate by computer all graphs which can exist up to eighth order on a finite periodic lattice. The size of the lattice is varied to check that all relevant graphs are included. It is found, as expected, that at any given order in V the lattice used need only be big enough to include all connected diagrams. This is because there exists a connected formalism for the lattice perturbation theory. Thus, at eighth order a periodic lattice of six sites suffices. One of the diagrams which demands this size is



The following results are obtained: Two types of energy denominator enter, which we label

$$\alpha = 1 + 2\mu, \qquad \beta = 3 + 2\mu \tag{3.89}$$

The vacuum energy density is

$$\frac{2\sqrt{x}}{g}\frac{E_0}{N} = -\frac{x^2}{\alpha} + \frac{3x^4}{\alpha^3} - \frac{(58+40\mu)}{\alpha^5\beta}x^6 + \frac{(1443+2000\mu+700\mu^2)}{\alpha^7\beta^2}x^8 + O(x^{10}). \tag{3.90}$$

The pseudoscalar particle mass is

$$\frac{2\sqrt{x}}{g} M_1^- = 1 + 2\mu + \frac{2x^2}{\alpha} - \frac{(10+4\mu)}{\alpha^3} x^4 + \frac{(236 + 272\mu + 96\mu^2 + 16\mu^3)}{\alpha^5\beta} x^6 - \frac{(6626 + 12112\mu + 7868\mu^2 + 2376\mu^3 + 432\mu^4 + 32\mu^5)}{\alpha^7\beta^2} x^8 + O(x^{10}) \tag{3.91}$$

and the scalar particle mass is

$$\frac{2\sqrt{x}}{g} M_1^+ = 1 + 2\mu + \frac{6x^2}{\alpha} - \frac{(26+4\mu)}{\alpha^3} x^4 + \frac{(572 + 448\mu + 16\mu^2 - 16\mu^3)}{\alpha^5\beta} x^6 - \frac{(15810 + 23264\mu + 9020\mu^2 - 56\mu^3 - 208\mu^4 + 32\mu^5)}{\alpha^7\beta^2} x^8 + O(x^{10}). \tag{3.92}$$

Results for these quantities have previously been presented by Carroll, Kogut, Sinclair and Susskind (1976). Their results for the vacuum energy density and scalar particle mass are wrong and are corrected in subsequent errata.

Before discussing the continuum estimates which can be obtained from the eighth order results, it is worth considering the non-relativistic limit of the lattice theory. We know that, from the point of view of the low-energy bound states, in the limit of large quark mass the Schwinger model reduces to the non-relativistic linear potential model. The exact continuum solution of this model is known. Since we also know that the corresponding lattice theory has the correct continuum limit, it is interesting to compare it with the non-relativistic limit of the lattice Schwinger model. This limit is discussed by Hamer (1977). It corresponds to letting

$$\frac{m}{g} \text{ or } \mu = \frac{2m}{ag^2} \to \infty \tag{3.93}$$

with

$$mg^2 = \text{const.} < \infty$$

and fixed lattice spacing a. The quantity

$$u = \frac{x^2}{\mu} \tag{3.94}$$

(c.f. (2.14)) remains finite, and the expansion, (3.91) and (3.92) for the pseudoscalar and scalar particle binding energies become in this limit

$$\frac{2\sqrt{x}}{g}\left(M_1^- - 2m\right)_{N.R.} = 1 + u - \frac{u^2}{2} + \frac{u^3}{4} - \frac{u^4}{16} + O(u^5) \tag{3.95}$$

and

$$\frac{2\sqrt{x}}{g}\left(M_1^+ - 2m\right)_{N.R.} = 1 + 3u - \frac{u^2}{2} - \frac{u^3}{4} - \frac{u^4}{16} + O(u^5) \tag{3.96}$$

These are just the expansions to fourth order of $\frac{2\sqrt{x}}{g} E_o^{odd}$ and $\frac{2\sqrt{x}}{g} E_1^{odd}$ of (2.44) and (2.45) respectively. That we should get agreement with the odd-lattice version of the linear potential model is not surprising, because it is implicit in our formulation of the lattice Schwinger model which only allows quark-antiquark pairs an odd number of links apart. This correspondence between the two lattice theories persists to all orders in perturbation theory. For the lattice Schwinger model, the only graphs which survive in the non-relativistic limit (3.93) are those in which each alternate intermediate state consists of a quark-antiquark pair an odd number of links

apart joined by a flux line (the linear potential), e.g. (3.77). These can be identified with the graphs occurring in the perturbation expansion for the linear potential; in the case of (3.77) the corresponding graph is (2.27).

Apart from providing a check of our eighth order results (3.91) and (3.92), this observation has several important consequences. First, it gives us a way of calculating the non-relativistic binding energies in the lattice Schwinger model to very high orders in x. Secondly, it tells us that the non-relativistic limit of the lattice Schwinger model has the correct continuum limit. Finally, and most important of all, it warns us of the dangers involved in naively taking our continuum estimates to be the $x \to \infty$ limit of Padé approximants. In the light of this correspondence between one coupling constant regime of the lattice Schwinger model and the lattice linear potential, it seems likely that the most reliable continuum estimates (perhaps for all values of m/g) will come from evaluating the Schwinger model Padé approximants at finite values of x.

With this in mind we proceed to obtain continuum limit estimates from (3.91) and (3.92). Recall that these are really series expansions in $z = \sqrt{x}$ valid to order $(\sqrt{x})$.[19] For individual particle masses we consider diagonal Padé approximants to the functions

$$f^{\pm}(x) = \frac{d}{d\sqrt{x}} \frac{\sqrt{x}}{g}\left(M_1^{\pm} - 2m\right) \qquad (3.97)$$

In the ultra-relativistic limit, $m/g \to 0$ this is just the particle mass sought by Carroll et al. (1976), whereas, in the non-relativistic limit, $m/g \to \infty$, it is the binding energy of the quark-antiquark pair and can be compared with our result for the linear potential model.

The Padé approximants to the pseudoscalar particle binding energy, $\bar{f}(x)$, are plotted as functions of $\sqrt{x}$ for a wide range of values of m/g in fig. 3.4. This series of graphs bears a remarkable resemblence to fig. 2.3 for the linear potential binding energy. It is evident that the function $\bar{f}(x)$ is represented well by the Padé approximants for $x \lesssim 1$, and this range of agreement increases with m/g. At the large-x end of this range all the Padé approximants seem to agree that $\bar{f}(x)$ 'turns a corner', but thereafter fail to show any hint of uniform convergence. As mentioned in the context of the linear potential, this sort of behaviour may be due to an essential singularity in the function at $x = \infty$. In this situation we can only rely on the Padé approximants at finite values of x. The best continuum estimate might be expected to come from the values of the Padé approximants at the largest value of x for which they have already converged. This is generally the peak value. We base all our estimates on the [8,8] Padé approximant, because it includes the eighth order results and is usually reasonably well-behaved. These peak-value estimates, together with the values of the [8,8] Padé approximant at $x = \infty$ are plotted for the pseudoscalar meson in fig. 3.5 and for the scalar meson in fig. 3.6. Also plotted are the exact continuum results known in the massless region from (3.24) and (3.26), and in the non-relativistic region from the solution of the linear potential model (the pseudoscalar particle has symmetric spatial wavefunction and hence binding energy given by (2.6); the scalar particle has antisymmetric spatial wavefunction and hence binding energy given by (2.8)).

It is clear from these graphs that the peak-values of the [8,8] Padé approximants represent the continuum results over the whole range

at $\frac{m}{g}$ better than the values of $x = \infty$. Specifically, the power-law behaviour is approximately correct in the regions where it is known. As was found for the non-relativistic linear potential model, the numerical values obtained for the lowest-lying state (pseudoscalar) are more accurate than for the first excited state (scalar). In the strong-coupling limit we find for the pseudoscalar particle

$$\frac{M_1^-}{g} \xrightarrow[\frac{m}{g}\to 0]{} 0.470 \quad \text{(peak value)} \tag{3.98}$$

which is correct to within 17%. This is to be compared with the eighth order estimate of Carroll et al. (1976). They took the $x \to \infty$ limit in the massless lattice Schwinger model and obtained 0.769, which is 36% too high. Our peak-value estimate for the corresponding binding energy in the non-realtivistic limit is in excellent agreement with the exact continuum result. The scalar particle mass, which we get by the same method, in strong coupling is

$$\frac{M_1^+}{g} \xrightarrow[\frac{m}{g}\to 0]{} 1.600 \quad \text{(peak value)} \tag{3.99}$$

and is 42% too high.

In the non-relativistic regime we expect to reproduce the behaviour of the linear potential model. Thus an alternative estimate of the continuum binding energy can be obtained by evaluating the Padé approximants at u = constant, where u is defined in (2.14). This relates x to $\frac{m}{g}$ via

$$\sqrt{x} = \left(2u\frac{m}{g}\right)^{1/3}. \tag{3.100}$$

Since the [8,8] Padé approximant in $\sqrt{x}$ should reduce to the [2,2] Padé approximant in u in the non-relativistic limit, the appropriate constant value of u can be obtained from the fourth order results of Chapter 2, following the arguments of Carroll et al. (1977) presented there. This method gives an improvement over our estimates from the peak value, as shown for the scalar particle in fig. 3.6. The peak in the Padé approximants follows closely the equation u = constant for $\frac{m}{g} \gtrsim 1$, and this is the reason why our estimates based on the peak value are qualitatively correct in the non-relativistic region.

Our estimates for the ratio of the scalar to pseudoscalar masses are obtained by considering diagonal Padé approximants to

$$R(x) \equiv \frac{M_1^+ - 2m}{M_1^- - 2m} \qquad (3.101)$$

These are plotted as functions of $\sqrt{x}$ in fig. 3.7. Here again we consider just the binding energies so as to be able to check the non-relativistic limit. The feature which distinguishes these graphs from fig. 3.4 for a single binding energy is the absence of a peak in the function. Some of the Padé approximants, notably the [9,9], tend to the value 3 at large x, even for strong coupling. This behaviour is observed in the linear potential model (see fig. 2.4) and all the Padé approximants in the non-relativistic limit. Its persistence at small values of m/g for a few of the Padé approximants is presumably spurious and can be disregarded. The remaining Padé approximants appear to converge uniformly, and so it seems reasonable to base our estimate of the continuum limit on the value of the [8,8]

Padé approximant at $x = \infty$. At least, this is approximately the value of the ratio at the largest x for which all the higher order Padé approximants agree. This estimate is plotted in fig. 3.8. Hence, we cannot improve on the strong-coupling result of Carroll et al. (1976) who obtain

$$\left.\frac{M_1^+}{M_1^-}[8,8]\right|_{\frac{m}{g}=0} = 1.949 \qquad (3.102)$$

Our estimate agrees with the continuum result:

$$\frac{M_1^+ - 2m}{M_1^- - 2m} = 2 + 2\sqrt{\pi}\,\frac{m}{g} + O\left(\frac{m}{g}\right)^2 \qquad (3.103)$$

to within 3% for $\frac{m}{g} \lesssim 0.005$. However, it overshoots the continuum result in the non-relativistic regime (2. 9). There our results are amenable to the methods of Carroll et al. (1977) (see previous paragraph). Evaluating the [8,8] Padé approximant at $u = 1.261$ (c.f. (2.66)) improves our agreement with the exact result to within 10% for $\frac{m}{g} \gtrsim 10$.

(d) Half-Asymptotic Particles in the Lattice Theory.

We conclude with a brief remark on the vacuum of the lattice Schwinger model for $|\theta| = \pi$, specifically $\theta = -\pi$. Recall that for this value of θ the continuum theory undergoes a phase transition between strong and weak coupling, with the weak-coupling vacuum being capable of supporting half-asymptotic particles. We are interested whether or not this occurs in the lattice theory.

The Hamiltonian for general θ is given in (3.55). We pick $\theta = -\pi$ and consider the strong-coupling limit, $m/g \ll 1$. Then the rescaled lattice Hamiltonian can be written:

$$W(\theta = -\pi) = W_o + xV \tag{3.104}$$

where

$$W_o = \sum_n L(n)\left[L(n) - \overline{1}\right] + \mu \sum_n (-1)^n \phi^+(n)\phi(n) \tag{3.105}$$

and

$$V = i \sum_n \left[\phi^+(n) U(n,n+1) \phi(n+1) + \phi(n) U^+(n,n+1) \phi^+(n+1)\right]. \tag{3.106}$$

At zeroth order, the vacuum is chosen to minimise $\langle 0|W_o|0\rangle$. This uniquely determines the fermion configuration, as a result of the mass term:

$$\langle 0|\phi^+(n)\phi(n)|0\rangle = \begin{cases} 1 & n \text{ odd} \\ 0 & n \text{ even} \end{cases} \tag{3.107}$$

but leaves the gauge-field configuration indeterminate,

$$\langle 0|L(n)|0\rangle = 0 \text{ or } 1. \tag{3.108}$$

The degeneracy is lifted at second order in V. The shift in the vacuum energy is

$$\delta w = x^2 \langle 0| V \frac{Q}{w^{(0)} - W_0} V |0\rangle$$

$$= -x^2 \sum_{n\ \mathrm{odd}} \langle 0| \frac{1}{[L(n)-1][L(n)-2]+2\mu} |0\rangle$$

$$- x^2 \sum_{n\ \mathrm{even}} \langle 0| \frac{1}{[L(n)+1]L(n)+2\mu} |0\rangle \qquad (3.109)$$

where we have used the known fermion configuration (3.107) and the commutation relations (3.51a,b). δw is minimised by

$$\langle 0|L(n)|0\rangle = \begin{cases} 1 & n \text{ odd} \\ 0 & n \text{ even} \end{cases} \qquad (3.110)$$

This vacuum state is easier to understand if we use the language of electric fields (3.47) and work relative to the Dirac sea, defined by (3.107). Then the strong-coupling vacuum for $\theta = -\pi$ is shown in fig. 3.9. The value of the electric field is shown above the links and the open circles denote vacant sites. Recall that from (3.39) and (3.107) a quark (antiquark) can be created on any empty even (odd) site. In such a vacuum a single quark (or antiquark) has infinite energy on a lattice of infinite extent. This is because Gauss' law requires that the quark be accompanied by an electric field of strength g emanating from it either to the right or left. But such a field configuration has infinite energy, because on every other link on one half of the lattice, the field is of magnitude $3g/2$.

For $\theta = -\pi$, the sort of vacuum state which can support an isolated quark of finite energy is shown in fig. 3.10. An example of such a

single quark state is shown in fig. 3.11. The electric flux changes through an amount g as we go from one side of the occupied site to the other, satisfying Gauss' law, but the magnitude of the electric field on any link remains $\frac{1}{2}g$. Thus the gauge field configuration contributes zero energy and the state has total unperturbed energy μ. The vacuum of fig. 3.10 is certainly degenerate with the strong-coupling vacuum at zeroth order, but is pushed up in energy by the second order term.

We argue that the vacuum of fig. 3.10 is favoured for weak coupling, $\frac{m}{g} >> 1$. Consider the perturbation expansions for the energies of the two types of vacuum. We have already seen that in the non-relativistic limit, the only graphs which contribute have every alternate intermediate state consisting of a widely separated quark-antiquark pair connected by a line of electric flux. At Nth order in V for the strong-coupling vacuum, the dominant intermediate states are those shown in fig. 3.12. These both correspond to energy denominators $\sim \frac{N}{2} + 2\mu$. So for $\frac{m}{g} >> 1$ the dominant Nth order contribution to the energy is proportional to

$$-\left(\frac{1}{\frac{N}{2}+2\mu}+\frac{1}{\frac{N}{2}+2\mu}\right) \underset{N\gg 1}{\sim} -\frac{4}{N}. \qquad (3.111)$$

However, for the vacuum of fig. 3.10, although the same type of graph dominates, the contributions of the intermediate states are differnt. The two important intermediate states are shown in fig. 3.13. In fig. 3.13(a) the electric field changes sign between the quark-antiquark pair, but contributes nothing to the energy. So this intermediate state corresponds to an energy denominator 2μ. When the quark is on

the right of the antiquark, as is the case in fig. 3.13(b), the electric field between them has magnitude 3g/2 and so contributes an energy 2 for each link separating them. So the corresponding energy denominator is $\sim N + 2\mu$. Hence, for $\frac{m}{g} >> 1$ the dominant Nth order contribution to the energy of the vacuum in fig. 3.10 is proportional to

$$-\left(\frac{1}{2\mu} + \frac{1}{N+2\mu}\right) \underset{N>>1}{\sim} -\frac{1}{2\mu} \qquad (3.112)$$

This effect eventually brings the energy of the vacuum supporting half-asymptotic particles, below that of the strong-coupling vacuum, when $\frac{m}{g} >> 1$. The resulting half-asymptotic particles are just the quark and antiquark escaping to the left and right respectively.

Summary

The massive Schwinger model provides a well-known exercise for lattice techniques. This is because it is a confining field theory whose low-energy particle spectrum is known in both the strong and weak coupling limits. Previous good results for strong coupling can be extended throughout the coupling constant range if a simple precaution is taken. For weak coupling, equivalence with the lattice theory of the non-relativistic linear potential indicates that the Padé approximants may suffer from convergence problems in the zero-lattice-spacing limit. Indeed they do, and so continuum estimates have to be based on their values at non-zero lattice spacing. The resulting estimates are in good agreement with known weak coupling results. Where they differ from previous estimates for strong coupling, they are generally better.

CHAPTER 4

MATRIX METHODS

The original proposal for obtaining continuum predictions from lattice theories was to use the zero-lattice-spacing limit of the sequence of Padé approximants to the strong-coupling expansion. In practice, we have found that non-zero-lattice-spacing estimates are usually necessary to repair the non-uniform convergence of this sequence. When eighth order calculations are available, the resulting predictions are good. Despite this, the need for extra precautions is a little unsatisfactory.

Aside from this misgiving, it is difficult to see how the theory can develop, unless some new techniques are found. As it stands, more accurate predictions can only come from higher orders in perturbation theory. These seem prohibitively difficult in most cases. The problem is particularly acute in 3+1 dimensions, where we cannot manage perturbative calculations much beyond fourth order. Thus, while there is no strong desire on our part to significantly alter the approach, a few new ideas wouldn't come amiss. Specifically, we seek a modification which would enable us to include, in comparatively low-order calculations, effects which, at present, are only accessible to high orders of perturbation theory.

(a) Matrix Padé Approximants.

One area where there may be room for improvement is in the choice of initial unperturbed state. As a rule, the lattice provides for an unambiguous identification of the lowest-energy state. But there are always states of higher energy, with the same quantum numbers, which contribute to the same continuum state. These are just those states which are connected to our original choice by the perturbation. Since we are usually satisfied with working to a specific order in perturbation theory, the number of relevant states is quite small; perhaps two or three. It may be reasonable to assume that none of these states, by itself, is a good starting point for the lattice calculation. Then a better approximation to the continuum state is to be expected from diagonalising the perturbation expansion for the Hamiltonian in this subspace.

If all the relevant states are degenerate at zeroth order this problem is handled using traditional degenerate perturbation theory. But, more often than not, all the relevant states are non-degenerate. Then we require an extension to the formalism of degenerate perturbation theory, which describes the mixing of non-degenerate states. This is quasi-degenerate perturbation theory and the necessary formulae are derived in appendix B. The result in both cases is a matrix for the Hamiltonian in the chosen subspace. Of course, for non-degenerate unperturbed states, the eigenvalues of this matrix are just the results we would have obtained from using non-degenerate perturbation theory for each state in turn. Padéing these to obtain continuum estimates is just what we did before. We appear to have gained nothing. However, a new continuation method is now available to us. Instead of first

diagonalising the matrix and then taking the continuum limit, we form a matrix Padé approximant to the series and obtain the continuum limit of the matrix for H. Then we diagonalise it. The hope behind this is that the matrix Padé approximant takes into account better the mixing of lattice states at any given order. The result ought to be better continuum estimates than can be obtained using conventional perturbation theory to the same order. In the long run, it is this sort of generalisation which may hold the key to a more realistic calculation of the pion mass in 3+1 dimensional QCD.

The application of quasi-degenerate perturbation theory produces a series expansion for the matrix of the Hamiltonian in the chosen subspace of states. The coefficients of this series are square matrices and continuum physics lies in the limit of infinite expansion parameter. So we are led to consider matrix Padé approximants. First, we must check that these entities are well-defined (Baker 1975, Zinn-Justin 1971). Let $\underline{A}(z)$ be an analytic matrix function of z, having a Taylor series expansion:

$$\underline{A}(z) = \sum_{k=0}^{\infty} \underline{A}_k z^k \qquad (4.1)$$

where $\{\underline{A}_k\}$ is a sequence of square matrices. The [m,n] Padé approximant to this series is defined as

$$\underline{A}[m,n] \equiv (\underline{N}_0 + \underline{N}_1 z + \cdots + \underline{N}_m z^m)(\underline{I} + \underline{D}_1 z + \cdots + \underline{D}_n z^n)^{-1} \qquad (4.2)$$

where the coefficients $\{\underline{N}_i, \underline{D}_j\}$ are determined from

$$\underline{A}[m,n] \equiv \sum_{k=0}^{m+n} \underline{A}_k z^k + O(z^{m+n+1}). \qquad (4.3)$$

There would seem to be an ambiguity in the definition (4.2), depending on whether the denominator is put on the R.H.S. or L.H.S. of the numerator. But it is easily proved, using (4.3), that this definition is unique.

The symmetry properties of matrix Padé approximants are essentially the same as for the scalar case (Baker 1975, Zinn-Justin 1971). The main justification for their use, as always, comes from successful applications in cases when exact continuum results are known. It is possible to derive a simple formula for the continuum limit of any Padé approximant. We illustrate it for the case we will need the most: the [4,4] Padé approximant. Taking the definition (4.2), the continuum limit is

$$\lim_{z\to\infty} \underline{A}[4,4](z) = \underline{N}_4 \underline{D}_4^{-1} \qquad (4.4)$$

We obtain $\underline{N}_4$ and $\underline{D}_4$ by multiplying through by the denominator in (4.2) and (4.3), and equating the coefficients of powers of z. The result is a system of linear simultaneous equations for $\underline{N}_0, \ldots, \underline{N}_4$ and $\underline{D}_1, \ldots, \underline{D}_4$. These can be written as a single big matrix equation and the result is a formula for (4.4) which is readily generalisable:

$$\lim_{z\to\infty} \underline{A}[4,4](z) = \underline{A}_0 - (\underline{A}_4\underline{A}_3\underline{A}_2\underline{A}_1)\begin{pmatrix} \underline{A}_5 & \underline{A}_4 & \underline{A}_3 & \underline{A}_2 \\ \underline{A}_6 & \underline{A}_5 & \underline{A}_4 & \underline{A}_3 \\ \underline{A}_7 & \underline{A}_6 & \underline{A}_5 & \underline{A}_4 \\ \underline{A}_8 & \underline{A}_7 & \underline{A}_6 & \underline{A}_5 \end{pmatrix}^{-1}\begin{pmatrix} \underline{A}_1 \\ \underline{A}_2 \\ \underline{A}_3 \\ \underline{A}_4 \end{pmatrix} \tag{4.5}$$

provided

$$\det\begin{pmatrix} \underline{A}_5 & \underline{A}_4 & \underline{A}_3 & \underline{A}_2 \\ \underline{A}_6 & \underline{A}_5 & \underline{A}_4 & \underline{A}_3 \\ \underline{A}_7 & \underline{A}_6 & \underline{A}_5 & \underline{A}_4 \\ \underline{A}_8 & \underline{A}_7 & \underline{A}_6 & \underline{A}_5 \end{pmatrix} \neq 0. \tag{4.6}$$

Similarly, a useful off-diagonal Padé approximant is the [5,4] with continuum limit

$$\lim_{z\to\infty} \frac{1}{z}\underline{A}[5,4](z) = \underline{A}_1 - (\underline{A}_5\underline{A}_4\underline{A}_3\underline{A}_2)\begin{pmatrix} \underline{A}_6 & \underline{A}_5 & \underline{A}_4 & \underline{A}_3 \\ \underline{A}_7 & \underline{A}_6 & \underline{A}_5 & \underline{A}_4 \\ \underline{A}_8 & \underline{A}_7 & \underline{A}_6 & \underline{A}_5 \\ \underline{A}_9 & \underline{A}_8 & \underline{A}_7 & \underline{A}_6 \end{pmatrix}^{-1}\begin{pmatrix} \underline{A}_2 \\ \underline{A}_3 \\ \underline{A}_4 \\ \underline{A}_5 \end{pmatrix} \tag{4.7}$$

provided, again, that the big matrix is non-singular. For completeness we state the other formulae we will need:

$$\lim_{z\to\infty} \underline{A}[1,1](z) = \underline{A}_0 - \underline{A}_1\underline{A}_2^{-1}\underline{A}_1 \tag{4.8}$$

$$\lim_{z\to\infty} \frac{1}{z}\underline{A}[2,1](z) = \underline{A}_1 - \underline{A}_2\underline{A}_3^{-1}\underline{A}_2 \tag{4.9}$$

and

$$\lim_{z\to\infty} \underline{A}[2,2](z) = \underline{A}_0 - (\underline{A}_2\,\underline{A}_1)\begin{pmatrix} \underline{A}_3 & \underline{A}_2 \\ \underline{A}_4 & \underline{A}_3 \end{pmatrix}^{-1}\begin{pmatrix} \underline{A}_1 \\ \underline{A}_2 \end{pmatrix}. \qquad (4.10)$$

All have simple derivations.

(b) Matrix Methods for the Linear Potential Model.

Although the linear potential model, introduced in Chapter 2, is a crude description of confined quarks, it gives us considerable insight into the lattice method. Its study revealed a potentially disasterous short-coming of the Padé approximant continuation scheme. As a consequence, it has established itself as a proving-ground for any new technique intended for application in lattice gauge theories. Also, because the linear potential model describes the low-lying bound states of the Schwinger model in the non-relativistic limit, it provides a guide to the measure of success that can be exprected there.

Recall that the lattice theory is defined by the rescaled Hamiltonian (2.14):

$$W = W_o + uV \qquad (4.12)$$

$$W_o = |n| \qquad (4.13)$$

$$V = 2 - d^+ - d^- \qquad (4.14)$$

As an illustration of the matrix method we calculate the energies of the lowest-lying bound states. Within the odd-lattice formulation the lowest-energy eigenstates of the unperturbed Hamiltonian (4.13) are

(c.f. (2.16), (2.17)):

$$|0\rangle \equiv \frac{1}{\sqrt{2}}\left(|n=1\rangle + |n=-1\rangle\right) \tag{4.15a}$$

$$|1\rangle \equiv \frac{1}{\sqrt{2}}\left(|n=1\rangle - |n=-1\rangle\right) \tag{4.15b}$$

$$|2\rangle \equiv \frac{1}{\sqrt{2}}\left(|n=3\rangle + |n=-3\rangle\right) \tag{4.15c}$$

$$|3\rangle \equiv \frac{1}{\sqrt{2}}\left(|n=3\rangle - |n=-3\rangle\right) \tag{4.15d}$$

etc., alternating in parity. V, (4.14), only connects states of the same parity. So we use quasi-degenerate perturbation theory to obtain matrices for W in the subspaces spanned by the two lowest parity-even states $\{|0\rangle, |2\rangle\}$ and by the two lowest parity-odd states $\{|1\rangle, |3\rangle\}$. The two calculations are similar, so we do the calculation explicitly for the excited parity-odd states and include the results for the parity-even states in parentheses whenever they differ.

The relevant formula for the perturbation expansion is given in (B.32). At zeroth order, the matrix is

$$\omega_1^{(0)} P_1 + \omega_3^{(0)} P_3 \tag{4.16}$$

where

$$\omega_1^{(0)} = 1 \ , \quad \omega_3^{(0)} = 3 \tag{4.17}$$

are the unperturbed energy eigenvalues. Thus,

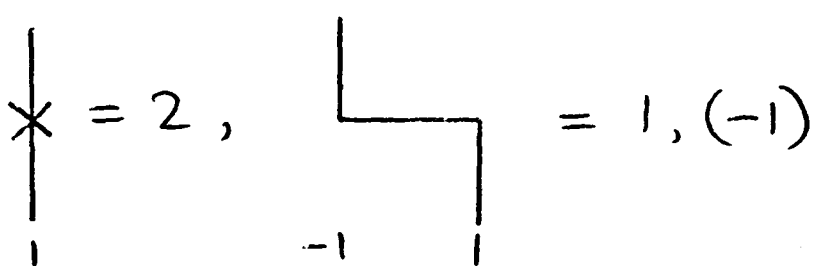
$$\text{zeroth order} = \begin{pmatrix} 1 & 0 \\ 0 & 3 \end{pmatrix} \tag{4.18}$$

At first order, the matrix is

$$PVP \tag{4.19}$$

and its elements are given as follows:

$\langle 1|V|1\rangle$:



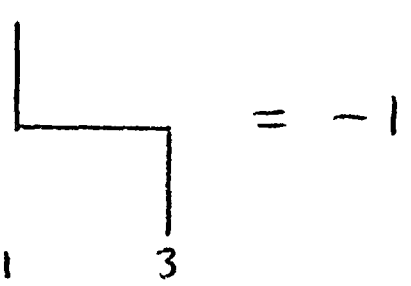
(4.20)

where the $*$ denotes insertion of a factor 2 from (4.14) and we restrict the 'incoming' particle to one site (n = 1), but allow it to 'leave' by either site, just as before. The second graph is the only one to distinguish different parity states. Hence, adding the two contributions in (4.20) gives

$$\langle 1|V|1\rangle = 3, (1). \tag{4.21}$$

The states on sites n = ±1 and n = ±3 are connected at first order by the $d^{\pm}$ operators in V:

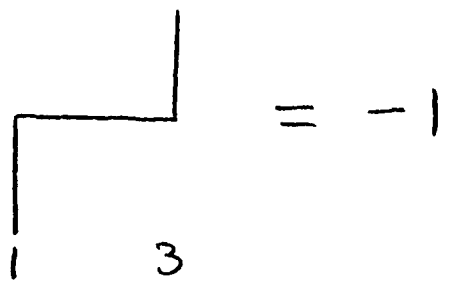
$\langle 1|V|3\rangle$:



(4.22)

and

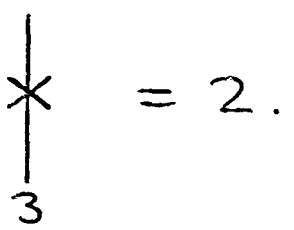
$\langle 3|V|1\rangle$:



(4.23)

Finally, for the states on sites n = ±3 the only graph contributing to the diagonal matrix element at first order is

$\langle 3|V|3\rangle$:



(4.24)

Thus,

$$\text{first order} = u\begin{pmatrix} 3,(1) & -1 \\ -1 & 2 \end{pmatrix} \tag{4.25}$$

The second order matrix element is

$$PVg_1VP_1 + PVg_3VP_3. \tag{4.26}$$

Here the g's forbid the states $|n = \pm 1\rangle$ and $|n = \pm 3\rangle$ from being intermediate states. As a result of V only connecting sites at most two links apart, it follows that

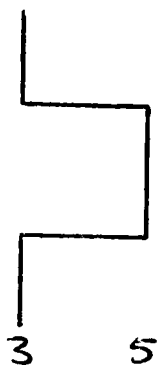
$$g_1VP_1 = P_1Vg_3 = 0. \tag{4.27}$$

Hence the matrix immediately simplifies to

$$P_3Vg_3VP_3 \tag{4.28}$$

and so the only non-zero matrix element is

$\langle 3|Vg_3V|3\rangle$:



$$= \frac{1}{3-5} = -\frac{1}{2} \tag{4.29}$$

Thus,

$$\text{second order} = u^2 \begin{pmatrix} 0 & 0 \\ 0 & -\frac{1}{2} \end{pmatrix}. \tag{4.30}$$

Finally, the third order matrix is

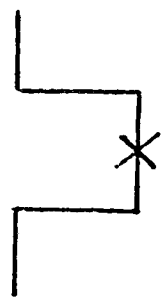
$$PVg_1Vg_1VP_1 + PVg_3Vg_3VP_3 - PVg_1^2VP(P_1VP_1) - PVg_3^2VP(P_3VP_3)$$
$$- PVg_1g_3VP(P_1VP_3 + P_3VP_1). \tag{4.31}$$

Using (4.27), this can be reduced to

$$P_3Vg_3Vg_3VP_3 - P_3Vg_3^2VP(P_3VP_3) - P_3Vg_1g_3VP(P_3VP_1). \tag{4.32}$$

The diagonal elements are

$\langle 3|Vg_3Vg_3V|3\rangle$:



$$= 2 \cdot \frac{1}{(3-5)^2} = \frac{1}{2} \tag{4.33}$$

together with the "subtraction term", obtained from (4.29) and (4.24),

$$\langle 3|Vg_3^2V|3\rangle\langle 3|V|3\rangle = \frac{1}{4} \cdot 2 = \frac{1}{2}. \tag{4.34}$$

So these two terms cancel. There remains just the off-diagonal element, which from (4.29) and (4.23) is

$$\langle 3|V g_1 g_3 V|3\rangle\langle 3|V|1\rangle = \frac{1}{(1-5)}\cdot\frac{1}{(3-5)}\cdot(-1) = -\frac{1}{8} \tag{4.35}$$

and so

$$\text{third order} = u^3\begin{pmatrix} 0 & 0 \\ \frac{1}{8} & 0 \end{pmatrix}. \tag{4.36}$$

This expansion to third order is sufficient to construct the first non-trivial matrix Padé approximant. We have generated the series:

$$\underline{W}^{-(+)} = \begin{pmatrix} 1 & 0 \\ 0 & 3 \end{pmatrix} + u\begin{pmatrix} 3(1) & -1 \\ -1 & 2 \end{pmatrix} + u^2\begin{pmatrix} 0 & 0 \\ 0 & -\frac{1}{2} \end{pmatrix} + u^3\begin{pmatrix} 0 & 0 \\ \frac{1}{8} & 0 \end{pmatrix} + O(u^4) \tag{4.37}$$

The eigenvalues of $\underline{W}^{\pm}$ are of the form (c.f. (2.13),(2.14)):

$$\left(\frac{16mu}{g^4}\right)^{1/3} E_i \tag{4.38}$$

and so we must cube the series before we can express it as a rational function. The results are:

$$(\underline{W}^{+})^{3} = \begin{pmatrix} 1 & 0 \\ 0 & 27 \end{pmatrix} + u\begin{pmatrix} 3 & -13 \\ -13 & 54 \end{pmatrix} + u^{2}\begin{pmatrix} 8 & -19 \\ -19 & \frac{59}{2} \end{pmatrix}$$

$$+ u^{3}\begin{pmatrix} 5 & -\frac{9}{2} \\ -\frac{23}{8} & -5 \end{pmatrix} + O(u^{4}) \qquad (4.39a)$$

and

$$(\underline{W}^{-})^{3} = \begin{pmatrix} 1 & 0 \\ 0 & 27 \end{pmatrix} + u\begin{pmatrix} 9 & -13 \\ -13 & 54 \end{pmatrix} + u^{2}\begin{pmatrix} 32 & -29 \\ -29 & \frac{59}{2} \end{pmatrix}$$

$$+ u^{3}\begin{pmatrix} 35 & -\frac{33}{2} \\ -\frac{119}{8} & -3 \end{pmatrix} + O(u^{4}). \qquad (4.39b)$$

Now, for large u, the eigenvalues of the matrix function on the LHS grow with u, so it is sensible to approximate the power series on the RHS by an off-diagonal Padé; the [2,1] approximant. This has continuum limit given by (4.9). So, for the even-parity states,

$$\lim_{u\to\infty} \frac{1}{u}(\underline{W}^{+})^{3}[2,1] = \frac{1}{607}\begin{pmatrix} 7645 & -6973 \\ -3723 & 7379 \end{pmatrix}. \qquad (4.40)$$

with smallest eigenvalue

$$\lambda = 3.979. \qquad (4.41)$$

The corresponding ground-state energy is

$$E_{0} = 0{\cdot}629\ \frac{g^{4/3}}{m^{1/3}} \quad (\text{exact} : 0{\cdot}642) \qquad (4.42)$$

correct to within 2%. Similarly, for the odd-parity states

$$\lim_{u\to\infty} \frac{1}{u}\left(\underline{W}^{-}\right)^{3}[2,1] = \frac{1}{5607}\begin{pmatrix} 6415 & -58053 \\ -60731 & 320289 \end{pmatrix}, \tag{4.43}$$

whose eigenvalue

$$\lambda = 59.059 \tag{4.44}$$

corresponds to an energy

$$E_1 = 1.546\ \frac{g^{4/3}}{m^{1/3}} \quad (\text{exact}: 1.473). \tag{4.45}$$

which is correct to within 5%. It appears as if our simple calculation gives astonishingly accurate results for the lowest eigenvalue. In contrast, the higher-energy state in each case is treated very badly. This is taken to be a fault of the low-order perturbation theory and not the matrix Padé continuation method. The higher excited states are unlikely to be represented well at low orders, because their wavefunctions are not allowed to spread across a sufficient number of lattice sites to give a reasonable approximation to the continuum wavefunction (2.4).

In order to test the matrix method for energy ratios, we extend the previous calculation to the next even order, i.e. fourth, so as to be able to form [1,1] and [2,2] diagonal Padé approximants. We focus on the ratio of the energy of the first excited state to the energy of the ground state. Then we need only do the fourth-order matrix calculation for the pair of odd-parity states. We get the energy ratio by dividing

the resulting matrix by the ground state energy to fourth order previously obtained using ordinary perturbation theory, (2.44). After all, this is just the eigenvalue of $\underline{W}^+$ which corresponds to the ground state.

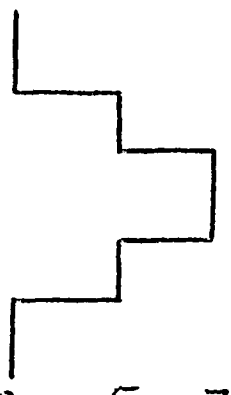
The fourth-order calculation for $\underline{W}^-$ proceeds as follows: Using (4.27) the general formula (B.32) for the fourth-order matrix element simplifies to

$$P_3Vg_3Vg_3Vg_3VP_3 - (P_3Vg_3^2Vg_3VP + P_3Vg_3Vg_3^2VP)(P_3VP_3)$$
$$+ \frac{1}{\omega_3^{(0)}-\omega_1^{(0)}}\,(P_3Vg_3Vg_3VP - P_3Vg_1Vg_1VP)(P_3VP_1)$$
$$- P_3Vg_3^2VP(P_3Vg_3VP_3) + P_3Vg_3^3\,VP(P_3VP_3VP_3)$$
$$+ P_3Vg_1^2g_3VP(P_3VP_1VP_1) + P_3Vg_1g_3^2VP(P_3VP_1VP_3 + P_3VP_3VP_1). \qquad (4.46)$$

So the only non-zero matrix elements are <3|....|3> and <3|...|1> .

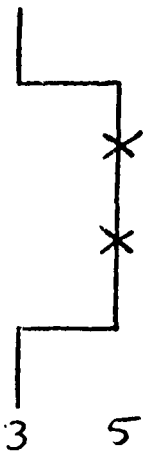
Considering the diagonal matrix element first, we have

$\langle 3|Vg_3Vg_3Vg_3V|3\rangle$



$$= \frac{1}{(3-5)^2(3-7)} = -\frac{1}{16} \qquad (4.47)$$

and



$$= \frac{2^2}{(3-5)^2} = -\frac{1}{2}. \qquad (4.48)$$

So, adding the contributions from the two graphs, gives

$$\langle 3|Vg_3Vg_3Vg_3V|3\rangle = -\frac{9}{16} \tag{4.49}$$

The subtraction terms are all obtained from the preceding lower-order calculations

$$\left(\langle 3|Vg_3^2Vg_3V|3\rangle + \langle 3|Vg_3Vg_3^2V|3\rangle\right)\langle 3|V|3\rangle$$

$$= 2\cdot\frac{2}{(3-5)^3}\cdot 2 = -1, \tag{4.50}$$

$$\langle 3|Vg_3^2V|3\rangle\langle 3|Vg_3V|3\rangle = \frac{1}{(3-5)^3} = -\frac{1}{8}, \tag{4.51}$$

$$\langle 3|Vg_3^3V|3\rangle\left(\langle 3|V|3\rangle\right)^2 = \frac{1}{(3-5)^3}\cdot 2^2 = -\frac{1}{2} \tag{4.52}$$

and

$$\langle 3|Vg_1g_3^2V|3\rangle\langle 3|V|1\rangle\langle 1|V|3\rangle = \frac{(-1)^2}{(3-5)^2(1-5)} = -\frac{1}{16} \tag{4.53}$$

Adding all the contributions (4.49)-(4.53) with the appropriate signs, it turns out that the diagonal matrix element vanishes. There remains just the off-diagonal matrix element, comprised of three terms:

$$\frac{1}{\omega_3^{(0)}-\omega_1^{(0)}}\left(\langle 3|Vg_3Vg_3V|3\rangle - \langle 3|Vg_1Vg_1V|3\rangle\right)\langle 3|V|1\rangle$$

$$= \frac{1}{3-1}\left[\frac{1}{2} - 2\cdot\frac{1}{(1-5)^2}\right]\cdot(-1) = -\frac{3}{16} \tag{4.54}$$

$$\langle 3|V g_1^2 g_3 V|3\rangle\langle 3|V|1\rangle\langle 1|V|1\rangle$$

$$= \frac{1}{(1-5)^2(3-5)} \cdot (-1) \cdot 3 = \frac{3}{32}, \tag{4.55}$$

and

$$\langle 3|V g_1 g_3^2 V|3\rangle\langle 3|V|3\rangle\langle 3|V|1\rangle$$

$$= \frac{1}{(1-5)(3-5)^2} \cdot 2 \cdot (-1) = \frac{1}{8}. \tag{4.56}$$

Adding (4.54)-(4.56) with appropriate signs gives 1/32 and so

$$\text{fourth order} = u^4 \begin{pmatrix} 0 & 0 \\ \frac{1}{32} & 0 \end{pmatrix}. \tag{4.57}$$

Next, we obtain the matrix for the ratio of $\underline{W}^-$ with the ground-state energy by dividing $\underline{W}^-$ by (2.44). The result is

$$\underline{W}^-/\omega_0 = \begin{pmatrix} 1 & 0 \\ 0 & 3 \end{pmatrix} + u\begin{pmatrix} 2 & -1 \\ -1 & -1 \end{pmatrix} + u^2\begin{pmatrix} -3/2 & 1 \\ 1 & 2 \end{pmatrix}$$

$$+ u^3\begin{pmatrix} \frac{9}{4} & -\frac{3}{2} \\ -\frac{11}{8} & -\frac{13}{4} \end{pmatrix} + u^4\begin{pmatrix} -\frac{55}{16} & \frac{9}{4} \\ \frac{69}{32} & \frac{75}{16} \end{pmatrix} + O(u^5) \tag{4.58}$$

The eigenvalues of the L.H.S. should become independent of u as $u \to \infty$, so we form diagonal Padé approximants to this series. Both the [1,1] and [2,2] approximants are accessible to us, and their continuum limits are given by (4.8) and (4.10) respectively. The smallest eigenvalues

of the resulting matrices give us the required estimate of the continuum energy ratio. They are

$$\frac{E_1}{E_0}[1,1] = 1.894 \quad (2\text{-state}) \tag{4.59a}$$

and

$$\frac{E_1}{E_0}[2,2] = 2.186 \quad (2\text{-state}). \tag{4.59b}$$

The estimate from the [2,2] matrix Padé is within 5% of the exact result 2.295, given in (2.9), and improves considerably on the single-state calculation (2.64).

The obvious next step is to include more states in the matrix for W. If we add

$$|5\rangle \equiv \frac{1}{\sqrt{2}}\left(|n=5\rangle - |n=-5\rangle\right) \tag{4.60}$$

to the set of unperturbed odd-parity states and divide the resulting matrix by the ground-state energy, we obtain

$$\underline{W}^-/\omega_0 = \begin{pmatrix} 1 & 0 & 0 \\ 0 & 3 & 0 \\ 0 & 0 & 5 \end{pmatrix} + u\begin{pmatrix} 2 & -1 & 0 \\ -1 & -1 & -1 \\ 0 & -1 & -3 \end{pmatrix}$$
$$+u^2\begin{pmatrix} -\frac{3}{2} & 1 & 0 \\ 1 & 5/2 & 1 \\ 0 & 1 & 5 \end{pmatrix} + u^3\begin{pmatrix} 9/4 & -3/2 & 0 \\ -3/2 & -15/4 & -3/2 \\ 0 & -11/8 & -31/4 \end{pmatrix}$$
$$+u^4\begin{pmatrix} -55/16 & 9/4 & 0 \\ 9/4 & 87/16 & 9/4 \\ 0 & 17/8 & 181/16 \end{pmatrix} + O(u^5). \tag{4.61}$$

Again the continuum limits of the [1,1] and [2,2] matrix Padés are obtained using (4.8) and (4.10). The smallest eigenvalues are

$$\frac{E_1}{E_0}[1,1] = 1.652 \quad \text{(3-state)} \tag{4.62a}$$

and

$$\frac{E_1}{E_0}[2,2] = 2.103 \quad \text{(3-state)} \tag{4.62b}$$

That these results should be less accurate than the two-state calculation seems a little surprising at first. It is presumably further indication that, to any fixed order in perturbation theory, predictions for bound-state energies get worse as we go to higher excited states. The fourth order calculation we have done treats the fifth excited state more crudely than either the first or third, and this influences all the eigenvalues of $\underline{\bar{W}}$ for the worse. However, if we could go to higher orders in perturbation theory, we might find that the smallest eigenvalue converges to the exact result quicker for the three-state calculation than for the two-state calculation. There is a slight suggestion of this in fig. 4.1, where we collect all our results.

(c) Matrix Methods for the Schwinger Model.

A number of eigenstates of the unperturbed lattice Hamiltonian W_o, (3.57) mix strongly in the perturbative calculation of the scalar and pseudoscalar meson masses. In addition to the basic one-link, quark-antiquark states, (3.66) and (3.67),

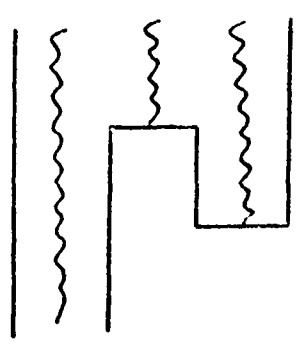
$$|1\pm\rangle \equiv \frac{1}{\sqrt{N}} \sum_n \left[\phi^+(n)\, U(n,n+1)\, \phi(n+1) \pm \phi(n)\, U^+(n,n+1)\, \phi^+(n+1)\right]|0\rangle, \qquad (4.63)$$

used in the original perturbative calculation, all those states, obtained by applying products of V's, (3.58), to these two, contribute to some extent. Since we work to a fixed order in perturbation theory (usually fourth), some of these will be more important than others. The most important ones are obtained when V acts once or twice.

The states generated in this way are of two types. The first type we shall consider are radial excitations of the quark-antiquark pair and are direct analogues of the excited states used in the matrix calculation for the linear potential. It is the odd-lattice formulation of the linear potential that is of relevance here, and so the first radial excitation of $|1\pm\rangle$ has the quark-antiquark pair three links apart:

$$|3\pm\rangle \equiv \frac{1}{\sqrt{N}} \sum_n \left[\phi^+(n) U(n,n+1) U(n+1,n+2) U(n+2,n+3) \phi(n+3) \pm \phi(n) U^+(n,n+1) U^+(n+1,n+2) U^+(n+2,n+3) \phi^+(n+3)\right]|0\rangle \qquad (4.64)$$

and is obtained from $|1\pm\rangle$ at second order, as is clear from the diagram



The five-link states

$$|5\pm\rangle \equiv \frac{1}{\sqrt{N}} \sum_n \Big[\phi^+(n) \prod_{\ell=n}^{n+4} U(\ell,\ell+1)\, \phi(n+5) \pm \phi(n) \prod_{\ell=n}^{n+4} U^+(\ell,\ell+1)\, \phi^+(n+5) \Big] |0\rangle \qquad (4.65)$$

are likely to be of less importance in a fourth order matrix calculation. They are included for completeness, but we expect the matrix calculation for one-, three- and five-link states to be subject to the same limitations as for the linear potential.

The other type of state which might be included in a matrix calculation is the two-particle state

$$|2,1\pm\rangle \equiv \frac{i}{\sqrt{N}} \sum_n \Big[\phi^+(n) U(n,n+1) \phi(n+1) \phi^+(n+2) U(n+2,n+3) \phi(n+3) \pm \phi(n) U^+(n,n+1) \phi^+(n+1) \phi(n+2) U^+(n+2,n+3) \phi^+(n+3) \Big] |0\rangle \qquad (4.66)$$

which mixes with $|1\pm\rangle$ at first order. In principle, the two quark-antiquark pairs may be separated by any number of links

$$|2,2m\pm\rangle = \frac{i}{\sqrt{N}} \sum_n \Big[\phi^+(n) U \phi(n+1) \phi(n+2m+1) U^+ \phi^+(n+2m+2) \pm \phi(n) U^+ \phi^+(n+1) \phi^+(n+2m+1) U \phi(n+2m+2) \Big] |0\rangle \qquad (4.67a)$$

$$|2,(2m+1)\pm\rangle \equiv \frac{i}{\sqrt{N}} \sum_n \Big[\phi^+(n) U \phi(n+1) \phi^+(n+2m+2) U \phi(n+2m+3) \pm \phi(n) U^+ \phi^+(n+1) \phi(n+2m+2) U^+ \phi^+(n+2m+3) \Big] |0\rangle \qquad (4.67b)$$

but we will argue that the dominant contribution comes from the state (4.66) with quark-antiquark pairs just one link apart. All two-particle states are connected to the one-particle states (4.63) at first order in V, and appear to be on equal footing. However, the existence of a connected formalism for perturbation theory means that at low orders, the states with quark-antiquark pairs far apart do not contribute, and the most important state has them closest together. In considering just this two-particle state, (4.66), we face problems at fourth order due to its degeneracy with the states (4.67). This problem and its resolution will be discussed later. For the time begin, we concentrate on the radial excitations.

Initially, we consider just the one- and three-link states. We sketch the calculation for the pseudoscalar particle mass matrix, noting different results for scalars in parentheses. The rescaled lattice Hamiltonian is the same as before, (3.56)-(3.58) and so is the vacuum energy to fourth order:

$$\langle 0|W|0\rangle = -\frac{Nx^2}{1+2\mu} + \frac{3Nx^4}{(1+2\mu)^3} + O(x^6). \qquad (4.68)$$

The perturbation expansion, (B.32), for the matrix of W in the subspace {|1->, |3->} simplifies, because

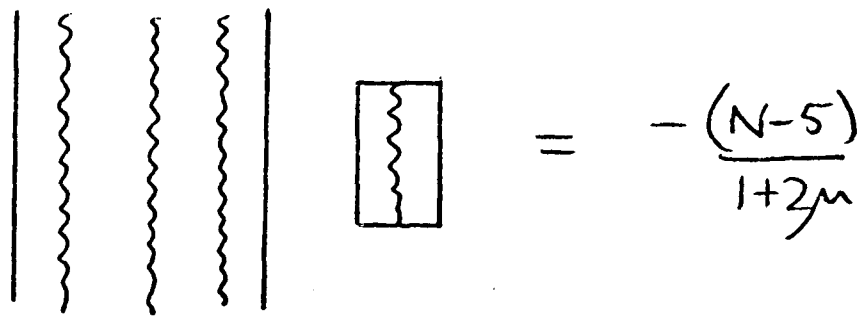
$$PVP = 0 \qquad (4.69)$$

and all terms of odd order in V vanish similarly. The diagram rules have already been introduced in Chapter 3.

At zeroth order the mass matrix is

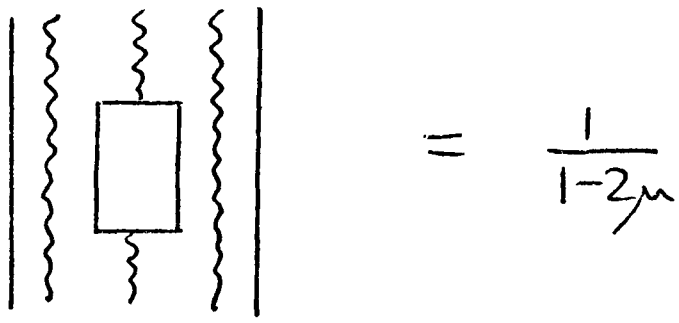
$$\begin{pmatrix} 1+2\mu & 0 \\ 0 & 3+2\mu \end{pmatrix}. \qquad (4.70)$$

At second order, the diagonal matrix element $\langle 1-|Vg_1V|1-\rangle$ is given in (3.75). The diagonal matrix element between three-link states is the same for both scalar and pseudoscalar, and receives contributions from two graphs:



$$= -\frac{(N-5)}{1+2\mu} \qquad (4.71)$$

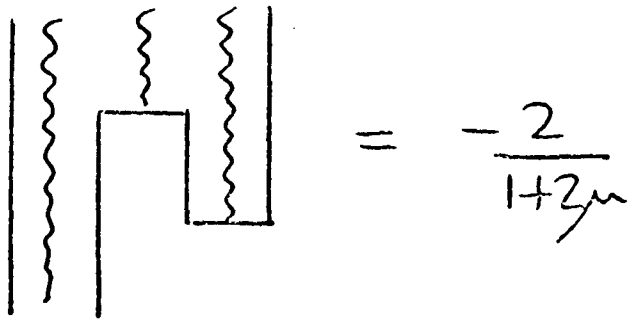
and



$$= \frac{1}{1-2\mu} \qquad (4.72)$$

The off-diagonal matrix elements are

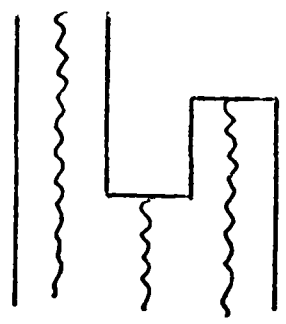
$\langle 3-|Vg_1V|1-\rangle$:



$$= -\frac{2}{1+2\mu} \qquad (4.73)$$

and

$\langle 1- | V g_3 V | 3- \rangle$:



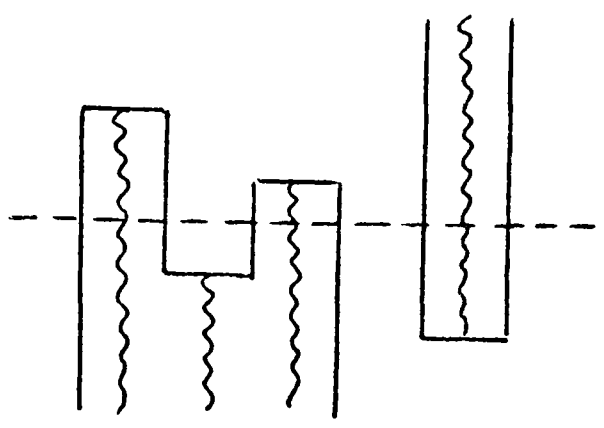
$= \frac{2}{1-2\mu}$ (4.74)

(two orientations of each). Hence, combining (3.75) and (4.71)-(4.74) gives

$$2^{nd}\text{ order} = x^2 \begin{pmatrix} -\frac{(N-2)}{1+2\mu}, \left[-\frac{(N-6)}{1+2\mu}\right] & \frac{2}{1-2\mu} \\ \frac{-2}{1+2\mu} & -\frac{(N-5)}{1+2\mu} + \frac{1}{1-2\mu} \end{pmatrix} \quad (4.75)$$

As usual, subtracting the vacuum energy renders it intensive.

The fourth order calculation proceeds along similar lines. The diagonal matrix element between one-link states is essentially the same as that calculated in Chapter 3, with the omission of graphs like (3.77). However, a problem arises in the scalar mass matrix, which has disastrous consequences for the eighth order computer calculation. The N-dependence of some off-diagonal matrix elements does not cancel out. Offending graphs are always of the type



(4.76)

in which a scalar particle is created out of the vacuum. But the scalar particle ought to be orthogonal to the vacuum, and it is for non-zero momentum. The problem occurs because of our choice of zero-momentum scalar state. The extensive character of graphs like (4.76) is spurious and goes away when particle energies are calculated at non-zero momentum. Although, on a finite lattice the momentum spectrum is discrete, it becomes continuous, $k\varepsilon\ (\frac{-\pi}{a}, \frac{\pi}{a}]$ as $N \to \infty$. So it is sensible to calculate the particle energies for $k \neq 0$ and identify masses with static energies obtained in the limit $k \to 0$. Then graphs, like (4.76), in which incoming and outgoing particles are n links apart, are weighted by a factor e^{ikna} instead of 1. So the sum over final configurations gives

$$\sum_n e^{ikna} \sim \delta(k) = 0$$

for $k \neq 0$, instead of N. Taking the $k \to 0$ limit at the end of the calculation, is equivalent to dropping the spurious N's. It is clear why a similar problem does not occur for pseudoscalars; they are just scalar particles at momentum $\frac{\pi}{a}$.

The result to fourth order for the pseudoscalar mass matrix is

$$W_{11}^{-} = 1+2\mu + \frac{2x^2}{1+2\mu} + x^4\left[\frac{-8}{(1+2\mu)^3} - \frac{4}{(1+2\mu)^2(1-2\mu)}\right] + O(x^6), \tag{4.77}$$

$$W_{13}^{-} = \frac{2x^2}{1-2\mu} + x^4\left[\frac{4}{(1+2\mu)(1-2\mu)^2} - \frac{2}{(1-2\mu)^3}\right] + O(x^6), \tag{4.78}$$

$$W_{31}^{-} = -\frac{2x^2}{1+2\mu} + x^4\left[\frac{5}{(1+2\mu)^3} - \frac{1}{(1+2\mu)^2(3+2\mu)} - \frac{2}{(1+2\mu)^2(1-2\mu)}\right] + O(x^6), \tag{4.79}$$

$$W_{33}^{-} = 3+2\mu + x^2\left(\frac{5}{1+2\mu} + \frac{1}{1-2\mu}\right) + x^4\left[\frac{-2}{(1+2\mu)^2} - \frac{17}{(1+2\mu)^3} - \frac{1}{(1-2\mu)^3} + \frac{2}{(1+2\mu)(1-2\mu)}\left(\frac{1}{1+2\mu} + \frac{1}{1-2\mu}\right)\right] + O(x^6), \tag{4.80}$$

and for the scalar mass matrix is

$$W_{11}^{+} = 1+2\mu + \frac{6x^2}{1+2\mu} + x^4\left[\frac{-24}{(1+2\mu)^3} - \frac{4}{(1+2\mu)^2(1-2\mu)}\right] + O(x^6), \tag{4.81}$$

$$W_{13}^{+} = \frac{2x^2}{1-2\mu} + x^4\left[\frac{8}{(1+2\mu)(1-2\mu)^2} - \frac{2}{(1-2\mu)^3}\right] + O(x^6), \tag{4.82}$$

$$W_{31}^{+} = -\frac{2x^2}{1+2\mu} + x^4\left[\frac{3}{(1+2\mu)^3} + \frac{5}{(1+2\mu)^2(3+2\mu)} - \frac{2}{(1+2\mu)^2(1-2\mu)}\right] + O(x^6), \tag{4.83}$$

$$W_{33}^{+} = W_{33}^{-} + O(x^6). \tag{4.84}$$

It is straightforward to check that (3.82) and (3.83) are eigenvalues of $\underline{W}^{-}$ and $\underline{W}^{+}$ respectively.

These mass matrices are regarded as series expansions in z, (3.84), valid to order z^{11}. Their eigenvalues are of the form 2zM/g, and so they should be replaced by [5,4] matrix Padé approximants. The formula for the corresponding continuum limit is given in (4.7). The resulting predictions for individual masses are rather poor. In the strong coupling region their behaviour is so dominated by poles and zeros that it is difficult to say anything except that there is a tendency for both the scalar and pseudoscalar meson masses to vanish with the quark mass. For $\frac{m}{g} \gtrsim 1$ the smallest eigenvalue in each case takes the value 2m/g i.e. the sum of the masses of the constituent quarks. Binding energies, $(M^{\pm}-2m)/g$ are negative.

Our estimates for the ratio of the continuum binding-energies, $(M^{+}-2m)/(M^{-}-2m)$, are more encouraging. These are obtained by dividing the scalar mass matrix, $\underline{W}^{+}$, by the eigenvalue, (3.82), of the pseudoscalar mass matrix corresponding to the one-link state, both with the sum of the constituent quark masses subtracted out. A [4,4] Padé approximant is taken of the resulting series. In the continuum limit, (4.5), its smallest eigenvalue is

$$\frac{M^{+}-2m}{M^{-}-2m} = \frac{5004f^4-1308-\left[(1152f^4-306)^2-4(432f^4-90)(216f^4-64)\right]^{1/2}}{2(1062f^4-283)} \qquad (4.85)$$

with

$$\frac{M^{+}-2m}{M^{-}-2m} \xrightarrow[\frac{m}{g}\to 0]{} 1\cdot 842 \quad \text{(2-state)} \qquad (4.86)$$

and

$$\frac{M^+-2m}{M^--2m} \xrightarrow[\frac{m}{g}\to\infty]{} 1.896 \quad (2\text{-state}) \tag{4.87}$$

(4.85) is plotted in fig. 4.2. This result is a considerable improvement over the one-state calculation, (3.86). In the strong-coupling limit, the estimate (4.86) is within 8% of the exact answer (3.27). As we go towards weak coupling, the binding energy ratio (4.85) increases, as it should, and reaches an asymptotic value (4.87) which is within 18% of the exact answer (2.9). This non-relativistic limit agrees well with the estimate (4.59a) from the equivalent calculation for the linear potential model.

Also shown in fig. 4.2 is the binding-energy ratio obtained when the five-link state, (4.65), is included in the fourth order calculation of the scalar mass matrix. The strong-coupling expansion is given in table 4.1. The continuum estimate for strong coupling

$$\frac{M^+-2m}{M^--2m} \xrightarrow[\frac{m}{g}\to 0]{} 1.845 \quad (3\text{-state}) \tag{4.88}$$

is only a marginal improvement on the two-state calculation. A little disappointingly, the non-relativistic limit

$$\frac{M^+-2m}{M^--2m} \xrightarrow[\frac{m}{g}\to\infty]{} 1.732 \quad (3\text{-state}) \tag{4.89}$$

is considerably worse. This would seem to confirm the trend, previously

oberved in the linear potential model, c.f. (4.62a), for estimates a fixed order to get worse as higher excited states are included in the matrix calculation.

Attempts to extend the matrix calculation to eighth order in V have failed. The source of the trouble is the non-cancellation of the N-dependence of off-diagonal scalar mass matrix elements. Such extensive terms cannot be identified on the finite lattice used by the computer. The alternative is to do the calculation at non-zero momentum, but that is beyond the scope of existing programmes. There remains the pseudoscalar mass matrix. The calculation to eighth order has been carried out, but continuum estimates based on it bear little resemblance to known results. The fourth order calculation suffers from the same fault. At the moment, the reason for this bad result (and a similarly bad result for the linear potential) is not understood.

So we continue with an extension of the fourth order calculation to include the two-meson state (4.66) in the scalar mass matrix. There is no straightforward way of doing this, because it belongs to the degenerate subspace of states (4.67). Diagonalisation of the full Hamiltonian in this subspace is difficult. The alternative, which we follow, is to seek a modification of the Hamiltonian (Banks et al. 1977) which splits the one-link state $|2,1+\rangle$ from the other two meson states.

The relevant issue is the uniqueness of lattice Hamiltonians. The only requirement is that all lattice Hamiltonians give the same continuum physics. Thus, operators can be freely added to H provided they preserve the symmetries of the terms in H which contribute to the continuum limit and provided they do not survive as $a \to 0$. In addition

we ask that the extra terms remove the unwanted degeneracies in the zeroth order particle spectrum. An operator with these properties is (3.63),

$$W_{eff} = C\sum_n \rho(n)\rho(n+1) \qquad (4.90)$$

where C is a dimensionless parameter. Such a term is generated at second order in the perturbation expansion of our original Hamiltonian, and is the effective Hamiltonian which fixes the ground state of the massless theory. So our first criterion is automatically satisfied.

The irrelevance of (4.90) comes about as follows (Kogut 1976): In 1+1 dimensions the Thirring interaction,

$$G^2\int dx\,(\bar{\psi}\psi)^2 \qquad (4.91)$$

is renormalisable and hence its lattice version (Shigemitsu and Elitzur 1976),

$$H \sim \frac{G^2}{a}\sum_n \rho(n)\rho(n+1) \qquad (4.92)$$

survives in the continuum limit. But, because of our rescaling (3.56), the interaction (4.90) enters the lattice Hamiltonian multiplied by $\frac{ag^2C}{2}$, which corresponds to an effective coupling in the continuum theory of $\frac{a^2g^2}{2}C \xrightarrow[a\to 0]{} 0$. Hence, it should behave like an irrelevant operator. This does not mean that our low-order calculations will

produce continuum estimates independent of C, only that their dependence on C ought to be slight.

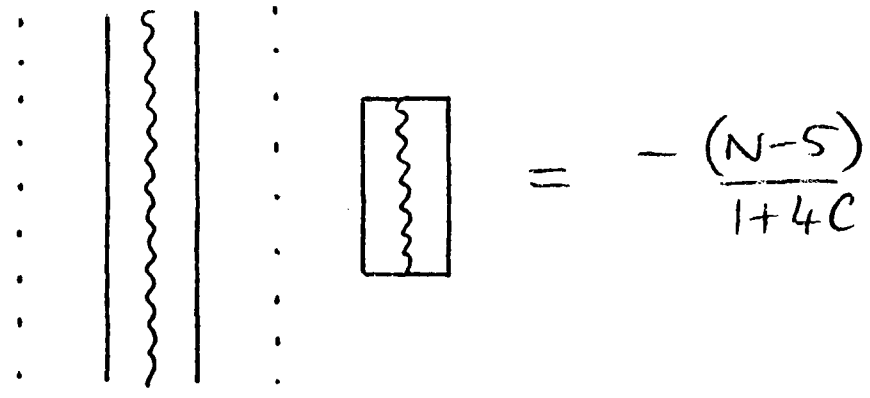
This claim can be checked by explicit low order calculations for the massless Schwinger model. The modified Hamiltonian is, c.f. (3.56)-(3.59),

$$W \equiv \frac{2}{ag^2} H = W_0 + x V \tag{4.93}$$

$$W_c = \sum_n \left[L(n)\right]^2 + C \sum_n \left[\rho(n)\rho(n+1) + 1\right] \tag{4.94}$$

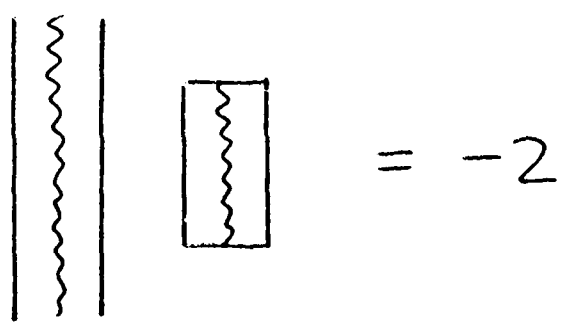
$$V = i \sum_n \left[\phi^\dagger(n) U(n,n+1) \phi(n+1) - h.c.\right] \tag{4.95}$$

The vacuum is unchanged, (3.65), and taken to be the zero of W_o. Now the extra static interaction in (4.94) acts to lower the energy of a quark-antiquark pair on neighbouring sites, relative to the energy they have when more than one link apart. Thus, the meson in (4.63) has zeroth order energy 1+4C, and the contribution from second order graphs depends on whether or not the components inhabit neighbouring sites. For example, the graphs with a vacuum fluctuation more than one link away from the through-going meson,



(4.96)

have higher intermediate energy than the graphs



(4.97)

in which they are closest together. For the same reason, the additional interaction (4.9)) removes the degeneracy problem in the two-meson subspace. The result of the fourth order calculation is an estimate for the continuum mass ratio

$$\frac{M_1^+}{M_1^-} = \frac{32C^2 - 8C + 5}{32C^2 - 8C + 3} \qquad (4.98)$$

shown in fig. 4.3. This agrees with our original calculation, (3.86), when $C = 0$, and for $C \lesssim 0.25$ agreement with the exact continuum result, (3.27), actually improves. For $C \gtrsim 0.4$, the four-fermion interaction produces large deviations from Schwinger model behaviour, which is to be expected since it then dominates the gauge field energy in (4.94).

We now calculate the scalar mass matrix in the subspace spanned by the one- and three-link single-meson states, (4.63) and (4.64), and the two-meson state (4.66). The mixing of these three states is expected to be important at fourth order. The modified Hamiltonian, (4.93)-(4.95), with the addition of a mass term, avoids the degeneracy problem in the two-meson subspace. At zeroth order, for the states (4.63), (4.64) and (4.66),

$$W_0|1+\rangle = (1+2\mu+4C)|1+\rangle \tag{4.99}$$

$$W_0|2,1+\rangle = (2+4\mu+4C)|2,1+\rangle \tag{4.100}$$

$$W_0|3+\rangle = (3+2\mu+8C)|3+\rangle \tag{4.101}$$

States consisting of two mesons separated by more than one link are split from these for C > 0, with

$$W_0|2,m+\rangle = (2+4\mu+8C)|2,m+\rangle, (m>1) \tag{4.102}$$

but, themselves, stay degenerate. For perturbative calculations around the state $|2,1+\rangle$, all that remains of the degeneracy problem are poles at C = 0. For this reason, we cannot trust continuum estimates near C = 0 and expect the most reliable predictions to come from $C \sim 0.25$.

Our calculation calls on the formula for quasi-degenerate perturbation theory around three states to fourth order, given in (B.31). The result for the strong-coupling expansion is given in table 4.2. Also required to construct the mass ratio is the $|1->$ pseudoscalar particle mass, obtained using ordinary perturbation theory:

$$\frac{2\sqrt{x}}{g} M_1^- = 1+2\mu+4C + x^2\left(\frac{6}{1+2\mu+4C} - \frac{4}{1+2\mu}\right)$$
$$+x^4\left[\frac{-36}{(1+2\mu+4C)^3} + \frac{14}{(1+2\mu+4C)^2(1+2\mu+2C)}\right.$$
$$+\frac{10}{(1+2\mu+4C)^2(1+2\mu)} - \frac{4}{(1+2\mu)^2(1+2\mu+4C)} + \frac{8}{(1+2\mu)^3}$$
$$\left.-\frac{2}{(1+2\mu)^2(1+2C)}\right] + O(x^6)$$

(4.103)

which, for C = 0, can be checked against (3.82). The scalar mass matrix is divided by (4.103), after subtracting the sum of the constituent quark masses from each, to obtain the binding-energy ratio. Our estimate for this quantity is taken to be the smallest eigenvalue of the continuum limit of the [4,4] matrix Padé approximant, given in (4.5).

First, we check the dependence of the result for the massless Schwinger model on C. This is shown in fig. 4.4. The poles around $C \simeq 0.025$ may be just a fault of the Padé approximant, because they are almost cancelled by nearby zeros. Outside this small region, the smallest eigenvalue shows very little variation with C over the range 0 to 0.25; its value falls from 1.8 to around 1.1. This supports our expectation that the operator (4.90) should become irrelevant in the continuum limit.

As a consequence, we propose to study the massive Schwinger

model at values of $C \sim 0.1$. The reason is that for much smaller values of C, poles in the strong-coupling expansion, resulting from the degeneracy of the two-meson states at $C = 0$, have a strong influence. This leads to quite wild behaviour of the eigenvalues as functions of $\frac{m}{g}$; they have poles and zeros, and occasionally two of them go complex. Values of C much larger than 0.1 are too far removed from Schwinger-model behaviour.

A typical result for the binding-energy ratio, as a function of $\frac{m}{g}$, is shown in fig. 4.5. Here $C = 0.1$. Apart from a rather low value in the massless limit, this estimate is not too bad. For $\frac{m}{g} \gtrsim 1$, two of the eigenvalues are large, or complex, while the smallest eigenvalue quickly settles down to the asymptotic value

$$\frac{M^+ - 2m}{M^- - 2m} \xrightarrow[\frac{m}{g} \to \infty]{} 2.371 \quad (3\text{-state};\ C = 0.1) \tag{4.104}$$

This agrees with the exact result, (2.9), for the linear potential to within 3%, and is an improvement on the estimates from other matrix calculations, (4.87) and (4.89). In fact, for C between 0.05 and 0.25, there is little deviation of this non-relativistic estimate from the exact result, as can be seen in fig. 4.6. This is encouraging, for it betters any other fourth-order calculation.

Thus, the matrix calculation, based around the three states which we expect to dominate at fourth order is, in part, successful and, in part, disappointing. Although for weak coupling the results are good, for strong coupling the mass ratio is no better than that

obtained from other fourth order calculations. The dependence on quark mass, absent in the single-state calculation, has been retrieved. But for $\frac{m}{g} \sim 1$ it is doubtful that the behaviour of the binding-energy ratio is anything but qualitatively correct.

Summary

Lattice strong-coupling expansions may be carried out about a subspace of non-degenerate states, instead of a single state. The subspace chosen, consists of the original state and any of those intermediate states which mix strongly with it at the order of perturbation theory being considered. The hope is that the resulting Hamiltonian matrix better represents the continuum physics than any one of its eigenvalues. Matrix Padé approximants are used to extrapolate the whole matrix to the continuum limit, at which point its smallest eigenvalue is associated with the energy (or energy ratio) being sought.

With a few notable exceptions, the estimates obtained are more accurate than those from single-state calculations. When the basis states are radial excitations of the quark-antiquark pair, it is the two-state calculation at fourth order which comes out best of all. Inclusion of higher excited states has a detrimental effect on all the eigenvalues at this order. There is no improvement for individual masses in the Schwinger model, but the mass ratio derived from the scalar mass matrix has a much more realistic dependence on quark mass. In contrast, the pseudoscalar mass matrix behaves badly and ruins the eighth order computer calculation.

For weak coupling an even better treatment of the mass ratio is achieved by including a two-meson state as well as the first radial excitation of the quark-antiquark pair. The addition of a four-fermion interaction to the Hamiltonian is required to remove a degeneracy in the two-meson subspace. Continuum estimates are almost independent of the corresponding coupling constant over the range 0.05 to 0.25.

CHAPTER 5

THE SU(2) FLAVOUR SCHWINGER MODEL

1+1 dimensional QED of two massive Dirac particles - an 'electron' and a 'muon' - takes us one step nearer reality. Actually, the confining nature of the interaction means this can be mistaken for the QCD of non-strange particles if the fundamental fermions are called 'up' and 'down' quarks. The two quark flavours need not have equal mass, but if they do the theory has a global isospin symmetry. It shares with QCD an isotriplet of pseudoscalar mesons whose mass vanishes with the fermion mass. So it provides an opportunity of studying the application of our methods to a theory with a pion-like excitation. The advantage of the 1+1 dimensional model is that, like the ordinary massive Schwinger model, some exact results are known about the low-energy particle spectrum for both strong and weak coupling (Coleman 1976). Simply doubling the number of fermions has some unexpected dynamical consequences. These may turn out to be peculiarities of 1+1 dimensional physics, but they are just as likely to foretell of surprises to come in QCD.

(a) The Continuum Theory.

Specifically, if we take the two fermion species ψ_i $(i = 1,2)$ to have masses m_i and equal electric charges g, the Lagrangian of the theory is

$$\mathcal{L} = \sum_{i=1,2} \bar{\psi}_i (i\partial\!\!\!/ - m_i - g A\!\!\!/)\psi_i - \frac{1}{4} F_{\mu\nu} F^{\mu\nu} \qquad (5.1)$$

where

$$F_{\mu\nu} = \partial_\mu A_\nu - \partial_\nu A_\mu . \qquad (5.2)$$

For $m_1 = m_2 = m$ the theory has an internal global SU(2) symmetry which we call isospin. The Dirac fields $\begin{pmatrix}\psi_1\\ \psi_2\end{pmatrix}$ form an isodoublet; the electromagnetic field A_μ is an isosinglet. Since the coupling constant has positive mass dimension, the theory is superrenormalisable and hence asymptotically free.

The strong-coupling limit is $\frac{m}{g} \ll 1$, but now the massless theory differs qualitatively from the theory with non-zero, but small fermion mass. There should be a restoration of (chiral) SU(2) x SU(2) symmetry as $\frac{m}{g} \to 0$, because there is no spontaneous breakdown of continuous internal symmetries in 1+1 dimensions (Coleman 1973). This is signalled by the vanishing of the $I^P = 1^-$ and 0^+ meson masses (Coleman 1976). Furthermore, the massless model does not confine quarks (Kurak, Schroer and Swieca 1977)! A more economic confinement scheme than usual prevails. Only the charges coupled to the gauge fields are confined; the fundamental flavour representation appears among the physical states as electrically neutral (colourless), $I = \frac{1}{2}$ particles.

We shall concentrate on the massive theory. The introduction of the mass term filters out the $I = \frac{1}{2}$ neutral particles, except when the

background field $\theta = \pm\pi$ (Kurak et al. 1977). In all other cases the confinement mechanism is the traditional one and the particle spectrum consists solely of mesons, which can be thought of as quark-antiquark pairs, tied together with gauge strings of constant tension. In the isospin-symmetric theory, these mesons reside in isomultiplets. The lowest-lying multiplet is an isotriplet of pseudoscalar mesons which can be identified with the 'pion'. For strong coupling these low-lying particles respect isospin symmetry even when it is broken at the level of the quark masses (Coleman 1976). This result may have relevance to 3+1 dimensions, where it can be argued (Weinberg 1977) that the effective masses of the u and d quarks in the QCD Lagrangian should be

$$m_u \simeq 4.2 \text{ MeV}, \; m_d \simeq 7.5 \text{ MeV}. \qquad (5.4)$$

despite the success of isospin symmetry.

The strongly coupled theory is best tackled in the equivalent language of boson fields. The arguments run parallel to those of Chapter 3(a). For simplicity we consider just the isospin-symmetric theory ($m_1 = m_2 = m$) and introduce two Bose fields, c.f. (3.11) and (3.12), one for each of the fermion flavours (Coleman 1976):

$$N_m[\bar{\psi}_i \gamma^\mu \psi_i] = \frac{1}{\sqrt{\pi}} \epsilon^{\mu\nu} \partial_\nu \phi_i \qquad (5.5)$$

and

$$N_m[\bar{\psi}_i \psi_i] = -cm N_m[\cos(2\sqrt{\pi}\phi_i)] \qquad (5.6)$$

(no sum on i). This leads us to the Hamiltonian, c.f. (3.17):

$$\mathcal{H} = N_m \Big[\tfrac{1}{2}\dot{\phi}_1^2 + \tfrac{1}{2}\dot{\phi}_2^2 + \tfrac{1}{2}(\partial_1\phi_1)^2 + \tfrac{1}{2}(\partial_1\phi_2)^2 - cm^2\cos(2\sqrt{\pi}\phi_1) - cm^2\cos(2\sqrt{\pi}\phi_2) + \frac{q^2}{2\pi}\left(\phi_1+\phi_2+\frac{\theta}{2\sqrt{\pi}}\right)^2\Big]. \tag{5.7}$$

If we define

$$\phi_+ \equiv \frac{1}{\sqrt{2}}\left(\phi_1+\phi_2+\frac{\theta}{2\sqrt{\pi}}\right) \tag{5.8}$$

$$\phi_- \equiv \frac{1}{\sqrt{2}}\left(\phi_1-\phi_2\right) \tag{5.9}$$

and

$$\mu \equiv \sqrt{\frac{2}{\pi}}\, g, \tag{5.10}$$

this becomes

$$\mathcal{H} = N_m \Big[\tfrac{1}{2}\dot{\phi}_+^2 + \tfrac{1}{2}(\partial_1\phi_+)^2 + \frac{\mu^2}{2}\phi_+^2 + \tfrac{1}{2}\dot{\phi}_-^2 + \tfrac{1}{2}(\partial_1\phi_-)^2 - 2cm^2\cos\left(\sqrt{2\pi}\phi_+ - \frac{\theta}{2}\right)\cos\left(\sqrt{2\pi}\phi_-\right)\Big] \tag{5.11}$$

Equation (5.11) is to be the starting point for our analysis of the low-lying particle spectrum for strong coupling, $m \ll \mu$. It displays the theory as that of two scalar fields, one heavy and one light, with weak self-interactions. Isospin invariance has become rather obscure, but it is still present. Using (5.5), the electric charge density is

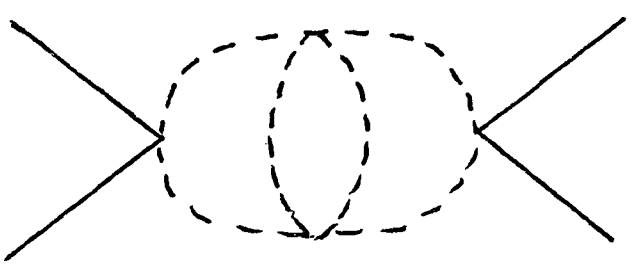
$$j_0 = N_m\left[\psi_1^+\psi_1 + \psi_2^+\psi_2\right] = \frac{1}{\sqrt{\pi}}\,\partial_1(\phi_1+\phi_2) \qquad (5.12)$$

and so ϕ_+ is an isosinglet. On the other hand, ϕ_- has complicated non-linear transformation properties under a general isospin transformation (Coleman 1976). All three isospin currents can be written as functions of ϕ_-, but only the third is represented simply:

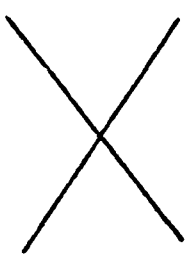
$$j_3^\mu = \tfrac{1}{2}N_m\left[\bar\psi_1\gamma^\mu\psi_1 - \bar\psi_2\gamma^\mu\psi_2\right] = \frac{1}{\sqrt{2\pi}}\,\epsilon^{\mu\nu}\partial_\nu\phi_- \qquad (5.13)$$

using (5.5) and (5.9). Also, the theory defined by (5.11) is still periodic in θ, with period 2π.

In contrast to the ordinary massive Schwinger model, we cannot investigate the particle spectrum of (5.11) using straightforward mass perturbation theory. This is because the scale of the ϕ_- mass and the magnitude of the ϕ_- couplings are given by the same small parameter m. So, for example, the higher order correction



to ϕ_+ scattering (solid lines are heavy mesons; broken lines are light mesons) is of order m^2, the same as the tree approximation:



Thus, although we can be fairly sure there is a ϕ_+ meson (possibly unstable) with mass close to μ, it is no easy matter to compute the corrections to its mass, or search for possible multi-meson bound states.

Coleman's approach is to forget about these high-mass states and concentrate on ϕ_- Green functions. Graphs with internal ϕ_+ lines are down by powers of m/μ and can be reasonably neglected. The only possible source of trouble comes from graphs involving the contraction of two ϕ_+ fields at the same vertex, since these are proportional to $\ell n(m/\mu)$. Fortunately, they can be removed by re-normal-ordering:

$$N_m\left[\cos\left(\sqrt{2\pi}\,\phi_+\right)\right] = \left(\frac{\mu}{m}\right)^{1/2} N_\mu\left[\cos\left(\sqrt{2\pi}\,\phi_+\right)\right] \qquad (5.14)$$

Now we can ignore ϕ_+ altogether. Also, at this stage we set $\theta = 0$. Everything that follows is true, with minor modifications to the mass scale, for non-zero background field, except for the pathological case $|\theta| = \pi$ which must be treated separately anyway. Then (5.11) reduces to

$$\mathcal{H} = N_m\left[\tfrac{1}{2}\dot{\phi}_-^2 + \tfrac{1}{2}\left(\partial_1\phi_-\right)^2 + 2cm^{3/2}\mu^{1/2}\cos\left(\sqrt{2\pi}\,\phi_-\right)\right] \qquad (5.15)$$

and re-normal-ordering:

$$\mathcal{H} = N_{m'}\left[\tfrac{1}{2}\dot{\phi}_-^2 + \tfrac{1}{2}(\partial_i\phi_-)^2 + m'^2\cos\left(\sqrt{2\pi}\,\phi_-\right)\right] \tag{5.16}$$

where

$$m' = \left[2cm\left(\frac{2g^2}{\pi}\right)^{1/4}\right]^{2/3} \tag{5.17}$$

is the only mass parameter in the problem. So the particles we have thrown away are $O(\mu/m') = O(g/m)^{2/3}$ times more massive than the particles we have retained. Because ϕ_+ is an isosinglet, this approximation does not destroy isospin invariance. What is more surprising is that if the two quark flavours have different masses, the same result, (5.16), is obtained apart from a change in m' (Coleman 1976).

Equation (5.16) is a special case of the sine-Gordon Hamiltonian whose interaction term is $N_{m'}[m'^2 \cos \beta\phi]$. This is known (Dashen, Hasslacher and Neveu 1975; Luther 1976; Schroer, Truong and Weisz 1976) to contain two particles of equal mass

$$M = \frac{8}{\beta'^2}\left(\beta\right)^{\beta'^2/\beta^2} m' \tag{5.18}$$

where

$$\beta'^2 = \frac{\beta^2}{1-\beta^2/8\pi} \tag{5.19}$$

called the soliton and antisoliton. If one defines the conserved current,

$$j^{\mu} = \frac{\beta}{2\pi} \epsilon^{\mu\nu} \partial_{\nu} \phi \qquad (5.20)$$

then the soliton and antisoliton have "charge" plus and minus one. In addition, for $\beta^2 < 4\pi$, the theory possesses soliton-antisoliton bound states, all with charge zero and masses given by

$$M_n = 2M \sin\left(\frac{\beta'^2 n}{16}\right) \qquad (5.21)$$

for $n = 1, 2, \ldots, < 8\pi/\beta'^2$.

For the low-lying states of the SU(2) Schwinger model in the strong coupling limit

$$\beta^2 = 2\pi \text{ and } \beta'^2 = \frac{8\pi}{3} . \qquad (5.22)$$

Comparing (5.20) and (5.13), we see that the soliton and antisoliton have $I_3 = \pm 1$ and, like ϕ_-, are pseudoscalar (Dashen et al. 1975). They are of mass

$$M = \frac{3}{\pi} (2\pi)^{2/3} m' \qquad (5.23)$$

which, using (5.17) and (3.16), is

$$M = \frac{3}{\pi} \left[2 e^{\gamma} m \left(\frac{2g^2}{\pi} \right)^{1/4} \right]^{2/3} \qquad (5.24)$$

There are just two soliton-antisoliton bound states, with $I_3 = 0$ and masses

$$M_n = 2M \sin\left(\frac{n\pi}{6}\right), \quad n = 1, 2. \qquad (5.25)$$

The lowest-lying of these has mass M and completes the pseudoscalar isotriplet. The other has the P and C transformation properties of a two-meson bound state (Dashen et al. 1975) and mass

$$M_2 = 2M \sin\left(\frac{\pi}{3}\right) = \sqrt{3}M. \qquad (5.26)$$

So it is a scalar particle and, being all alone, must be an isosinglet. All the other particles have masses up around μ. Amongst these is the ϕ_+ meson which is a pseudoscalar isosinglet.

For weak coupling the results are just the obvious generalisations of those for the one-flavour model. There are four times as many particles, arranged in isotriplets and isosinglets. The lowest-lying states are the pseudoscalars $I^P = 1^-,0^-$ with binding energy given by (2.6). Above them are the scalar particles 1^+, 0^+ with binding energy given by (2.8). If the quark flavours have different masses, the corresponding results are given by (2.1) with m replaced by the reduced mass. Notice that in the passage from weak to strong coupling the 0^- and 0^+ levels cross. The 0^- meson acquires a high mass, whereas the 0^+ meson, (5.26), follows the pseudoscalar isotriplet, (5.24) to zero mass:

$$\frac{M_1^-}{g} \xrightarrow[\frac{m}{g}\to 0]{} 2.066\left(\frac{m}{g}\right)^{2/3} \qquad (5.27)$$

and

$$\frac{M_0^+}{g} \xrightarrow[\frac{m}{g}\to 0]{} 3.578\left(\frac{m}{g}\right)^{2/3} \qquad (5.28)$$

in the ratio

$$\frac{M_0^+}{M_1^-} \xrightarrow[\frac{m}{g}\to 0]{} \sqrt{3}\,. \qquad (5.29)$$

We conclude with what Coleman (1976) discovers for $|\theta| = \pi$. Here he is able to relate the strongly-coupled theory to a sine-Gordon Hamiltonian with

$$\beta^2 = 8\pi - 0\left(\frac{m}{g}\right)^2 \qquad (5.30)$$

According to Dashen et al. (1975), for $\beta^2 > 4\pi$ the only particles in the theory are the soliton and antisoliton with topological charges ± 1. But, from (5.20) and (5.13),

$$I_3 = \frac{\sqrt{2\pi}}{\beta} \times \text{topological charge} \qquad (5.31)$$

and so these particles have isospin $\frac{1}{2}$. They are electrically neutral and are the remnant of the "bleached" free quark states present in the massless theory. For weak coupling there are two half-asymptotic isodoublets, quark and antiquark, carrying electric charges $\pm g$. So Coleman proposes that here there may be a phase transition between weak and strong coupling, as there is for the one-flavour model.

(b) The Lattice Theory.

At a first glance, we might not expect to learn much more about lattice gauge theories from the SU(2) Schwinger model than we got out of the ordinary one-species case. The shortcomings of our Padé approximant continuation method have received ample attention and the more complicated

model seems unlikely to alter the conclusions already reached. But a little extra thought reveals two important reasons for studying the two-flavour lattice theory. First of all, the continuum theory itself held a few surpises. Even if we ignore the phenomenon of 'bleaching' which allows free quark states in the massless theory, there is the pion-like excitation, and the persistence of isospin symmetry in the low-energy spectrum of the strongly-coupled theory, regardless of the quark mass-splitting. The extent to which these features are reproduced in the lattice theory is considered in the next chapter. Of more immediate interest is the way in which flavour symmetry is built into the lattice theory. This derives its significance from our technique of splitting the fermion degrees of freedom in order to counteract the appearance of unwanted particle states in the continuum limit. As a result, some of the internal symmetries get mixed with discrete spatial symmetries of the lattice. For example, in the 3+1 dimensional lattice QCD of non-strange particles (Banks et al. 1977, Susskind 1977) a shift along a face diagonal of the cubic lattice is a discrete isospin rotation. With more than one flavour or spatial dimension there is more than one way of distributing the fermion degrees of freedom around the unit cell. Consequently, there is an ambiguity in the interpretation of lattice symmetries. Perhaps only one choice of lattice theory is 'natural'. Certainly it is to be hoped that all choices belong to the same universality class as the continuum theory. Nevertheless, for non-zero lattice spacing the theories are likely to be quite different and there is no reason to suppose that they will exhibit similar convergence properties. The SU(2) Schwinger model is the simplest theory to possess this ambiguity. It has just two distinct lattice formulations. So, how do

they compare?

We seek a Hamiltonian lattice formulation of the theory defined by (5.1) and (5.2). The argument follows the same lines as for the single-species model apart from the treatment of fermion fields. Recall that when we originally tried to place a two component fermion field on each lattice site we ended up with a theory containing two real fermions in the continuum limit. This is just what we want now. So, at each site n define a pair of single-component fermion fields $\phi_i(n)$ (i = 1,2) obeying

$$\{\phi_i(m), \phi_j(n)\} = 0 , \quad \{\phi_i^+(m), \phi_j(n)\} = \delta_{ij}\delta_{mn} . \tag{5.32}$$

We identify the fields $\phi_i(n)$ with separate spinor components of the two continuum Dirac fields. The two distinct identifications, which will hereafter be referred to as "lattice I" and "lattice II" are:

$$\text{Lattice I:} \quad \frac{1}{\sqrt{a}}\phi_i(n) \equiv \psi_i^{(n+i \bmod 2)}(na) \tag{5.33}$$

$$\text{Lattice II:} \quad \frac{1}{\sqrt{a}}\phi_i(n) \equiv \psi_i^{(n+i \bmod 2)}(na) \tag{5.34}$$

where the upper index is the Dirac index. Thus, lattice I is the usual staggered lattice used by Hamer (1977) and Steinhardt (1977) in which quarks of each flavour reside on even sites and antiquarks on odd sites. It is the obvious generalisation of the lattice chosen for the single-species Schwinger model. Lattice II, however, has a quark and antiquark of different flavour on each site, where one type of quark lives on even sites and the other on odd sites. It is obtained from lattice I by

shifting the lattice for type 2 fields one spacing relative to that for type 1 fields. The quark-hopping Hamiltonian is the same for both lattices:

$$H_{K.E.} = \frac{i}{2a} \sum_{i,n} \left[\phi_i^+(n)\, \phi_i(n+1) - \phi_i^+(n+1)\, \phi_i(n) \right] \tag{5.35}$$

for then the equations of motion are

$$\begin{aligned} \dot{\phi}_i(n) &= i \left[H_{K.E.} , \phi_i(n) \right] \\ &= \frac{1}{2a} \left[\phi_i(n+1) - \phi_i(n-1) \right] \end{aligned} \tag{5.36}$$

Using (5.33) or (5.34), these are equivalent to

$$\dot{\psi}_i(na) = \begin{pmatrix} 0 & 1 \\ 1 & 0 \end{pmatrix} \frac{1}{2a} \left[\psi_i((n+1)a) - \psi_i((n-1)a) \right] \tag{5.37}$$

which has the Dirac equation

$$\dot{\psi}_i = \alpha \partial_1 \psi_i \tag{5.38}$$

as its continuum ($a \to 0$) limit. (We use the representation (3.31) for the Dirac algebra).

The fully gauge-invariant Hamiltonian for each lattice is obtained by introducing the gauge connections (3.44) into (5.35), and adding the gauge-field energy (3.49) and the relevant mass term. The result for zero background field is (Kenway and Hamer 1978):

$$H_I = \frac{ag^2}{2}\sum_n [L(n)]^2 + \sum_{i,n}(-1)^n m_i \phi_i^+(n)\phi_i(n)$$
$$+\frac{i}{2a}\sum_{i,n}[\phi_i^+(n)U(n,n+1)\phi_i(n+1) + \phi_i(n)U^+(n,n+1)\phi_i^+(n+1)] \quad (5.39)$$

and

$$H_{II} = \frac{ag^2}{2}\sum_n [L(n)]^2 + \sum_{i,n}(-1)^{n+i+1} m_i \phi_i^+(n)\phi_i(n)$$
$$+\frac{i}{2a}\sum_n[\phi_i^+(n)U(n,n+1)\phi_i(n+1)+\phi_i(n)U^+(n,n+1)\phi_i^+(n+1)] \quad (5.40)$$

These differ only in the sign of m_2. It is straightforward to check that the interaction terms in (5.39) and (5.40) have the correct continuum limit and that both lattice formulations reduce to the classical continuum Hamiltonian

$$H = \int dx\left[\sum_i \Psi_i(i\partial\!\!\!/ + m_i - gA\!\!\!/)\Psi_i + \frac{1}{2}(\partial_0 A_1)^2\right] \quad (5.41)$$

in the limit $a \to 0$ ($A_0 = 0$ gauge, of course). However, for $a \neq 0$ the two lattices respect different symmetries. In terms of the field vector

$$\Phi(n) \equiv \begin{pmatrix}\phi_1(n)\\ \phi_2(n)\end{pmatrix} \quad (5.42)$$

the two Hamiltonians have the form

$$H_{I,II} = \frac{ag^2}{2}\sum_n [L(n)]^2 + \sum_n (-1)^n \Phi^+(n)\begin{pmatrix} m_1 & 0\\ 0 & \pm m_2\end{pmatrix}\Phi(n)$$
$$+\frac{i}{2a}\sum_n\left[\Phi^+(n)U(n,n+1)\Phi(n+1) + \Phi(n)U^+(n,n+1)\Phi^+(n+1)\right] \quad (5.43)$$

where the + sign refers to lattice I and the - sign to lattice II. Translation by even integers is a symmetry of both and is the remnant of ordinary translational invariance. However, translation by odd integers, which for both lattices is equivalent to the discrete chiral symmetry

$$\psi_i \longmapsto \gamma_5 \psi_i \qquad (5.44)$$

(+ an ordinary translation) is broken by the non-zero masses. There is a global SU(2) symmetry on the lattice

$$\Phi(n) \longmapsto R\,\Phi(n), \quad R \in SU(2) \qquad (5.45)$$

provided R commutes with the mass matrix in (5.43). Thus H_I is invariant for equal-mass quarks, whereas H_{II} is invariant only in the massless limit. In the former case (5.45) is our original isospin invariance; in the latter case it is axial isospin. Consequently, the spectrum of H_I is comprised of isospin multiplets, even for strong coupling. The spectrum of H_{II} is unlikely to be similar. Obviously, both Hamiltonians are the same in the massless limit.

We employ the usual technique of solving for the particle spectra of the two lattice theories in the limit when the dimensionless coupling constant, ag, is large. This still leaves us free to vary the two parameters m_i/g. In this limit the static terms in the Hamiltonian dominate the kinetic terms. This is evident if we rescale H and write:

$$W_{I,II} \equiv \frac{2}{ag^2} H_{I,II} \equiv W^{\circ}_{I,II} + xV \qquad (5.46)$$

where

$$W_I^\circ \equiv \sum_n \left[L(n)\right]^2 + \sum_{i,n} (-1)^n \mu_i \phi_i^\dagger(n)\phi_i(n), \tag{5.47}$$

$$W_{II}^\circ \equiv \sum_n \left[L(n)\right]^2 + \sum_{i,n} (-1)^{n+i+1} \mu_i \phi_i^\dagger(n)\phi_i(n), \tag{5.48}$$

$$V \equiv i \sum_{i,n} \left[\phi_i^\dagger(n) U(n,n+1) \phi_i(n+1) + \phi_i(n) U^\dagger(n,n+1) \phi_i^\dagger(n+1)\right] \tag{5.49}$$

$$x \equiv \frac{1}{a^2 g^2} \tag{5.50}$$

and

$$\mu_i \equiv \frac{2m_i}{ag^2} = 2\sqrt{x}\,\frac{m_i}{g}. \tag{5.51}$$

Then the term xV is small and we can treat the eigenstates by standard Rayleigh-Schrödinger perturbation theory.

The first task to which we must address ourselves is the determination of the vacua of the unperturbed Hamiltonians (5.47) and (5.48). The argument we follow (Steinhardt 1977) starts from the massless theory and so can be applied to either lattice. The ground state is fluxless,

$$\langle 0|L(n)|0\rangle = 0 \quad \forall\, n, \tag{5.52}$$

but all configurations of the fermion fields are degenerate at zeroth order. To determine the vacuum uniquely we apply degenerate perturbation theory and diagonalise the perturbation in the degenerate subspace. The lowest non-zero order is

$$\delta\omega = x^2 \langle 0 | V \frac{Q}{-W^\circ} V | 0 \rangle \qquad (5.53)$$

where

$$W^\circ \equiv \sum_n \left[L(n) \right]^2 \qquad (5.54)$$

and Q forbids fluxless intermediate states. A convenient way of specifying the fermion configuration at a given site n is to define the local number operator for each flavour, c.f. (3.62):

$$\rho_i(n) \equiv \left[\phi_i^+(n), \phi_i(n) \right], (i = 1,2) \qquad (5.55)$$

This takes values ±1 depending on whether or not the site n is occupied by a fermion of flavour i. It can be thought of as one of a pair of Ising spins at each site which points 'up' ($\rho_i(n) = +1$) or 'down' ($\rho_i(n) = -1$). Hence there are four possibilities for the fermion configuration at any site, shown in fig. 5.1, which we call <up>, <down>, <in> and <out>.

Now the vacuum state must respect the following four symmetries, assuming that none is spontaneously broken:

(a) Translation invariance: $|0\rangle$ must be invariant under shifts by even integers.

(b) Isospin symmetry: $|0\rangle$ must have zero total isospin. The current density for the third component of lattice isospin is

$$j_3^\circ(n) = \frac{1}{2} \left\{ \phi_1^+(n) \phi_1(n) - \phi_2^+(n) \phi_2(n) \right\}$$

$$= \frac{1}{4} \left\{ \rho_1(n) - \rho_2(n) \right\} \qquad (5.56)$$

and so the vacuum must satisfy

$$\sum_n j_3^0(n)|0\rangle = 0. \tag{5.57}$$

(c) Charge conjugation: $|0\rangle$ must have zero total charge. The lattice charge current density is

$$j^0(n) = \tfrac{1}{2}g\{[\phi_1^\dagger(n), \phi_1(n)] + [\phi_2^\dagger(n), \phi_2(n)]\}$$

$$= \tfrac{1}{2}g\{\rho_1(n) + \rho_2(n)\} \tag{5.58}$$

and so this requirement is

$$\sum_n j^0(n)|0\rangle = 0. \tag{5.59}$$

(d) Local gauge invariance: $|0\rangle$ must be annihilated by the generator of local gauge transformations,

$$G(n) \equiv gL(n) - j^0(n) + \rho_{vac}(n) \tag{5.60}$$

where ρ_{vac} is the charge density of the vacuum. Thus,

$$G(n)|0\rangle = 0 \qquad \forall n. \tag{5.61}$$

We proceed to show that all fluxless states obeying (a)-(d) can be written either as a linear combination of basis states each of which has only <in> or <out> fermion configurations on each lattice site, or as a single basis state with only <up> or <down> fermion configuration on each site.

Consider an arbitrary fluxless state. In general, this is a linear combination of basis states in which the fermion configuration on each site is specified to be one of the four types in fig. 5.1. Then, for

each of these basis states, (b) implies that the number of <in> sites equals the number of <out> sites, while (c) implies that the number of <up>sites equals the number of <down> sites. Translational invariance, (a), requires that if one basis state has a specific fermion configuration at site n, then there exists another basis state (possibly the same one) in the same linear combination, with an identical fermion configuration at site n+2m, for all integers m. Finally, local gauge invariance, (d), requires that each basis state in the linear combination must be an eigenstate of $j^{o}(n)$ corresponding to the same eigenvalue $\rho_{vac}(n)$.

Suppose our fluxless state $|0\rangle$ is a linear combination of basis states, one of which has non-zero charge density at some site n (i.e. <up> or <down>). Then the last point requires that all the basis states have the same charge density at site n, and this must be repeated on all sites n+2m, by translational invariance. Charge conjugation then requires that the charge density on all the other sites is equal and opposite to that on site n. Hence, just one basis state comprises the linear combination which is $|0\rangle$ and it is either

$$|\text{even sites <down>; odd sites <up>>} \qquad (5.62a)$$

or

$$|\text{even sites <up>; odd sites <down>>}. \qquad (5.62b)$$

The only alternative is that $|0\rangle$ be a linear combination of basis states with <in> and <out> configurations at each lattice site. Local gauge invariance imposes no constraint on this vacuum since each site has zero charge density. The only requirement is that the state be translationally invariant with equal numbers of <in> and <out> sites.

Since the two subspaces cannot mix to form the vacuum, the perturbation can be diagonalised separately in the {<in>,<out>} and {<up>,<down>} subspaces and the state of minimum energy determined. Inserting (5.49) in (5.53) and using

$$W^{o}V|0\rangle = V|0\rangle, \tag{5.63}$$

the problem of minimising δw reduces to that of finding the ground state of the effective Hamiltonian

$$W_{eff} = x^2 \sum_n \left[4\, \underline{\tau}(n).\underline{\tau}(n+1) + \frac{1}{4}\left(\rho_1(n)+\rho_2(n)\right)\left(\rho_1(n+1)+\rho_2(n+1)\right) - 1 \right] \tag{5.64}$$

where

$$\tau_+(n) \equiv \tau_1(n) + i\tau_2(n) \equiv \phi_1^{+}(n)\phi_2(n) \tag{5.65}$$

$$\tau_-(n) \equiv \tau_1(n) - i\tau_2(n) \equiv \phi_2^{+}(n)\phi_1(n) \tag{5.66}$$

$$\tau_3(n) \equiv \frac{1}{2}\left\{ \phi_1^{+}(n)\phi_1(n) - \phi_2^{+}(n)\phi_2(n) \right\} \tag{5.67}$$

so that

$$\left[\tau_i(n), \tau_j(m)\right] = i\,\epsilon_{ijk}\,\tau_k(n)\,\delta_{nm}. \tag{5.68}$$

Consider first the {<up>, <down>} subspace. Recall (fig. 5.1) that the fermion configuration at each site has isospin zero, so the $\underline{\tau}(n).\underline{\tau}(n+1)$ interaction in (5.64) vanishes. The remaining term is simplified by defining

$$S(n) \equiv \frac{1}{2}\left\{ \rho_1(n) + \rho_2(n) \right\}. \tag{5.69}$$

Then S(n) takes values ±1 and the effective Hamiltonian is

$$W_{eff} = x^2 \sum_n \left[S(n) S(n+1) - 1 \right] \qquad (5.70)$$

which is just an Ising antiferromagnetic chain. For this reason the {<up>,<down>} subspace will be called the Ising subspace. The ground state of (5.70) is well known. It is the doubly-degenerate state with

$$\langle 0 | S(n) | 0 \rangle = - \langle 0 | S(n+1) | 0 \rangle \quad \forall n \qquad (5.71)$$

c.f. (3.63) and (3.64). The two vacua are related by a shift through one lattice spacing. They are just the states (5.62a) and (5.62b). The existence of two solutions corresponds to spontaneous breaking of discrete chiral symmetry on the lattice, as was the case for the single-species Schwinger model. The energy density for the Ising ground state (at second order) is

$$\frac{\omega_o}{N} = -2x^2 \qquad (5.72)$$

on a periodic lattice of N (even) sites.

In the {<in>,<out>} subspace, it is the Ising term in (5.64) which vanishes, leaving

$$W_{eff} = x^2 \sum_n \left[4 \underline{\tau}(n) . \underline{\tau}(n+1) - 1 \right] \qquad (5.73)$$

This is the Hamiltonian for a quantum Heisenberg antiferromagnetic spin-$\frac{1}{2}$ chain. So we will call the {<in>,<out>} subspace the Heisenberg subspace. The determination of the vacuum is considerably more complicated than the comparable problem for an Ising chain. Bethe (1931) and later Hulthén (1938) first solved the problem (see Thompson 1972, and references therein) and found the vacuum to be a linear combination of all basis states containing an equal number of $\tau_3 = +\frac{1}{2}$ and $\tau_3 = -\frac{1}{2}$ sites with total spin zero. The vacuum is non-degenerate, and so is symmetric under discrete chiral transformations. The energy density is a function of the number of lattice sites N, and

$$\frac{\omega_0}{N} \xrightarrow[N\to\infty]{} -(4\ln 2)x^2 = -2.77x^2 \qquad (5.74)$$

This result is only valid to second order in x, but it shows (c.f. (5.72)) that the massless theory for either lattice favours the Heisenberg vacuum. Further, it confirms our expectation that there should be no spontaneous breakdown of the SU(2) x SU(2) symmetry of the massless lattice theory (Coleman 1973).

Next consider what happens when the fermion masses are switched on. The behaviour of the vacuum is easiest to understand when the two flavours have equal masses, though the results are qualitatively the same for arbitrary non-zero masses. It is important to recognise the relative magnitudes of the mass terms and the interactions in (5.64). To this end we factor out the dependence on $\sqrt{x}$ by defining

$$f \equiv \frac{4m}{g}, \qquad z \equiv \sqrt{x} \qquad (5.75)$$

so that, from (5.51),

$$2\mu \equiv fz. \tag{5.76}$$

Then, from (5.47) and (5.48), the mass terms are

$$\begin{aligned} M_I &= \frac{f\beta}{4} \sum_n (-1)^n [\rho_1(n) + \rho_2(n)] \\ &= \frac{f\beta}{2} \sum_n (-1)^n S(n) \end{aligned} \tag{5.77}$$

for lattice I, and

$$M_{II} = f\beta \sum_n (-1)^n \tau_3(n) \tag{5.78}$$

for lattice II, where we have used (5.55), (5.69) and (5.67). These have to be compared with the effective Hamiltonian for the massless theory (5.64):

$$W_{eff} = \beta^4 \sum_n [4\underline{\tau}(n).\underline{\tau}(n+1) + S(n)S(n+1) - 1] \tag{5.79}$$

The vacua of the two lattice theories behave quite differently as functions of f. For lattice I the mass term (5.77) contributes zero energy in the Heisenberg subspace. In the Ising subspace it selects the one configuration,

$$\langle 0|S(n)|0\rangle = (-1)^{n+1} \quad \forall n, \tag{5.80}$$

corresponding to (5.62a), with the lower energy density of $-\frac{1}{2}fz$. Hence, for lattice I, the total energy densities of the lowest-lying states in each subspace are:

$$\left(\frac{\omega_o}{N}\right)_I = -\frac{1}{2} fz - 2z^4 \quad \text{(Ising subspace)} \qquad (5.81)$$

and

$$\left(\frac{\omega_o}{N}\right)_I = -2.77\, z^4 \qquad \text{(Heisenberg subspace)} \qquad (5.82)$$

These results are valid in perturbation theory to order z^4. To this order, the true vacuum for lattice I is whichever of these two states has lowest energy for the given value of f. For f large enough (weak coupling) the spontaneous-symmetry-breaking Ising vacuum must win for any finite z. Hence there is a phase transition on lattice I, between chirally symmetric and unsymmetric phases. It is interesting to compare this behaviour with the single-species Schwinger model, where the mass term also breaks chiral symmetry, but this symmetry remains broken in the massless limit.

The phase transition on lattice I is first order, because there is no other state in the Ising subspace which becomes degenerate with the ground state at any order of perturbation theory. Further, there is a discontinuity in the derivative of the ground state energy at the transition; see fig. 5.2. Of course, we can only trust our results for the vacuum energy for small values of z where higher order terms in the perturbation expansions (5.81) and (5.82) can be neglected. So, for sufficiently large lattice spacing, the line of first order transitions separating the Ising and Heisenberg subspaces is

$$f^* \simeq 1.55\, z^3 + \cdots \qquad (5.83)$$

and the resulting phase diagram is shown in fig. 5.3. The dashed line is meant to indicate that for large z higher order terms will be important and could modify the phase diagram.

Remarkably the situation for lattice II is a lot different. The mass term (5.78) always favours the Heisenberg subspace, as does W_{eff} (5.79). So the vacuum belongs to this subspace for all values of f. It is the ground state of the effective Hamiltonian

$$W_{eff} = \sum_n \left[4\beta^4 \underline{\tau}(n).\underline{\tau}(n+1) + (-1)^n f\beta \tau_3(n) \right] \qquad (5.84)$$

which is just the Heisenberg antiferromagnet in an applied staggered magnetic field. There is no phase transition in this model; as f varies, the vacuum changes continuously. For $f \neq 0$ the ground state is very strongly magnetised, since z is small. Effectively, only the single basis state for which

$$\langle \tau_3(n) \rangle = \frac{(-1)^{n+1}}{2} \qquad (5.85)$$

contributes to the linear combination which is the vacuum. So, again, chiral symmetry is broken (by the mass term). But now, as f decreases to zero, other basis states with equal numbers of <in> and <out> sites contribute more and more to the vacuum, until exactly at $f = 0$ all these basis states contribute equally, forming the isotropic Heisenberg antiferromagnetic ground state. The region over which this

transition to a chirally symmetric vacuum occurs is $f \lesssim 4z^3$ and is vanishingly small for perturbation theory.

Of course, the description of the phase diagram for lattice II, offered by (5.84), is valid only to the extent that we can trust the low order perturbative calculations. Nevertheless, it indicates that the continuum physics for small fermion masses may be more accessible to lattice II than lattice I.

Perturbation theory on the lattice is an expansion around $z = 0$. So, for both lattice theories the perturbative vacuum, on which to base our calcualtions of the particle spectrum, is the single "classical" Néel state with antiparallel spins; either (5.80) or (5.85). For weak coupling ($m >> g$) this approach has not been discredited. Even for strong coupling ($m << g$) this may not be such a bad starting point for calculating the low-lying excitations of the Heisenberg antiferromagnet (e.g. Mattis 1965), particularly for lattice II when $0 < m/g << 1$. What is worrying is that the continuum theory appears to be separated from lattice I by a phase transition.

It is difficult to say anything quantitative about the particle spectrum for strong coupling, when the vacuum is a non-trivial state in the Heisenberg subspace. A perturbative calculation around such a vacuum is very difficult. At best we can talk about the low-lying excitations of the Heisenberg antiferromagnet, bearing in mind that this only corresponds to the first non-trivial order in our perturbation expansion. Certainly, for small x, the lowest-lying particle excitations must themselves belong to the Heisenberg subspace. This is because they must be fluxless if they are not to have high masses of order ag^2.

Immediately, this reveals another shortcoming of lattice I. The perturbative calculation we are leading up to, is based on the Ising vacuum, which cannot support fluxless states. So, in this formulation all the particle states start at zeroth order with masses of order ag^2. Not until our perturbation expansions are valid for quite large values of $x \sim (g/m)^{4/3}$ can we expect convergence to the strong-coupling results (5.27) or (5.28). Lattice II fares better; since it always remains in the Heisenberg subspace, even the perturbative vacuum supports fluxless states. However, now we have to expect the perturbation expansion to involve mass poles $\sim \left(\frac{m}{g}\right)^{-1}$, heralding the degeneracy problem which develops as $\frac{m}{g} \to 0$.

Little is known about the low-energy excitations of the Heisenberg antiferromagnet. In the zero-mass limit the isotropic Hamiltonian (5.73) applies to both models. This is well-known to have massless excitations as a consequence of rotational invariance. These form a triplet of spin 1 magnons (Des Cloizeaux and Pearson 1962) and correspond to the pseudoscalar isotriplet of the SU(2) Schwinger model. For example, the $I_3 = +1$ member of this isotriplet is created by applying τ_+ to the vacuum. The resulting state can be interpreted as a quark of flavour 1 and an antiquark of flavour 2 on the same site, propagating along the lattice with momentum k. The energy of this state is proportional to $\frac{1}{a}|\sin ka|$ and so the particle is massless in the continuum limit. Since it consists of a quark and antiquark on the same site, the state can only have even spatial parity and hence odd total parity. So these spin 1 magnons are just what remains of the 'pions' discovered by Coleman in the continuum theory. Notice that if

a small, but non-zero, mass is given to the quarks the rotational symmetry of the effective Hamiltonian is broken. A gap appears in the excitation spectrum, giving the spin-1 magnons a mass which vanishes with the quark mass.

Coleman also finds a low-lying 0^+ state. This should occur amongst the two spin-1 magnon bound states, if any exist. Recent calculations by Endo and Ishikawa (1974) suggest that one such bound state with spin zero (i.e. isospin zero), which fits the bill, does exist below the free two-magnon band. If there are no other low-lying excitations of the Heisenberg antiferromagnet, then the qualitative agreement with the strongly coupled continuum SU(2) Schwinger model is remarkable.

Summary

Doubling the number of fermion species in the Schwinger model results in a non-trivial extension of both the continuum and lattice theories. Both derive their motivation from the QCD of non-strange hadrons, but differ in having a restoration of chiral symmetry as the quark mass vanishes. The low-energy spectrum of the continuum theory is known for both strong and weak coupling, and includes a pion-like excitation. This makes the lattice theory worth studying. However, an ambiguity arises in the lattice formulation. Two theories are possible which for large lattice spacing are quite distinct. There are indications that the two approximation schemes converge at different rates.

CHAPTER 6

PARTICLE SPECTRUM CALCULATIONS FOR THE SU(2) SCHWINGER MODEL

Our investigation into lattice methods culminates with a calculation of the particle spectrum of the SU(2) Schwinger model. Although this does not take us out of one spatial dimension, it is still a demanding test of the theory. The continuum model has a non-trivial spectrum for strong coupling and all the techniques, which were developed in simpler contexts, are called upon to extract reliable continuum predictions over the whole coupling constant range.

We ask for the extent to which various features of the continuum theory are reproduced by the lattice calculation. Of particular concern is the vanishing of the 'pion' mass with that of the fermion. An understanding of how this may be achieved in 1+1 dimensions, may shed some light on the 3+1 dimensional problem. The underlying question seems to be the ambiguity in the lattice formulation, which allows two distinct cut-off theories. At low orders in perturbation theory these have quite different particle spectra. So it is important to compare the rates of convergence of the two approximation schemes as the cut-off is removed. Given that there is a practical limit on the order of the perturbation expansion, one might provide a better treatment of the 'pion' than the other. This can only be tested by explicit calculations.

The calculations are more complicated than for the single-species Schwinger model. Lattice I requires just a straightforward extension of the method used there. But for lattice II there are several sources of difficulty. One problem is that there is not always a unique choice of unperturbed lattice state which can be expected to give convergence for all coupling strengths. This drives us to doing matrix calculations. For practical reasons, these are only carried out to fourth order in the perturbation. Also, our experience with the single-species model suggests that dependence of the continuum estimates on the fermion mass will be trivial until eighth order. Unfortunately, at that order, the lattice II calculation faces unpleasant degeneracy problems, which require careful handling. For both lattices, the reliance on non-zero-lattice-spacing estimates is no different from the single-species calculation.

(a) The Unperturbed Particle States.

Particle states on either lattice are gauge invariant combinations of quarks, antiquarks and flux lines. The zero momentum states are constructed by allowing the appropriate lattice versions of the spatial integrals of various continuum currents to operate on the vacuum. This does not uniquely determine the lattice states; we select the lowest-lying eigenstate of $W^{o}_{I,II}$ (5.47), (5.48), with the correct quantum numbers, as the basis of our perturbation expansion. The relevant quantities are parity and flavour content (actually, we can use isospin on lattice I when $m_1 = m_2$). Thus, for example, a meson composed of a quark of flavour i and an antiquark of flavour j carries labels $i\bar{j}$, plus a parity designation.

The low-lying states of lattice I are reminiscent of the single-species model. Recall that the perturbative vacuum, $|0\rangle_I$, belongs to the Ising subspace and is given by, (5.80),

$$\phi_i(2n)|0\rangle_I = \phi_i^\dagger(2n+1)|0\rangle_I = 0 \quad (i=1,2) \tag{6.1}$$

The pseudoscalar meson states are obtained by applying the spatial integral of the vector current $\bar{\psi}_i\gamma_1\psi_j$ to $|0\rangle_I$. Using the identification (5.33) and inserting the connection to ensure local gauge invariance, gives

$$|i\bar{j}-\rangle_I = \frac{1}{\sqrt{N}}\sum_n \left[\phi_i^\dagger(n)\,U(n,n+1)\,\phi_j(n+1) - \phi_j(n)\,U^\dagger(n,n+1)\,\phi_i^\dagger(n+1)\right]|0\rangle_I \tag{6.2}$$

Here we abide by the usual convention of normalising all states to unity on a finite periodic lattice of N(even) sites. The scalar density $\bar{\psi}_i\psi_j$ is diagonal for $i = j$ and annihilates the vacuum for $i \neq j$. The alternative is to use the kinetic part of the Hamiltonian, (5.49), to create scalar excitations:

$$|i\bar{j}+\rangle_I = \frac{1}{\sqrt{N}}\sum_n \left[\phi_i^\dagger(n)\,U(n,n+1)\,\phi_j(n+1) + \phi_j(n)\,U^\dagger(n,n+1)\,\phi_i^\dagger(n+1)\right]|0\rangle_I \tag{6.3}$$

Both (6.2) and (6.3) are 1-link states at rest relative to the lattice. They are the lowest-lying eigenstates of W_I^o, (5.47),

$$W_I^o\,|i\bar{j}\pm\rangle_I = (1+\mu_i+\mu_j)\,|i\bar{j}\pm\rangle_I. \tag{6.4}$$

When the quark flavours have equal mass ($\mu_1 = \mu_2 = \mu$), W_I is isospin symmetric, so the states (6.2) and (6.3) can be given isospin classifications. The two multiplets (I^P)

$$1^-: \begin{cases} |1\bar{2}-\rangle_I \\ \frac{1}{\sqrt{2}}\left(|1\bar{1}-\rangle_I - |2\bar{2}-\rangle_I\right) \\ |2\bar{1}-\rangle_I \end{cases} \tag{6.5}$$

and

$$0^+: \frac{1}{\sqrt{2}}\left(|1\bar{1}+\rangle_I + |2\bar{2}+\rangle_I\right) \tag{6.6}$$

correspond to the continuum particle states which have low mass for strong coupling. Of the remaining isomultiplets

$$0^-: \frac{1}{\sqrt{2}}\left(|1\bar{1}-\rangle_I + |2\bar{2}-\rangle_I\right) \tag{6.7}$$

corresponds to the pseudoscalar isosinglet, and

$$1^+: \begin{cases} |1\bar{2}+\rangle_I \\ \frac{1}{\sqrt{2}}\left(|1\bar{1}+\rangle_I - |2\bar{2}+\rangle_I\right) \\ |2\bar{1}+\rangle_I \end{cases} \tag{6.8}$$

corresponds to the scalar isotriplet both of which have high mass in the strong-coupling limit.

The low-energy eigenstates of W^{o}_{II}, (5.48), are quite different. There is no isospin symmetry in the massive theory and the perturbative vacuum, $|0\rangle_{II}$, is the "classical" state, (5.85),

$$\phi_1(2n)|0\rangle_{II} = \phi_1^{+}(2n+1)|0\rangle_{II} = 0$$

$$\phi_2^{+}(2n)|0\rangle_{II} = \phi_2(2n+1)|0\rangle_{II} = 0. \qquad (6.9)$$

This vacuum supports fluxless states which have lower zeroth order energy than states containing flux.

First, we consider the low-energy eigenstates of W^{o}_{II} corresponding to the continuum particles which have low mass for strong coupling. Using the vector currents $\bar{\psi}_1\gamma_1\psi_2$ and $\bar{\psi}_2\gamma_1\psi_1$ as before, but now with prescription (5.34), leads to the zero-momentum states

$$|1\bar{2}-\rangle_{II} = \sqrt{\frac{2}{N}} \sum_{n\ even} \phi_1^{+}(n)\phi_2(n)|0\rangle_{II} \qquad (6.10)$$

and

$$|2\bar{1}-\rangle_{II} = \sqrt{\frac{2}{N}} \sum_{n\ odd} \phi_2^{+}(n)\phi_1(n)|0\rangle_{II}. \qquad (6.11)$$

These are locally gauge invariant, because they only involve products of quark fields at the same site. (6.10) and (6.11) contribute to the $I_3 = \pm 1$ pseudoscalar states respectively, and, consisting of just a quark-antiquark pair, are the lowest energy eigenstates of W^{o}_{II} to do so. They have unperturbed energy $\mu_1 + \mu_2$, which vanishes with the quark masses. Notice that these states are obtained by applying $\tau_{\pm}$ of (5.65), (5.66) to the Néel state $|0\rangle_{II}$, and so conform to the naive

idea of spin waves in a Heisenberg antiferromagnet.

The $I_3 = 0$ member of the pseudoscalar isotriplet does not have a unique counterpart on lattice II. The vector currents $\bar{\psi}_1\gamma_1\psi_1$ and $\bar{\psi}_2\gamma_1\psi_2$ and prescription (5.34) suggest the states

$$|i\bar{i}\rangle_{II} = \frac{1}{\sqrt{N}}\sum_n \left[\phi_i^+(n)\,U(n,n+1)\,\phi_i(n+1) - \phi_i(n)\,U^+(n,n+1)\,\phi_i^+(n+1)\right]|0\rangle_{II} \tag{6.12}$$

(no sum on i). These contain one unit of flux, and are not the best choice. The perturbation V, (5.49), connects these to the lower-lying state

$$|1\bar{2},2\bar{1}\rangle_{II} = \frac{i}{\sqrt{N}}\sum_n \left[\phi_1^+(n)\phi_2(n)\,\phi_2^+(n+1)\phi_1(n+1) - \phi_2^+(n)\phi_1(n)\,\phi_1^+(n+1)\phi_2(n+1)\right]|0\rangle_{II}. \tag{6.13}$$

This is a four-quark state, consisting of two quark-antiquark pairs on neighbouring sites. Its unperturbed energy is $2\mu_1 + 2\mu_2$, to be compared with $1 + 2\mu_i$ for the two states in (6.12). Thus (6.13) is a better choice for perturbation theory, and its flavour-symmetric mass should favour the restoration of isospin symmetry. Nevertheless, for weak coupling the appropriate linear combination of two-quark states (6.12) is expected to dominate. Thus, we can anticipate the possibility of level-crossing (or, more likely, level-repulsion) as m_i/g varies, and the need for quasi-degenerate perturbation theory to give a complete treatment of this state. Notice that the important state in the strong coupling regime, (6.13), looks rather like a bound state of two spin waves in the linearised Heisenberg antiferromagnet.

The remaining continuum particle which has low mass for strong coupling, also has $I_3 = 0$; it is a scalar isosinglet. The same problem of identifying the relevant lattice state occurs. The appropriate choice is the even parity version of (6.13):

$$|1\bar{2}, 2\bar{1}+\rangle_{II} = \frac{i}{\sqrt{N}} \sum_n \left[\phi_1^+(n)\phi_2(n)\phi_2^+(n+1)\phi_1(n+1) + \phi_2^+(n)\phi_1(n)\phi_1^+(n+1)\phi_2(n+1) \right] |0\rangle_{II} \quad (6.14)$$

with unperturbed energy $2\mu_1 + 2\mu_2$. But for weak coupling a linear combination of the states

$$|i\bar{i}+\rangle_{II} = \frac{1}{\sqrt{N}} \sum_n \left[\phi_i^+(n) U(n,n+1) \phi_i(n+1) + \phi_i(n) U^+(n,n+1) \phi_i^+(n+1) \right] |0\rangle_{II} \quad (6.15)$$

whose unperturbed energies are $1 + 2\mu_i$ respectively, becomes important.

The identification of lattice II states corresponding to continuum particles which have high masses for strong coupling will concern us less. These states should contain at least one unit of flux. The lowest-energy eigenstates of W^o_{II} which correspond (in some linear combination) to the pseudoscalar isosinglet, 0^-, are just those in (6.12). Likewise, the $I_3 = 0$ member of the scalar isotriplet, 1^+, can be identified with the linear combination of states in (6.15) which is orthogonal to the combination used for the 0^+ particle. There is an ambiguity now in the identification of the $I_3 = \pm 1$ members of this isotriplet. The lowest-lying two-quark states involve two units of flux:

$$|1\bar{2}+\rangle_{II} = \frac{1}{\sqrt{N}} \sum_{n\ \text{even}} [\phi_1^+(n) U(n,n+1) U(n+1,n+2) \phi_2(n+2) + \phi_2(n) U^+(n,n+1) U^+(n+1,n+2) \phi_1^+(n+2)] |0\rangle_{II} \tag{6.16}$$

and similarly for $|2\bar{1}+\rangle_{II}$. But these are connected by the perturbation to four-quark states

$$|1\bar{2}, 2\bar{2}+\rangle_{II} = \frac{i}{\sqrt{N}} \sum_n [\phi_1^+(n)\phi_2(n)\phi_2^+(n+1) U(n+1,n+2)\phi_2(n+2) + \phi_2(n) U^+(n,n+1)\phi_2^+(n+1)\phi_2(n+2)\phi_1^+(n+2)] |0\rangle_{II} \tag{6.17}$$

and

$$|1\bar{1}, 1\bar{2}+\rangle_{II} = \frac{i}{\sqrt{N}} \sum_n [\phi_1^+(n) U(n,n+1)\phi_1(n+1)\phi_1^+(n+2)\phi_2(n+2) + \phi_2(n)\phi_1^+(n)\phi_1(n+1) U^+(n+1,n+2)\phi_1^+(n+2)] |0\rangle_{II} \tag{6.18}$$

which contain only one unit of flux, and so have lower energy for large lattice spacing. (The six-quark states obtained by applying V a second time, all vanish).

The zeroth order particle spectra of the two lattice theories are clearly quite different. For large lattice spacing, the low-lying particle states of lattice I are approximately degenerate, with rescaled masses ~ 1. While, on lattice II, those states identified with the continuum particles which Coleman (1976) finds have low mass for strong coupling, start with approximately zero rescaled mass, whereas the states identified with high mass continuum particles start with rescaled masses ~ 1. This seems to favour lattice II above lattice I as a starting point for perturbation theory in the strong-coupling regime.

The opposite may be true for weak coupling. In addition, lattice I possesses isospin symmetry when the quarks have equal mass, which may give it an advantage.

(b) Mass Matrices for $(1,0)^-$ and 0^+ Mesons of Lattice II.

For arbitrary quark masses there are three states around which a perturbation expansion for the $(I, I_3)^P = (1,0)^-$ (or 0^+) meson mass can be constructed. These are (6.12) and (6.13) (or (6.14) and (6.15)). The four-quark states are expected to dominate the strong-coupling region ($m_i \ll g$), while the two-quark states take over in the weak-coupling region ($m_i \gg g$). So a good convergence of this mass, at all coupling strengths, is unlikely to result from a perturbation expansion about one of the states alone, although they are non-degenerate. Instead, quasi-degenerate perturbation theory is necessary and the resulting expansion for the Hamiltonian diagonalised in the subspace spanned by the three states.

Even to fourth order this calculation is difficult. It can be simplified if we concern ourselves solely with equal-mass quarks. Then the problem reduces to a two-state calculation, because it is possible to diagonalise the full Hamiltonian in the degenerate subspace spanned by the two-quark states. The results are not sufficiently encouraging to make the three-state calculation worthwhile. Nevertheless, the two-state calculation serves as a useful illustration, and provides access to both ordinary and matrix Padé approximants for the meson mass.

For equal-mass quarks, the pairs of states connected by the perturbation are:

$$(1,0)^-: \begin{cases} |4q-\rangle \equiv |1\bar{2}, 2\bar{1}-\rangle_{II} \\ |2q-\rangle \equiv \frac{1}{\sqrt{2}}\left(|1\bar{1}-\rangle_{II} - |2\bar{2}-\rangle_{II}\right) \end{cases} \qquad (6.19)$$

and

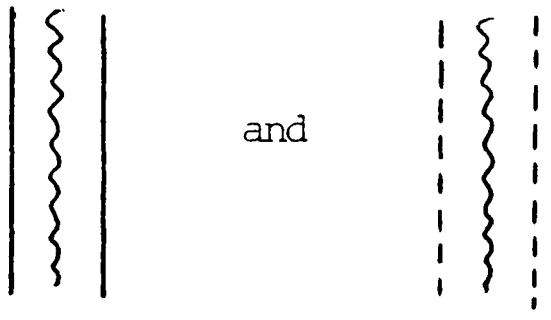
$$0^+: \begin{cases} |4q+\rangle \equiv |1\bar{2}, 2\bar{1}+\rangle_{II} \\ |2q+\rangle \equiv \frac{1}{\sqrt{2}}\left(|1\bar{1}+\rangle_{II} + |2\bar{2}+\rangle_{II}\right) \end{cases} \qquad (6.20)$$

We expand the Hamiltonian in each subspace to fourth order in V. The whole calculation would take too long to present here, so we content ourselves with describing the first non-trivial contribution to each matrix element. The calculations for the pseudoscalar and scalar mass matrices are carried out side-by-side; where the two results differ, the one for the scalar meson is given afterwards in parentheses.

The general formula for the perturbation expansion is given in (B.32). Only even orders contribute to diagonal matrix elements and only odd orders to off-diagonal matrix elements. In the diagrams there is a solid (broken) vertical line for each quark of flavour 1(2) and a vertical wiggly line for each unit of flux. Thus, the zeroth order four-quark state is represented by



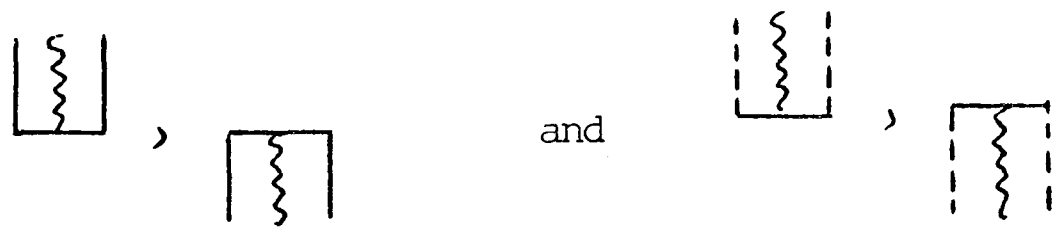
and the zeroth order two-quark states are represented by



The matrix for W^{o}_{II}, (5.48), in either subspace (6.19), or (6.20), is

$$\text{zeroth order} = \begin{pmatrix} 4\mu & 0 \\ 0 & 1+2\mu \end{pmatrix} \qquad (6.21)$$

The action of the perturbation V, (5.49), is to create and destroy quark-antiquark pairs with the same flavour, denoted by the vertices

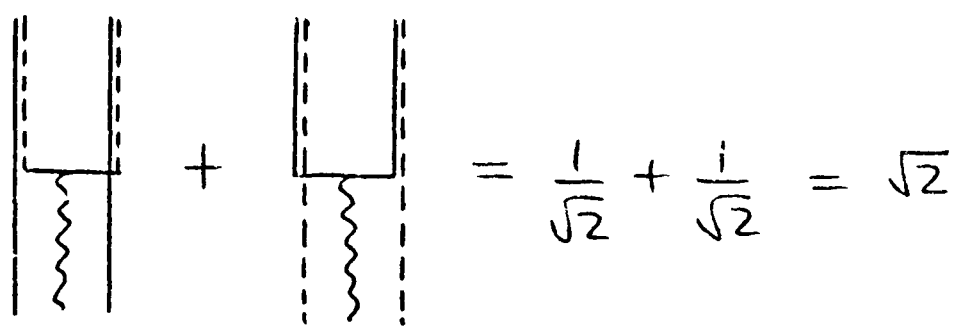


Now fermi statistics allows a maximum of two fermions per site, provided they have different flavours. This leads to the appearance of overlapping graphs. Otherwise, the diagrammatics is much the same as for the ordinary Schwinger model (Banks et al. 1976).

The first order matrix is

$$PVP \qquad (6.22)$$

and only its off-diagonal elements are non-zero. These are equal and given by



(6.23)

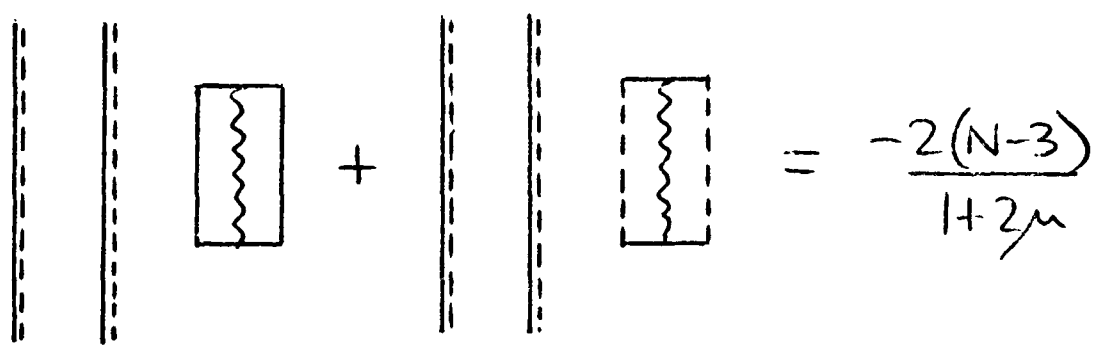
This result follows directly from the definitions of the states in (6.19). So,

$$\text{first order} = \chi \begin{pmatrix} 0 & \sqrt{2} \\ \sqrt{2} & 0 \end{pmatrix} \tag{6.24}$$

The second order matrix is

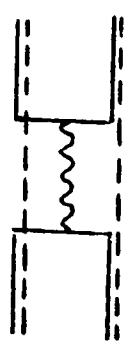
$$PVg_4VP_4 + PVg_2VP_2 \tag{6.25}$$

and only its diagonal elements are non-zero. The one between four-quark states is the same for scalar and pseudoscalar. It is

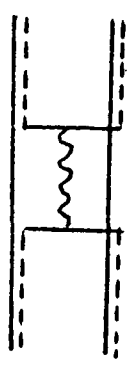


(6.26)

Here fermi statistics forbids the vacuum fluctuation from occupying the two links adjacent to the through-going particle. Notice that the graphs

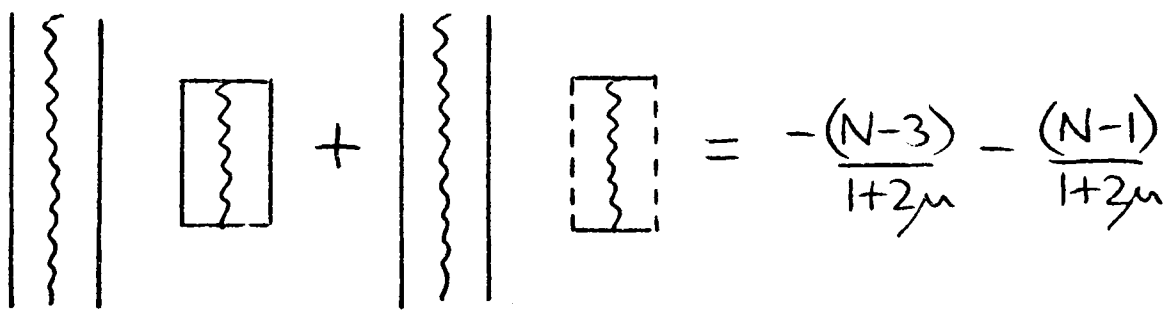


and



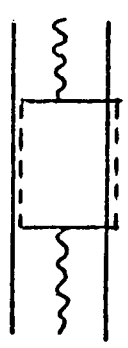
allowed in the ordinary perturbation expansion for the mass of the four-quark state, are forbidden here by g_4.

To save space when calculating the diagonal element between two-quark states, we just draw the graphs for which the incoming quark-antiquark pair have flavour 1. The graphs are of two types. Those involving a single vacuum fluctuation,

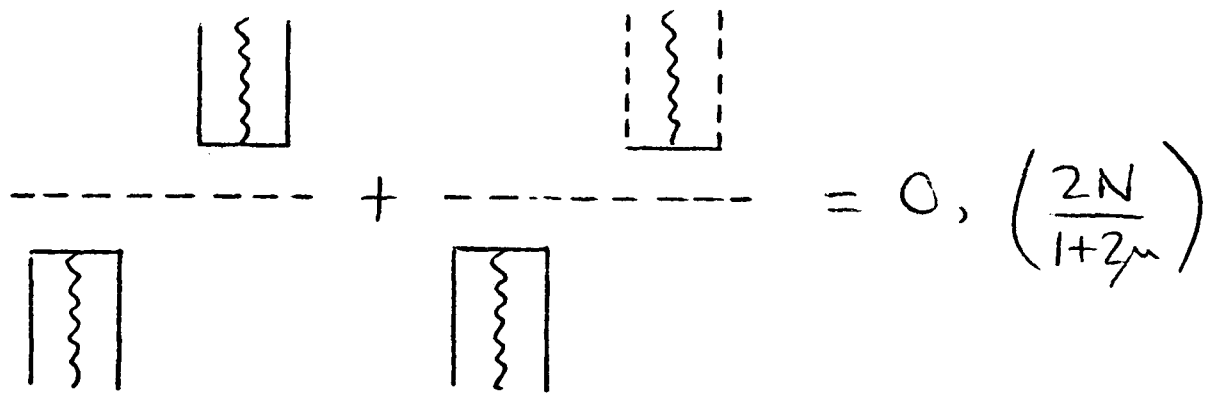


(6.27)

are the same for scalar and pseudoscalar. Notice that the vacuum fluctuation is allowed on the two links adjacent to the through-going particle when the flavours of the quarks comprising the two are different. Again, the overlapping graph

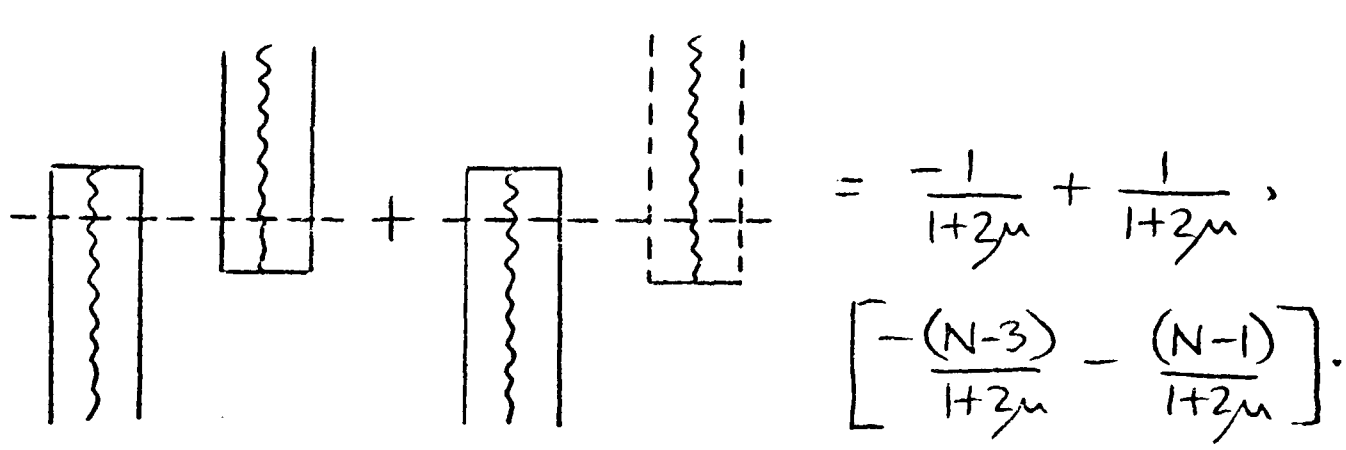


allowed in the ordinary perturbation expansion for the two-quark state's mass, is forbidden here by g_2. In the second type of graph, the perturbation destroys the incoming state and recreates it on another (possibly the same) site. The intermediate state may be the vacuum:



(6.28)

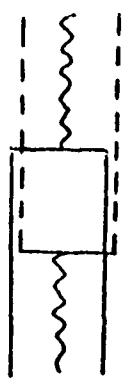
or a two particle state



(6.29)

For pseudoscalars, care must be taken in counting these graphs, because, when the incoming and outgoing particle are on adjacent links or separated by an even number of links the graph carries an extra minus sign.

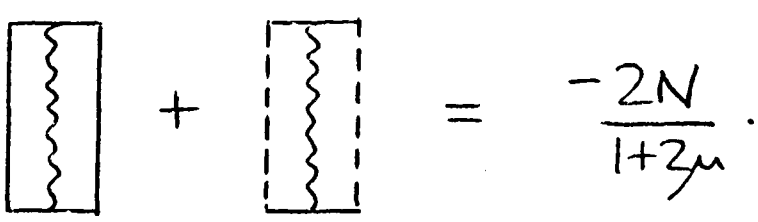
The overlapping graph



is again forbidden by g_2. Collecting the contributions (6.26)-(6.29) gives

$$\text{second order} = x^2 \begin{pmatrix} -\frac{2(N-3)}{1+2\mu} & 0 \\ 0 & -\frac{2(N-2)}{1+2\mu}, \left[-\frac{2(N-4)}{1+2\mu}\right] \end{pmatrix} \tag{6.30}$$

Of course, at second order there is a shift in the vacuum energy, given by



$$= \frac{-2N}{1+2\mu}. \tag{6.31}$$

Subtracting this form (6.30) restores the intensive character of the mass matrix.

Continuing in the same vein, we obtain to fourth order in V, the pseudoscalar mass matrix

$$\underline{W}^- = \begin{pmatrix} 4\mu & 0 \\ 0 & 1+2\mu \end{pmatrix} + x\begin{pmatrix} 0 & \sqrt{2} \\ \sqrt{2} & 0 \end{pmatrix}$$

$$+x^2\begin{pmatrix} \frac{6}{1+2\mu} & 0 \\ 0 & \frac{4}{1+2\mu} \end{pmatrix} + x^3\begin{pmatrix} 0 & \frac{1}{\sqrt{2}\mu(1+2\mu)} \\ 0 & 0 \end{pmatrix}$$

$$+x^4\begin{pmatrix} \frac{3-24\mu-4\mu^2}{\mu(1+2\mu)^3} & 0 \\ 0 & \frac{2-16\mu-4\mu^2}{\mu(1+2\mu)^3} \end{pmatrix} + O(x^5)$$

(6.32)

and the scalar mass matrix

$$\underline{W}^+ = \begin{pmatrix} 4\mu & 0 \\ 0 & 1+2\mu \end{pmatrix} + x\begin{pmatrix} 0 & \sqrt{2} \\ \sqrt{2} & 0 \end{pmatrix}$$

$$+x^2\begin{pmatrix} \frac{6}{1+2\mu} & 0 \\ 0 & \frac{8}{1+2\mu} \end{pmatrix} + x^3\begin{pmatrix} 0 & \frac{-3}{\sqrt{2}\mu(1+2\mu)} \\ \frac{-2\sqrt{2}}{1+2\mu} & 0 \end{pmatrix}$$

$$+x^4\begin{pmatrix} \frac{3-24\mu-4\mu^2}{\mu(1+2\mu)^3} & 0 \\ 0 & \frac{6-44\mu-12\mu^2}{\mu(1+2\mu)^3} \end{pmatrix} + O(x^5).$$

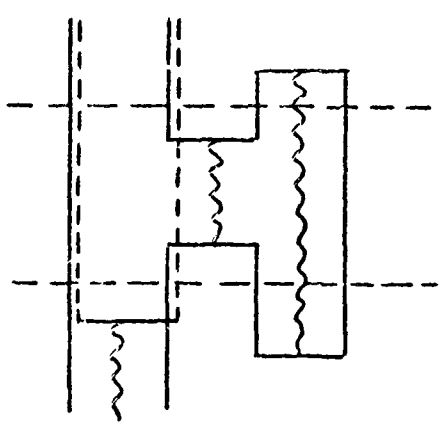
(6.33)

Because of the $\sqrt{x}$-dependence of μ, these must be regarded as series expansions in $\sqrt{x}$. But now the appearance of denominators proportional to μ (the mass poles which warn us that all fluxless states become degenerate in the massless limit) means that at any given order in V there may be contributions to lower order in $\sqrt{x}$ than we might naively expect from regarding μ as a constant. In particular, our perturbation expansion to fourth order in V may not be valid to eighth order in $\sqrt{x}$, because of contributions coming from higher orders in V, which we have neglected. This must be checked before we can proceed to construct Padé approximants.

At fifth order in V only the off-diagonal matrix elements are non-vanishing. These involve subtraction terms which are potentially $\sim x^5/\mu^3$. However, they are all multiplied by

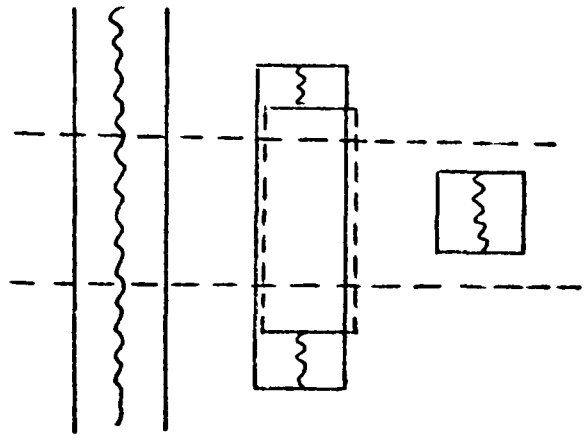
$$\langle 2q|V|2q\rangle = 0 \text{ , or } \langle 4q|V|4q\rangle = 0.$$

So the worst contribution is $\sim x^5/\mu^2$ and comes from direct fifth-order graphs, like



As a consequence the off-diagonal terms in $\underline{W}^{\pm}$ are only valid to order $(\sqrt{x})^7$. Similarly, the terms from sixth order in V, which contribute to

the lowest order in $\sqrt{x}$, are $\sim x^6/\mu^2$ and come from graphs like



So the diagonal terms in $\underline{W}^{\pm}$ are valid to order $(\sqrt{x})^9$.

The elements of the matrices $\underline{W}^{\pm}$ in (6.32) and (6.33) are known sufficiently accurately to determine the eigenvalues correctly to order $(\sqrt{x})^9$. This is because only the product of off-diagonal elements enters the eigenvalues, and this is known to order $(\sqrt{x})^9$. The eigenvalues of the pseudoscalar mass matrix are

$$\frac{2\sqrt{x}}{g} M_{(1,0)^-}\Big|_{4\text{quark}} = 4\mu + x^2\left(\frac{6}{1+2\mu} - \frac{2}{1-2\mu}\right) + x^4\left[\frac{-2}{(1+2\mu)^2} - \frac{28}{(1+2\mu)^3} + \frac{2}{\mu(1+2\mu)^2} + \frac{4}{(1-2\mu)^3} - \frac{4}{(1+2\mu)^2(1-2\mu)} - \frac{4}{(1+2\mu)(1-2\mu)^2}\right] + O(x^5) \quad (6.34)$$

and

$$\frac{2\sqrt{x}}{g} M_{(1,0)^-}\Big|_{2\text{quark}} = 1+2\mu + x^2\left(\frac{4}{1+2\mu} + \frac{2}{1-2\mu}\right) + x^4\left[-\frac{2}{(1+2\mu)^2} - \frac{18}{(1+2\mu)^3} + \frac{3}{\mu(1+2\mu)^2} - \frac{4}{(1-2\mu)^3} + \frac{4}{(1+2\mu)^2(1-2\mu)} + \frac{4}{(1+2\mu)(1-2\mu)^2}\right] + O(x^5). \quad (6.35)$$

The eigenvalues of the scalar mass matrix are

$$\frac{2\sqrt{x}}{g} M_{0^+}\Big|_{4\text{quark}} = 4\mu + x^2\left(\frac{6}{1+2\mu} - \frac{2}{1-2\mu}\right)$$
$$+ x^4\left[\frac{-2}{(1+2\mu)^2} + \frac{4}{(1+2\mu)(1-2\mu)} - \frac{28}{(1+2\mu)^3} + \frac{6}{\mu(1+2\mu)^2}\right.$$
$$\left. + \frac{12}{(1+2\mu)^2(1-2\mu)} + \frac{4}{(1+2\mu)(1-2\mu)^2} + \frac{4}{(1-2\mu)^3}\right] + O(x^5)$$

(6.36)

and

$$\frac{2\sqrt{x}}{g} M_{0^+}\Big|_{2\text{quark}} = 1+2\mu + x^2\left(\frac{8}{1+2\mu} + \frac{2}{1-2\mu}\right)$$
$$+ x^4\left[\frac{-2}{(1+2\mu)^2} - \frac{50}{(1+2\mu)^3} + \frac{3}{\mu(1+2\mu)^2} - \frac{4}{(1-2\mu)^3}\right.$$
$$\left. - \frac{20}{(1+2\mu)^2(1-2\mu)} - \frac{4}{(1+2\mu)(1-2\mu)^2}\right] + O(x^5). \quad (6.37)$$

These are, of course, the same as the results obtained from ordinary non-degenerate perturbation theory (Kenway and Hamer 1978). They can be expanded as power series in $z = \sqrt{x}$ and Padé approximants constructed. The expansions based around the two-quark states, (6.35) and (6.37), require [5,4] Padé approximants, but the continuum estimates obtained are no better than for the single-species Schwinger model, c.f. (3.87), (3.88) i.e. linear dependence on m/g. For the four-quark states z divides out of the series (6.34) and (6.36), allowing [4,4] Padé approximants to be taken. The corresponding continuum estimates are shown in fig. 6.1. Results for the $(1,0)^-$ meson are not unreasonable, but those for the 0^+ meson are badly disfigured by the pole near $\frac{m}{g} = 0$. In each case, the

dashed lines are the exact continuum results. For strong coupling these are (5.27) and (5.28); for weak coupling both masses should be approximately the sum of the constituent quark masses.

Different continuum estimates can be obtained by taking matrix Padé approximants of the series (6.32) and (6.33). In doing so, we make the unjustified assumption that the eigenvalues of the [5,4] matrix Padé approximant are insensitive to the off-diagonal terms of order $(\sqrt{x})^8$. The only alternative, in the absence of higher-order calculations, would be to use lower-order Padé approximants; but these are poorly behaved.

The eigenvalues of the continuum mass matrices, obtained from the [5,4] Padé approximants to (6.32) and (6.33), are plotted as functions of m/g in fig. 6.2. The smallest eigenvalue, in each case, is taken to be our estimate for the particle mass. The estimates for both the pseudoscalar and scalar particles are distorted by poles in the strong-coupling limit. Nevertheless, for $\frac{m}{g} \gtrsim 0.1$ there is a slight hint of the correct strong-coupling behaviour. Again, for weak coupling, the linear dependence on the quark mass is qualitatively correct. Throughout the coupling-constant range, there is a marginal improvement on the results from ordinary Padé approximants.

The construction of matrix Padé approximants to the mass ratio is not so simple. On the whole, at the orders we have available, these are badly behaved. An interesting ratio (which behaves better than average) is obtained by dividing the scalar mass matrix (6.33) by the eigenvalue of the pseudoscalar mass matrix corresponding to the four-quark state. Because the series, (6.34), for this eigenvalue begins

at order $\sqrt{x}$, we need the expansion to order $(\sqrt{x})^{10}$. This is extracted from the computer calculation (see later). The result is a series expansion for a matrix with eigenvalues $zM_{0^+}/M_{(1,0)^-}$, so we take the [5,4] Padé approximant. The continuum eigenvalues are plotted in fig. 6.3. Despite the complicated structure around $\frac{m}{g} \sim 0.25$, this graph has two encouraging features. In the strong-coupling limit one eigenvalue is infinitely large, while the other gives an estimate

$$\frac{M_{0^+}}{M_{(1,0)^-}} \xrightarrow[\frac{m}{g}\to 0]{} 1.214 \qquad (6.38)$$

within 30% of the exact result (5.29). Also, in the weak-coupling limit, both eigenvalues tend to 1, as they should. Although far from satisfactory, this is the best estimate we can obtain from the fourth order calculation.

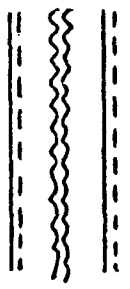
Two conclusions seem forced on us. At fourth order, the matrix calculation does better than ordinary perturbation theory. However, neither gives a true account of the strong-coupling behaviour.

(c) The Strong-Coupling Expansion to High Orders.

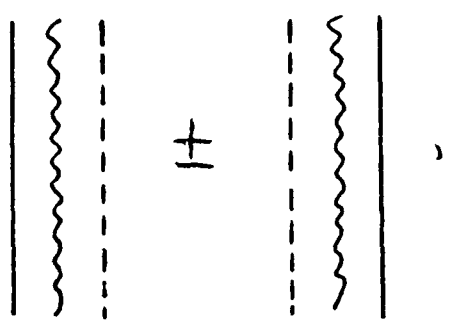
Accurate predictions for the behaviour of continuum particle masses over a wide range of coupling strengths demand lattice calculations to high orders in $\sqrt{x}$. The highest order in perturbation theory currently feasible is eighth. So we strive for consistent expansions of the bound-state masses which incorporate eighth order effects. Since we always work to a fixed order in $\sqrt{x}$, these sometimes

require the inclusion of a few contributions from beyond eighth order in perturbation theory. The matrix calculations are generally too difficult. So, with a few important exceptions, our calculations are based on non-degenerate perturbation theory around single states. All need a computer.

The calculation for lattice I is the more straightforward, because it amounts to a direct generalisation of the techniques used for the single-species Schwinger model. The diagram rules differ slightly from those for lattice II, introduced in the preceding section. This is due solely to the shift of the field for one flavour by one lattice spacing relative to the other. So, for example, a two-quark, two-antiquark state on neighbouring sites now carries two units of flux:



For arbitrary (non-zero) quark masses, the "$I_3 = \pm 1$" states, $|1\bar{2}\pm\rangle_I$ and $|2\bar{1}\pm\rangle_I$, can all be handled by standard non-degenerate perturbation theory. The zeroth order graphs are



where the relative sign between quark-antiquark pairs on different links is determined by the parity of the state. The formula for the perturbation expansion is given in (A.32); only even orders contribute.

For unequal quark masses, the "$I_3 = 0$" states, $|1\bar{1}\pm\rangle_I$ and $|2\bar{2}\pm\rangle_I$, require quasi-degenerate perturbation theory; the perturbation expansion is diagonalised in the two subspaces $\{|1\bar{1}-\rangle_I, |2\bar{2}-\rangle_I\}$ and $\{|1\bar{1}+\rangle_I, |2\bar{2}+\rangle_I\}$. The alternative, when the quarks have equal mass, is to use isospin symmetry to diagonalise the full Hamiltonian in these (degenerate) subspaces. The resulting isospin eigenstates

$$|I=1, I_3=0\pm\rangle_I = \frac{1}{\sqrt{2}}\left(|1\bar{1}\pm\rangle_I - |2\bar{2}\pm\rangle_I\right) \qquad (6.39)$$

and

$$|I=0\pm\rangle_I = \frac{1}{\sqrt{2}}\left(|1\bar{1}\pm\rangle_I + |2\bar{2}\pm\rangle_I\right) \qquad (6.40)$$

are treated by non-degenerate perturbation theory. It turns out that the counting problem is more complicated using the latter method, so it is quicker to treat it as a special case of the calculation for $\mu_1 \neq \mu_2$. However, performing the calculation both ways provides a highly non-trivial check of our results.

The vacuum energy and all the particle masses are calculated to eighth order in V by computer. As for the single-species model, the calculations can be carried out on a finite lattice, big enough to contain all the connected quark-string configurations which occur at eighth order. These are no worse than for one species, so a minimum of six lattice sites is needed. The vacuum energy is subtracted from the particle masses to obtain a finite result independent of the

lattice size. Our results for arbitrary quark masses are presented in table 6.1. The sixth and eighth order results are not included due to lack of space. The number of distinct denominators grows from around 75 at sixth order, to around 750 at eighth order! The results simplify considerably for equal quark masses, and so these are given to sixth order in table 6.2. All results for lattice I have been checked against hand calculations to sixth order in V (Kenway and Hamer 1978).

It is important to understand the validity of these perturbation expansions. As we have already noted, the lattice I formulation does not allow fluxless states. Consequently, there are no energy denominators proportional to μ_i, at any order. (There are, however, denominators proportional to $\mu_1 - \mu_2$ which arise from diagonalising the mass matrices for the "$I_3 = 0$" states). This means that matrix elements which are nth order in V are also nth order in x. Hence, the results of our calculation to eighth order in V are valid to order $(\sqrt{x})^{19}$.

The calculation for the particle spectrum of lattice II proceeds along the lines started in section (b), using standard or quasi-degenerate perturbation theory, whichever is necessary. The problem associated with the degeneracy of all fluxless states in the massless limit afflicts all lattice II calculations. In addition, at eighth order in V there is a more serious degeneracy problem amongst the fluxless states, which must be taken into account.

Those states which correspond to Coleman's (1976) "high mass" particles, receive the usual treatment. The most important of these

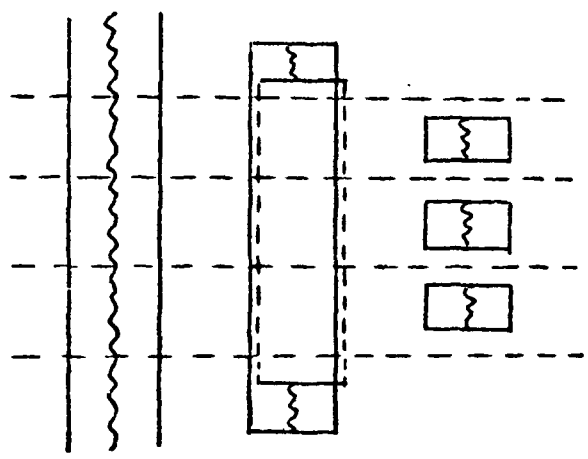
is the fundamental 0^- meson. Its mass is calcualted by diagonalising the perturbation expansion in the subspace $\{|1\bar{1}->_{II}, |2\bar{2}->_{II}\}$, (6.12). The other eigenvalue provides an estimate for the "low mass" $(1,0)^-$ meson. It is not expected to be very accurate for strong coupling, where the four-quark state dominates, but may be our best estimate of this mass for weak coupling. For equal quark masses, the full Hamiltonian may be diagonalised in subspace (6.12); the appropriate combination of states for the 0^- meson is

$$0^- : \frac{1}{\sqrt{2}}\left(|1\bar{1}->_{II} + |2\bar{2}->_{II}\right) \tag{6.41}$$

with the orthogonal combination for the $(1,0)^-$ meson, (6.19).

The other "high mass" particle, whose identification with a lattice state is unambiguous, is the $(1,0)^+$ meson. Its mass is obtained similarly by diagonalising the perturbation expansion in the $\{|1\bar{1}+>_{II}, |2\bar{2}+>_{II}\}$, (6.15), subspace. The other eigenvalue is taken as an estimate for the 0^+ particle mass, and should be good for weak coupling. The masses of the $I_3 = \pm 1$ members of the scalar isotriplet are more difficult to calculate. Even if we ignore the need for a matrix calculation in the subspace spanned by (6.16)-(6.18), the graphical expansion to eighth order for states which spread over two links is too unwieldy for existing computer programmes. Our results (Kenway and Hamer 1978) are given to fourth order for unequal quark masses in table 6.3 and to sixth order for equal quark masses in table 6.4.

The validity of these perturbation expansions to eighth order in V should be questioned. For the states discussed above, which contain at least one unit of flux, the only problem comes from denominators proportional to μ. At any fixed order in V, the leading order in $1/\mu$ comes from graphs like this tenth order one:

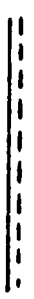


$$\sim \frac{x^{10}}{\mu^4} \qquad (6.42)$$

Thus, at nth order in V there are contributions of order $(\sqrt{x})^{(3n+2)/2}$, but none of lower order in $\sqrt{x}$. In particular, there are contributions of order $(\sqrt{x})^{16}$ from graphs which are tenth order in V. These are not included in the preceding calculation, which is consequently valid only to order $(\sqrt{x})^{15}$.

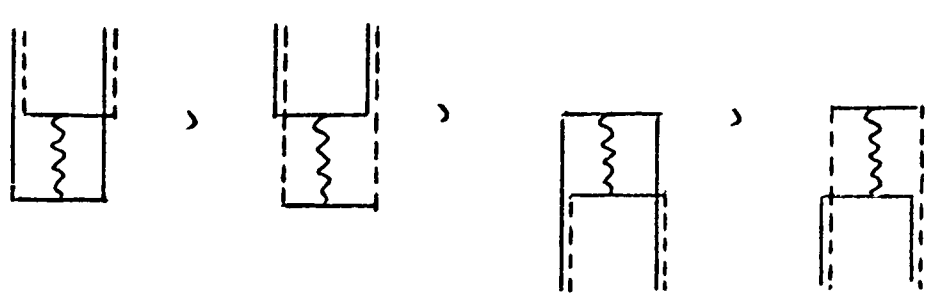
The mass poles only cause trouble for strong coupling. In the non-relativistic (weak coupling) regime the theory is equivalent to the lattice linear potential (with m replaced by the reduced mass $m_R = 2m_i m_j/(m_i + m_j)$ for constituents of flavour i and j, if $m_1 \neq m_2$). All the graphs containing mass poles can be neglected in this limit (see the discussion for the ordinary Schwinger model) and so our perturbation expansions are trustworthy to eighth order in x. This correspondence with the lattice linear potential model is important for providing a check on the computer calculation, and for warning us of the need to take precautions when making continuum estimates.

In the strong coupling regime, Coleman's (1976) light mesons have been identified with the fluxless states, (6.10), (6.11), (6.13) and (6.14) of lattice II to which we turn our attention. The $I_3 = \pm 1$ pseudoscalar states, (6.10) and 6.11), are represented at zeroth order by



Their degeneracy with other fluxless states is broken at order $\sqrt{x}$. So their masses are calculated using non-degenerate perturbation theory; the low-order results are quoted in tables 6.3 and 6.4.

When the quarks have equal masses, the problem of obtaining the leading terms in $1/\mu$ has an easy solution for the fluxless states. At any order in perturbation theory, the graphs which contribute to leading order in $1/\mu$ must have alternate intermediate states which are fluxless, c.f. (6.42). Since the action of the perturbation is to create or destroy a unit of flux, successive vertices can be paired together; they are either



(6.43)

or,



(6.44)

It is possible to write an effective Hamiltonian which has just these interactions. We have already done so; it is (5.84). This describes all second order interactions between fluxless states.

There is a one-to-one correspondence between the graphical expansion of W_{eff} and the graphs which contribute to leading order in $1/\mu$. (5.84) can be written as

$$W_{eff} = W^{o}_{eff} + z^{4} W_{eff}. \tag{6.45}$$

where

$$W^{o}_{eff} = \sum_{n} \left[4\beta^{4} \tau_3(n)\tau_3(n+1) + (-1)^{n} f_\beta \tau_3(n) \right] \tag{6.46}$$

and

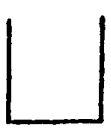
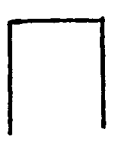
$$V_{eff} = 2\sum_{n} \left[\tau_+(n)\tau_-(n+1) + \tau_-(n)\tau_+(n+1) \right]. \tag{6.47}$$

Then, doing perturbation theory in $z^{4} V_{eff}$ corresponds to allowing just the vertices (6.43). The "boxes", (6.44), are included as the static "Thirring" interaction in the unperturbed Hamiltonian W^{o}_{eff}. This means that only even orders in V_{eff} contributed to diagonal matrix elements, but energy denominators should be expanded as power series

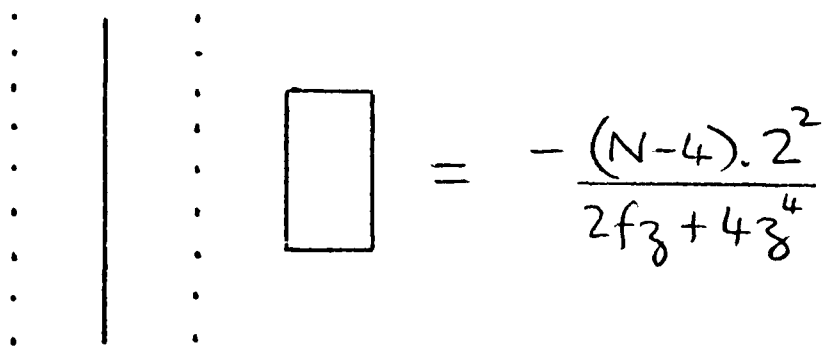
in z. The result is a series of the form $\sum_{k=0}^{\infty} a_k z^{3k+1}$, as anticipated for the leading terms in $1/\mu$. In this way, the calculation to fourth order in V_{eff} generates all the leading terms in $1/\mu$ which occur to tenth order in V in the full theory.

The perturbation expansion for (6.45) is like that for the ordinary Schwinger model with a Thirring interaction. The ground state of W^{o}_{eff}, for $f > 0$, is the perturbative vacuum, (5.85), of the full theory. It is taken to have zero unperturbed energy. Our fluxless states are readily identified with the low-energy eigenstates of W^{o}_{eff}, e.g. $I_3 = \pm 1$ states, (6.10) and (6.11), correspond to flipping one spin, and the $I_3 = 0$ states, (6.13) and (6.14), correspond to flipping a pair of neighbouring spins. If a vertical line is drawn to represent each flipped spin, the $I_3 = \pm 1$ states at zeroth order are

with unperturbed energy $fz + 4z^4$, and the vertices, (6.43), are

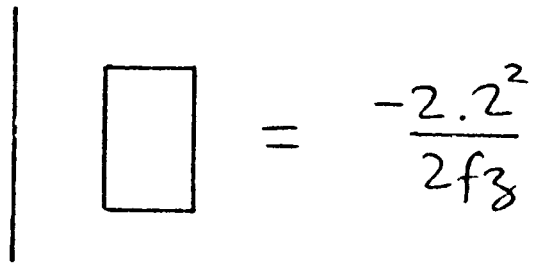
 and 

So, at second order in V_{eff}, this mass receives contributions from disconnected graphs,



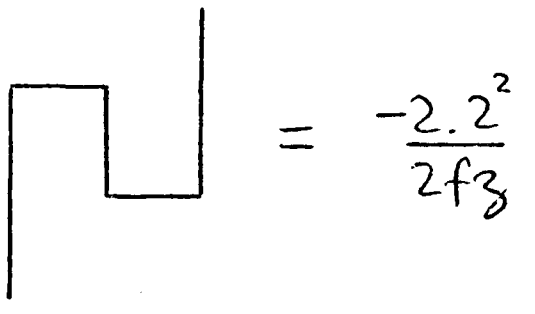
$$= -\frac{(N-4).2^2}{2f_3+4_3^4} \qquad (6.48)$$

in which the vacuum fluctuation is more than one link away from the flipped spin (the dotted lines prevent adjacent spins being flipped) from disconnected graphs



$$= \frac{-2.2^2}{2f_3} \qquad (6.49)$$

in which they are one link apart, and from the connected graphs

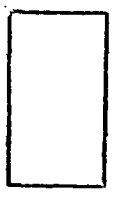


$$= \frac{-2.2^2}{2f_3} \qquad (6.50)$$

Notice how the Thirring interaction gives a lower energy to the spin configuration forming the intermediate state in (6.49) and (6.50), than to the one in (6.48). Adding the three terms gives

$$\text{second order} = 3^8\left[\frac{-2(N-4)}{f_3+4_3^4} - \frac{8}{f_3}\right]. \qquad (6.51)$$

As usual, there is a shift in the vacuum energy, due to the graph



$$= \frac{-N.2^2}{2f\zeta + 4\zeta^4}, \tag{6.52}$$

which must be subtracted from (6.51). The contribution from fourth order in V_{eff} begins at z^{13}. So, expanding the energy denominator to order z^{10} gives

$$\frac{2\zeta}{g} M_{(1,1)^-} = f\zeta + 4\zeta^4 - \frac{16}{f^2}\zeta^{10} + O(\zeta^{13}), \tag{6.53}$$

which may be checked against the results in table 6.4. For the fluxless states we are interested in, and the vacuum, the calculation to fourth order in V_{eff} gives

$$\frac{2\zeta}{g}\frac{E_0}{N} = -\frac{2}{f}\zeta^7 + \frac{4}{f^2}\zeta^{10} - \frac{2}{f^3}\zeta^{13} - \frac{24}{f^4}\zeta^{16} + O(\zeta^{19}) \tag{6.54}$$

$$\frac{2\zeta}{g} M_{(1,1)^-} = f\zeta + 4\zeta^4 - \frac{16}{f^2}\zeta^{10} + \frac{44}{f^3}\zeta^{13} + \frac{48}{f^4}\zeta^{16} + O(\zeta^{19}) \tag{6.55}$$

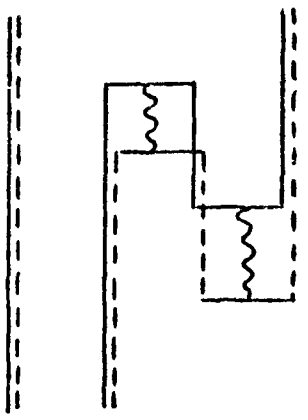
$$\frac{2\zeta}{g} M_{(1,0)^-} = 2f\zeta + 4\zeta^4 + \frac{4}{f}\zeta^7 - \frac{24}{f^2}\zeta^{10} + \frac{40}{f^3}\zeta^{13} + \frac{146}{f^4}\zeta^{16} + O(\zeta^{19}) \tag{6.56}$$

and

$$\frac{2\zeta}{g} M_{0^+} = 2f\zeta + 4\zeta^4 + \frac{12}{f}\zeta^7 - \frac{40}{f^2}\zeta^{10} + \frac{40}{f^3}\zeta^{13} + \frac{276}{f^4}\zeta^{16} + O(\zeta^{19}). \tag{6.57}$$

To order z^{13} these provide a check on the computer calculation for strong coupling (recall that the linear potential provides a check for weak coupling). The terms of order z^{16} in (6.54)-(6.57) include the leading terms in $1/\mu$ which come from tenth order in V, and so can be used to extend the validity of our computer calculation.

We are not out of the wood yet. The results, (6.56) and (6.57), quoted for the $I_3 = 0$ meson masses, are actually just the diagonal matrix elements in a calculation using quasi-degenerate perturbation theory. This is a reflection of a new degeneracy problem which afflicts the full eighth order lattice II calculation. The four-quark states in which the two quark-antiquark pairs are one and three links apart are degenerate. They are connected at fourth order in V by the graphs



and, as intermediate states in non-degenerate Rayleigh-Schrödinger perturbation theory, lead to vanishing energy denominators at eighth order. This simply tells us that we should be using degenerate perturbation theory in the subspace of four-quark states. (The corresponding states in the calculation using the effective Hamiltonian (6.45), are split at "zeroth order" by the Thirring interaction, and so can be treated using quasi-degenerate perturbation theory).

Of course, all four-quark states in which the two quark-antiquark pairs are an odd number of links apart are degenerate. The next one of importance is the five-link state, but this does not enter into the calculation of the energy of the one-link state until sixteenth order, being connected to the one-link state at eighth order and the three-link state at fourth order. So, only the one- and three-link states are relevant for the eighth order calculation.

The masses of the $I_3 = 0$ pseudoscalar and scalar mesons are calculated using degenerate perturbation theory in the subspaces spanned by the one-link states

$$|4q,1\pm\rangle \equiv |\bar{1}2,2\bar{1}\pm\rangle_{II}, \tag{6.58}$$

given in (6.13) and (6.14), and the three-link states

$$|4q,3\pm\rangle \equiv \frac{i}{\sqrt{N}} \sum_n \left[\phi_1^+(n)\phi_2(n)\phi_2^+(n+3)\phi_1(n+3) \pm \phi_2^+(n)\phi_1(n)\phi_1^+(n+3)\phi_2(n+3) \right] |0\rangle_{II}. \tag{6.59}$$

We seek a consistent expansion, to order z^{15}, of the eigenvalue of each mass matrix which corresponds to the one-link state. This makes available [7,7] Padé approximants (the [8,8] Padé approximants require that the expansions be valid to order z^{17}, and this last order is difficult to obtain). The mass matrix for both pseudoscalars and scalars has the form

$$\underline{W} = \begin{pmatrix} \omega^{(0)}+a & c \\ d & \omega^{(0)}+b \end{pmatrix} \tag{6.60}$$

where

$$\omega^{(0)} = 2\mu_1 + 2\mu_2 \tag{6.61}$$

and a, b start at second order in V, and c, d start at fourth order in V. The eigenvalue corresponding to the one-link state can be obtained iteratively through

$$\lambda = \omega^{(0)} + a + \frac{cd}{\lambda - \omega^{(0)} - b} . \tag{6.62}$$

Because there are denominators proportional to z, these matrix elements have to be determined to sufficiently high orders to make possible a consistent expansion of λ to order z^{15}.

The calculation has three parts. First of all, the diagonal matrix element, a, corresponding to the one-link state, is calculated. This is an eighth order calculation, using the formula (A.32). The degeneracy with the three-link state only begins to cause trouble at eighth order in V, so the calculation can be carried out as if it were a non-degenerate treatment of the one-link state, except that terms with vanishing denominators which contribute to the eighth order matrix element are ignored and replaced by

$$-\langle 4q,1|(V_q^2 V_q V_q V + V_q V_q^2 V_q V + V_q V_q V_q^2 V)|4q,3\rangle \times \langle 4q,3|V_q V_q V_q V|4q,1\rangle \tag{6.63}$$

Our results to fourth order in V for unequal quark masses are given in table 6.3; those for equal quark masses are also presented to fourth order in table 6.4. From our discussion of the effective Hamiltonian (6.45), we know these results are valid to order z^{15}.

Secondly, the off-diagonal matrix elements, c and d, are required to sixth order in V. Only even orders in V contribute, so the relevant formula is again (A.32). Our results are presented in Table 6.5, where the sixth order result for arbitrary quark masses has been omitted to save space. The effective Hamiltonian, (6.45), tells us that the expansions for c and d start at order z^7, and are valid to order z^{12}. Consequently, the expansion for their product, required in (6.62), begins at order z^{14} and is valid to order z^{19}.

Finally, we need the mass of the three-link state to fourth order in V, given in table 6.3. The resulting expansion for the mass difference, a-b, begins at order z^4 and is valid to order z^9. It follows that (6.62) need only be iterated once and that

$$\lambda = \omega^{(0)} + a + \frac{cd}{a-b} + O(z^{16}) \qquad (6.64)$$

is the required result for the mass of the one-link state.

Thus, the mass of each low-lying particle state of lattice II has been expanded as a power series in z to order z^{15}. In most cases, the next order in z can be obtained simply from the effective Hamiltonian, (6.45), if needed. But the terms of order z^{17} demand a lot more work. This is in contrast to lattice I, where our series expansions are valid to order z^{19}. However, the strong-point of lattice II is expected to be its treatment of the strong-coupling region. Our series expansions to order z^{15} do include all contributions from eighth order in V which are proportional to $1/\mu$, and these presumably dominate for strong coupling. So our inability to expand the lattice II masses further is not seen as a serious handicap.

(d) Continuum Estimates for Particle Masses.

At non-zero lattice spacing the particle spectra of the two lattice theories differ considerably; not just at zeroth order, but also within perturbation theory. Yet they ought to describe the same continuum physics. We have a well-tried method for extracting continuum predictions. It is applied here to compare the rate of convergence of the two approximation schemes.

Each continuum particle of interest is assigned one, or more, low-energy bound state of each lattice. The rescaled masses, $2zM/g$, of these states are known as series expansion in z, valid to order z^{19} for lattice I and z^{15} for lattice II. These, and related series for mass ratios, can be extrapolated away from $z = 0$ using Padé approximants.

The individual masses are of two types. When the series expansion for the rescaled mass begins at O(1), as is the case for lattice I and some of the states of lattice II, we form diagonal Padé approximants to the function

$$\frac{d}{dz}\, z\left(\frac{M_{i\bar{j}} - m_i - m_j}{g}\right) \qquad (6.65)$$

The masses of the constituent quarks are subtracted out in order to be able to compare our results with those for the linear potential model in the non-relativistic limit ($m_i >> g$). In the strong-coupling limit ($m_i << g$), (6.65) reduces to the meson mass, and our predictions for the continuum value can be directly compared with Coleman's (1976)

results. When a factor of z can be divided out of the series expansion for the rescaled mass, as is the case for the fluxless states of lattice II, we are able to approximate the binding energy

$$\frac{M_{i\bar{j}} - m_i - m_j}{g} \qquad (6.66)$$

itself by diagonal Padé approximants.

As functions of z, the Padé approximants to (6.65) for the lattice I results have very similar structure to the graphs of fig. 3.4 for the ordinary Schwinger model. The lattice II results differ from fig. 3.4 only in that the peak value for $\frac{m}{g} \lesssim 1$ appears to decrease with m/g, whereas for the ordinary Schwinger model and the lattice I results it remains approximately constant. Since, following our analysis of the ordinary Schwinger model, we propose the peak value as our best estimate of the continuum mass over the whole range of m/g (except $\frac{m}{g} = 0$), this qualitative distinction between the strong-coupling behaviour of the two lattices is significant.

Mass ratios are handled similarly. Again, for ease of checking the non-relativistic results with those for the linear potential model, we consider ratios of binding energies and approximate them by sequences of diagonal Padé approximants. The latter have the same functional form as those for the single-species Schwinger model, shown in fig. 3.7. Hence, we estimate the continuum limit in the same way, by taking the asymptotic value of the [7,7] or [8,8] Padé approximant at $z = \infty$. As has already been remarked, all particle

masses on the same lattice appear to have similar strong-coupling behaviour (i.e. power-law behaviour in $\frac{m}{g}$). For this reason, we might expect our estimates for the mass ratios to become constant, independent of $\frac{m}{g}$ in this limit. This is just what happens.

These techniques for estimating the continuum results apply for all values of $\frac{m}{g}$. However, in the non-relativistic regime our estimates for both individual binding energies and their ratios can usually be improved by employing the method of Carroll et al. (1977). This relies on the knowledge that our series expansions become identical to those for the lattice theory of the linear potential model in this limit. Carroll et al. (1977) propose that Padé approximants for the latter model should be evaluated at finite values of the expansion parameter (2.14),

$$u = \frac{g}{2m} z^3 \qquad (6.67)$$

Their choice of u can be translated, for any given m/g, into a value of z at which to evaluate the corresponding Schwinger-model Padé approximant, as demonstrated for the one-species model in chapter 3. In the lattice II version of the two-species model, there are states like the ($I_3 = \pm 1$) mesons for which it is the even lattice formulation of the linear potential model which is relevant, rather than the odd lattice formulation.

We will concentrate on our results for equal-mass quarks. We begin with a consideration of the 1^- and 0^+ mesons, which Coleman (1976) finds have low masses, (5.27), (5.28) for strong coupling.

On lattice I the estimates for these masses are qualitatively wrong in the strong-coupling region, as shown in fig. 6.4 for the binding energy of the 1^- state. Both the $z \to \infty$ value, (a), and the peak value, (b) of the [8,8] Padé approximant miss the power-law behaviour (5.27). However, at the other coupling extreme, when $\frac{m}{g} \gtrsim 2$, both the peak-value estimate and the estimate, (c), at $u = 0.88$ (Carroll et al.'s value for the non-relativistic linear potential model: see fig. 2.2) are within 13% of the non-relativistic result (2.6). Our estimates for the 0^+ mass on lattice I are similar.

In contrast, results for these states on lattice II show qualitative agreement with the continuum theory in both the strong- and weak coupling regions. We start by discussing the lightest particles; the pseudoscalar isotriplet.

In the strong coupling regime we expect our best estimates to come from the calculations based on fluxless states. Indeed they do. The predictions for the $I_3 = 1$ and $I_3 = 0$ meson masses, derived from [7,7] Padé approximants, are shown in fig. 6.5. For both masses, the peak-value estimates, (b), follow quite closely the power-law behaviour (5.27) for $\frac{m}{g} \lesssim 10^{-1}$, and the $I_3 = 1$ particle mass is in excellent numerical agreement with the exact continuum result there. The traditional $z \to \infty$ estimates, (a), are not very reliable. There is some agreement with the peak value for the $I_3 = 1$ member of the isotriplet, but not for the other.

As we move towards weak coupling, the four-quark state used for the $(1,0)^-$ meson starts to give anomalous results, as shown in fig. 6.6. Instead of mass estimates which correspond to a weakly bound quark-

antiquark pair in a linear potential, the peak value, (b), follows closely $4m/g$ for $m/g \gtrsim 0.5$. This was anticipated; the two-quark state, (6.19), should start to take over as a better description of the $I_3 = 0$ meson in the non-relativistic limit.

The results for the two-quark state are shown in fig. 6.7 and confirm our expectations. The strong-coupling behaviour of the peak value, (b), is in the right direction, but is not as good as the four-quark state in figs 6.5 and 6.6. However, for $\frac{m}{g} \gtrsim 1$, it is the two-quark state which gives a much better account of the continuum physics. Comparing it with the $I_3 = 1$ member of the isotriplet, shown in fig. 6.5, we see that both peak-value estimates agree in this region, indicative of a partial restoration of the isospin symmetry, lost in the lattice II formulation. The resulting estimates for the non-relativistic binding energy of the isotriplet have approximately the correct power-law behaviour (2.6), and the estimates for the $I_3 = 1$ meson, fig. 6.5(c), from the [7,7] Padé approximant evaluated at $u = 0.2$, which is the value obtained when the method of Carroll et al. (1977) is applied to the corresponding Padé approximant in the even-lattice formulation of the linear potential model, are in perfect agreement with (2.6).

Our discussion of the other light particle on lattice II, the 0^+ meson, is similar. We find that the four-quark state provides the most accurate estimates in the strong-coupling region, fig. 6.8(b). However, neither it, nor the two-quark state, (6.20), gives a good description for weak coupling. For $\frac{m}{g} \gtrsim 1$, the estimate, fig. 6.9, for the mass of the four-quark scalar state, like the pseudoscalar,

follows the anomalous value 4m/g. In the same region, the estimate for the two-quark state is less badly behaved, but still misses the behaviour (2.8) by a long way.

The mass ratio for the light mesons in the strong-coupling region, which can be derived from the individual masses of the four-quark states, is

$$\frac{M_{0^+}}{M_{(1,0)^-}}\left(\frac{m}{g} \lesssim 10^{-2}\right) \simeq 1.73 \qquad (6.68)$$

and is in excellent agreement with the exact result (5.29). However, Padé approximants to the mass ratio for these states are badly behaved. So instead, we present the 0^+ to 1^- binding energy ratio for lattice I and the two-quark states of lattice II in fig. 6.10. Our estimates, (a), are based on zero-lattice-spacing limits, as mentioned earlier. For strong coupling, lattice I is remarkably accurate, considering its poor treatment of the individual masses. In the same region, the result for lattice II is too low, but this is to be expected, because the two-quark states do not describe strong coupling well. Both lattices give identical predictions for the non-relativistic limit, which can be improved, (b), by evaluating the Padé approximants at the Carroll et al. (1977) value for the linear potential model of u = 1.26. The reason for the success of lattice I in the strong-coupling limit is not clear. It may be that effects which are responsible for the slow convergence of individual particle masses, cancel when the ratio is taken. Equally, it may be accidental.

Next we turn to the 0^- and 1^+ mesons which Coleman (1976) finds have high masses, around $\sqrt{\frac{2}{\pi}}g$, c.f. (5.10), for strong coupling. These are treated poorly by lattice II; it predicts strong-coupling behaviour similar to that for the other two-quark states, figs. 6.7 and 6.8. Our lattice I results for the 0^- and 1^+ mesons are shown in fig. 6.11. The strong-coupling behaviour is certainly qualitatively correct in both cases, and is within 5% of the exact result for the 0^- meson. We find that the scalar isotriplet is almost twice as massive in this limit. In the non-relativistic regime, our peak-value estimates give the correct power-law behaviour. The results for the 0^- binding energy agree with the continuum linear potential model to within 10% for $\frac{m}{g} \gtrsim 1$. Those for the 1^+ binding energy are improved by evaluating the [8,8] Padé approximant at u = 1.0 following Carroll et al. (1977).

Our estimates for the ratios of the high to low mass states all fail to reproduce the correct strong-coupling behaviour. This is probably due to the fact that each lattice seems to treat only one type of particle well(i.e. either those which have high mass or those which have low mass for strong coupling). As expected,the non-relativistic results all agree with the continuum values after treatment by the method of Carroll et al. (1977). In the case of the 0^- to 1^- binding-energy ratio, which should go to 1 for large $\frac{m}{g}$, this value is attained by the $z \to \infty$ limit of the [8,8] Padé approximant and no further refinement is necessary.

Finally, we note that for intermediate coupling strengths (i.e. $\frac{m}{g} \gtrsim 0.5$) there is general qualitative (and sometimes quantitative) agreement between the peak-value estimates from the two lattice

formulations for a given particle mass. This may be indicative of some convergence of the lattice theories sufficiently far away from the region of the transition to a chirally symmetric vacuum.

One of the unexpected results which Coleman (1976) reports is the restoration of isospin symmetry for the low-mass states in strong coupling even if there is a large quark-mass splitting. Thus, even if one quark mass is ten times the other, Coleman finds that the lightest particles form a degenerate isotriplet. We can check to what extent this occurs in the lattice theory. It is only a sensible question to ask for lattice II, because it is only these results which we can trust for the low-mass particles. The masses of the $1\bar{2}$ and $1\bar{1}$ pseudosclar mesons for strong coupling, when one quark flavour is ten times heavier than the other, are shown in fig. 6.12. Note that here we plot actual masses (i.e. $\frac{M}{g}$) and not binding energies. Comparison of the peak values of the [7,7] Padé approximants indicates isospin breaking of about 27% and comparison of their $z = \infty$ values indicates breaking of about 19% for $\frac{m_1}{g} \sim 10^{-2}$. Thus the lattice theory favours Coleman's result rather than the additive quark model, which predicts an isospin breaking of 80%

Summary

Masses of the low-lying bound states of the two lattice theories can be calculated perturbatively to eighth order in V. A problem arises with lattice II due to the degeneracy of all fluxless states for zero quark mass, which restricts the validity of the series

expansions. For both lattices the results are extrapolated to small lattice spacing using Padé approximants. Continuum estimates are obtained by evaluating these at the smallest lattice spacing for which their convergence seems assured.

The predictions for the non-relativistic limit are well understood in terms of the linear potential model. For intermediate values of the coupling constant ($\frac{m}{g} \sim 1$), where exact continuum results are unknown, there is some indication of convergence. Both lattice theories are in reasonable agreement here. But for strong coupling neither lattice gives a satisfactory account of the complete particle spectrum. Lattice I seems to treat the high mass particles better and lattice II the low-mass particles. Qualitative features of these particle masses agree well with the continuum theory and occasionally there is good quantitative agreement.

CHAPTER 7

RESULTS AND CONCLUSIONS

Underlying our work is the simple, one-dimensional, non-relativistic linear potential model. This is because it describes the low-energy bound states of the Schwinger model in the non-relativistic limit. In addition, both continuum and lattice theories can be solved exactly. It should not be scorned for its simplicity. It displays the non-uniform convergence of Padé approximants and is instrumental in developing non-zero-lattice-spacing estimates to remedy this defect.

The equivalence of the lattice Schwinger model to the lattice linear potential model for weak coupling warns us that non-zero-lattice-spacing estimates are needed in the massive theory. Inspection of the Padé approximants for individual meson masses, as functions of the lattice spacing, reveals that the best continuum estimates for all values of m/g come from their peak values.

The extension to two fermion flavours has interesting consequences for the strongly-coupled continuum theory. The lowest-lying particles form a degenerate pseudoscalar isotriplet, even for large mass-splitting between the flavours. The next state, 0^+, lies a factor $\sqrt{3}$ higher in mass, while all the rest, like the 0^-, have much larger masses (by a factor of $(g/m)^{2/3}$).

Two distinct lattice formulations, I and II, are possible, associated with an ambiguity in the identification of continuum fermion fields with

their lattice counterparts. Unlike the one-flavour model, or QCD, both have a restoration of chiral symmetry as the fermion mass vanishes. For lattice II this transition is smooth, but lattice I appears to undergo a first order phase transition. The SU(2) chirally symmetric vacuum, relevant for strong coupling, is too complicated to do a perturbative calculation beyond second order, where the low-lying states are those of a Heisenberg antiferromagnetic chain. Our lattice calculations are built around the unsymmetric vacua appropriate for the massive theories, so their convergence for strong coupling is expected to be slow.

The two lattices have quite different zeroth order spectra and perturbation expansions. Lattice I is like the ordinary Schwinger model. Lattice II supports fluxless states, which dominate the low-energy spectrum for strong coupling and render the eighth order calculation valid only to order $(\sqrt{x})^{15}$. Continuum estimates for individual meson masses are based on peak values of the Padé approximants. They are well understood for weak coupling in terms of the linear potential model. At intermediate coupling strengths, where there are no continuum results for comparison, there is some indication of convergence. But for strong coupling neither lattice can account for the whole particle spectrum. Lattice I treats the high mass particles well, e.g. it predicts a mass for the 0^- meson very close to the exact result $\sqrt{\frac{2}{\pi}}\,g$, but fails for the low mass particles. Meanwhile, on lattice II the high mass particles are treated badly, whereas the 0^+ and 1^- meson masses, in units of g, fall off with approximately the power law $\left(\frac{m}{g}\right)^{2/3}$, in the ratio $\sqrt{3}$, as they should. Also, approximate degeneracy of the pseudoscalar isotriplet, on lattice II, indicates a partial restoration of the isospin symmetry, lost in this

formulation, and there are signs that the effect persists when the flavours are given different masses. The disparity in the two lattice treatments confirms the slow convergence expected for strong coupling.

Matrix methods are an attempt to improve the convergence of low order lattice calculations. Comparison of the results from fourth order single-state and matrix calculations for the ordinary Schwinger model, provide some encouragement. Continuum estimates for the mass ratio, derived from several scalar mass matrices, have a more realistic dependence on the quark mass. Agreement with the known results for strong and weak coupling is improved, and is within 10% for certain choices of unperturbed states. In contrast the pseudoscalar mass matrix behaves badly. For the SU(2) Schwinger model, a fourth order matrix calculation is carried out for the low-lying particles of lattice II, but is rather inconclusive.

Three aspects of our work may have wider significance; though none will out-last lattice QCD. First of all, non-uniform convergence of the sequence of Padé approximants to individual bound-state masses is a common feature of all our 1+1 dimensional calculations. It is a warning that precautions must be taken before trusting zero-lattice-spacing estimates. Secondly, matrix methods may have useful applications in 3+1 dimensions. However, this will depend on being able to understand the reason for the failure of the pseudoscalar mass matrix in the Schwinger model. Finally, the lattice formulation of the SU(2) Schwinger model is not unique. Here, for strong coupling, where overall convergence of the two versions is expected to be slow, the estimates for any given continuum particle mass converge at quite different rates. Care should be exercised if similar ambiguities arise elsewhere.

As a calculational scheme, lattice QCD is in danger of stagnation. New techniques are needed to provide the impetus for more low-order calculations. Of themselves, these may never be conclusive. However, there is one tantalising prospect: the theoretical framework being created could justify a massive computing project. A brute-force approach may lack aesthetic appeal, but just might lead to the same sort of revolution in physics as occurred recently in mathematics (Appel and Haken 1977).

"Assumptions, hasty, crude, and vain,
Full oft to use will Science deign;
The corks the novice plies today
The swimmer soon shall cast away".

A. H. Clough (184C)

APPENDIX A

Rayleigh-Schrödinger Perturbation Theory

The backbone of lattice calculations is the Rayleigh-Schrödinger series for the eigenvalues of a Hamiltonian in powers of the perturbation. The formula for the perturbation expansion to high orders is required in a convenient form. Here we sketch the derivation to eighth order for both degenerate and non-degenerate eigenvalues of the unperturbed Hamiltonian.

The first step is to obtain the Brillouin-Wigner series for the eigenvalues of the Hamiltonian

$$H = H_o + V. \tag{A.1}$$

H_o is the unperturbed Hamiltonian and V is taken as a perturbation on H_o. Suppose H_o possesses a set of degenerate eigenstates $S = \{|\phi_i>\}$ (there may be just one), obeying

$$H_o|\phi_i> = \varepsilon\ |\phi_i> \qquad \forall i. \tag{A.2}$$

Let P be the projection operator onto the subspace S and let

$$Q = 1 - P. \tag{A.3}$$

Let $|\Psi>$ be an eigenstate of the full Hamiltonian satisfying

$$|\Psi> \xrightarrow[V \to 0]{} |\psi> \ \varepsilon\ S \tag{A.4}$$

and

$$H|\Psi\rangle = E|\Psi\rangle. \tag{A.5}$$

Thus we assume that

$$P|\Psi\rangle = |\psi\rangle \tag{A.6}$$

and

$$|\Psi\rangle = |\psi\rangle + |\chi\rangle \tag{A.7}$$

where $|\chi\rangle$ is orthogonal to S; in particular,

$$\langle\chi|\psi\rangle = 0. \tag{A.8}$$

(i.e. $|\Psi\rangle$ is not normalised). Then

$$P|\chi\rangle = 0 \text{ and } Q|\chi\rangle = |\chi\rangle, \tag{A.9}$$

so,

$$\begin{aligned} QH_o|\chi\rangle &= H_o|\chi\rangle - PH_o|\chi\rangle \\ &= H_o|\chi\rangle - \varepsilon P|\chi\rangle \\ &= H_o|\chi\rangle \\ &= H_o Q|\chi\rangle \end{aligned} \tag{A.10}$$

Now we can write (A.5) as

$$(E - H_o)|\Psi\rangle = V|\Psi\rangle \tag{A.11}$$

or, from (A.7),

$$(E - H_o)|\chi\rangle = V|\Psi\rangle - (E - \varepsilon)|\psi\rangle. \tag{A.12}$$

Operating on (A.12) with Q gives

$$(E - H_o)|\chi\rangle = QV|\Psi\rangle \tag{A.13}$$

while operating on (A.11) with P gives

$$(E - \varepsilon)|\psi\rangle = PV|\Psi\rangle. \qquad (A.14)$$

(A.13) and (A.14) are the basic equations from which the Brillouin-Wigner series is derived. (A.13) is written as

$$|\chi\rangle = \frac{Q}{E-H_o} V|\Psi\rangle \qquad (A.15)$$

where the operator

$$G(E) \equiv \frac{Q}{E-H_o} \qquad (A.16)$$

is well-defined provided E does not coincide with any eigenvalue of H_o. Combining (A.15) and (A.7) gives

$$|\Psi\rangle = |\psi\rangle + G(E)V|\Psi\rangle \qquad (A.17)$$

Define

$$\Omega \equiv 1 + G(E)V\Omega \qquad (A.18)$$

then

$$|\Psi\rangle = \Omega|\psi\rangle \qquad (A.18)$$

and (A.14) becomes

$$(E - \varepsilon)|\psi\rangle = PV\Omega|\psi\rangle \qquad (A.20)$$

Hence, we are led to an implicit equation for the matrix E:

$$E = \varepsilon + \mathcal{V}(E) \qquad (A.21)$$

where

$$\mathcal{V}(E) \equiv PV\Omega P \qquad (A.22)$$

and

$$V\Omega = V + V \frac{Q}{E-H_o} V\Omega. \qquad (A.23)$$

Equations (A.21)-(A.23) constitute the Brillouin-Wigner series. They may be combined into a single equation

$$E = \varepsilon + \sum_{n=0}^{\infty} PV\left(\frac{Q}{E-H_o} V\right)^n P \qquad (A.24)$$

which is meant to be solved iteratively for E, as a power series in V. The eigenvalues of E are just those eigenvalues of H which have ε as their limit when $V \to 0$.

The explicit solution of (A.24) is the Rayleigh-Schrödinger series, and is a more convenient form for most applications. It is obtained by expanding (A.16):

$$\begin{aligned} G(E) &= \frac{Q}{\varepsilon - H_o - (\varepsilon - E)} \\ &= \frac{Q}{\varepsilon - H_o}\left(1 - \frac{\varepsilon - E}{\varepsilon - H_o}\right)^{-1} \\ &= \sum_{n=0}^{\infty}\left(\frac{Q}{\varepsilon - H_o}\right)^{n+1}(\varepsilon - E)^n \end{aligned} \qquad (A.25)$$

Define

$$g \equiv \frac{Q}{\varepsilon - H_o} . \qquad (A.26)$$

Then, using (A.21), we can write (A.25) as

$$VG(E)V = \sum_{n=0}^{\infty} V g^{n+1} V \left[-\mathcal{T}(E)\right]^n \qquad (A.27)$$

which is in a form that can be used in conjunction with (A.24):

$$\mathcal{T}(E) = \sum_{n=0}^{\infty} PV\left[G(E)V\right]^n P, \qquad (A.28)$$

to perform the iteration. For exampl nd order (A.27) and (A.28) reduce to

$$\mathcal{V}(E) = PVP + PVgVP + O(V^3) \tag{A.29}$$

and to fourth order

$$\begin{aligned}\mathcal{V}(E) = PVP &+ \sum_{n=0}^{\infty} PVg^{n+1}VP\left[-\mathcal{V}(E)\right]^n \\ &+ \sum_{n,m=0}^{\infty} PVg^{n+1}Vg^{m+1}VP\left[-\mathcal{V}(E)\right]^{n+m} \\ &+ \sum_{n,m,\ell=0}^{\infty} PVg^{n+1}Vg^{m+1}Vg^{\ell+1}VP\left[-\mathcal{V}(E)\right]^{n+m+\ell} \\ &+ O(V^5)\end{aligned} \tag{A.30}$$

Then substituting (A.29) into the R.H.S. of (A.30), and discarding terms of order V^5 and higher, we obtain finally,

$$\begin{aligned}E = \varepsilon P &+ PVP + PVgVP + PVgVgVP - PVg^2VP(PVP) \\ &+ PVgVgVgVP - (PVg^2VgVP + PVgVg^2VP)(PVP) \\ &- PVg^2VP(PVgVP) + PVg^3VP(PVP)^2 + O(V^5).\end{aligned} \tag{A.31}$$

This formula is valid for both the degenerate and non-degenerate case with appropriate definitions for P and g.

For completeness we state the formula to eighth order in the case where only even orders in V are non-vanishing:

$$
\begin{aligned}
E(\text{even orders}) = {} & \varepsilon\, P + PVgVP \\
& + PVgVgVgVP - PVg^2VP(PVgVP) + PVgVgVgVgVgVP \\
& - PVg^2VP(PVgVgVgVP) - (PVg^2VgVgVP + PVgVg^2VgVP + PVgVgVg^2VP) \\
& \times (PVgVP) + PVg^2VP(PVg^2VP)(PVgVP) + PVg^3VP(PVgVP)(PVgVP) \\
& + PVgVgVgVgVgVgVP - PVg^2VP(PVgVgVgVgVgVP) \\
& - (PVg^2VgVgVgVgVP + PVgVg^2VgVgVgVP + PVgVgVg^2VgVgVP \\
& + PVgVgVgVg^2VgVP + PVgVgVgVgVg^2VP)(PVgVP) \\
& - (PVg^2VgVgVP + PVgVg^2VgVP + PVgVgVg^2VP) \times (PVgVgVgVP) \\
& + (PVg^3VgVgVP + PVgVg^3VgVP + PVgVgVg^3VP + PVg^2Vg^2VgVP \\
& + PVg^2VgVg^2VP + PVgVg^2Vg^2VP) \times (PVgVP)(PVgVP) \\
& + (PVg^2VgVgVP + PVgVg^2VgVP + PVgVgVg^2VP) \times (PVg^2VP)(PVgVP) \\
& + PVg^2VP(PVg^2VgVgVP + PVgVg^2VgVP + PVgVgVg^2VP)(PVgVP) \\
& + PVg^3VP(PVgVgVgVP)(PVgVP) + PVg^3VP(PVgVP)(PVgVgVgVP) \\
& + PVg^2VP(PVg^2VP)(PVgVgVgVP) - PVg^4VP(PVgVP)(PVgVP)(PVgVP) \\
& - PVg^3VP(PVg^2VP)(PVgVP)(PVgVP) - PVg^3VP(PVgVP)(PVg^2VP)(PVgVP) \\
& - PVg^2VP(PVg^3VP)(PVgVP)(PVgVP) - PVg^2VP(PVg^2VP)(PVg^2VP)(PVgVP) \\
& + O(V^{10}).
\end{aligned}
\tag{A.32}
$$

APPENDIX B

Quasi-Degenerate Perturbation Theory.

Consider the situation in which a set of non-degenerate eigenstates of the unperturbed Hamiltonian are mixed by the perturbation. Since we work to a definite order in perturbation theory, only a small number of states are involved. But no state alone will be a particularly good starting point for non-degenerate perturbation theory. Rather it is better to diagonalise the perturbation expansion for the Hamiltonian in the subspace spanned by these states. In the specific application to lattice theories, the idea is to take the continuum limit of the Hamiltonian matrix prior to diagonalisation.

The equivalent of the Rayleigh-Schrödinger series can be obtained from a modified version of the Brillouin-Wigner series, by a method similar to that used in Appendix A. Above fourth order the resulting formulae are extremely complicated. For this reason, we illustrate the method by sketching the derivation for three states to fourth order. The two-state formula follows as a special case.

Suppose the complete Hamiltonian is

$$H = H_o + V \qquad (B.1)$$

and we wish to do perturbation theory in V about three non-degenerate eigenstates of H_o:

$$|a\rangle, |b\rangle, |c\rangle$$

obeying

$$H_o|a\rangle = \varepsilon_a|a\rangle,\ H_o|b\rangle = \varepsilon_b|b\rangle,\ H_o|c\rangle = \varepsilon_c|c\rangle \tag{B.2}$$

with

$$\varepsilon_a < \varepsilon_b < \varepsilon_c. \tag{B.3}$$

To obtain the Brillouin-Wigner series, write

$$H = H_o - (\varepsilon_b - \varepsilon_a)P_b - (\varepsilon_c - \varepsilon_a)P_c + V + (\varepsilon_b - \varepsilon_a)P_b + (\varepsilon_c - \varepsilon_a)P_c \tag{B.4}$$

where

$$P_b = |b\rangle\langle b| \quad \text{and} \quad P_c = |c\rangle\langle c|. \tag{B.5}$$

So,

$$H = \hat{H}_o + \hat{V} \tag{B.6}$$

where

$$\hat{H}_o = H_o - \Delta_b P_b - \Delta_c P_c \tag{B.7}$$

$$\hat{V} = V + \Delta_b P_b + \Delta_c P_c \tag{B.8}$$

and

$$\Delta_b = \varepsilon_b - \varepsilon_a,\ \Delta_c = \varepsilon_c - \varepsilon_a. \tag{B.9}$$

Then

$$\hat{H}_o|a\rangle = \varepsilon_a|a\rangle,\ \hat{H}_o|b\rangle = \varepsilon_a|b\rangle,\ \hat{H}_o|c\rangle = \varepsilon_a|c\rangle, \tag{B.10}$$

and $|a\rangle$, $|b\rangle$, $|c\rangle$ are degenerate eigenstates of $\hat{H}_o$. So take S to be the subspace spanned by these vectors, with

$$P \equiv P_a + P_b + P_c \tag{B.11}$$

and

$$Q \equiv 1 - P. \tag{B.12}$$

Then, from (A.21)-(A.23) the basic equation for the Hamiltonian matrix E in this subspace is

$$E = \varepsilon_a + \mathcal{V}(E) \tag{B.13}$$

where

$$\mathcal{V}(E) \equiv P\hat{V}\Omega P \tag{B.14}$$

and

$$\hat{V}\Omega \equiv \hat{V} + \hat{V}\frac{Q}{E-\hat{H}_o}\hat{V}\Omega \tag{B.15}$$

Equations (B.13)-(B.15) are the required modified Brillouin-Wigner series.

Define
$$\begin{aligned}
\hat{G}(E) \equiv \frac{Q}{E-\hat{H}_o} &= \frac{Q}{E-H_o+\Delta_b P_b+\Delta_c P_c} \\
&= \frac{Q}{E-H_o}\left(1+\frac{\Delta_b P_b+\Delta_c P_c}{E-H_o}\right)^{-1} \\
&= \sum_{n=0}^{\infty}\frac{Q}{E-H_o}\left(\frac{-\Delta_b P_b-\Delta_c P_c}{E-H_o}\right)^n \\
&= \frac{Q}{E-H_o} \quad \text{since} \begin{cases} P_b Q = Q P_b = 0 \\ P_c Q = Q P_c = 0 \end{cases} \qquad \text{(B.16)} \\
&\equiv G(E)
\end{aligned}$$

(c.f. A.16). Thus,

$$\hat{V\Omega} = V + \Delta_b P_b + \Delta_c P_c + VG(E)V + VG(E)VG(E)V + \ldots\ldots \tag{B.17}$$

Next, define

$$g_a \equiv \frac{Q}{\varepsilon_a - H_o}\,, \quad g_b \equiv \frac{Q}{\varepsilon_b - H_o}\,, \quad g_c \equiv \frac{Q}{\varepsilon_c - H_o}\,. \tag{B.18}$$

In order to convert the Brillouin-Wigner formalism into Rayleigh-Schrödinger form, we rewrite (B.14) and (B.15) as an implicit equation for $\mathcal{V}(E)$. This is achieved by expanding G(E) in powers of $\mathcal{V}(E)$:

$$\begin{aligned} G(E) &= \frac{Q}{\varepsilon_a - H_o - (\varepsilon_a - E)} \\ &= \frac{Q}{\varepsilon_a - H_o}\left[1 - \left(\frac{\varepsilon_a - E}{\varepsilon_a - H_o}\right)\right]^{-1} \\ &= \sum_{n=0}^{\infty}\left(\frac{Q}{\varepsilon_a - H_o}\right)^{n+1}(\varepsilon_a - E)^n. \end{aligned} \tag{B.19}$$

So, using (B.13) and (B.18),

$$VG(E)V = \sum_{n=0}^{\infty} V g_a^{n+1} V\,[-\mathcal{V}(E)]^n. \tag{B.20}$$

Hence, the implicit equation for $\mathcal{V}(E)$, obtained from (B.14), (B.17) and (B.20) is

$$\mathcal{V}(E) = \Delta_b P_b + \Delta_c P_c + PVP + \sum_{n=0}^{\infty} PV g_a^{n+1} V \left[-\mathcal{V}(E)\right]^n + \sum_{n,m=0}^{\infty} PV g_a^{n+1} V g_a^{m+1} VP \left[-\mathcal{V}(E)\right]^{n+m} + \sum_{n,m,\ell=0}^{\infty} PV g_a^{n+1} V g_a^{m+1} V g_a^{\ell+1} VP \left[-\mathcal{V}(E)\right]^{n+m+\ell} + \ldots \tag{B.21}$$

As a first step we simply need the expansion for $\mathcal{V}(E)$ to second order. Iterating the last equation once gives

$$\mathcal{V}(E) = \Delta_b P_b + \Delta_c P_c + PVP + PV g_a V P_a + \sum_{n=0}^{\infty} PV g_a^{n+1} V P_b (-1)^n \Delta_b^n + \sum_{n=0}^{\infty} PV g_a^{n+1} V P_c (-1)^n \Delta_c^n + O(V^3). \tag{B.22}$$

Now, we can sum these series since

$$\sum_{n=0}^{\infty} g_a^{n+1} (-1)^n \Delta_b^n = g_a \sum_{n=0}^{\infty} \left(-g_a \Delta_b\right)^n = \frac{Q}{1/g_a + \Delta_b} = \frac{Q}{\varepsilon_b - H_0} \equiv g_b \tag{B.23}$$

with a similar result for the other sum. So, (B.22) is just

$$\mathcal{V}(E) = \Delta_b P_b + \Delta_c P_c + PVP + PVg_a VP_a + PVg_b VP_b + PVg_c VP_c + O(V^3). \tag{B.24}$$

All that remains to be done is to substitute (B.24) in (B.21) and expand the resulting expression consistently to fourth order in V. This is somewhat complicated, so we shall content ourselves with describing the steps involved and stating the important intermediate results.

It is the first sum in (B.21) which causes the most trouble. We have to expand the quantity

$$\sum_{n=0}^{\infty} PVg_a^{n+1} VP(-1)^n \left(\Delta_b P_b + \Delta_c P_c + PVP + PVg_a VP_a + PVg_b VP_b + PVg_c VP_c\right)^n \tag{B.25}$$

to fourth order in V. The lemma which tells us how to do this is: for $n \geq 4$,

$$\begin{aligned}
(\Delta_b P_b + \Delta_c P_c + X)^n &= \Delta_b^n P_b + \Delta_c^n P_c \\
&+ \Delta_b^{n-1}[P_b X + (n-2)P_b XP_b + XP_b] + \Delta_c^{n-1}[P_c X + (n-2)P_c XP_c + XP_c] \\
&+ D_{n-2}(P_b XP_c + P_c XP_b) + \Delta_b^{n-2}(P_b X^2 + XP_b X + X^2 P_b) \\
&+ \Delta_c^{n-2}(P_c X^2 + XP_c X + X^2 P_c) + (n-3)\Delta_b^{n-2}(P_b XP_b X + P_b X^2 P_b + XP_b XP_b) \\
&+ (n-3)\Delta_c^{n-2}(P_c XP_c X + P_c X^2 P_c + XP_c XP_c) + \tfrac{1}{2}(n-3)(n-4)\Delta_b^{n-2} P_b XP_b XP_b \\
&+ \tfrac{1}{2}(n-3)(n-4)\Delta_c^{n-2} P_c XP_c XP_c + D_{n-3}(P_b XP_c X + P_b X^2 P_c + XP_b XP_c) \\
&+ D_{n-3}(P_c XP_b X + P_c X^2 P_b + XP_c XP_b) \\
&+ \Delta_b^2 \frac{\partial}{\partial \Delta_b} D_{n-4}(P_b XP_b XP_c + P_b XP_c XP_b + P_c XP_b XP_b) + \Delta_c^2 \frac{\partial}{\partial \Delta_c} D_{n-4} \\
&\times (P_c XP_c XP_b + P_c XP_b XP_c + P_b XP_c XP_c) + O(X^3)
\end{aligned} \tag{B.26}$$

where

$$D_n \equiv \Delta_b^n \Delta_c + \Delta_b^{n-1} \Delta_c^2 + \ldots\ldots + \Delta_b \Delta_c^n \qquad (B.27)$$

$$D_o \equiv 0$$

which is proved by induction on n. Having carried out this expansion, we do the sums over n. The formulae we require, in addition to (B.23) are:

$$\sum_{n=1}^{\infty} (-1)^n g_a^{n+1} n \Delta_b^{n-1} = -g_b^2 \qquad (B.28)$$

$$\sum_{n=2}^{\infty} (-1)^n g_a^{n+1} \left(\Delta_b^{n-1} + D_{n-2} + \Delta_c^{n-1} \right) = g_a^2 - g_b g_c \qquad (B.29)$$

$$\sum_{n=2}^{\infty} (-1)^n g_a^{n+1} \tfrac{1}{2} n(n-1) \Delta_b^{n-2} = g_b^3 . \qquad (B.30)$$

The remaining two sums in (B.21) are simply more of the same, but are trivial by comparison with the first.

Eventually, after collecting all the terms, we arrive at the

the formula for the Hamiltonian matrix in the 3-state subspace, to fourth order in V:

$$\begin{aligned} E = {} & \varepsilon_a P_a + \varepsilon_b P_b + \varepsilon_c P_c + PVP + PVg_a VP_a + PVg_b P_b + PVg_c VP_c \\ & + PVg_a Vg_a VP_a + PVg_b Vg_b VP_b + PVg_c Vg_c VP_c - PVg_a^2 VP_a VP_a \\ & - PVg_b^2 VP_b VP_b - PVg_c^2 VP_c VP_c - PVg_a g_b VP(P_a VP_b + P_b VP_a) \\ & - PVg_b g_c VP(P_b VP_c + P_c VP_b) - PVg_c g_a VP(P_c VP_a + P_a VP_c) \\ & + PVg_a Vg_a Vg_a VP_a + PVg_b Vg_b Vg_b VP_b + PVg_c Vg_c Vg_c VP_c \\ & - (PVg_a^2 Vg_a VP + PVg_a Vg_a^2 VP) P_a VP_a - (PVg_b^2 Vg_b VP + PVg_b Vg_b^2 VP) P_b VP_b \end{aligned}$$

$$
\begin{aligned}
&- (PVg_c^2Vg_cVP + PVg_cVg_c^2VP)P_cVP_c + \frac{1}{\varepsilon_b-\varepsilon_c}(PVg_bVg_bVP - PVg_aVg_aVP) \\
&\times (P_aVP_b + P_bVP_a) + \frac{1}{\varepsilon_c-\varepsilon_a}(PVg_cVg_cVP - PVg_aVg_aVP)(P_aVP_c + P_cVP_a) \\
&+ \frac{1}{\varepsilon_c-\varepsilon_b}(PVg_cVg_cVP - PVg_bVg_bVP)(P_bVP_c + P_cVP_b) \\
&- PVg_a^2VP_aVg_aVP_a - PVg_b^2VP_bVg_bVP_b - PVg_c^2VP_cVg_cVP_c \\
&- PVg_ag_bVP(P_aVg_bVP_b + P_bVg_aVP_a) - PVg_bg_cVP(P_bVg_cVP_c + P_cVg_bVP_b) \\
&- PVg_cg_aVP(P_cVg_aVP_a + P_aVg_cVP_c) + PVg_a^3VP_aVP_aVP_a + PVg_b^3VP_bVP_bVP_b \\
&+ PVg_c^3VP_cVP_cVP_c + PVg_ag_b^2VP(P_aVP_bVP_b + P_bVP_aVP_b + P_bVP_bVP_a) \\
&+ PVg_a^2g_bVP(P_aVP_aVP_b + P_aVP_bVP_a + P_bVP_aVP_a) \\
&+ PVg_bg_c^2VP(P_cVP_cVP_b + P_cVP_bVP_c + P_bVP_cVP_c) \\
&+ PVg_b^2g_cVP(P_bVP_bVP_c + P_bVP_cVP_b + P_cVP_bVP_b) \\
&+ PVg_cg_a^2VP(P_aVP_aVP_c + P_aVP_cVP_a + P_cVP_aVP_a) \\
&+ PVg_c^2g_aVP(P_aVP_cVP_c + P_cVP_aVP_c + P_cVP_cVP_a) \\
&+ PVg_ag_bg_cVP(P_aVP_bVP_c + P_bVP_cVP_a + P_cVP_aVP_b + P_aVP_cVP_b + P_cVP_bVP_a \\
&+ P_bVP_aVP_c) + O(V^5).
\end{aligned}
$$

(B.31)

The result for two states can be obtained immediately from this formula, by dropping all terms involving the state $|c\rangle$:

$$
\begin{aligned}
E = {} & \varepsilon_a P_a + \varepsilon_b P_b + PVP + PVg_aVP_a + PVg_bVP_b + PVg_aVg_aVP_a + PVg_bVg_bVP_b \\
& - PVg_a^2VP_aVP_a - PVg_b^2VP_bVP_b - PVg_ag_bVP(P_aVP_b + P_bVP_a) \\
& + PVg_aVg_aVg_aVP_a + PVg_bVg_bVg_bVP_b - (PVg_a^2Vg_aVP + PVg_aVg_a^2VP)P_aVP_a \\
& - (PVg_b^2Vg_bVP + PVg_bVg_b^2VP)P_bVP_b + \frac{1}{\varepsilon_b-\varepsilon_a}(PVg_bVg_bVP - PVg_aVg_aVP) \\
& \times (P_aVP_b + P_bVP_a) - PVg_a^2VP_aVg_aVP_a - PVg_b^2VP_bVg_bVP_b \\
& - PVg_ag_bVP(P_aVg_bVP_b + P_bVg_aVP_a) + PVg_a^3VP_aVP_aVP_a + PVg_b^3VP_bVP_bVP_b \\
& + PVg_ag_b^2VP(P_aVP_bVP_b + P_bVP_aVP_b + P_bVP_bVP_a) \\
& + PVg_a^2g_bVP(P_aVP_aVP_b + P_aVP_bVP_a + P_bVP_aVP_a) + O(V^5).
\end{aligned}
\tag{B.32}
$$

The two-state formula to eighthorder in V has been used in our calculations, but is too long to be given here.

REFERENCES

Abramowitcz, M. and Stegun, I. A., 1965, 'Handbook of Mathematical Functions' (Dover, New York).

Appel, K. and Haken, W., 1977, Sci. Am. 237, No. 4.

Baker, G. A. Jnr., 1975, 'Essentials of Padé Approximants' (Academic Press, New York).

Banks, T., Susskind, L. and Kogut, J. B., 1976, Phys. Rev. D13, 1043.

Banks, T., Raby, S., Susskind, L., Kogut, J. B., Jones, D. R. T., Sharbach, P. N. and Sinclair, D. K., 1977, Phys. Rev. D15 1111.

Bethe, H. A., 1931, Z. Physik, 71 205.

Carroll, A., Kogut, J. B., Sinclair, D. K. and Susskind, L., 1976 Phys. Rev. D13 2270 and Erratum: Phys. Rev. D14 1729.

Carroll, A., Baker, G. A. Jnr., and Gammel, J. L., 1977, Nucl. Phys. B129 361.

Casher, A., Kogut, J. B. and Susskind, L., 1974, Phys. Rev. D10 732.

Coleman, S., 1973, Comm. Math. Phys. 31 259.

Coleman, S., 1975, Phys. Rev. D11 2088.

Coleman, S., 1976, Ann. of Phys. 101 239.

Coleman, S., Jackiw, R. and Susskind, L., 1975, Ann. of Phys. 93 267.

Dashen, R. F., Hasslacher, B. and Neveu, A., 1975, Phys. Rev. D11 3424.

Des Cloizeaux, J. and Pearson, J. J., 1962, Phys. Rev. 128 2131.

Drell, S. D., Weinstein, M. and Yankielowicz, S., 1976, Phys. Rev. D14 487.

Endo, Y. and Ishikawa, T., 1974, J.Phys.Soc. of Japan 37 681.

Hamer, C. J., 1977, Nucl. Phys. B121 159.

Hulthén, L., 1938, Arkiv. Mat. Astron. Fys. 26A No. 11.

Jackiw, R., 1973, Erice lectures.

Jurkiewicz, J. and Wosiek, J., 1978, Nucl. Phys. B135 416.

Kadanoff, L. P., 1976, Ann. of Phys. 100 359.

Kenway, R. D. and Hamer, C. J., 1978, Nucl. Phys. B139 85.

Kogut, J. B., 1976, 'Three Lectures on Lattice Gauge Theory' Cornell Preprint CLNS-347.

Kogut, J. B. and Susskind, L., 1975a, Phys. Rev. D11 3594.

Kogut, J. B. and Susskind, L., 1975b, Phys. Rep. 23C 348.

Kurak, V., Schroer, B. and Swieca, J. A., 1977, 'Comments on Confinement Criteria', CERN preprint TH.2374.

Lowenstein, J. H. and Swieca, J. A., 1971, Ann. of Phys. 68 172.

Luther, A., 1976, Phys. Rev. B14 2153.

Marciano, W. and Pagels, H., 1978, Phys. Rep. 36C 137.

Mattis, D. C., 1965, 'The Theory of Magnetism' (Harper and Row, New York).

Migdal, A. A., 1975, Zh. Eksp. Teor. Fiz. 69 810, 1477.

Paul c. 70 Lett. to Hebrews Ch. 11 vs. 3 (Revised Standard Version).

Schroer, B., Truong, T. T. and Weisz, P., 1976, Phys. Lett. 63B 422.

Schwinger, J., 1962, Phys. Rev. 128 2425.

Shigemitsu, J. and Elitzur, S., 1976, Phys. Rev. D14, 1988.

Steinhardt, P. J., 1977, Phys. Rev. D16 1782.

Susskind, L., 1976, Les Houches Lectures.

Susskind, L., 1977, Phys. Rev. D16 3031.

Thompson, C. J., 1972, 'Phase Transitions and Critical Phenomena' Vol. 1, ed. C. Domb and M. S. Green (Academic Press, London).

Weinberg, S., 1977, 'The Problem of Mass', Harvard Preprint HUTP-77/A057.

Wilson, K. G., 1974, Phys. Rev. D10 2445.

Wilson, K. G., 1975, Erice Lectures.

Zinn-Justin, J., 1971, Phys. Rep. 1C 55.

Table 2.1

Continuum limit ($u \to \infty$) of the Padé approximants for the odd-lattice formulation of the linear potential model.

N	1	2	3	4	5	6	7	8
$\frac{E_1^{odd}}{E_0^{odd}}$ [N,N]	3.000	3.286	1.284	1.283	2.161	2.330	1.754	1.712
$\frac{m^{1/3}}{g^{4/3}} E_0^{odd}$[N,N-1]	0.572	0.669	0.636	0.646	0.642	0.643	0.642	0.642
$\frac{m^{1/3}}{g^{4/3}} E_1^{odd}$[N,N-1]	0.826	-	1.501	-	2.791	-	6.218	-

Table 4.1

Scalar mass matrix elements in space of 1, 3 and 5 link states; $\alpha = 1+2\mu$, $\beta = 3+2\mu$, $\gamma = 1-2\mu$, $\delta = 5+2\mu$, $\varepsilon = 3-2\mu$.

Order	Term	W_{11}	W_{33}	W_{55}	W_{13}	W_{31}	W_{15}	W_{51}	W_{35}	W_{53}
zeroth	1	$1+2\mu$	$3+2\mu$	$5+2\mu$	0	0	0	0	0	0
second	x^2/α	6	5	7	0	-2	0	0	0	-2
	x^2/β	0	0	-1	0	0	0	0	0	0
	x^2/γ	0	1	2	2	0	0	0	2	0
fourth	x^4/α^3	-24	-17	-23	0	3	0	0	0	4
	$x^4/\alpha^2\beta$	0	0	0	0	5	0	-2	0	0
	$x^4/\alpha^2\gamma$	-4	-2	2	0	-2	0	0	0	-2
	$x^4/\alpha\gamma^2$	0	2	2	8	0	0	0	4	0
	x^4/γ^3	0	-1	-2	-2	0	0	0	-2	0
	x^4/β^3	0	0	1	0	0	0	0	0	0
	$x^4/\gamma^2\beta$	0	0	2	0	0	0	0	2	0
	$x^4/\gamma\beta^2$	0	0	-2	0	0	0	0	0	0
	x^4/α^2	0	0	-2	0	0	0	0	0	0
	$x^4/\gamma^2\varepsilon$	0	0	0	0	0	2	0	0	0
	$x^4/\alpha\beta\delta$	0	0	0	0	0	0	0	0	-2

Table 4.2

Strong-coupling expansion to fourth order for the scalar mass matrix in the subspace $\{|1+\rangle, |2,1+\rangle, |3+\rangle\}$ using the modified Hamiltonian (4.93). Notation: $\alpha = 1 + 2\mu + 4C$, $\beta = 1 + 2\mu + 2C$, $\gamma = 1 + 2\mu$, $\delta = 1 - 2\mu + 4C$, $\varepsilon = 1 + 2C$, $\xi = 1 - 2\mu$, $\eta = 3 + 2\mu + 4C$, $\nu = 3 + 2\mu + 8C$.

Order	Term	W^+_{11}	W^+_{22}	W^+_{33}	W^+_{12}	W^+_{21}	W^+_{13}	W^+_{31}	W^+_{23}	W^+_{32}
zeroth	1	$1 + 2\mu + 4C$	$2 + 4\mu + 4C$	$3 + 2\mu + 8C$	0	0	0	0	0	0
first	x	0	0	0	2	2	0	0	1	1
second	x^2/α	10	7	7	0	0	0	0	0	0
	x^2/γ	0	-4	-2	0	0	0	0	0	0
third	$x^3/\alpha C$	0	0	0	-2	0	0	0	0	0
	$x^3/\gamma C$	0	0	0	1	0	0	0	0	0
	$x^3/\alpha\beta$	0	0	0	0	-7	0	0	0	0
	$x^3/\alpha\gamma$	0	0	0	0	2	0	0	0	0

Table 4.2 (Continued)

third	x^3/α^2	0	0	0	0	-4	0	0	0	0
	$x^3/\gamma\varepsilon$	0	0	0	0	0	0	0	0	1
fourth	x^4/α^3	-68	-41	-41	0	0	0	0	0	0
	$x^4/\alpha^2\beta$	28	22	18	0	0	0	0	0	0
	$x^4/\alpha^2 C$	-4	0	0	0	0	0	0	0	0
	$x^4/\alpha^2\gamma$	-2	-2	3	0	0	0	0	0	0
	$x^4/\alpha\gamma^2$	-4	-4	2	0	0	0	0	0	0
	$x^4/\gamma^2 C$	2	1	0	0	0	0	0	0	0
	$x^4/\gamma^2\delta$	0	4	0	0	0	0	0	0	0
	$x^4/\gamma\delta\varepsilon$	0	-2	0	0	0	0	0	0	0
	$x^4/\gamma^2\varepsilon$	0	-4	1	0	0	0	4	0	0

Table 4.2(Continued)

fourth	x^4/γ^3	0	0	1	0	0	0	0	0	0
	x^4/γ^2	0	0	-2	0	0	0	0	0	0
	$x^4/\alpha\xi C$	0	0	0	0	0	2	0	0	0
	$x^4/\gamma\delta C$	0	0	0	0	0	-1	0	0	0
	$x^4/\gamma\delta\xi$	0	0	0	0	0	-4	0	0	0
	$x^4/\alpha\beta\nu$	0	0	0	0	0	0	7	0	0
	$x^4/\alpha\gamma\eta$	0	0	0	0	0	0	-2	0	0
	$x^4/\gamma\varepsilon\eta$	0	0	0	0	0	0	-2	0	0
	$x^4/\gamma^2\eta$	0	0	0	0	0	0	-4	0	0

Table 6.1.

Strong-coupling expansions for (rescaled) energy eigenvalues w_s on lattice I for unequal-mass quarks.

The first column in the table shows the order of the expansion in powers of x. The second column lists the terms which contribute at any given order, where we define: $\alpha_i = 1 + 2\mu_i$, $\beta = 4 + 2\mu_1 + 2\mu_2$, $\gamma_i = 3 + 2\mu_i$, $\varepsilon = 2\mu_1 - 2\mu_2$, $\xi_i = 1 - 2\mu_i$, $\tau = 2\mu_1 + 2\mu_2$. The remaining columns list the coefficients of each term associated with a given eigenstate.

Eigenstate:		Vacuum	$\|1\bar{2}\rangle$ ->	$\|1\bar{1}\rangle$ ->	$\|1\bar{2}\rangle_+$	$\|1\bar{1}\rangle_+$
Order	Term	w_o/N	$w^-_{1\bar{2}} - w_o$	$w^-_{1\bar{1}} - w_o$	$w^+_{1\bar{2}} - w_o$	$w^+_{1\bar{1}} - w_o$
zeroth	1	0	$1 + \mu_1 + \mu_2$	$1 + 2\mu_1$	$1 + \mu_1 + \mu_2$	$1 + 2\mu_1$
second	x^2/α_1	-1	1	2	3	6
	x^2/α_2	-1	1	1	3	1
	x^2/γ_2	0	0	-1	0	-1
fourth	x^4/α_1^3	3	-3	-8	-11	-24
	$x^4/\alpha_1^2\alpha_2$	1	-4	-2	-4	-6
	$x^4/\alpha_1\alpha_2^2$	1	-4	-2	-4	-6
	x^4/α_2^3	3	-3	-5	-11	-5
	$x^4/\alpha_1^2\beta$	-1	3	6	3	3
	$x^4/\alpha_1\alpha_2\beta$	-2	6	12	6	6
	$x^4/\alpha_2^2\,\beta$	-1	3	3	3	3
	x^4/α_2^2	0	$-\frac{1}{2}$	0	$-\frac{1}{2}$	0
	$x^4/\alpha_1\alpha_2$	0	-1	0	-1	0

Table 6.1. (Continued)

fourth	x^4/α_1^2	0	$-\frac{1}{2}$	-2	$-\frac{1}{2}$	-2
	$x^4/\alpha_2^2\varepsilon$	0	0	1	0	1
	$x^4/\alpha_2\gamma_2\varepsilon$	0	0	-2	0	-2
	$x^4/\alpha_2\gamma_2\beta$	0	0	6	0	0
	$x^4/\gamma_2^2\varepsilon$	0	0	1	0	1
	$x^4/\gamma_2^2\beta$	0	0	-3	0	0
	$x^4/\alpha_2\gamma_2^2$	0	0	2	0	2
	$x^4/\alpha_2^2\gamma_2$	0	0	2	0	2
	x^4/γ_2^3	0	0	1	0	1
	$x^4/\alpha_1^2\gamma_2$	0	0	-4	0	3
	$x^4/\gamma_2^2\alpha_1$	0	0	4	0	-3
	$x^4/\alpha_2\gamma_2\alpha_1$	0	0	-8	0	6

Table 6.2

Strong-coupling expansions for (rescaled) energy eigenvalues, w_s, on lattice I for equal-mass quarks. The format is the same as for Table 6.1, and the energy denominators are defined as follows: $\alpha = 1 + 2\mu$, $\beta = 4 + 4\mu$, $\gamma = 3 + 2\mu$, $\delta = 5 + 2\mu$, $\nu = 5 + 6\mu$.

Eigenstate:	Vacuum	$\|0 ->$	$\|1 ->$	$\|0 +>$	$\|1 +>$
Order	Term	w_o/N	$w_o^- - w_o$	$w_1^- - w_o$	$w_o^+ - w_o$	$w_1^+ - w_o$
zeroth	1	0	$1 + 2\mu$	$1 + 2\mu$	$1 + 2\mu$	$1 + 2\mu$
second	x^2/α	-2	4	2	8	6
	x^2/γ	0	-2	0	-2	0
fourth	x^4/α^3	8	-18	-14	-50	-30
	$x^4/\alpha^2\beta$	-4	12	12	12	12
	x^4/α^2	0	-2	-2	-2	-2
	$x^4/\alpha^2\gamma$	0	-4	0	20	0
	$x^4/\alpha\gamma^2$	0	4	0	-4	0
	x^4/γ^3	0	4	0	4	0
sixth	x^6/α^5	-70	178	152	514	296
	$x^6/\alpha^4\beta$	56	-160	-218	-192	-172
	$x^6/\alpha^3\beta^2$	16	-48	-50	-64	-64

Table 6.2 (Continued)

sixth	$x^6/\alpha^4\gamma$	-2	34	50	-238	-32
	x^6/α^4	0	20	22	20	18
	$x^6/\alpha^2\beta^2\delta$	0	-8	-8	-8	-8
	x^6/α^3	0	2	6	-2	$3\frac{1}{2}$
	$x^6/\alpha^2\gamma^3$	0	8	0	-88	0
	$x^6/\alpha\gamma^4$	0	-24	0	24	0
	$x^6/\alpha^3\gamma^2$	0	-20	0	92	0
	x^6/γ^5	0	-16	0	-16	0
	$x^6/\alpha^3\gamma$	0	-8	-10	-8	-9
	$x^6/\alpha^4\nu$	0	0	-12	0	0
	$x^6/\alpha^3\beta\nu$	0	0	-20	0	0
	$x^6/\alpha^2\beta^2\gamma$	0	0	-10	0	0
	$x^6/\alpha^3\beta$	0	0	-8	0	-8
	$x^6/\alpha^2\beta\delta$	0	0	-8	0	-8
	$x^6/\alpha^2\delta$	0	0	-2	0	-2
	$x^6/\alpha^2\beta^2\nu$	0	0	-8	0	0
	$x^6/\alpha^2\gamma$	0	0	-2	0	$-3\frac{1}{2}$
	$x^6/\alpha^3\beta\gamma$	0	0	-44	0	36

Table 6.3

Strong-coupling expansi

For an explanation of notati

Eigenstate:		Va
Order	Term	
zeroth	1	
second	x^2/α_1	
	x^2/α_2	
	x^2/ξ_2	
	x^2/ξ_1	
fourth	x^4/α_1^3	

$+ O(x^6)$.

ice II for unequal-mass quarks.

	$\lvert 1\bar{1} \rightarrow$	$\lvert 1\bar{1} +\rangle$
	$w^{-}_{1\bar{1}} - w_o$	$w^{+}_{1\bar{1}} - w_o$
	$1 + 2\mu_1$	$1 + 2\mu_1$
	2	6
	1	1
	1	1
	0	0
	-8	-24

Erratum

The strong-coupling expansio

is omitted from table 6.3. It is

$$w_{4q,3}^{\pm} - w_o = 2\mu_1 + 2\mu_2 + x^2\left(\frac{4}{\alpha_1} + \frac{4}{\alpha_2}\right) + x^4\left(-\frac{2}{\alpha_1^2} - \frac{2}{\alpha_2^2} - \frac{16}{\alpha_1^3} - \frac{4}{\alpha_1^2\alpha_2} - \frac{4}{\alpha_1\alpha_2^2} - \frac{16}{\alpha_2^3} + \frac{4}{\xi\alpha_1^2} + \frac{8}{\xi\alpha_1\alpha_2} + \frac{4}{\xi\alpha_2^2}\right)$$

Table 6.3

Strong-coupling expansions for (rescaled) energy eigenvalues w_s on lattice II for unequal-mass quarks. For an explanation of notation see the caption for Table 6.1.

Eigenstate:		Vacuum	$\|1\bar{2}$ ->	$\|1\bar{2},2\bar{1}$ ->	$\|1\bar{2},2\bar{1}$ +>	$\|1\bar{1}$ ->	$\|1\bar{1}$ +>
Order	Term	w_o/N	$w^-_{1\bar{2}} - w_o$	$w^-_{1\bar{2}2\bar{1}} - w_o$	$w^+_{1\bar{2}2\bar{1}} - w_o$	$w^-_{1\bar{1}} - w_o$	$w^+_{1\bar{1}} - w_o$
zeroth	1	0	$\mu_1 + \mu_2$	$2\mu_1 + 2\mu_2$	$2\mu_1 + 2\mu_2$	$1 + 2\mu_1$	$1 + 2\mu_1$
second	x^2/α_1	-1	2	3	3	2	6
	x^2/α_2	-1	2	3	3	1	1
	x^2/ξ_2	0	0	-1	-1	1	1
	x^2/ξ_1	0	0	-1	-1	0	0
fourth	x^4/α_1^3	3	-8	-11	-11	-8	-24

Table 6.3 (Continued)

fourth	$x^3/\alpha_1^2\tau$	-1	0	2	6	6	3
	$x^4/\alpha_1\alpha_2\tau$	-2	0	4	12	12	6
	$x^4/\alpha_2^2\tau$	-1	0	2	6	3	3
	x^4/α_2^3	3	-8	-11	-11	-5	-5
	$x^4/\alpha_1\alpha_2^2$	1	-2	-3	-3	-2	-5
	$x^4/\alpha_1^2\alpha_2$	1	-2	-3	-3	-2	-5
	x^4/α_1^2	0	-1	-1	-1	-2	-2
	$x^4/\alpha_1\alpha_2$	0	-2	0	3	0	0
	x^4/α_2^2	0	-1	-1	-1	0	0

Table 6.3 (Continued)

fourth	$x^4/\xi_2^2\varepsilon$	0	0	0	0	1	1
	$x^4/\xi_2\alpha_2\varepsilon$	0	0	0	0	2	0
	$x^4/\xi_2^2\tau$	0	0	0	0	-3	0
	$x^4\xi_2\alpha_2\tau$	0	0	0	0	-6	0
	$x^4/\alpha_2^2\varepsilon$	0	0	0	0	1	0
	x^4/ξ_2^3	0	0	1	1	-1	-1
	$x^4/\xi_2\alpha_2^2$	0	0	0	0	-2	-2
	$x^4/\xi_2\alpha_1^2$	0	0	-1	3	4	-3
	$x^4/\xi_2\alpha_2\alpha_1$	0	0	-1	0	8	-4

Table 6.3 (Continued)

fourth	$x^4/\alpha_1^2\xi_1$	0	0	0	0	0	0
	$x^4/\alpha_1\xi_1^2$	0	0	0	0	0	0
	x^4/ξ_1^3	0	0	1	1	0	0
	$x^4/\xi_1^2\xi_2$	0	0	1	1	0	0
	$x^4/\xi_1\xi_2^2$	0	0	1	1	0	0
	$x^4/\alpha_1\xi_1\alpha_2$	0	0	-1	0	0	0
	$x^4/\xi_1\xi_2\alpha_2$	0	0	0	0	0	0
	$x^4/\alpha_1^2\varepsilon$	0	0	0	0	0	1
	$x^4/\alpha_i\xi_2\varepsilon$	0	0	0	0	0	2

Table 6.3 (Continued).

fourth	$x^4/\xi_2^2\alpha_2$	0	0	0	0	2	2
	$x^4/\xi_2^2\alpha_1$	0	0	-1	3	4	-3
	x^4/ξ_1^2	0	0	-1	-1	0	0
	x^4/ξ_2^2	0	0	-1	-1	0	0
	$x^4/\alpha_1\xi_2$	0	0	$-\frac{1}{2}$	3	0	0
	$x^4/\alpha_2\xi_1$	0	0	$-\frac{1}{2}$	3	0	0
	$x^4/\xi_1\xi_2$	0	0	1	1	0	0
	$x^4/\xi_1^2\alpha_2$	0	0	-1	3	0	0
	$x^4/\xi_1\alpha_2^2$	0	0	-1	3	0	0

Table 6.4

Strong-coupling expansions for (rescaled) energy eigenvalues, w_s, on lattice II, for equal-mass quarks. The two-quark states are labelled $|I,I_3,P>$. The four-quark states are labelled $|4q,I,I_3,P>$ and are only given to fourth order. The energy denominators are: $\alpha = 1+2\mu$, $\xi = 1-2\mu$, $\gamma = 3+2\mu$, $\delta = 5+2\mu$, $\phi = 1-6\mu$, $\psi = 1+6\mu$.

Eigenstate:		Vacuum	$\|1,1,->$	$\|4q,1,0,->$	$\|1,0,->$	$\|0,0,->$	$\|1,0,+>$	$\|4q,0,0,+>$	$\|0,0,+>$
Order	Term	w_o/N	$w^-_{11} - w_o$	$w^-_{10} - w_o$	$w^-_{10} - w_o$	$w^-_{00} - w_o$	$w^+_{10} - w_o$	$w^+_{00} - w_o$	$w^+_{00} - w_o$
zeroth	1	0	2μ	4μ	$1 + 2\mu$	$1 + 2\mu$	$1 + 2\mu$	4μ	$1 + 2\mu$
second	x^2/α	-2	4	6	4	2	6	6	8
	x^2/ξ	0	0	-2	2	0	0	-2	2
fourth	x^4/α^3	8	-20	-28	-18	-14	-30	-28	-50
	$x^4/\alpha^2\mu$	-1	0	2	6	3	3	6	3
	x^4/α^2	0	-4	-2	-2	-2	-2	-2	-2
	$x^4/\xi^2\mu$	0	0	0	-3	0	0	0	0
	x^4/ξ^3	0	0	4	-4	0	0	4	-4
	$x^4/\alpha^2\xi$	0	0	-4	16	0	0	12	-20

Table 6.4 (Continued)

Order	Term	w_o/N	$w^-_{11} - w_o$	$w^-_{10} - w_o$	$w^-_{10} - w_o$	$w^-_{00} - w_o$	$w^+_{10} - w_o$	$w^+_{00} - w_o$	$w^+_{00} - w_o$
fourth	$x^4/\alpha\xi^2$	0	0	-4	16	0	0	4	-4
	$x^4/\alpha\xi$	0	0	0	0	0	0	4	0
sixth	x^6/α^5	-70	204		179	161	297		523
	$x^6/\alpha^4\mu$	14	-16		-84	-84	-52		-48
	$x^6/\alpha^3\mu^2$	1	-4		-6	-6	$-4\frac{1}{2}$		$-4\frac{1}{2}$
	$x^6/\alpha^4\gamma$	-2	4		8	-4	8		8
	x^6/α^4	0	40		0	22	18		26
	$x^6/\alpha^3\mu$	0	-8		0	-4	-4		0
	$x^6/\xi^3\mu^2$	0	0		$\frac{1}{2}$	0	0		0
	$x^6/\xi^2\mu^2\phi$	0	0		2	0	0		0
	$x^6/\alpha^4\psi$	0	0		16	0	0		0
	$x^6/\alpha^4\delta$	0	0		-1	-9	-1		-9
	$x^6/\alpha^3\delta$	0	0		-2	-6	-2		-6
	$x^6/\alpha^2\delta$	0	0		-1	-1	-1		-1

Table 6.4(continued)

Order	Term	w_o/N	$\bar{w}_{11} - w_o$	$\bar{w}_{10} - w_o$	$\bar{w}_{10} - w_o$	$\bar{w}_{00} - w_o$	$\dot{w}_{10} - w_o$	$\dot{w}_{00} - w_o$	$\dot{w}_{00} - w_o$
sixth	$x^6/\xi^4\mu$	0	0		38	0	0		0
	$x^6/\alpha^4\xi$	0	0		-142	-160	0		246
	$x^6/\alpha^2\xi$	0	0		-3	0	0		0
	x^6/ξ^5	0	0		16	0	0		16
	$x^6/\alpha\xi^4$	0	0		-176	0	0		24
	$x^6/\alpha^3\xi^2$	0	0		-140	-120	0		84
	$x^6/\alpha^2\xi^2$	0	0		8	0	0		4
	$x^6/\alpha^2\xi^3$	0	0		-168	0	0		88
	$x^6/\alpha\xi^2\mu\phi$	0	0		-32	0	0		0
	$x^6/\alpha^2\xi^2\psi$	0	0		-64	0	0		0
	$x^6/\alpha^2\xi^2\phi$	0	0		128	0	0		0
	$x^6/\alpha^2\xi\mu^2$	0	0		0	$2\frac{1}{2}$	0		0
	x^6/α^3	0	0		0	3	-1		-3
	$x^6/\alpha^2\xi^2\mu$	0	0		0	30	0		0
	$x^6/\alpha^3\xi$	0	0		0	0	0		16

Table 6.5

Strong coupling expansions for off-diagonal matrix elements between one- and three-link four-quark states on lattice II. Results are identical for scalars and pseudoscalars. For notation, see captions of Tables 6.1, 6.4.

Unequal Quark Masses:

Order	Term	$\langle 1\|W\|3\rangle$	$\langle 3\|W\|1\rangle$
fourth	$x^4/\alpha_1\alpha_2$	-2	-2
	$x^4/\alpha_1^2\tau$	-2	-2
	$x^4/\alpha_1\alpha_2\tau$	-4	-4
	$x^4/\alpha_2^2\tau$	-2	-2

Equal Quark Masses:

Order	Term	$\langle 1\|W\|3\rangle$	$\langle 3\|W\|1\rangle$
fourth	$x^4/\alpha^2\mu$	-2	-2
	x^4/α^2	-2	-2
sixth	$x^6/\alpha^3\mu^2$	-1	0
	$x^6/\alpha^2\xi\mu^2$	-1	0
	$x^6/\alpha^4\mu$	14	18
	$x^6/\alpha^3\mu$	-5	-5
	$x^6/\alpha^3\xi\mu$	-4	4

Table 6.5 (Continued)

Equal Quark Masses (Continued):

Order	Term	<1|W|3>	<3|W|1>
sixth	$x^6\alpha^2\xi\mu$	-1	-1
	$x^6/\alpha^2\xi^2\mu$	4	0
	x^6/α^4	14	18
	x^6/α^3	-2	0
	$x^6/\alpha^3\xi$	-4	4
	$x^6/\alpha^2\xi$	-2	0
	$x^6/\alpha^2\xi^2$	4	0

FIGURE CAPTIONS

Fig. 2.1: Linear potential.

Fig. 2.2: Diagonal Padé approximants to the ground state energy as functions of u (odd-lattice formulation of the linear potential model).

Fig. 2.3: Diagonal Padé approximants to the energy of the first excited state as functions of u (odd-lattice formulation of the linear potential model).

Fig. 2.4: Diagonal Padé approximants to the ratio of the energy of of the first excited state to the energy of the ground state as functions of u (odd-lattice formulation of the linear potential model).

Fig. 3.1: Dispersion law for massless fermions in the continuum.

Fig. 3.2: Dispersion law for eqn. (3.32).

Fig. 3.3: Dispersion law for eqn. (3.37).

Fig. 3.4: Diagonal Padé approximants to the pseudoscalar particle binding energy in the single-species Schwinger model as functions of $\sqrt{x}$. (a) is for $\frac{m}{g} = 0.01$; (b) is for $\frac{m}{g} = 0.1$; (c) is for $\frac{m}{g} = 1.0$; (d) is for $\frac{m}{g} = 10.0$.

Fig. 3.5: Estimates for the continuum binding energy of the pseudoscalar particle in the single-species Schwinger model,

Fig. 3.5: (Cont'd) based on the [8,8] Padé approximant. (a) is the value at $x = \infty$, and (b) is the peak value.

Fig. 3.6: Estimates for the continuum binding energy of the scalar particle in the single-species Schwinger model, based on the [8,8] Padé approximant. (a) is the value at $x = \infty$ and (b) is the peak value.

Fig. 3.6 (cont.): (c) is the value at u=1.01 corresponding to the estimate of Carroll et al. for the linear potential model.

(b) is for $\frac{m}{g} = 0.1$; (c) is for $\frac{m}{g} = 1.0$; (d) is for $\frac{m}{g} = 10.0$.

Fig. 3.8: Continuum estimates for the ratio of the scalar to pseudoscalar binding energies in the single-species Schwinger model, based on the [8,8] Padé approximant. (a) is the value at $x = \infty$ and (b) is the value at $u = 1.261$.

Fig. 3.9: Strong-coupling vacuum for $\theta = -\pi$.

Fig. 3.10: Vacuum state for $\theta \doteq -\pi$ capable of supporting a single quark with finite energy.

Fig. 3.11: An isolated quark with finite energy for $\theta = -\pi$.

Fig. 3.12: Dominant intermediate states for weak coupling in the vacuum of fig. 3.9.

Fig. 3.13: Dominant intermediate states for weak coupling in the vacuum of fig. 3.10.

Fig. 3.5: (Cont'd) based on the [8,8] Padé approximant. (a) is the value at $x = \infty$, and (b) is the peak value.

Fig. 3.6: Estimates for the continuum binding energy of the scalar particle in the single-species Schwinger model, based on the [8,8] Padé approximant. (a) is the value at $x = \infty$ and (b) is the peak value.

Fig. 3.7: Diagonal Padé approximants to the ratio of the scalar to pseudoscalar binding energies as functions of $\sqrt{x}$ in the single-species Schwinger model. (a) is for $\frac{m}{g} = 0.01$; (b) is for $\frac{m}{g} = 0.1$; (c) is for $\frac{m}{g} = 1.0$; (d) is for $\frac{m}{g} = 10.0$.

Fig. 3.8: Continuum estimates for the ratio of the scalar to pseudoscalar binding energies in the single-species Schwinger model, based on the [8,8] Padé approximant. (a) is the value at $x = \infty$ and (b) is the value at $u = 1.261$.

Fig. 3.9: Strong-coupling vacuum for $\theta = -\pi$.

Fig. 3.10: Vacuum state for $\theta \doteq -\pi$ capable of supporting a single quark with finite energy.

Fig. 3.11: An isolated quark with finite energy for $\theta = -\pi$.

Fig. 3.12: Dominant intermediate states for weak coupling in the vacuum of fig. 3.9.

Fig. 3.13: Dominant intermediate states for weak coupling in the vacuum of fig. 3.10.

Fig. 4.1: Estimates for the ratio of the energy of the first excited state to the energy of the ground state in the linear potential model.

Fig. 4.2: Continuum estimates for the ratio of the scalar to pseudoscalar binding energies in the ordinary Schwinger model, derived from [4,4] Padé approximants.

Fig. 4.3: Continuum estimate for the scalar/pseudoscalar mass ratio in the massless Schwinger model (4.98) as a function of the parameter C.

Fig. 4.4: Eigenvalues of the continuum limit of the matrix for the scalar/pseudoscalar mass ratio in the massless Schwinger model, as functions of the parameter C. (3-state calculation to fourth order).

Fig. 4.5: Scalar/pseudoscalar binding-energy ratio, obtained from the 3-state calculation with C = 0.1.

Fig. 4.6: Non-relativistic limit of scalar/pseudoscalar binding-energy ratio, obtained from the 3-state calculation, as a function of the parameter C.

Fig. 5.1: Allowed fermion configurations at any site in the lattice SU(2) Schwinger model.

Fig. 5.2: Ground-state energy to second order, as a function of the quark mass, for lattice I.

Fig. 5.3: Phase diagram for lattice I.

Fig. 6.1: Continuum estimates for (i) the $(1,0)^-$ meson mass and (ii) the 0^+ meson mass, derived from the fourth-order calculation for four-quark states of lattice II.

Fig. 6.2: Continuum eigenvalues of the mass matrix for (i) the $(1,0)^-$ meson, and (ii) the 0^+ meson. Dashed lines are the exact results expected for the smallest eigenvalue.

Fig. 6.3: Continuum eigenvalues of the matrix corresponding the $0^+/(1,0)^-$ meson mass ratio.

Fig. 6.4: Estimates for the binding energy of the 1^- state on lattice I, based on the [8,8] Padé approximant. (a) is the value at $x = \infty$; (b) is the peak value, and (c) is the value at $u = 0.88$.

Fig. 6.5: Estimates for the binding energies of (i) the $I_3 = 1$, and (ii) the $I = 1$, $I_3 = 0$ pseudoscalar mesons on lattice II, based on the [7,7] Padé approximant. (a) is the value at $x = \infty$, (b) is the peak value, and (c) is the value at $u = 0.2$.

Fig. 6.6: Estimate for $(1,0)^-$ meson mass from the four-quark-state calculation. (a) is the $x = \infty$ limit of the [7,7] Padé approximant, and (b) is its peak value.

Fig. 6.7: Estimate for the binding energy of the $(1,0)^-$ meson from the two-quark-state calculation on lattice II. (a) is the $x = \infty$ limit of the [7,7] Padé approximant, and (b) is its peak value.

Fig. 6.8: Estimates for the binding energy of the 0^+ meson on lattice II from calculations based on (i) the four-quark state and (ii) the two-quark state. (a) is the value of the [7,7] Padé approximant at $x = \infty$, and (b) is its peak value.

Fig. 6.9: Estimate for the 0^+ meson mass from the four-quark-state calculation. (a) is the $x = \infty$ limit of the [7,7] Padé approximant, and (b) is the peak value.

Fig. 6.10: Estimates for the ratio of the binding energies of the 0^+ to 1^- multiplets for (i) lattice I and (ii) lattice II, based on calculations for two-quark states. (a) is the value at $x = \infty$ of the [8,8] Padé approximant for lattice I and the [7,7] Padé approximant for lattice II. (b) is the value at $u = 1.26$. The dashed lines are the exact results in the strong- and weak-coupling limits.

Fig. 6.11: Estimates for the binding energies of (i) the 0^- meson, and (ii) the 1^+ meson on lattice I from [8,8] Padé approximant. (a) is the value at $x = \infty$, (b) is the peak value, and (c) is the value at $u = 1.0$.

Fig. 6.12: The $1\bar{2}$ and $1\bar{1}$ pseudoscalar meson masses in strong coupling for a quark-mass splitting $m_2 = 10m_1$. Curves are shown for both the $x \to \infty$ and peak-value estimates from the [7,7] Padé approximant on lattice II.

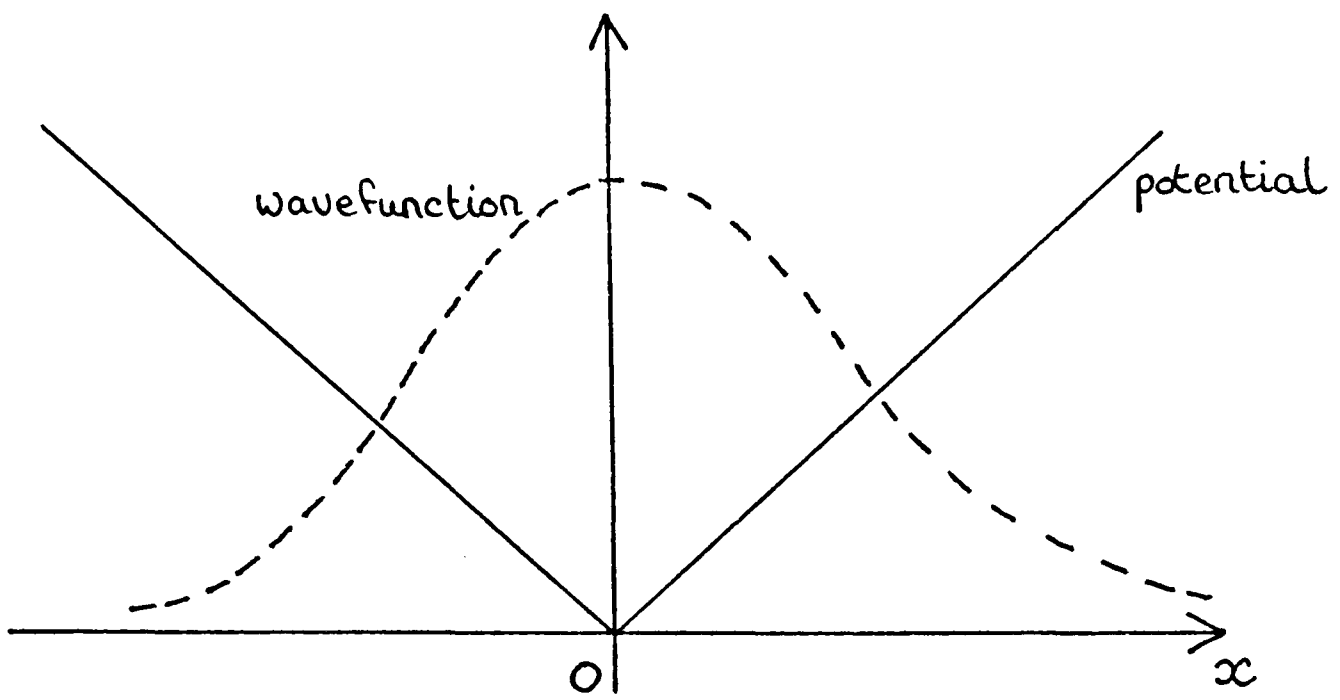


Fig. 2·1

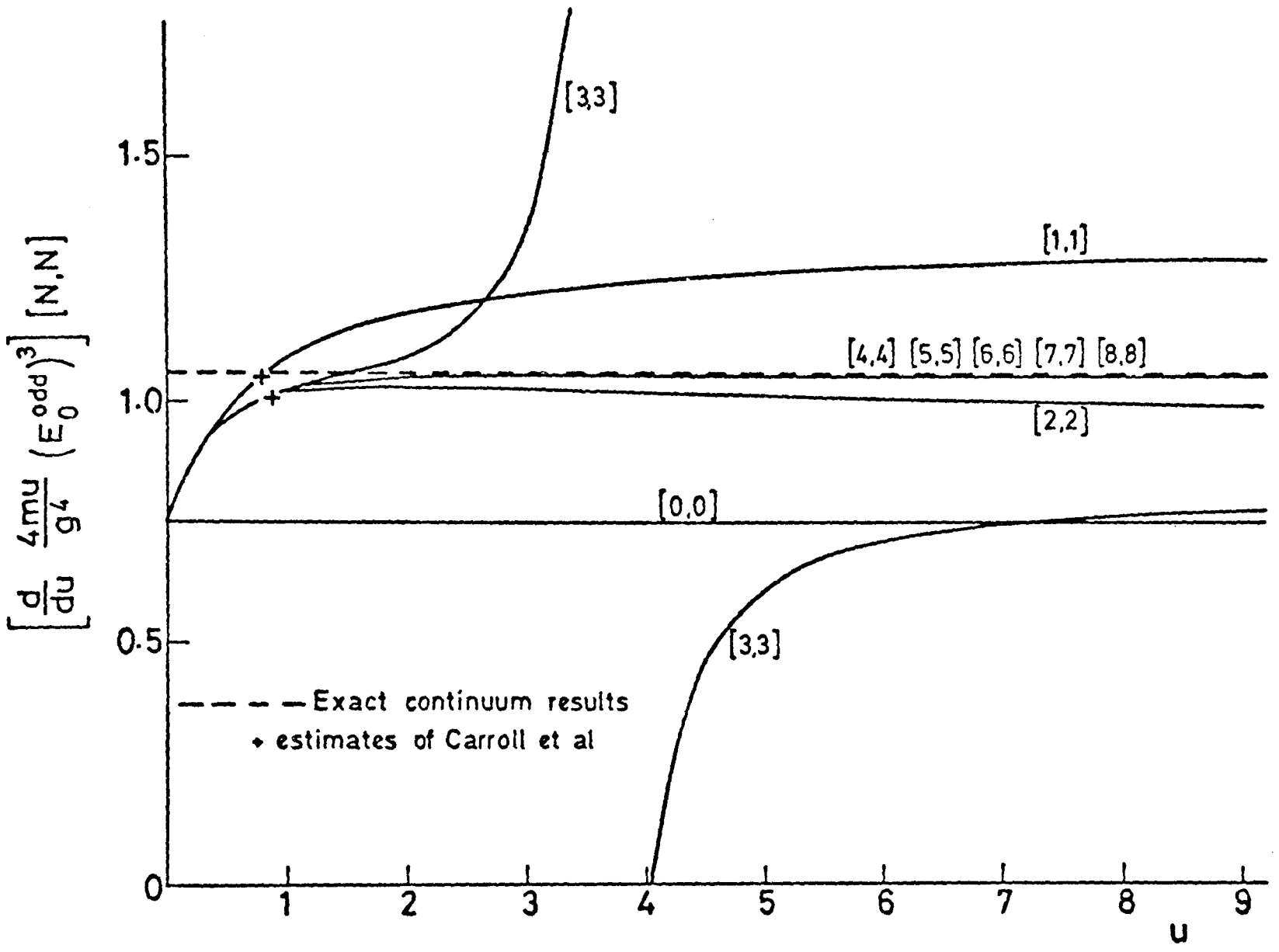

[3,3]
[1,1]
[4,4] [5,5] [6,6] [7,7] [8,8]
[2,2]
[0,0]
[3,3]
1.5
1.0
0.5
0
1
2
3
4
5
6
7
8
9
u
$\left[\frac{d}{du}\ \frac{4mu}{g^4}\ (E_0^{odd})^3\right][N,N]$
Exact continuum results
estimates of Carroll et al

Fig. 2·2

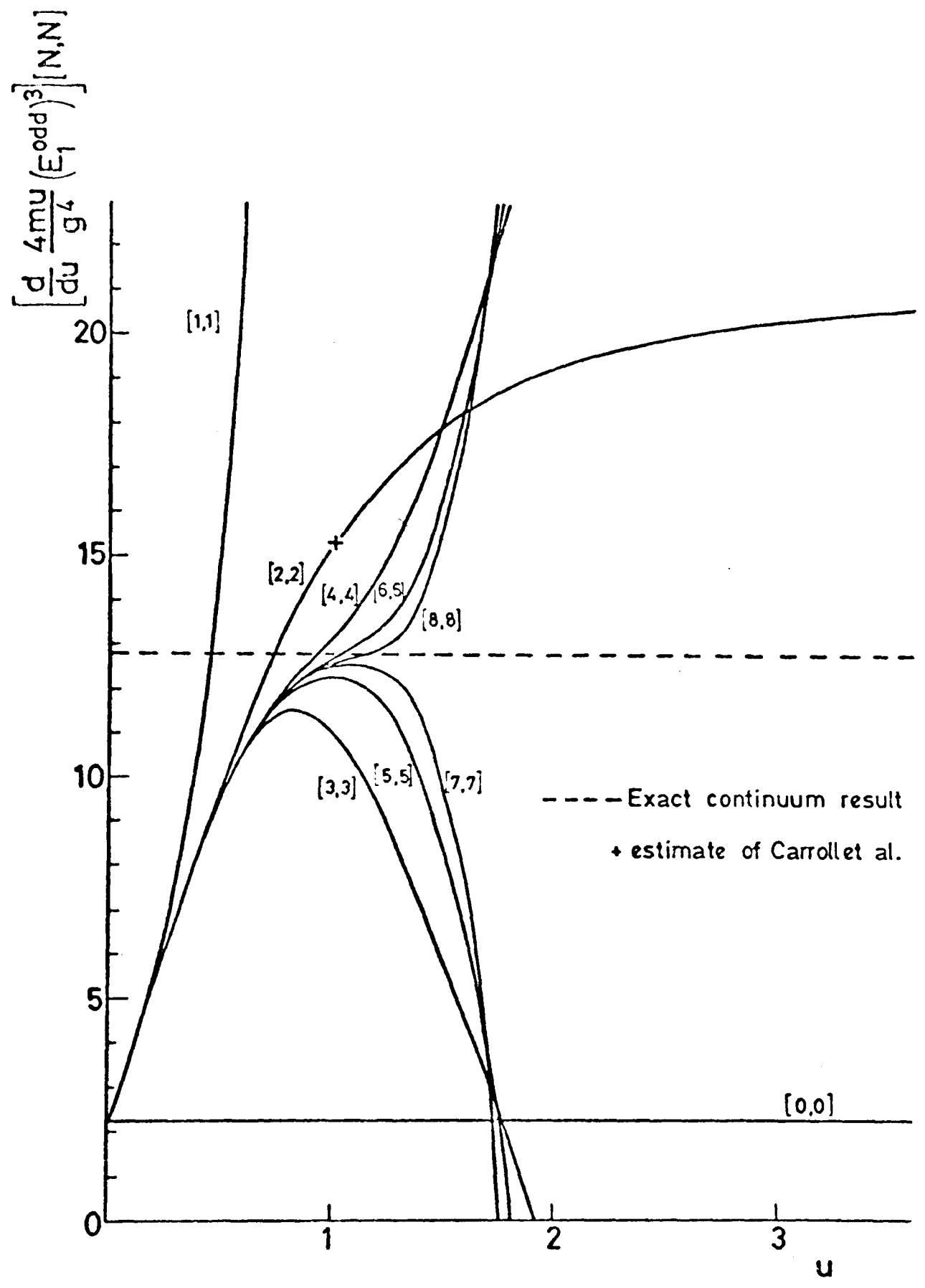

$\left[\frac{d}{du}\frac{4mu}{g^4}(E_1^{odd})^3\right][N,N]$
20
15
10
5
0
1
2
3
u
[1,1]
[2,2]
[4,4]
[6,6]
[8,8]
[3,3]
[5,5]
[7,7]
[0,0]
----Exact continuum result
+ estimate of Carroll et al.

Fig. 2·3

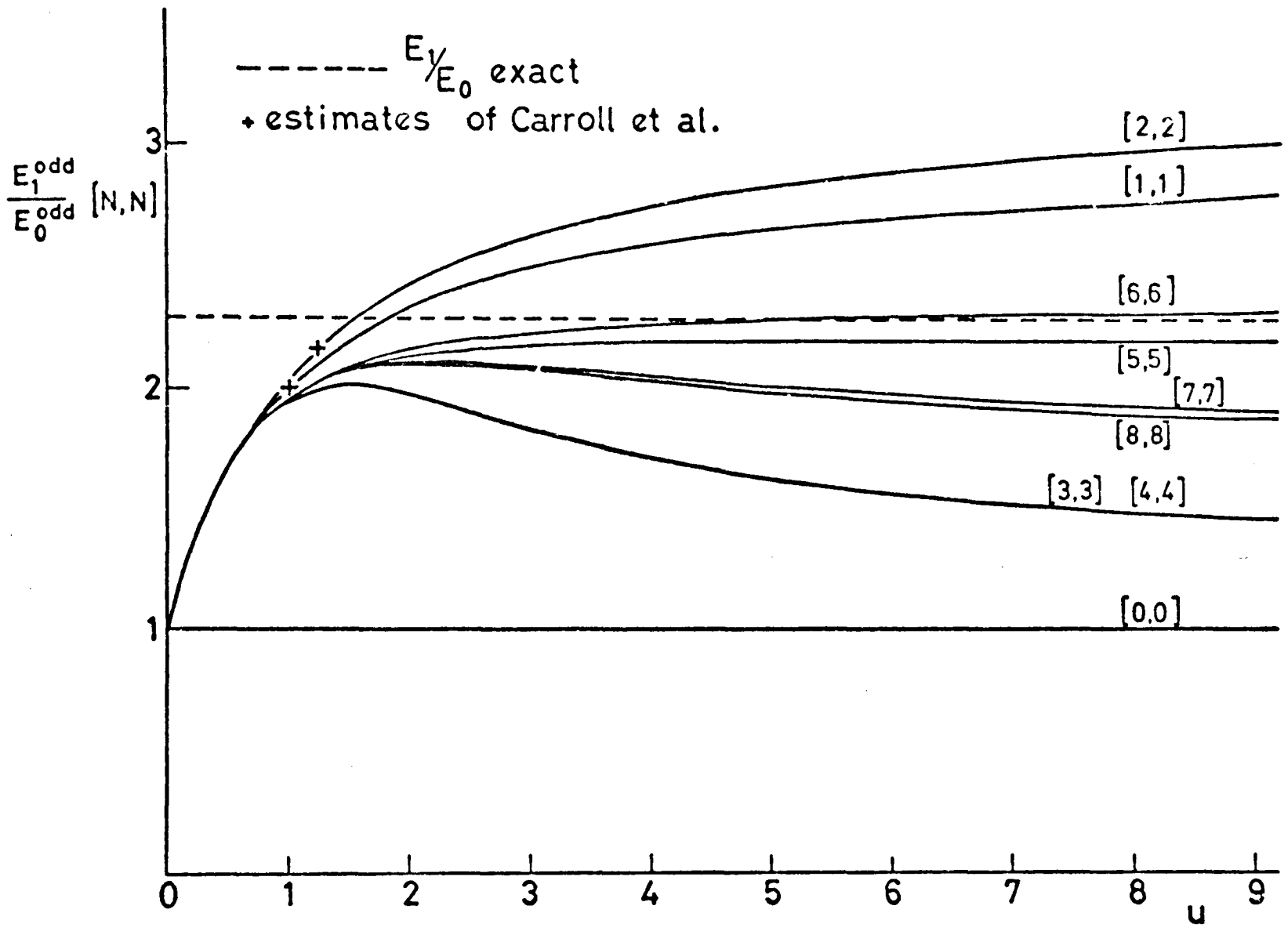

E_1/E_0 exact
estimates of Carroll et al.
$\frac{E_1^{odd}}{E_0^{odd}}$ [N,N]
3
2
1
[2,2]
[1,1]
[6,6]
[5,5]
[7,7]
[8,8]
[3,3] [4,4]
[0,0]
0 1 2 3 4 5 6 7 8 9
u

Fig. 2·4

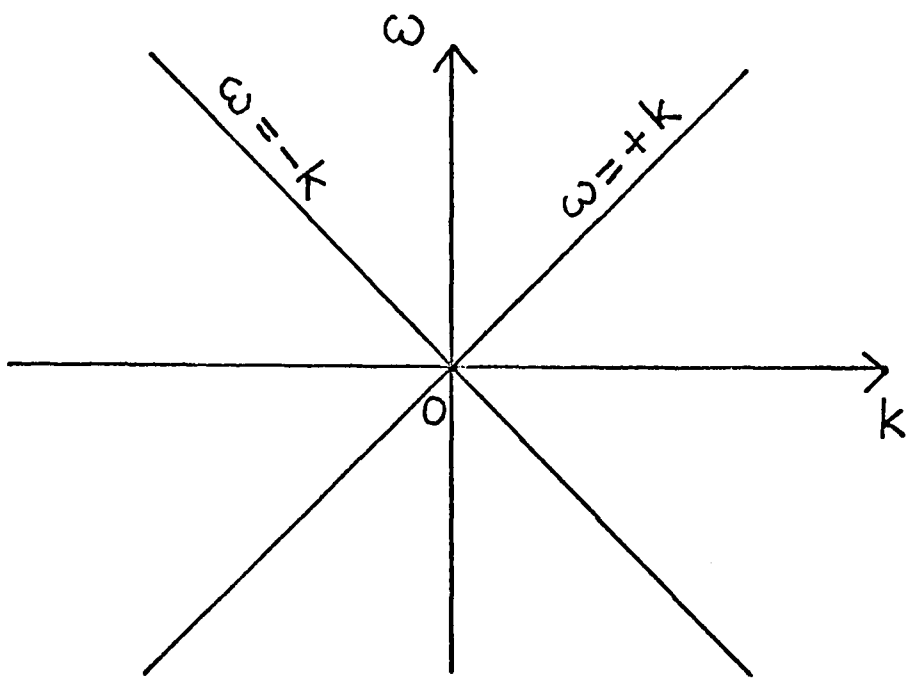


Fig. 3·1

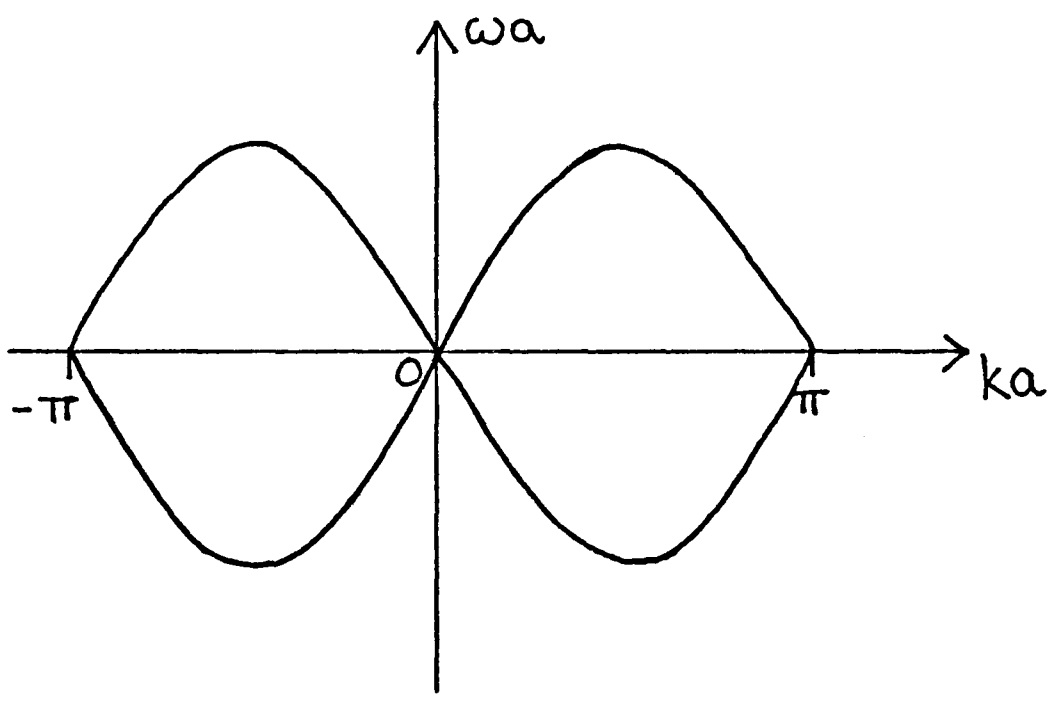


Fig. 3·2

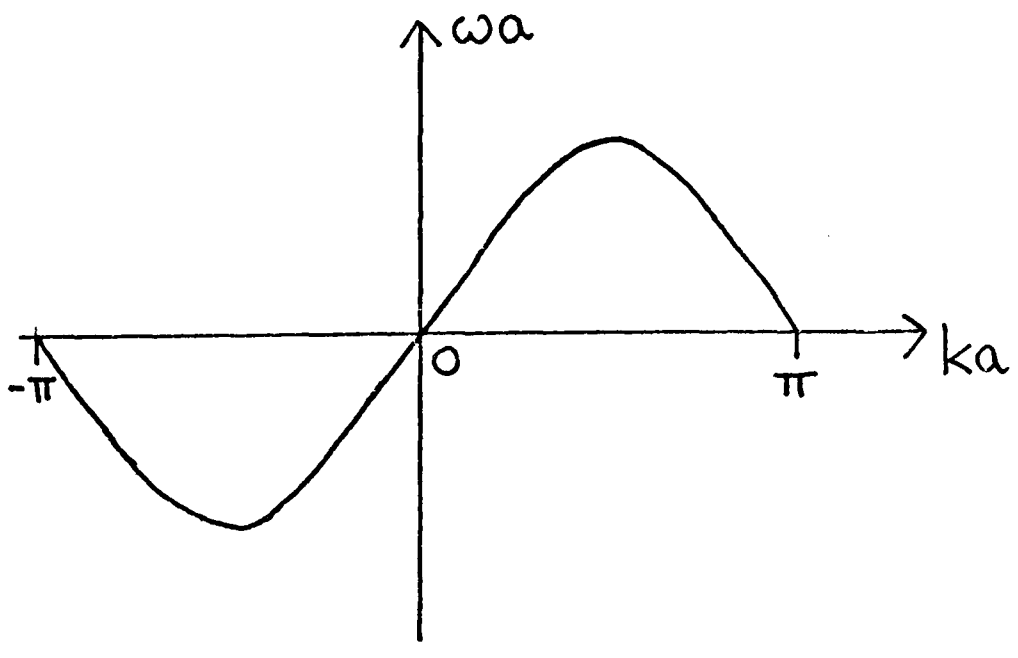


Fig. 3·3

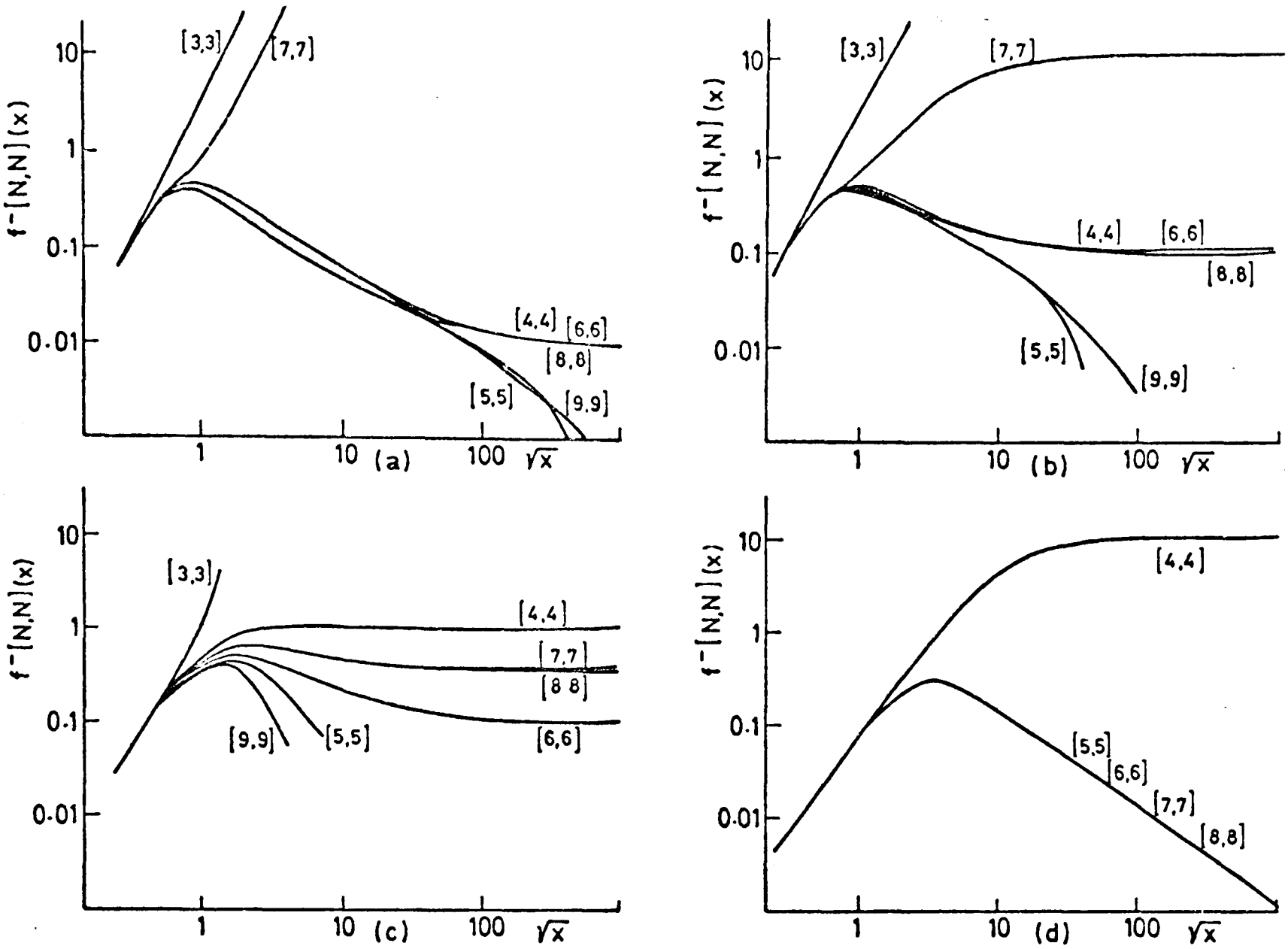

f⁻[N,N](x)
10
1
0.1
0.01
[3,3]
[7,7]
[4,4]
[6,6]
[8,8]
[5,5]
[9,9]
1
10
100
√x
(a)
(b)
(c)
(d)

Fig. 3·4

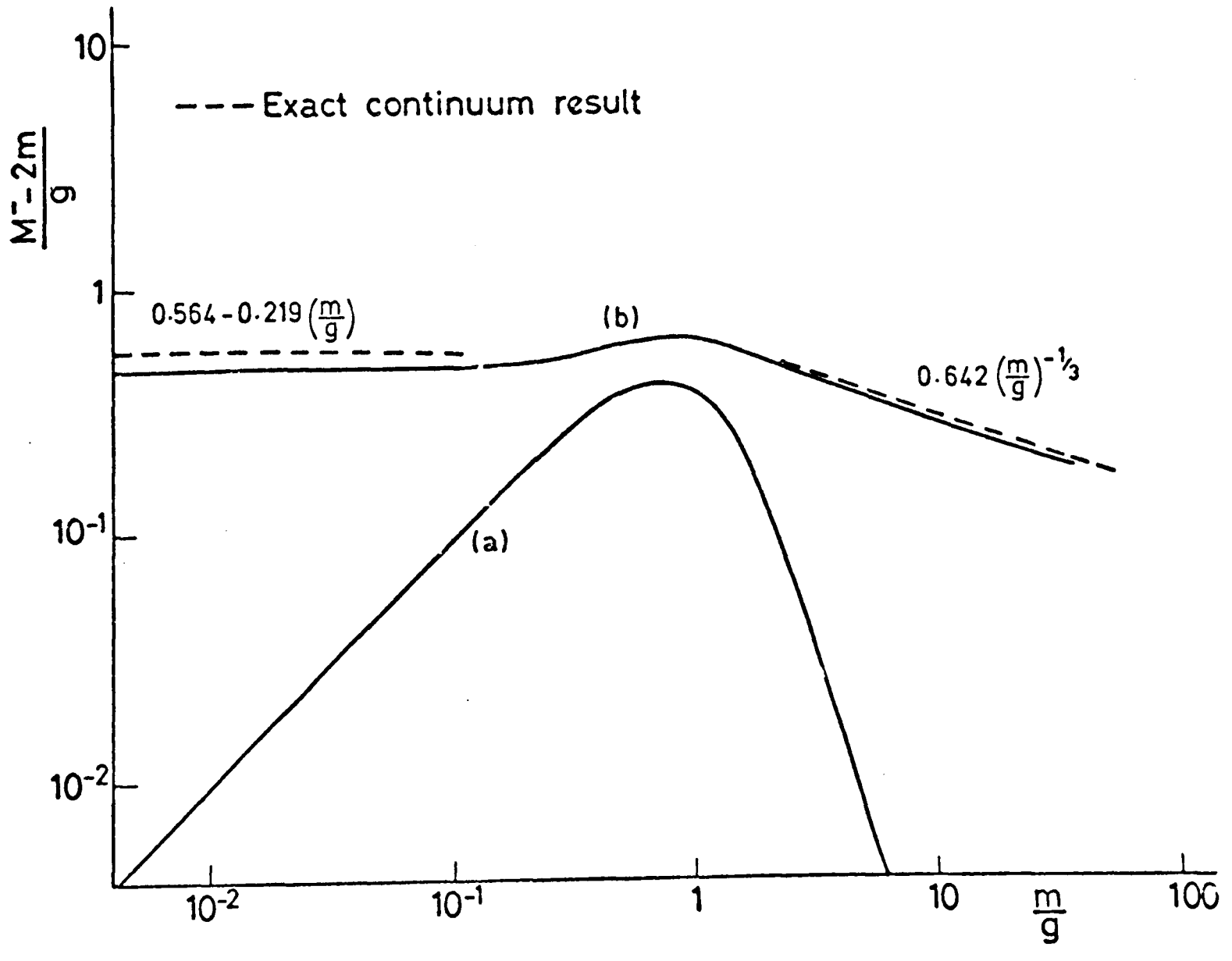

M⁻-2m/g
10
1
10⁻¹
10⁻²
Exact continuum result
0.564 - 0.219 (m/g)
(b)
0.642 (m/g)^-1/3
(a)
10⁻²
10⁻¹
1
10
100
m/g

Fig. 3·5

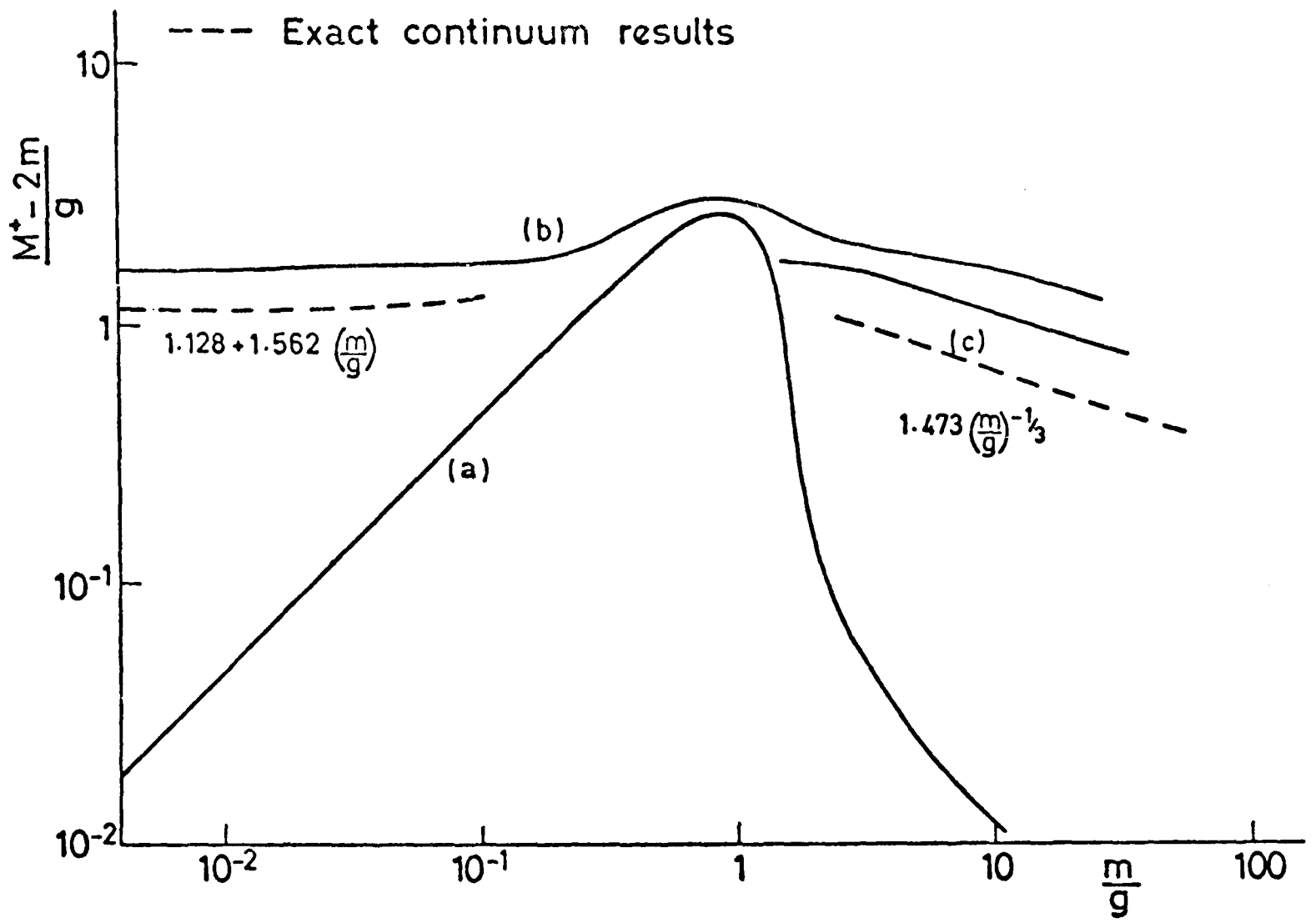

Exact continuum results
$\frac{M^+-2m}{g}$
10
1
10^{-1}
10^{-2}
(b)
(a)
(c)
$1.128+1.562\left(\frac{m}{g}\right)$
$1.473\left(\frac{m}{g}\right)^{-1/3}$
10^{-2}
10^{-1}
1
10
100
$\frac{m}{g}$

Fig. 3·6

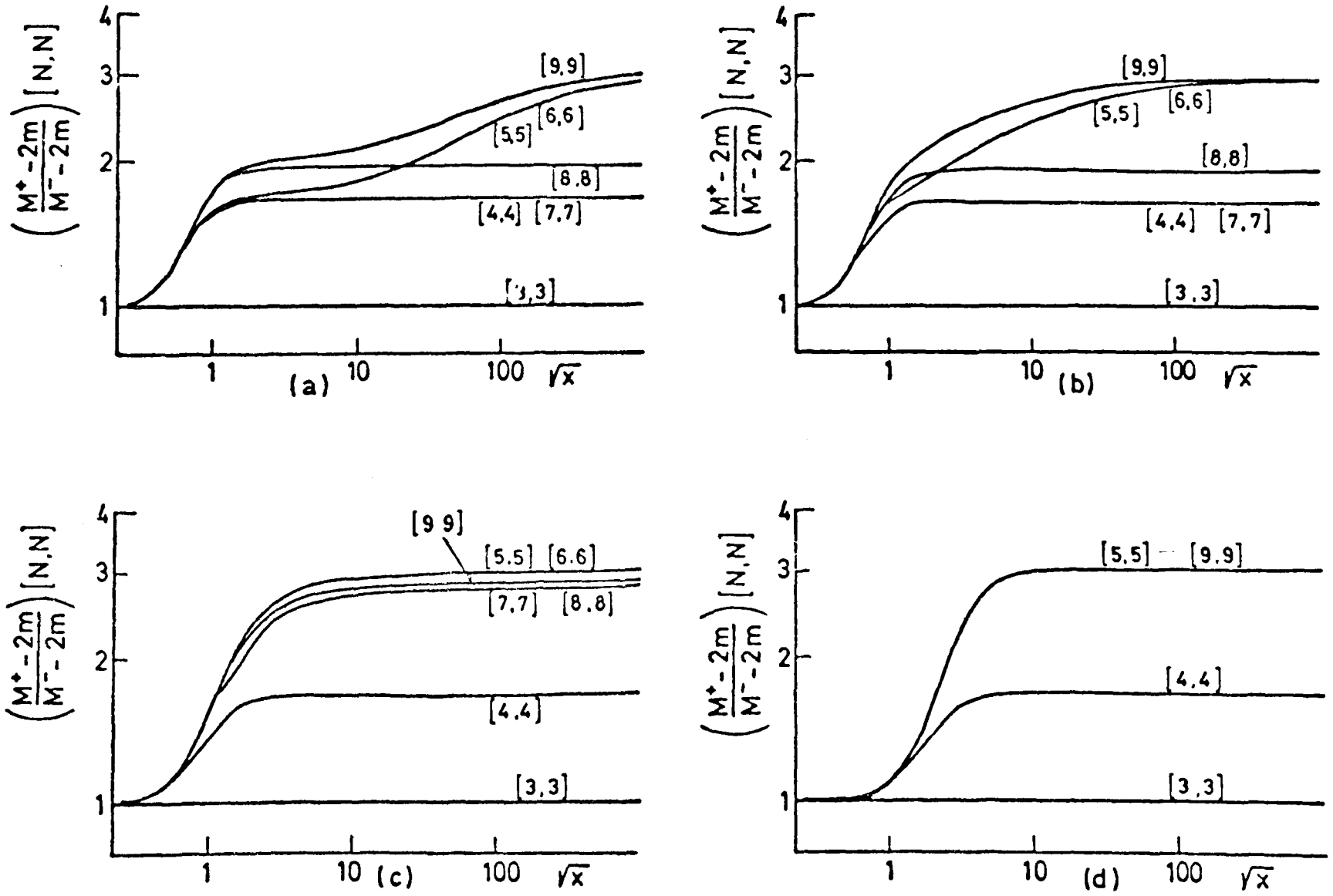

$\left(\frac{M^+-2m}{M^--2m}\right)[N,N]$
4
3
2
1
[9,9]
[6,6]
[5,5]
[8,8]
[4,4] [7,7]
[3,3]
1
10
100
$\sqrt{x}$
(a)
(b)
[9 9]
[5.5] [6.6]
[7,7] [8,8]
[4,4]
(c)
[5,5] [9,9]
(d)

Fig. 3·7

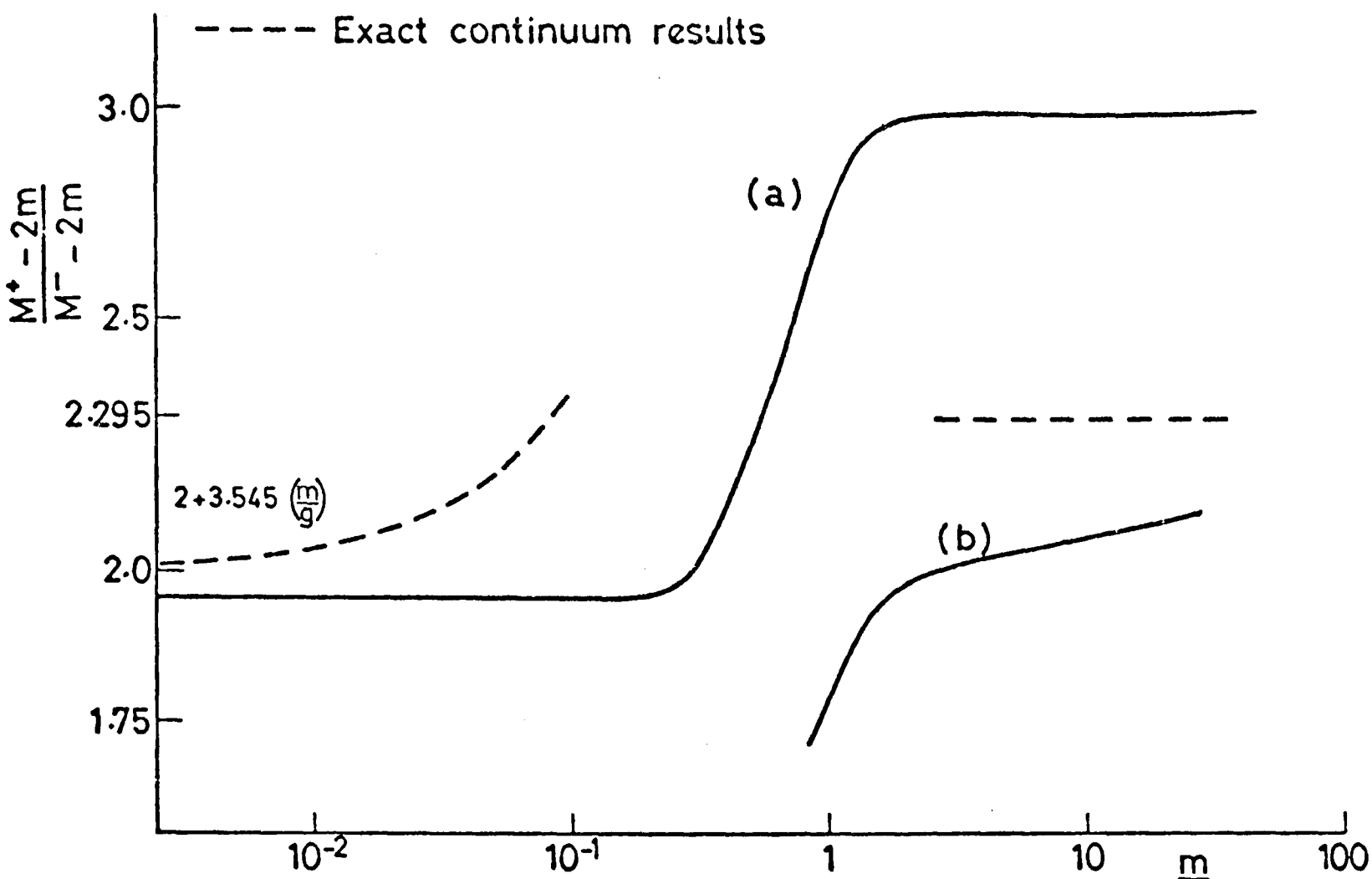

Exact continuum results
$\frac{M^+ - 2m}{M^- - 2m}$
3.0
2.5
2.295
2.0
1.75
2+3.545 $(\frac{m}{g})$
(a)
(b)
10^{-2}
10^{-1}
1
10
m
100
$\frac{m}{g}$

Fig. 3.8

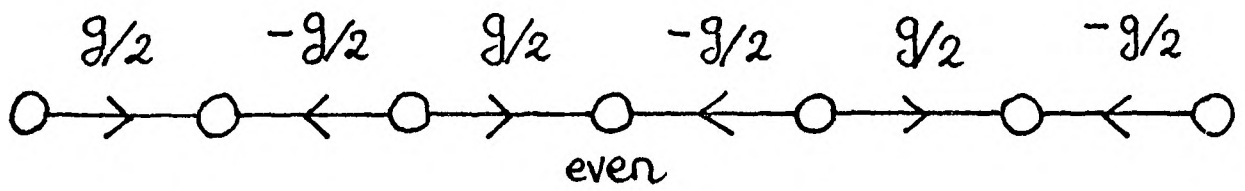


Fig. 3.9

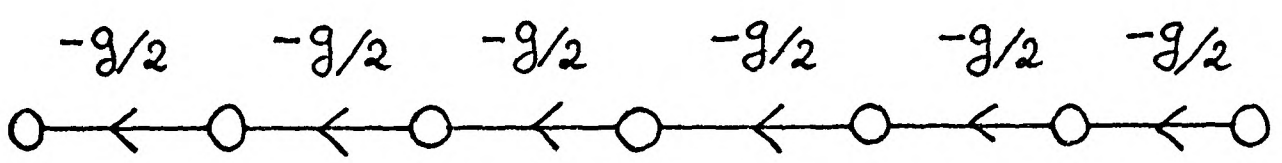


Fig. 3.10

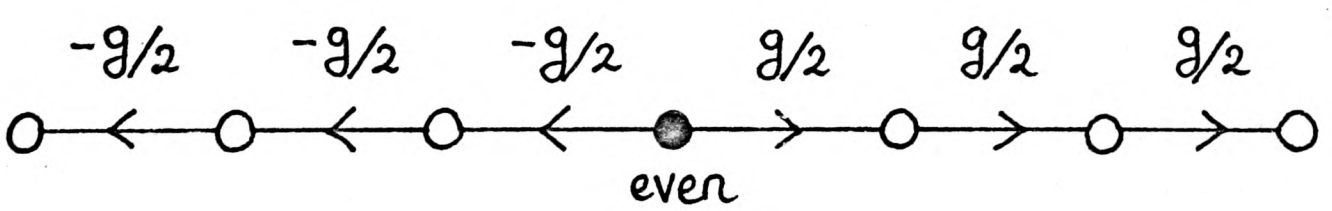
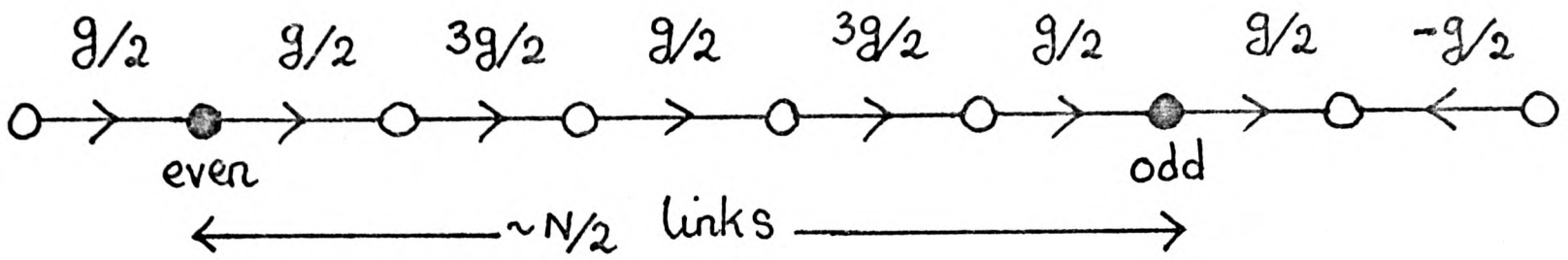


Fig. 3.11



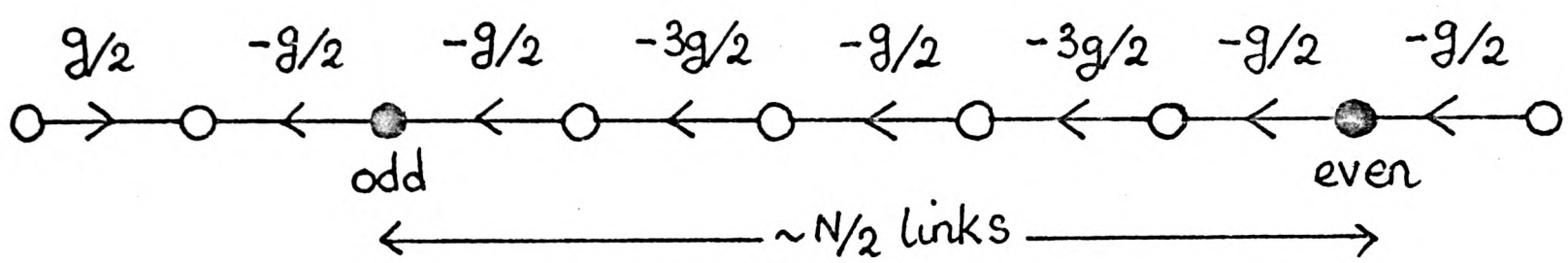
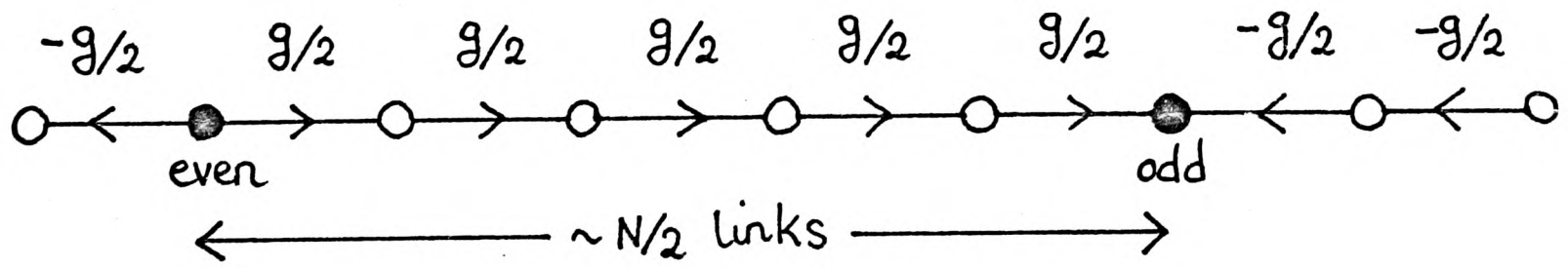
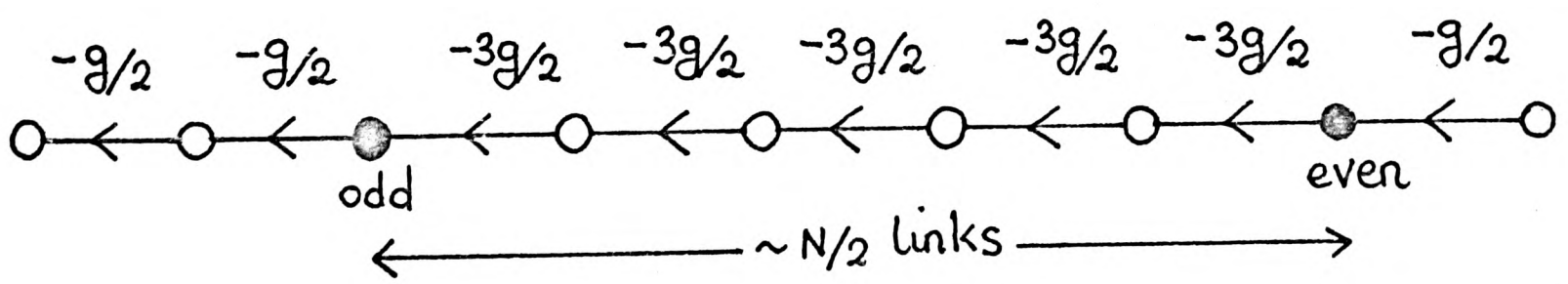


Fig. 3·12



(a)



(b)

Fig. 3·13

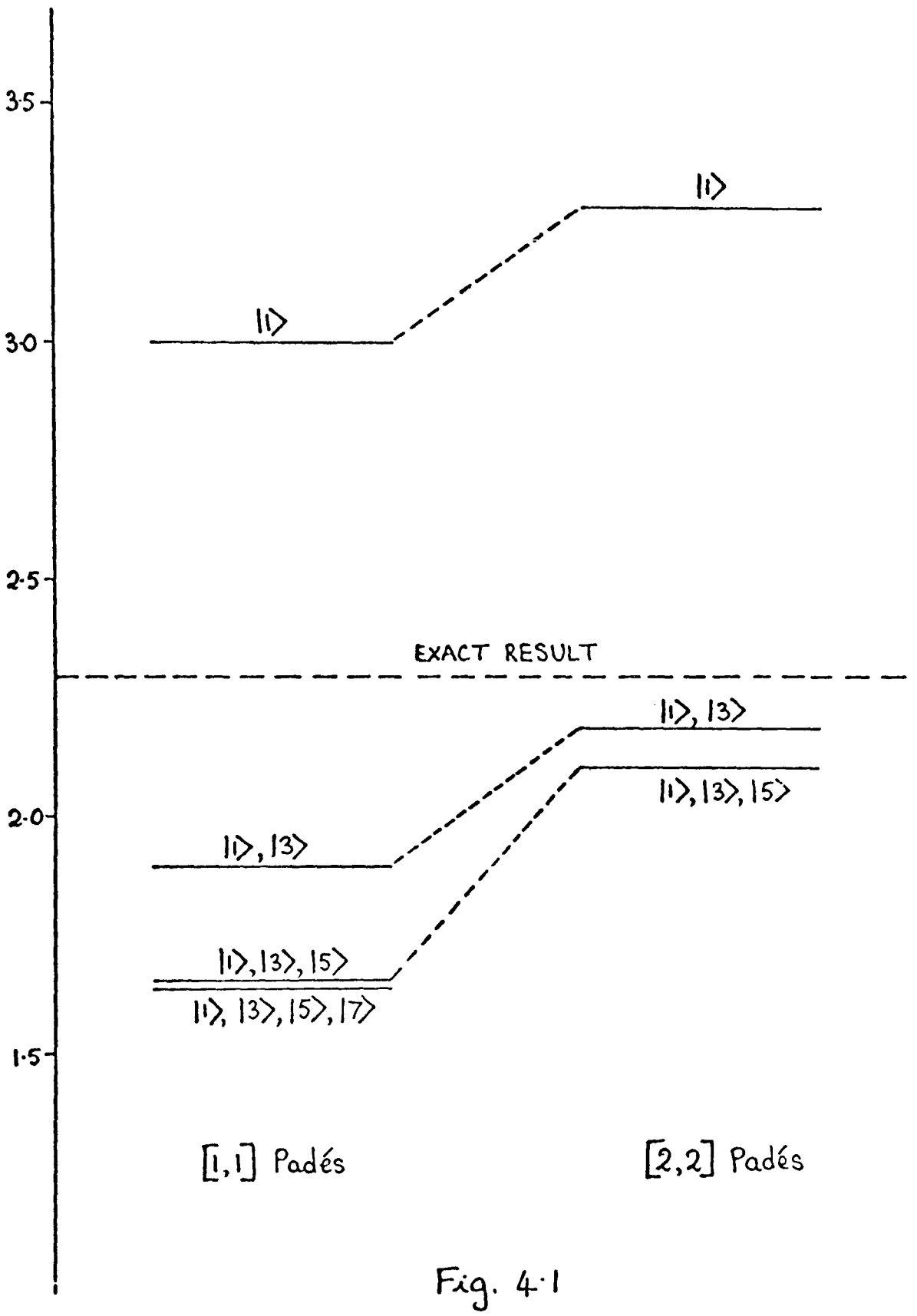


Fig. 4·1

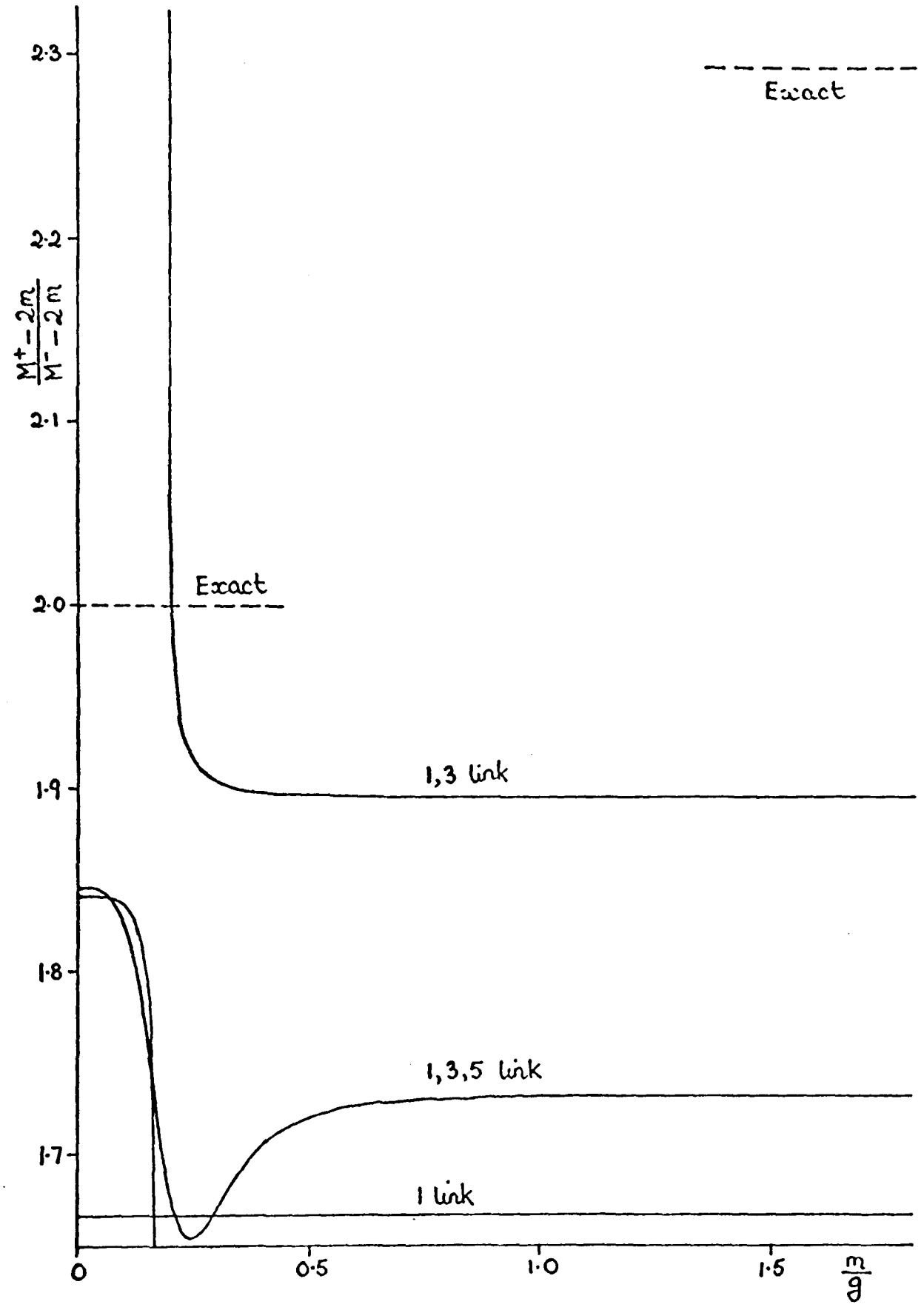

2·3
2·2
2·1
2·0
1·9
1·8
1·7
$\frac{M^+ - 2m}{M^- - 2m}$
Exact
Exact
1,3 link
1,3,5 link
1 link
0
0·5
1·0
1·5
$\frac{m}{g}$

Fig. 4·2

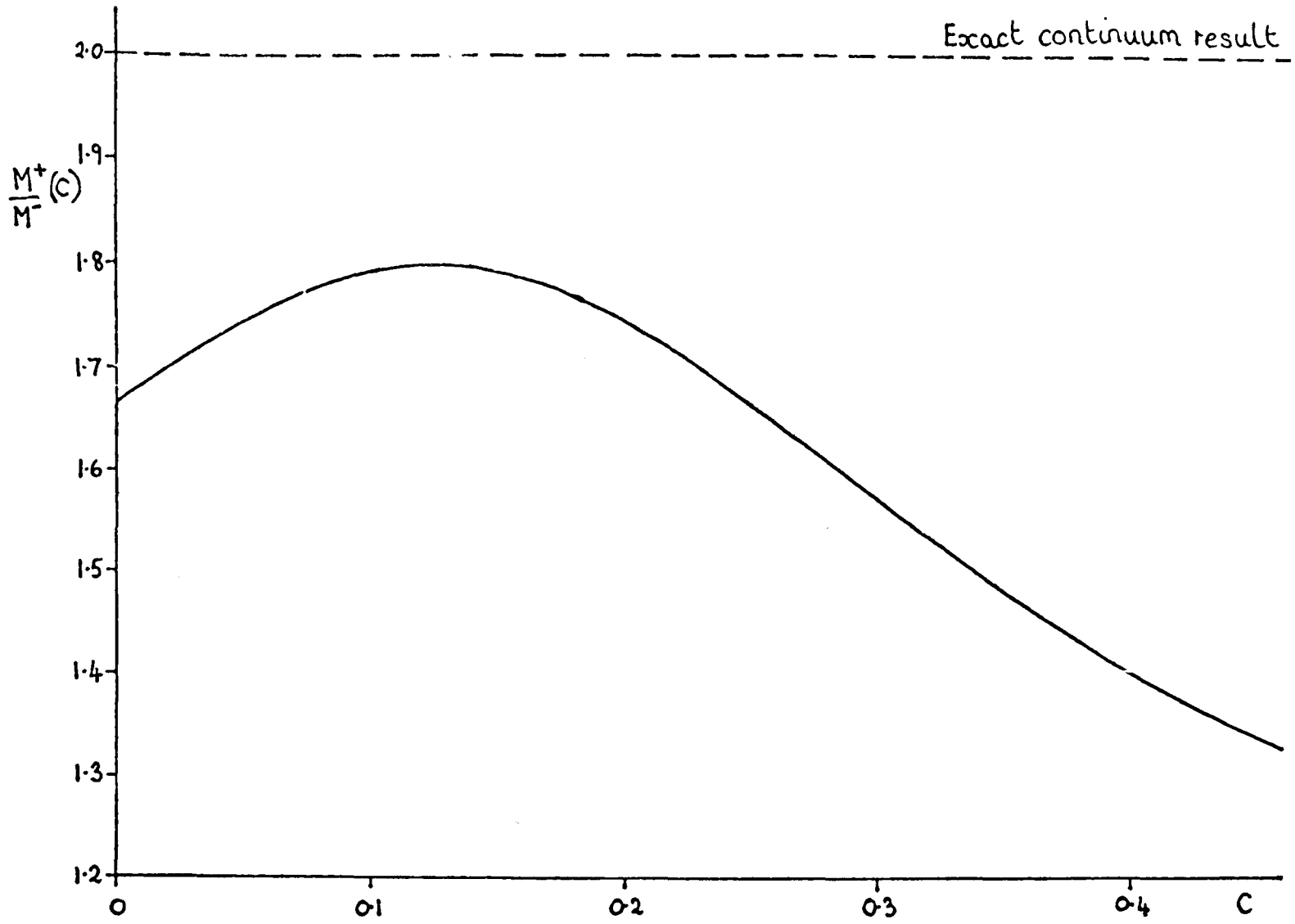

Exact continuum result
$\frac{M^+}{M^-}(c)$
2·0
1·9
1·8
1·7
1·6
1·5
1·4
1·3
1·2
0
0·1
0·2
0·3
0·4
c

Fig. 4·3

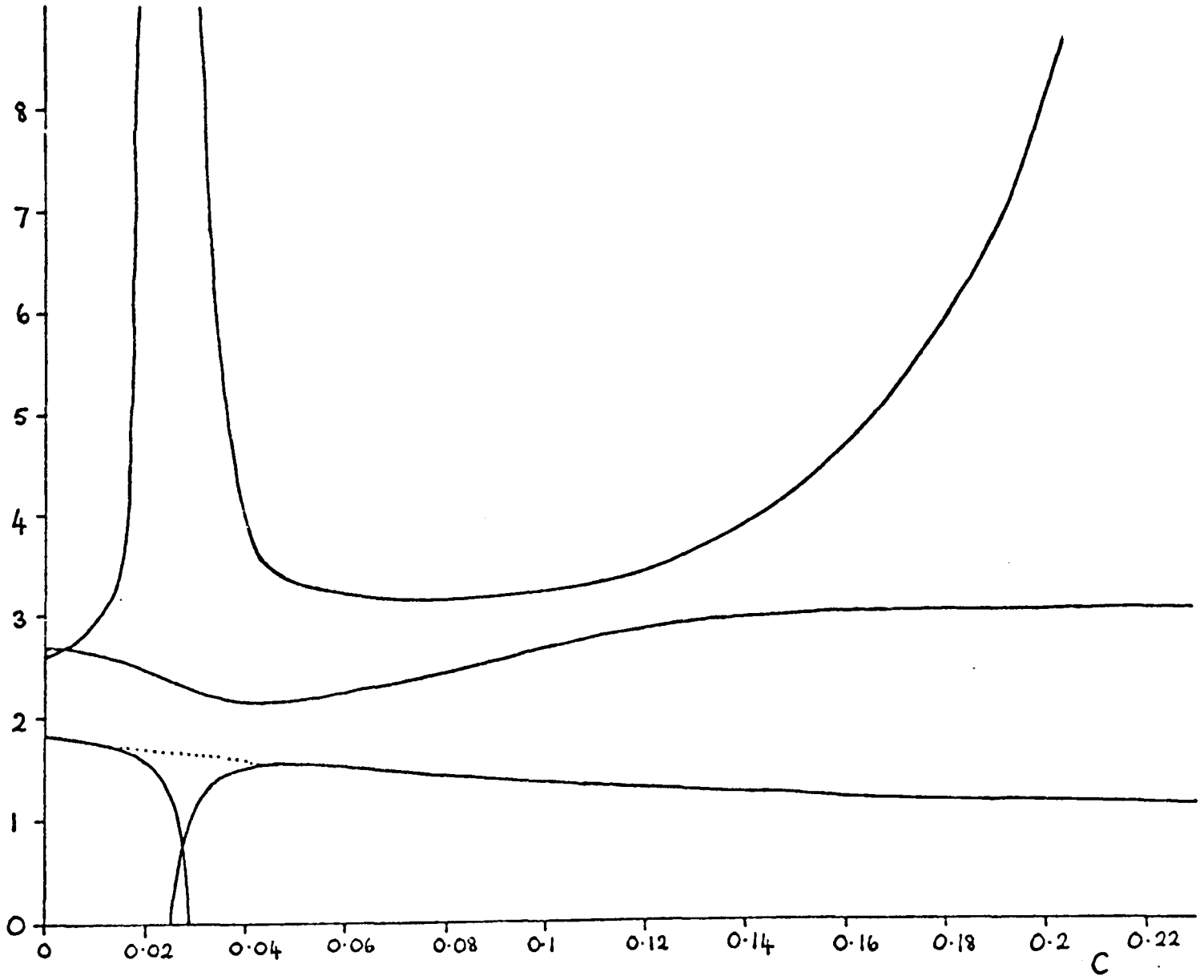

8
7
6
5
4
3
2
1
0
0
0·02
0·04
0·06
0·08
0·1
0·12
0·14
0·16
0·18
0·2
0·22
c

Fig. 4·4

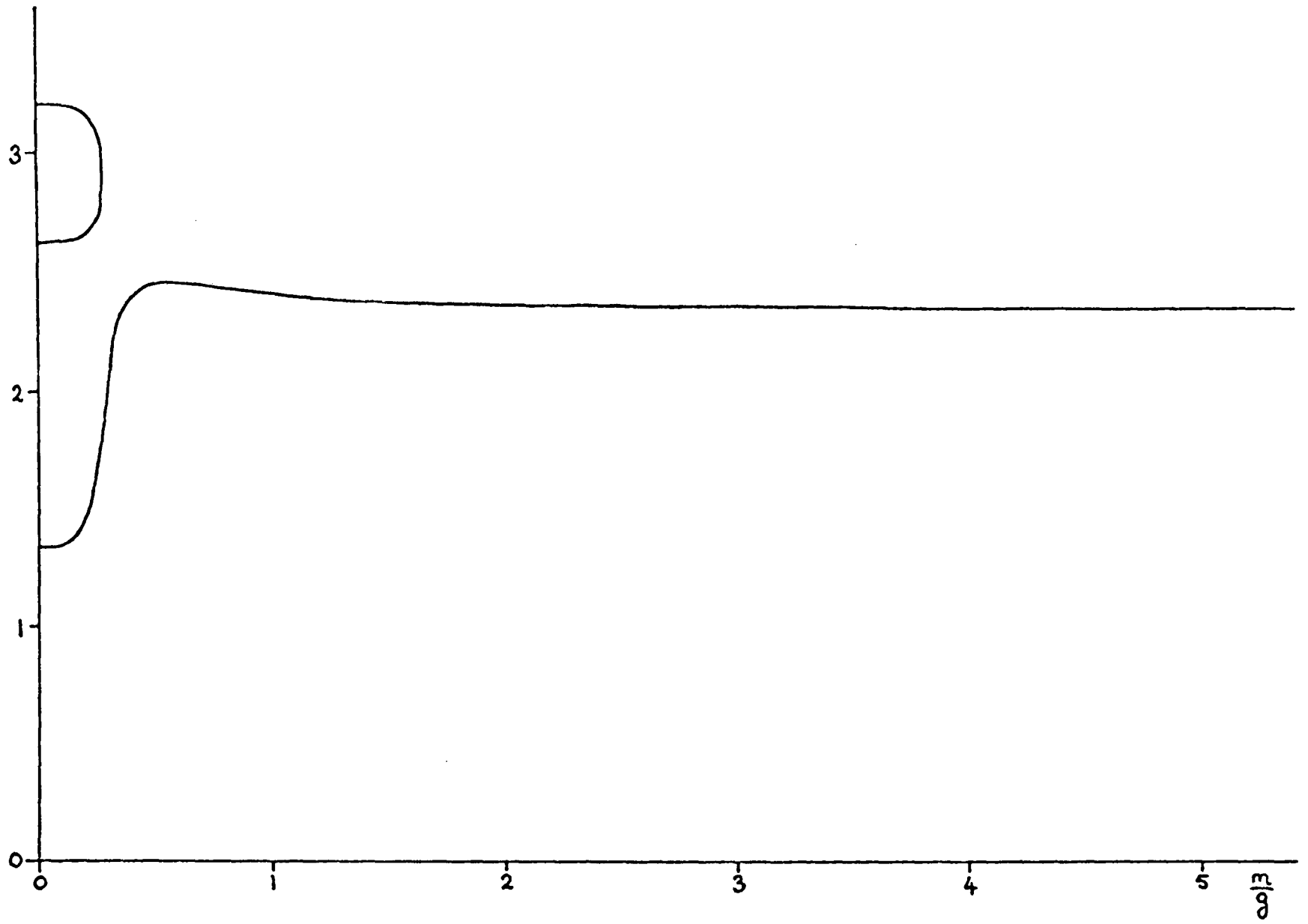

3
2
1
0
0
1
2
3
4
5
$a^{1/3}$

Fig. 4·5

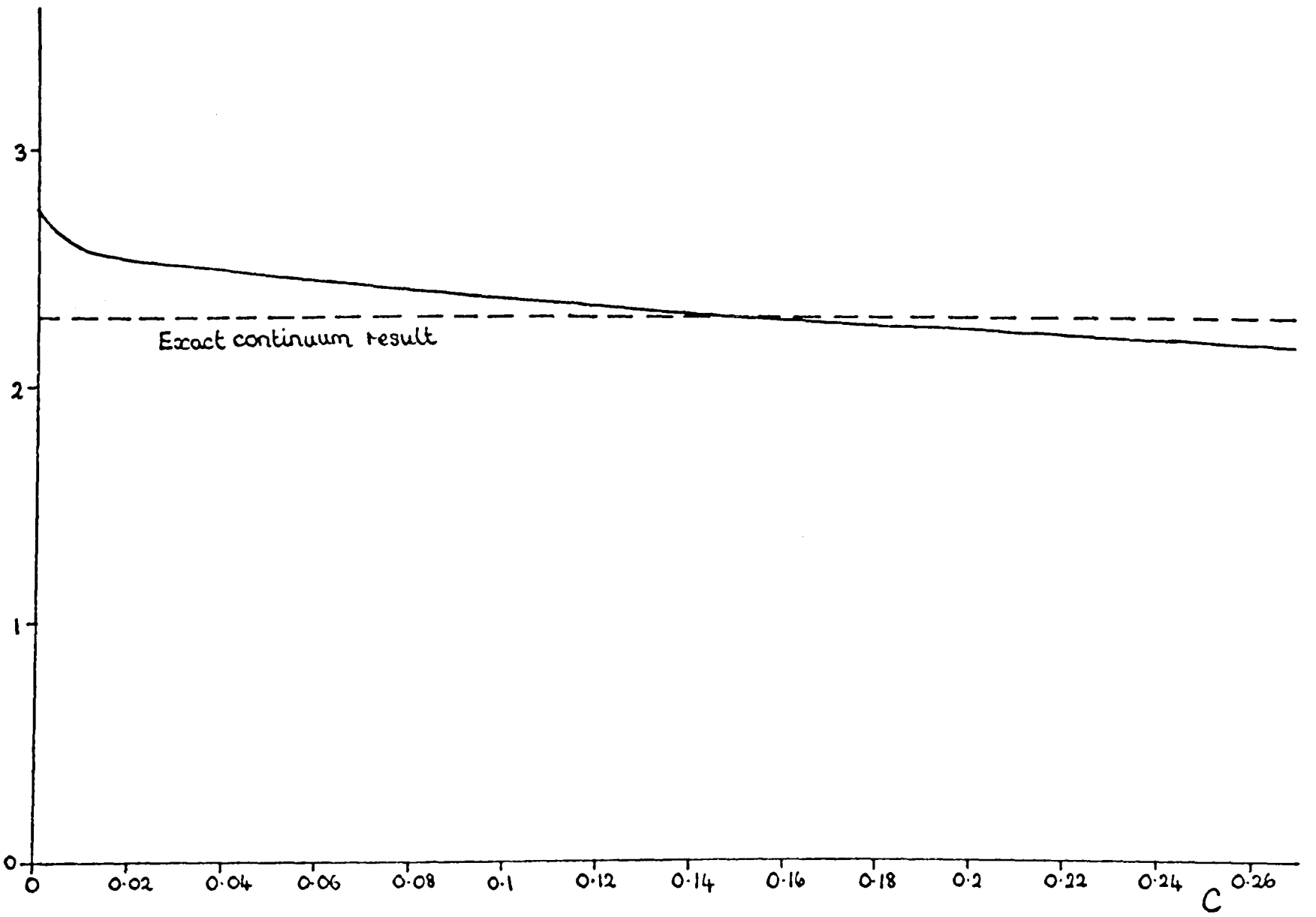

3
2
1
0
Exact continuum result
0
0·02
0·04
0·06
0·08
0·1
0·12
0·14
0·16
0·18
0·2
0·22
0·24
0·26
C

Fig 4·6

	$\langle$up$\rangle$	$\langle$down$\rangle$	$\langle$in$\rangle$	$\langle$out$\rangle$
ρ_1 :	$\uparrow$	$\downarrow$	$\downarrow$	$\uparrow$
ρ_2 :	$\uparrow$	$\downarrow$	$\uparrow$	$\downarrow$
I_3 :	0	0	$-\frac{1}{2}$	$\frac{1}{2}$
charge:	g	$-g$	0	0

Fig. 5.1

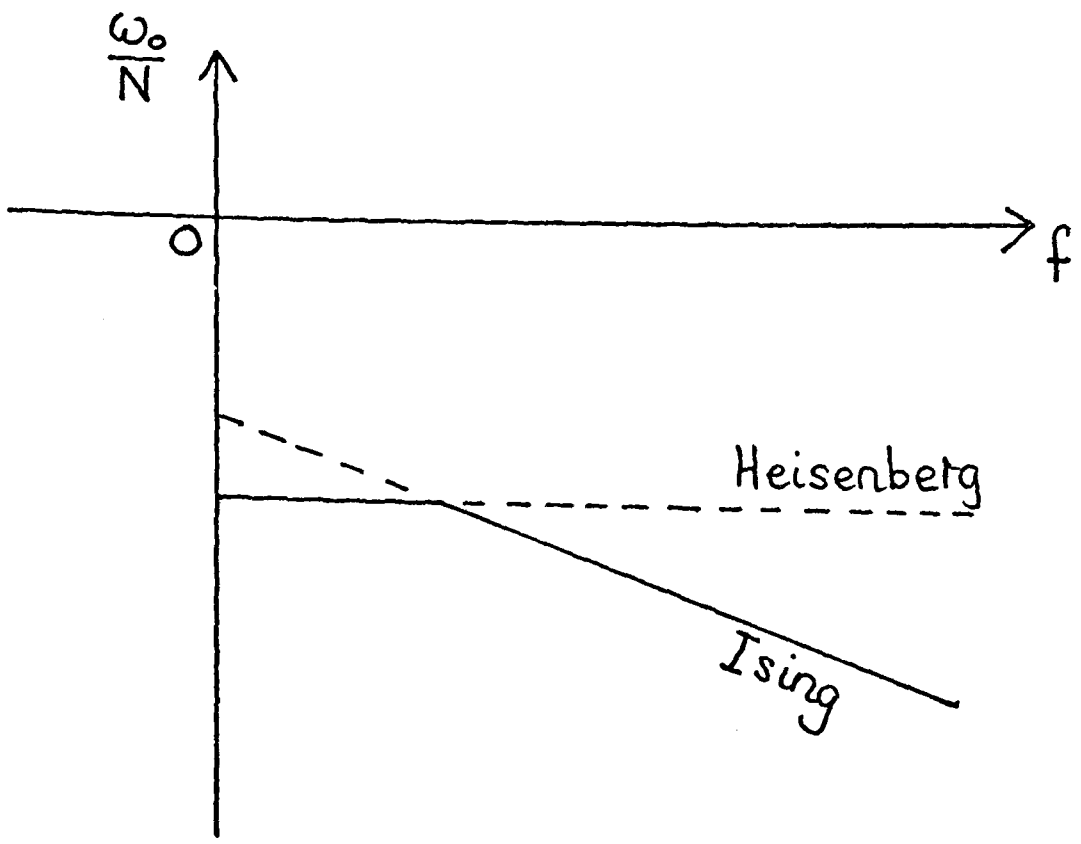


Fig. 5.2

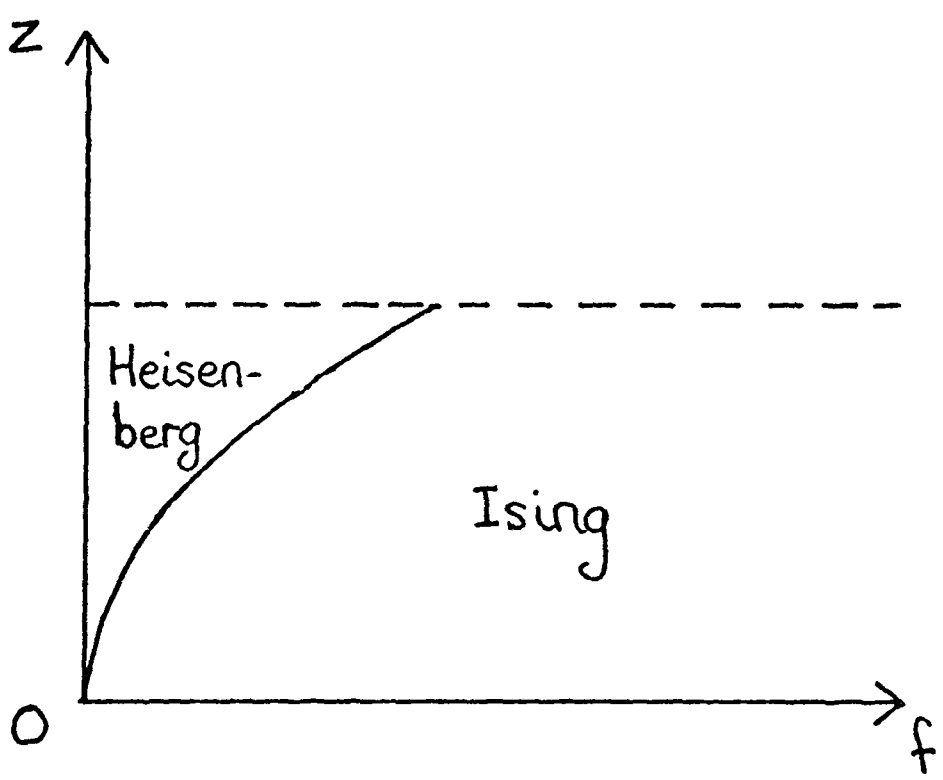
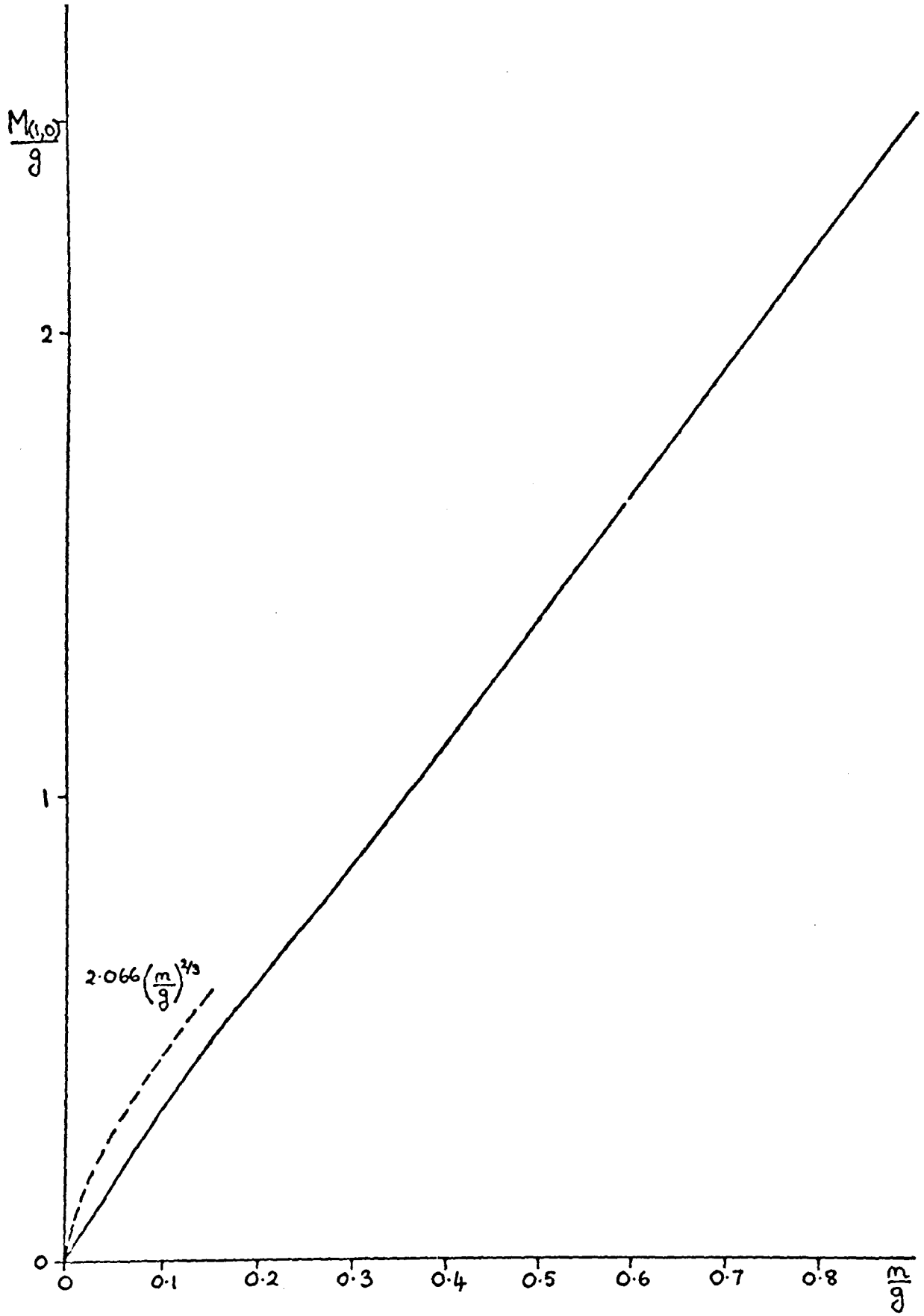
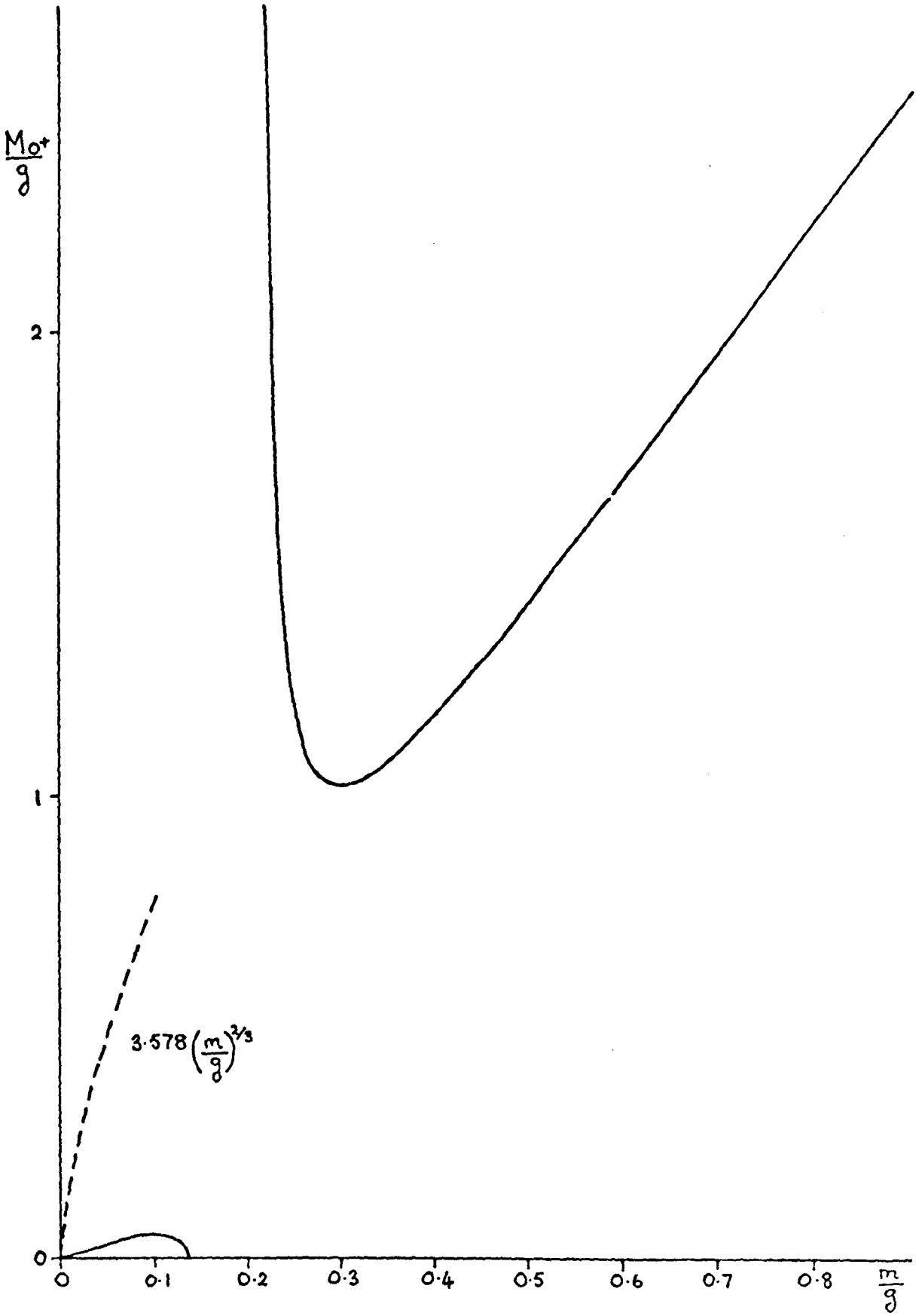


Fig. 5.3

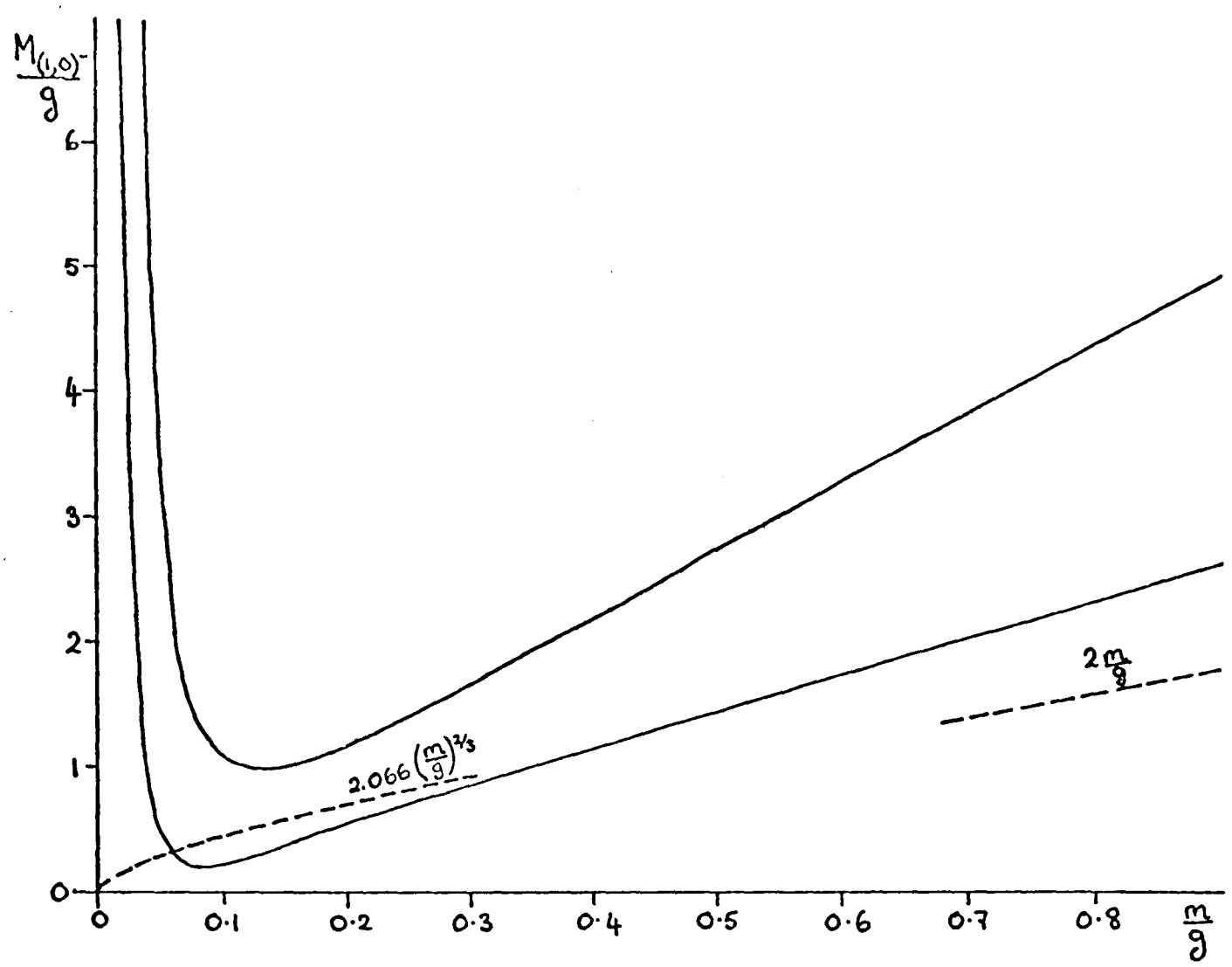

$\frac{M_{(1,0)}}{g}$
2
1
0
$2{\cdot}066\left(\frac{m}{g}\right)^{2/3}$
0
0·1
0·2
0·3
0·4
0·5
0·6
0·7
0·8
$\frac{m}{g}$

(i)

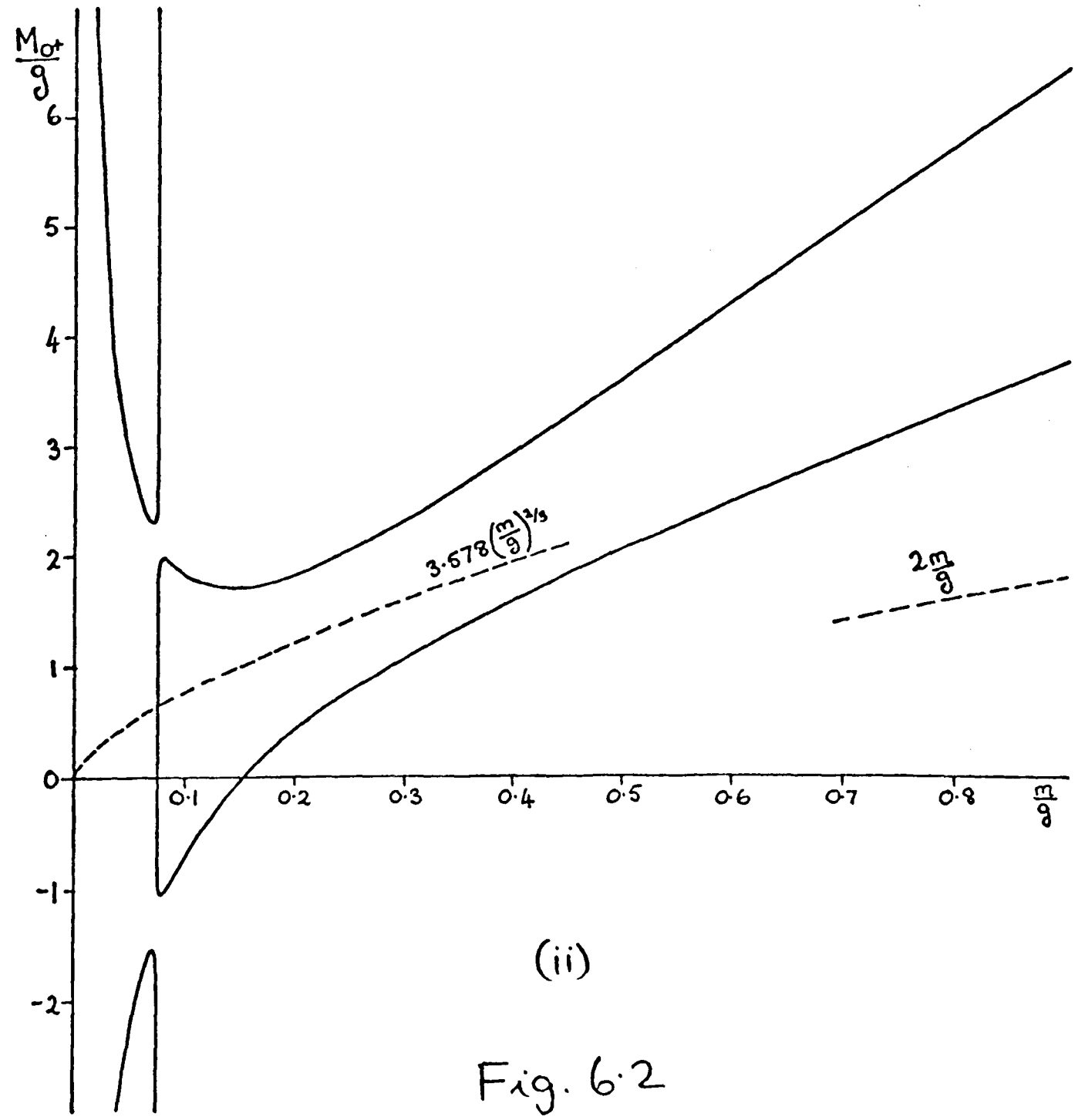

$\frac{M_{0^+}}{g}$
2
1
0
$3{\cdot}578\left(\frac{m}{g}\right)^{2/3}$
0
0·1
0·2
0·3
0·4
0·5
0·6
0·7
0·8
$\frac{m}{g}$

(ii)

Fig. 6·1


$\frac{M_{(1,0)^-}}{g}$
6
5
4
3
2
1
0
0
0·1
0·2
0·3
0·4
0·5
0·6
0·7
0·8
$\frac{m}{g}$
$2\frac{m}{g}$
$2.066\left(\frac{m}{g}\right)^{2/3}$

(i)


$\frac{M_{0^+}}{g}$
6
5
4
3
2
1
0
-1
-2
0·1
0·2
0·3
0·4
0·5
0·6
0·7
0·8
$\frac{m}{g}$
$2\frac{m}{g}$
$3.678\left(\frac{m}{g}\right)^{2/3}$

(ii)

Fig. 6·2

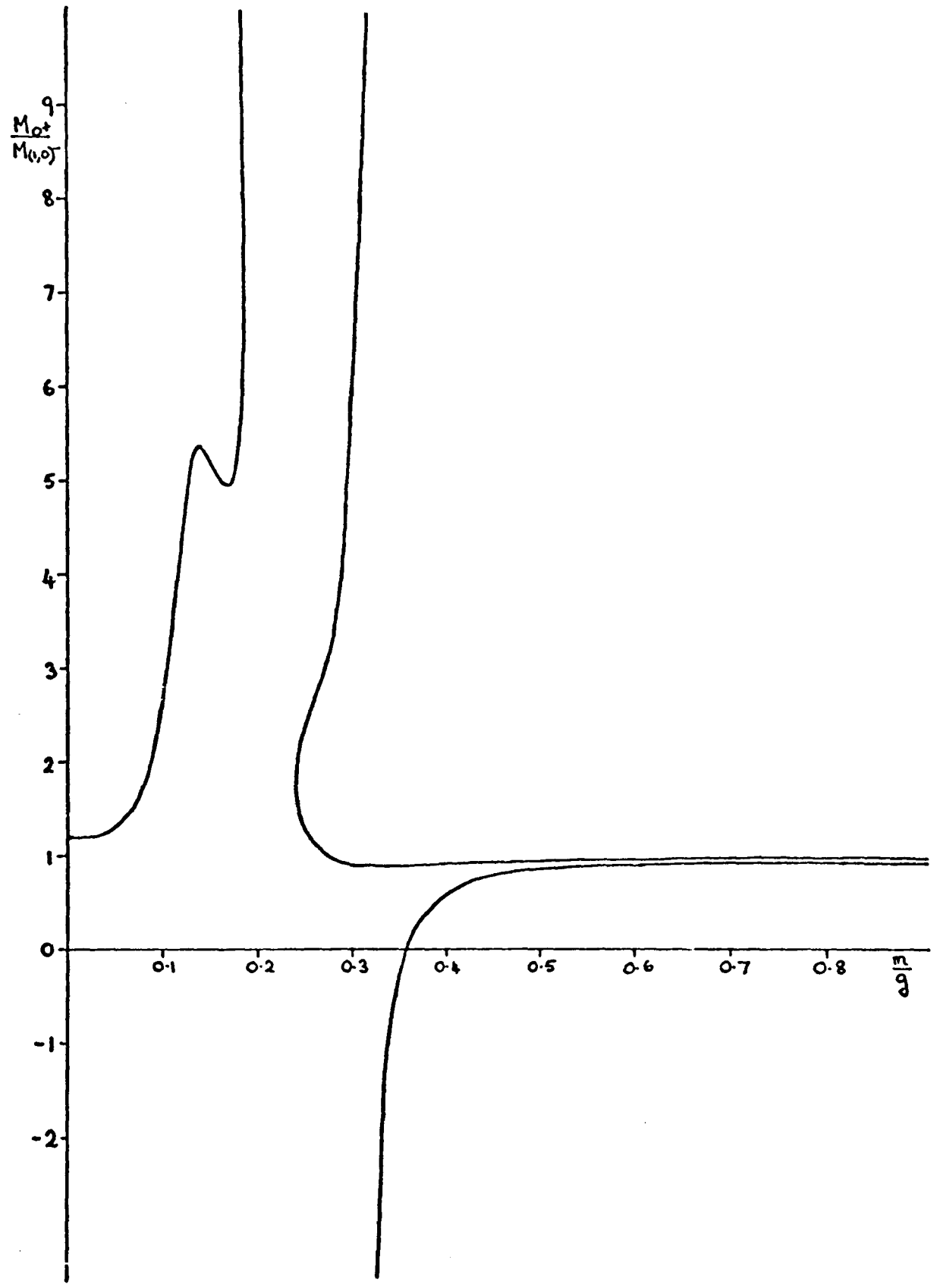


Fig. 6·3

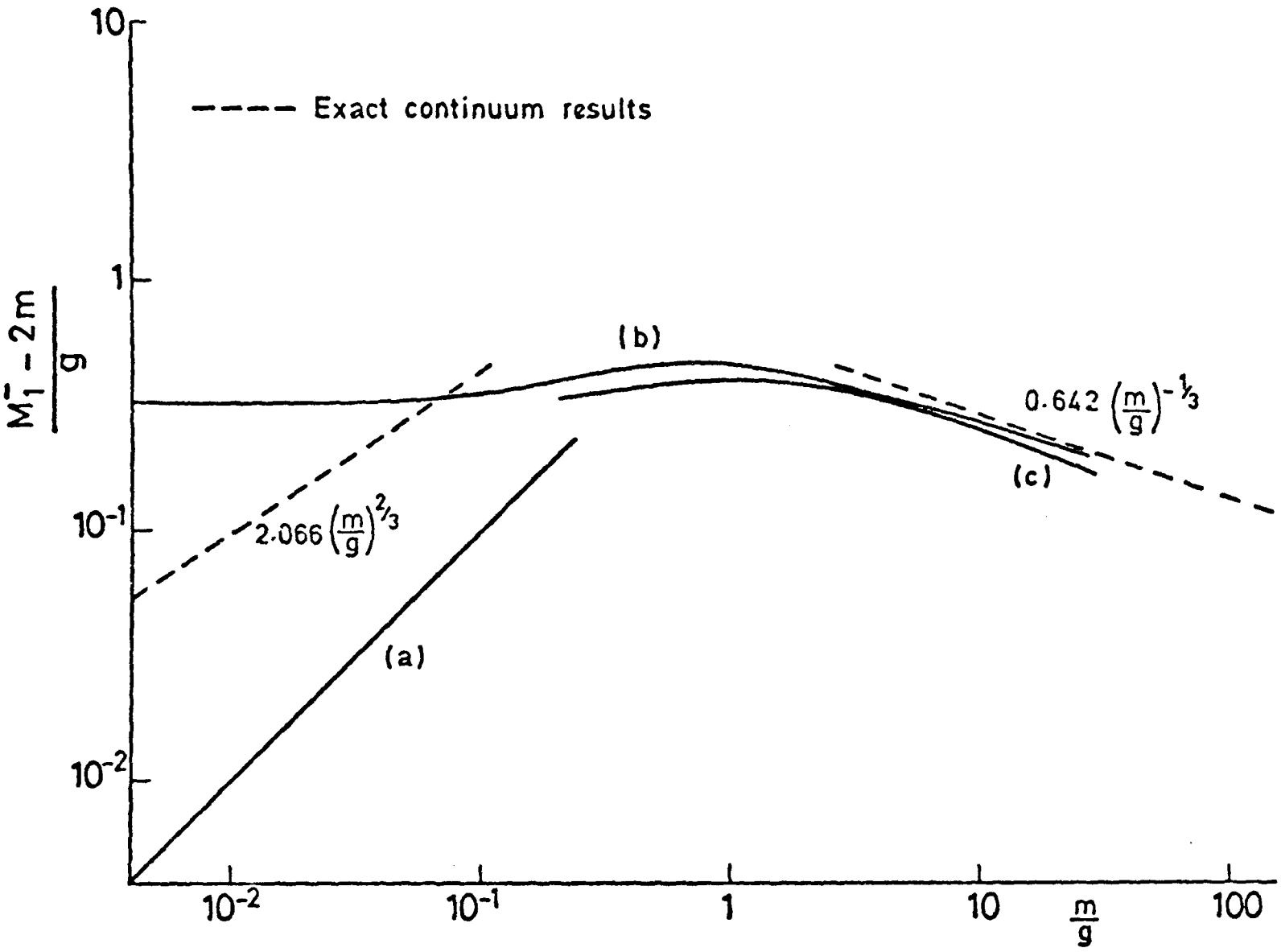
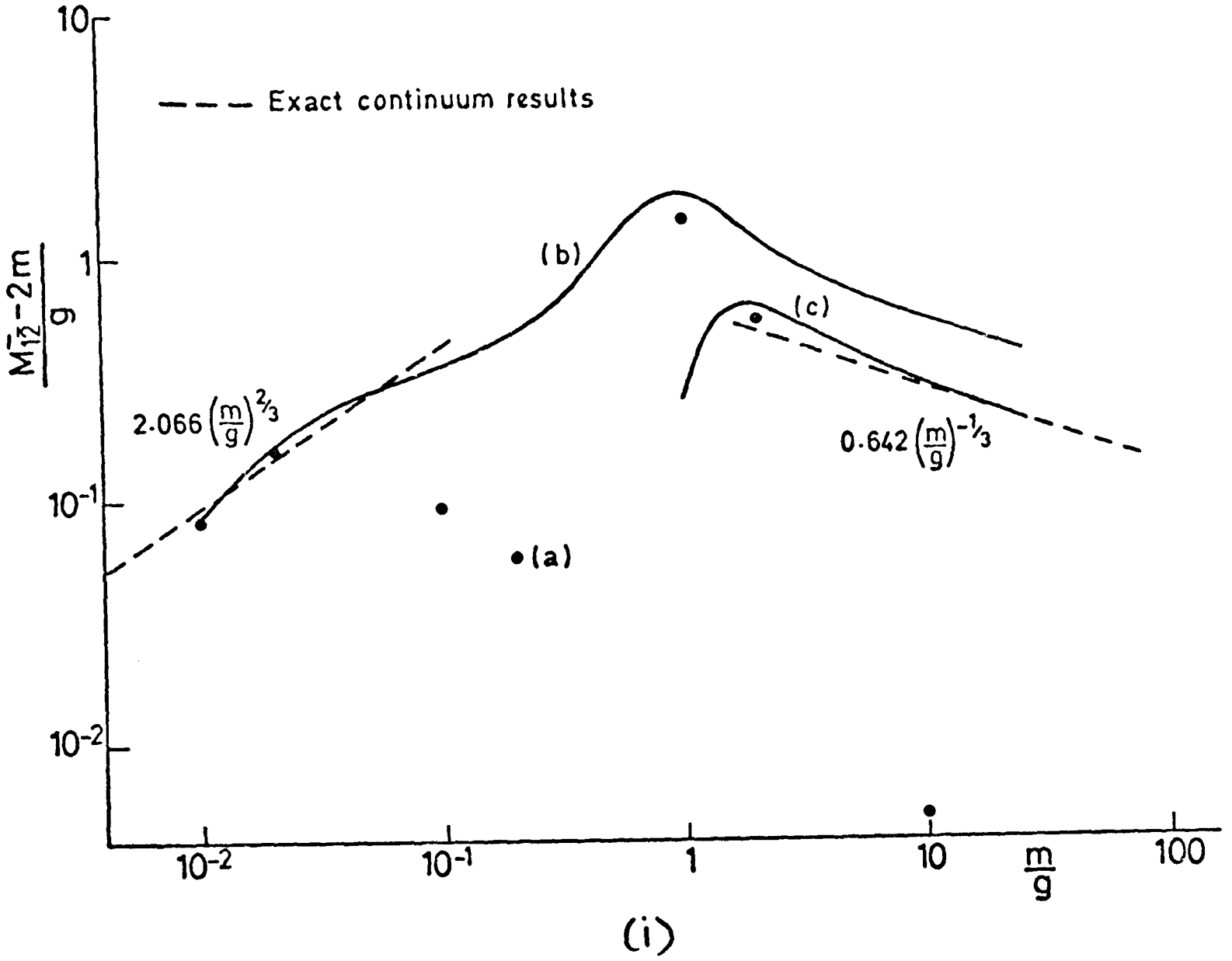
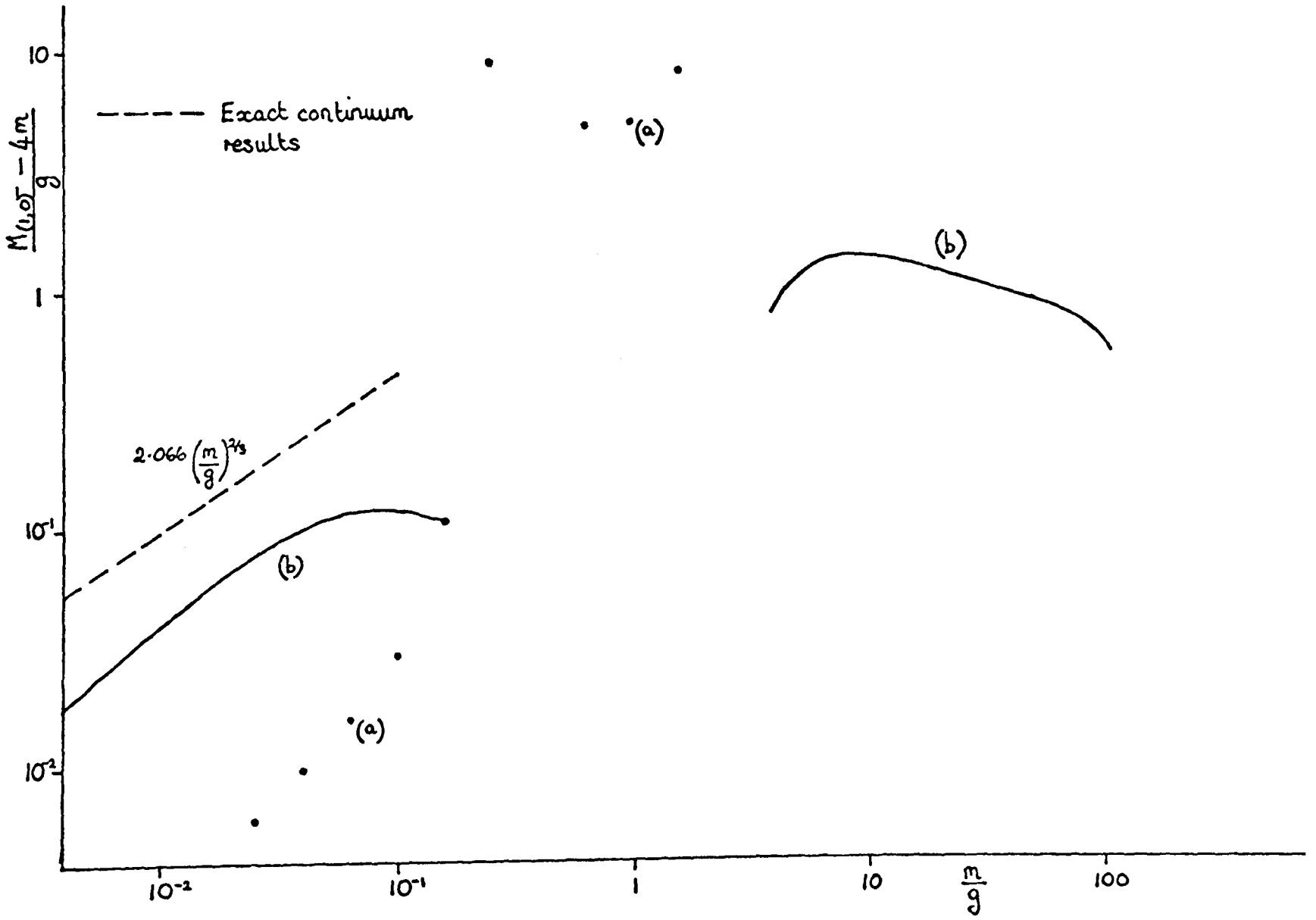

10
1
10^{-1}
10^{-2}
$\frac{M_1^- - 2m}{g}$
Exact continuum results
(b)
$0.642\left(\frac{m}{g}\right)^{-1/3}$
(c)
$2.066\left(\frac{m}{g}\right)^{2/3}$
(a)
10^{-2}
10^{-1}
1
10
100
$\frac{m}{g}$

Fig. 6·4


Exact continuum results
$\frac{M_{12}-2m}{g}$
(b)
(c)
(a)
$2.066\left(\frac{m}{g}\right)^{2/3}$
$0.642\left(\frac{m}{g}\right)^{-1/3}$
10
1
10^{-1}
10^{-2}
10^{-2}
10^{-1}
1
10
100
$\frac{m}{g}$

(i)


Exact continuum results
$\frac{M_{LOT}-4m}{g}$
(a)
(b)
$2.066\left(\frac{m}{g}\right)^{2/3}$
(b)
(a)
10
1
10^{-1}
10^{-2}
10^{-2}
10^{-1}
1
10
100
$\frac{m}{g}$

(ii)

Fig. 6·5

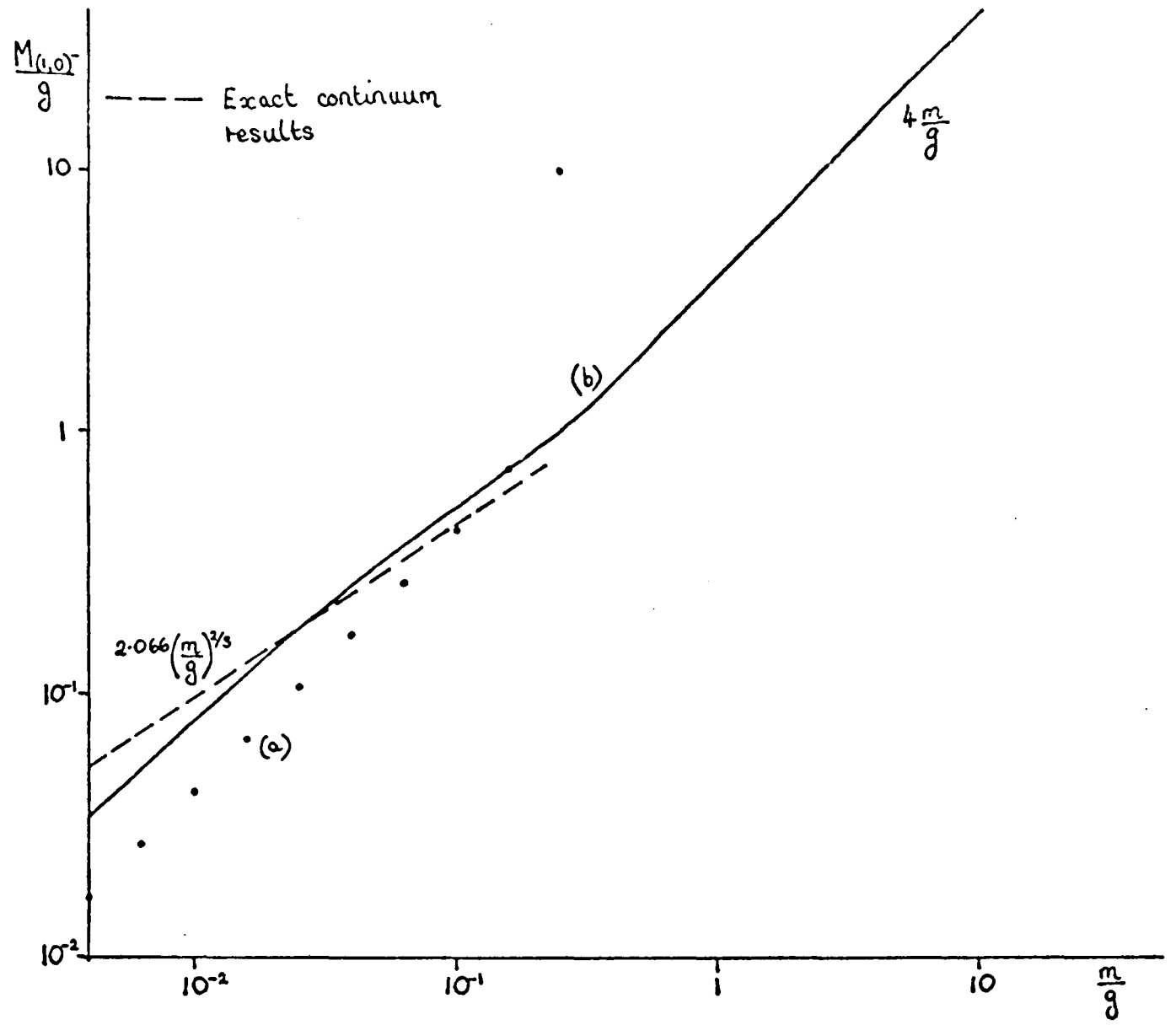

$\frac{M_{(1,0)^-}}{g}$
Exact continuum results
$4\frac{m}{g}$
10
1
10^{-1}
10^{-2}
$2.066\left(\frac{m}{g}\right)^{2/3}$
(a)
(b)
10^{-2}
10^{-1}
1
10
$\frac{m}{g}$

Fig. 6.6

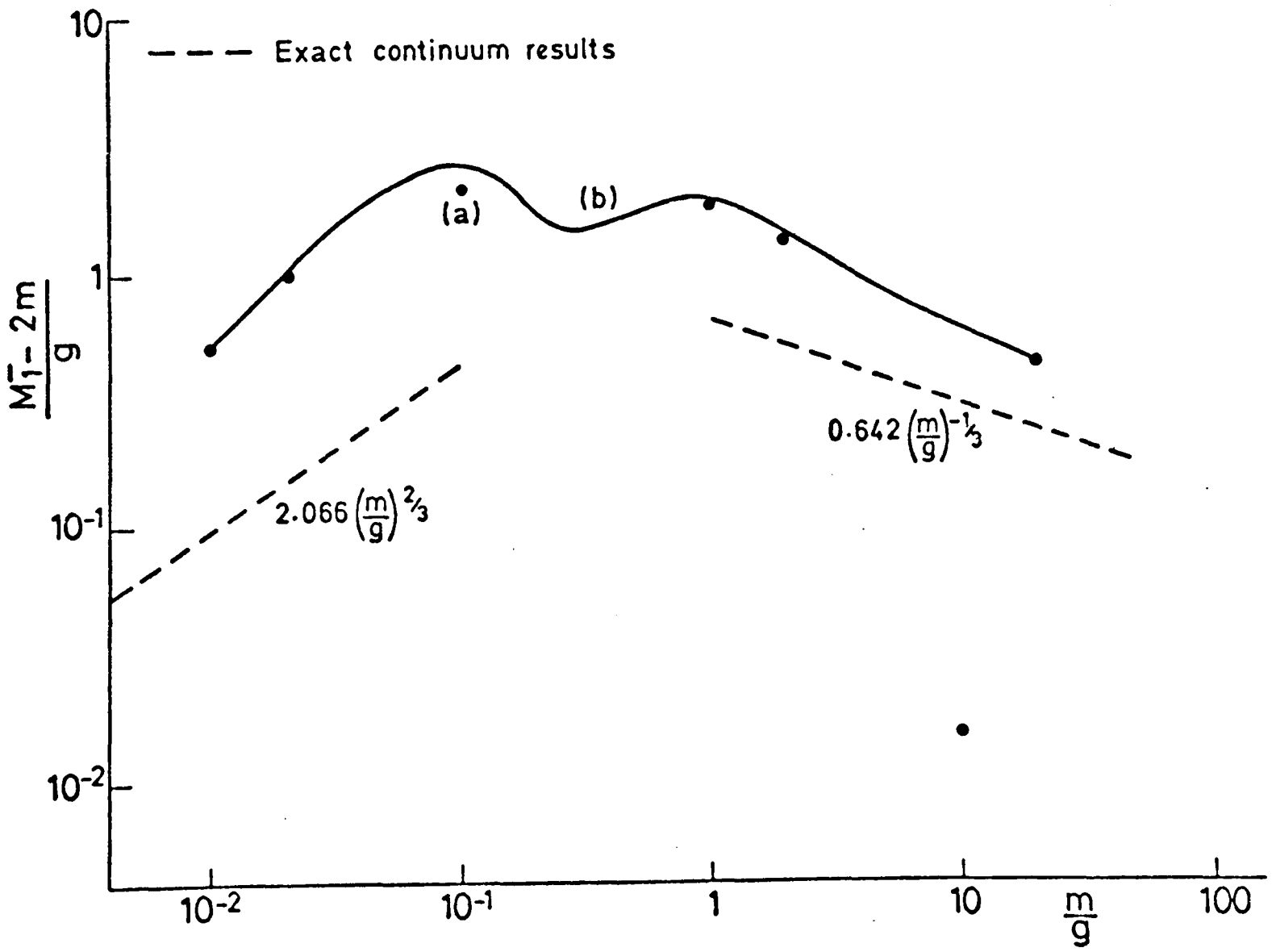
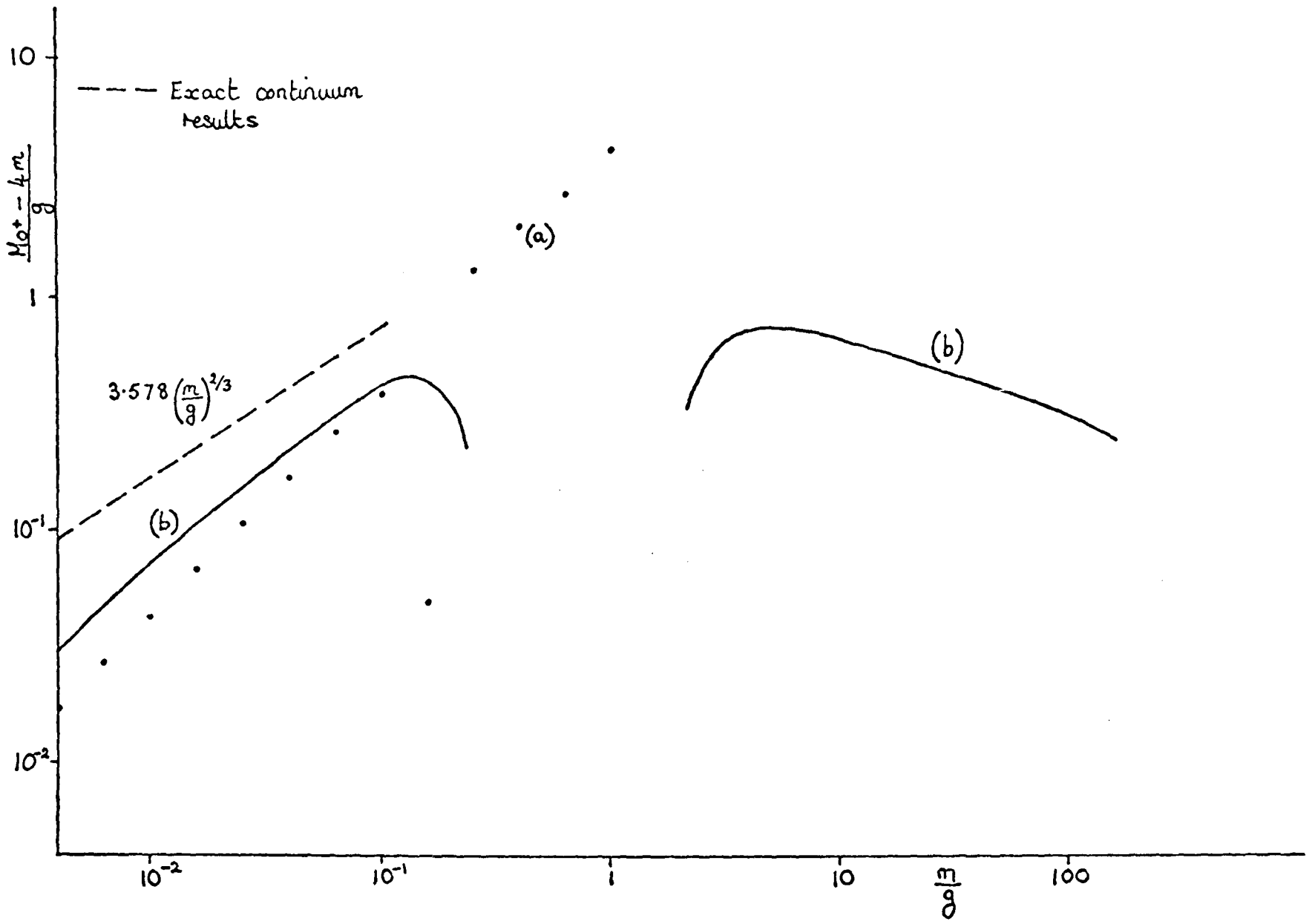
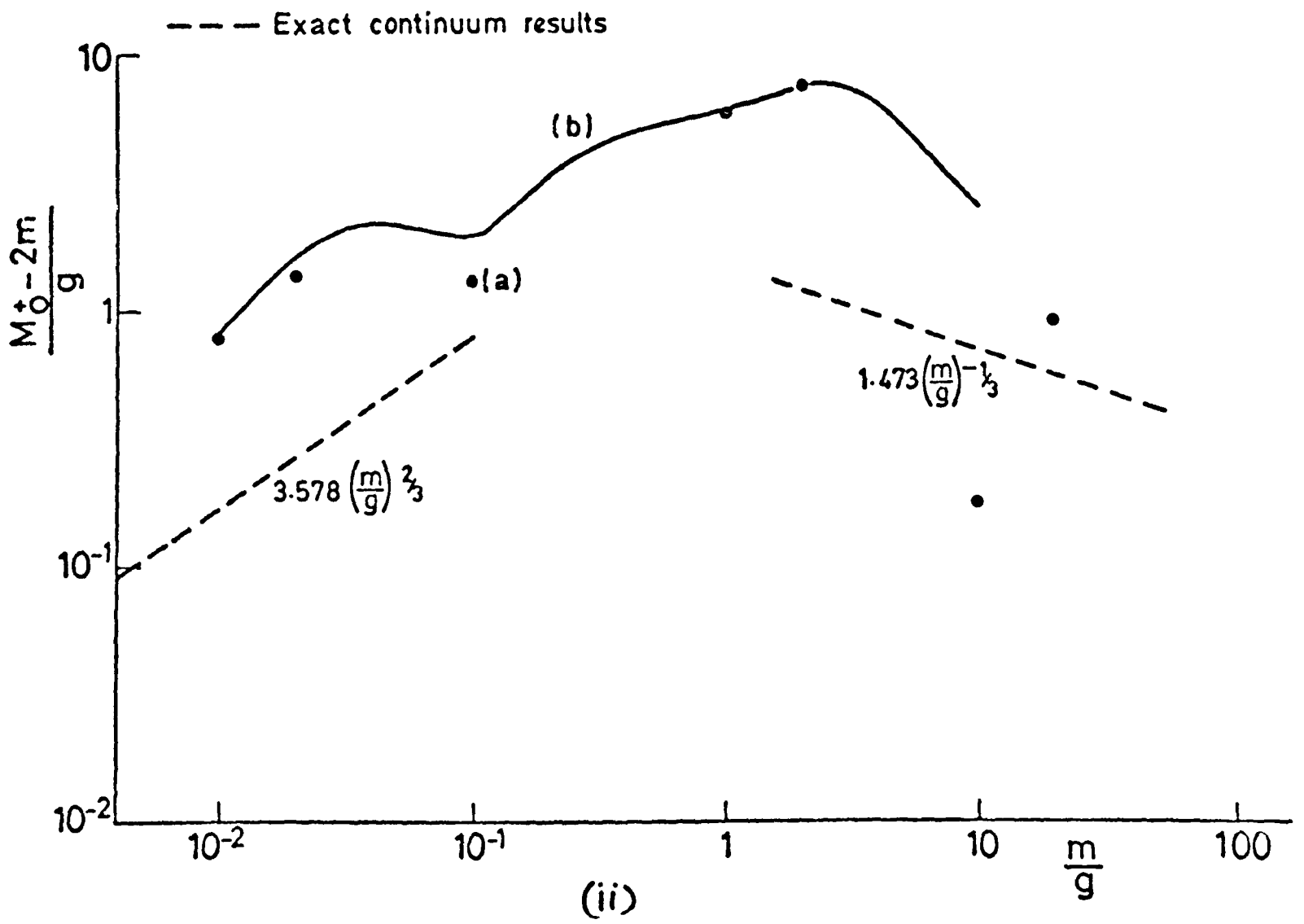

10
Exact continuum results
$\frac{M_{1^-} - 2m}{g}$
1
10^{-1}
10^{-2}
(a)
(b)
$2.066\left(\frac{m}{g}\right)^{2/3}$
$0.642\left(\frac{m}{g}\right)^{-1/3}$
10^{-2}
10^{-1}
1
10
100
$\frac{m}{g}$

Fig. 6.7


10
1
10^{-1}
10^{-2}
$\frac{M_0^+ - 4m}{g}$
Exact continuum results
$3{\cdot}578\left(\frac{m}{g}\right)^{2/3}$
(a)
(b)
(b)
10^{-2}
10^{-1}
1
10
100
$\frac{m}{g}$

(i)


Exact continuum results
10
1
10^{-1}
10^{-2}
$\frac{M_0^+ - 2m}{g}$
(b)
(a)
$1{\cdot}473\left(\frac{m}{g}\right)^{-1/3}$
$3{\cdot}578\left(\frac{m}{g}\right)^{2/3}$
10^{-2}
10^{-1}
1
10
100
$\frac{m}{g}$

(ii)

Fig. 6·8

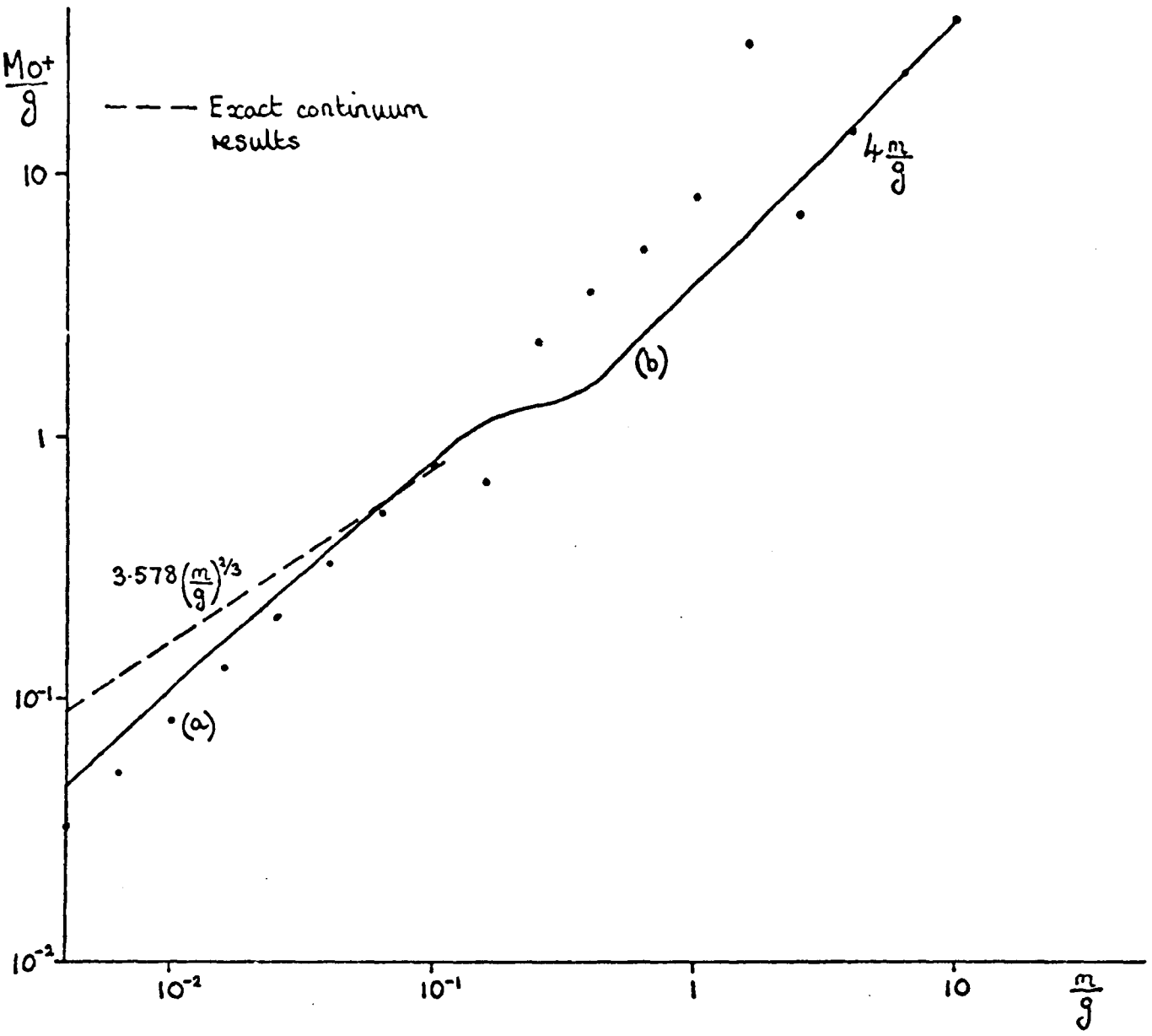
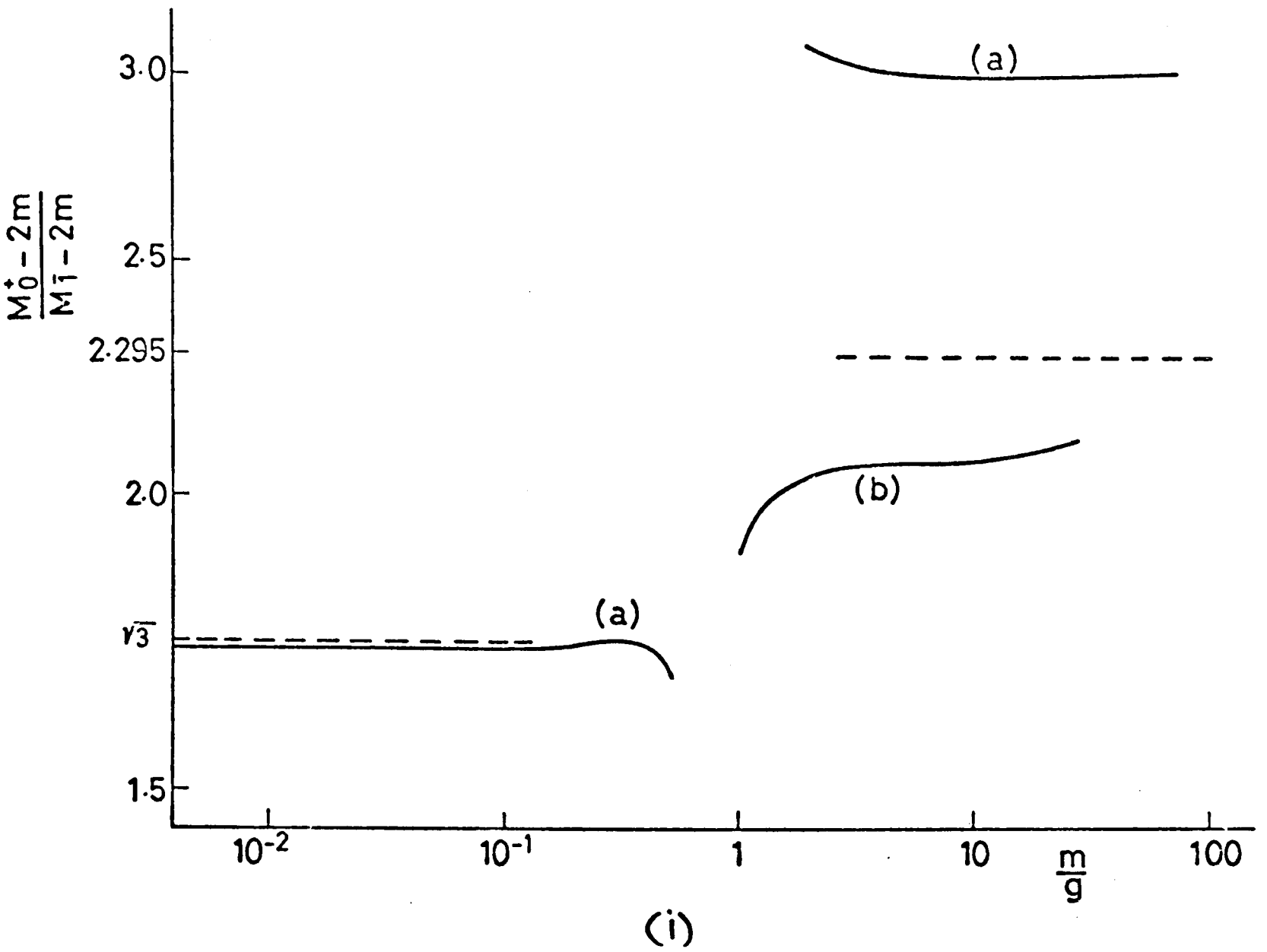

$\frac{M\sigma^+}{g}$
Exact continuum results
$4\frac{m}{g}$
$3{\cdot}578\left(\frac{m}{g}\right)^{2/3}$
(a)
(b)
10
1
10^{-1}
10^{-2}
10^{-2}
10^{-1}
1
10
$\frac{m}{g}$

Fig. 6·9


3·0
2·5
2·295
2·0
√3
1·5
(a)
(b)
(a)
$\frac{M_0^+ - 2m}{M_1^- - 2m}$
10^{-2}
10^{-1}
1
10
100
$\frac{m}{g}$
(i)

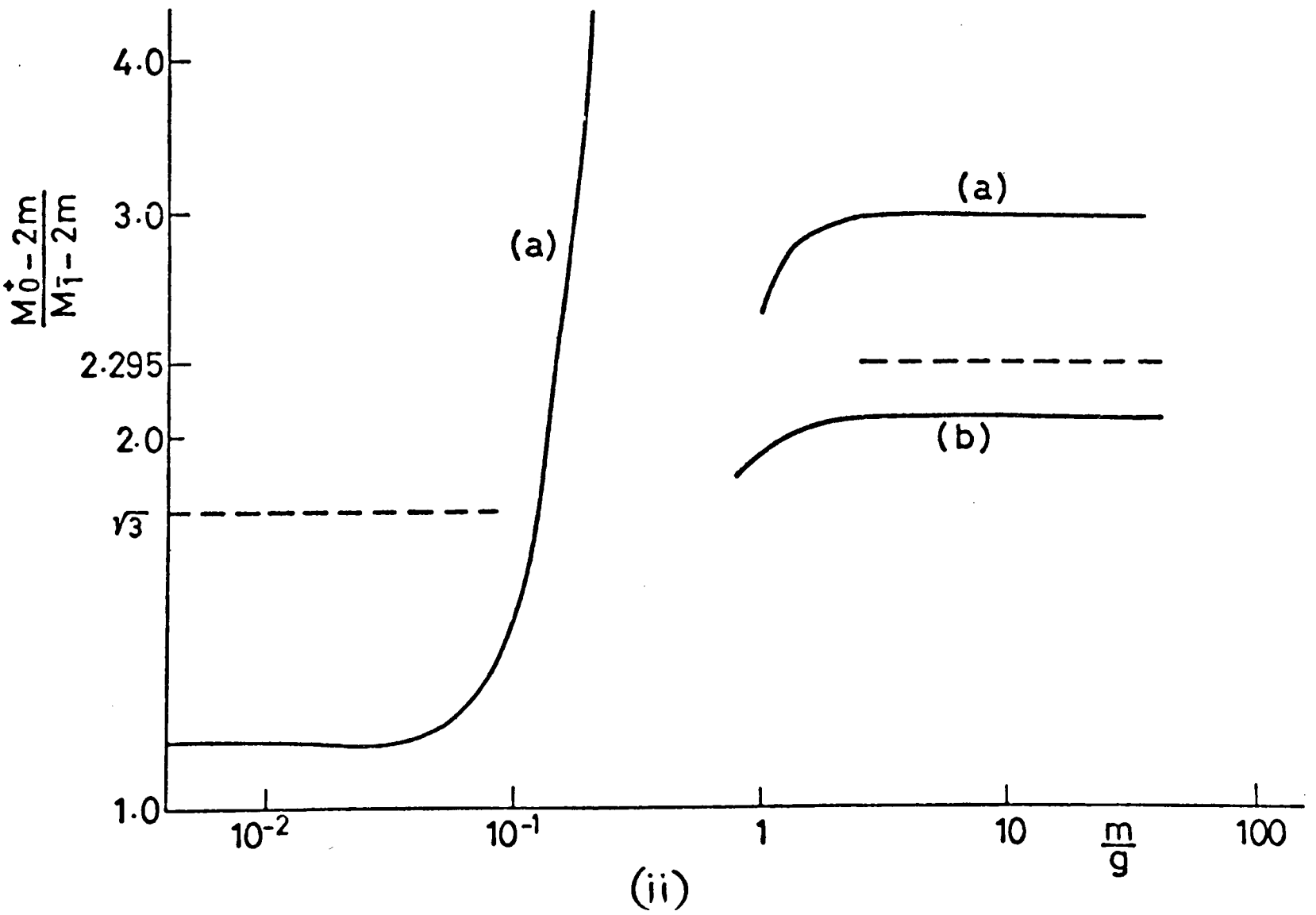
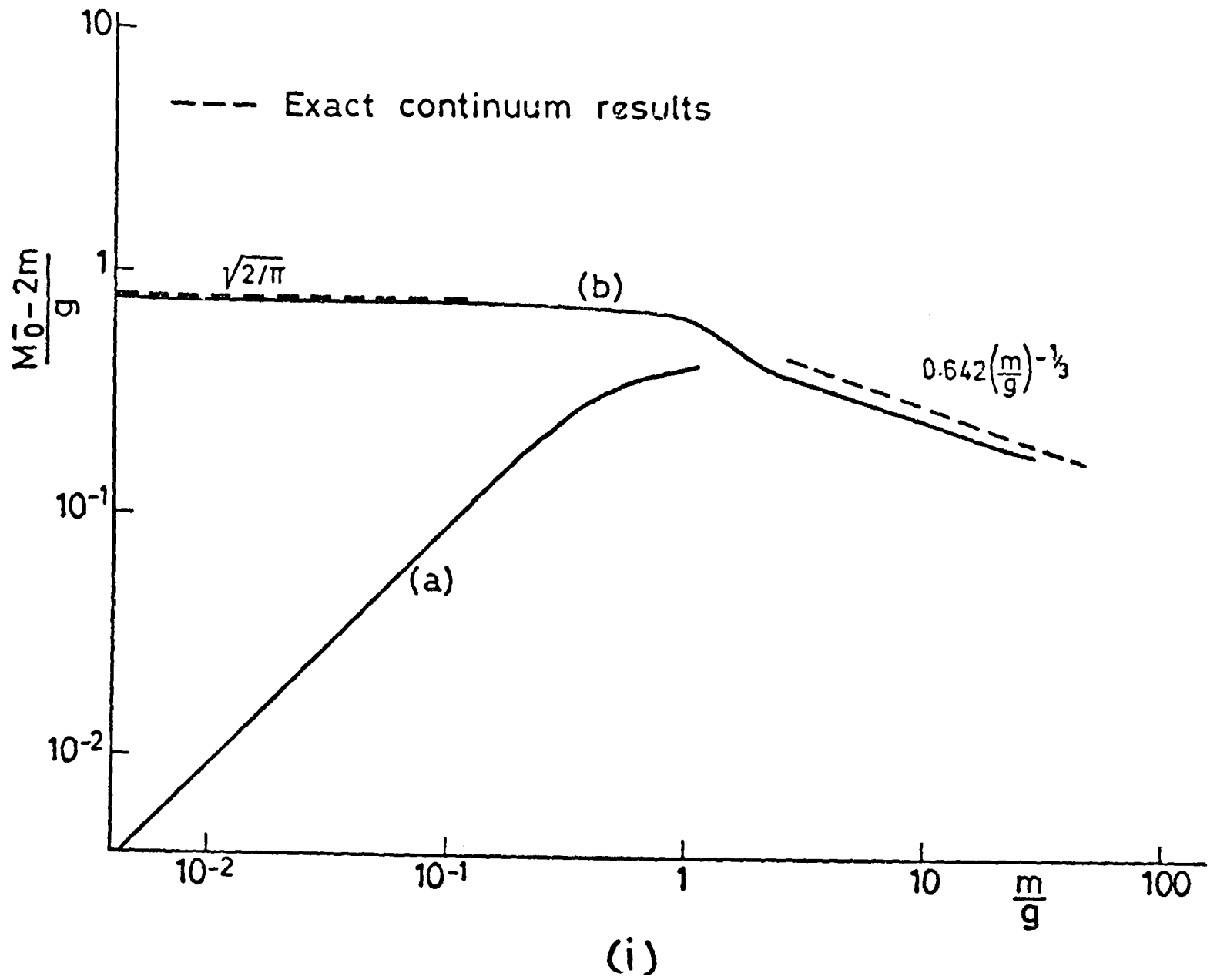
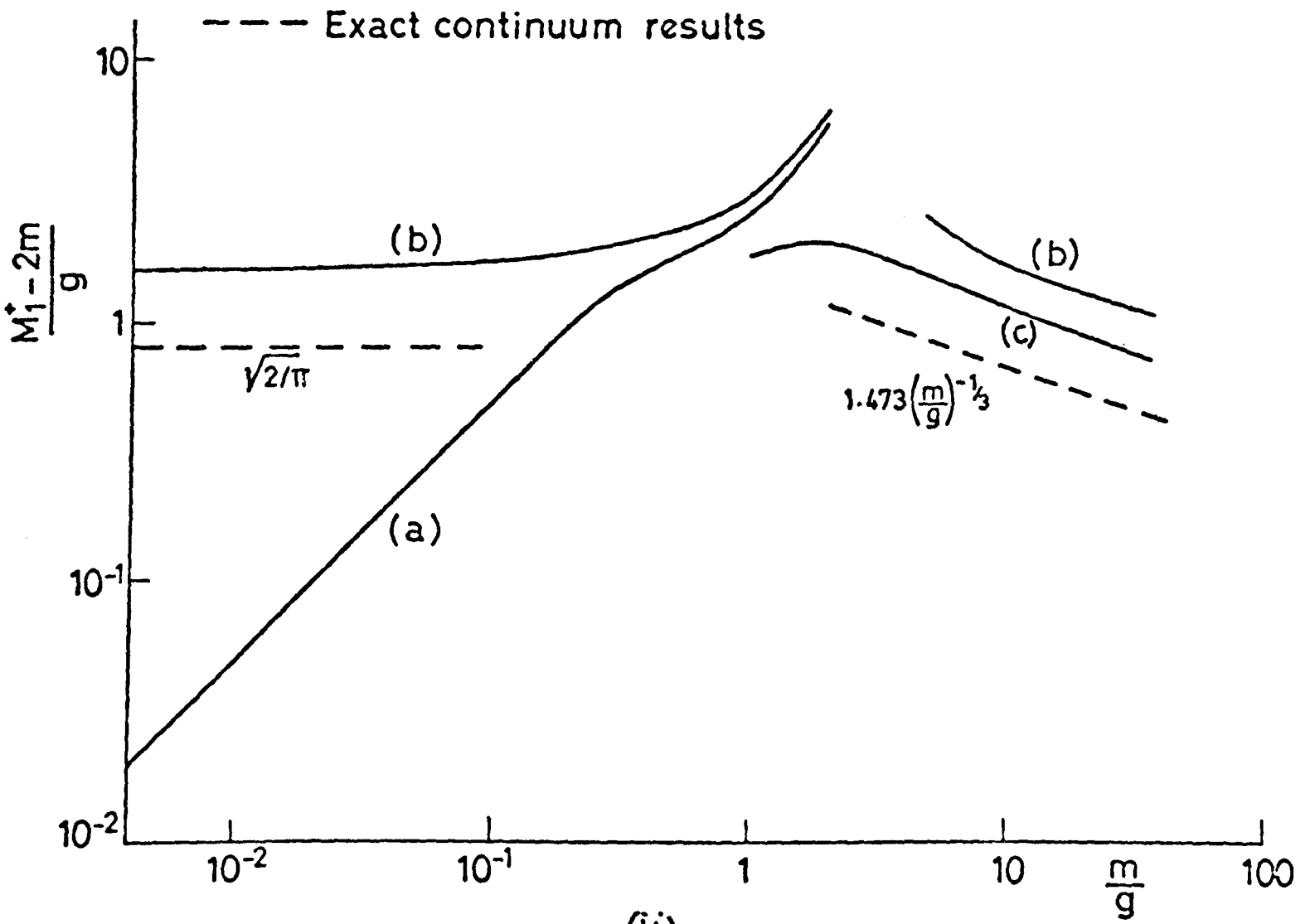

4·0
3·0
2·295
2·0
√3
1·0
(a)
(a)
(b)
$\frac{M_0^+ - 2m}{M_1^- - 2m}$
10^{-2}
10^{-1}
1
10
100
$\frac{m}{g}$
(ii)

Fig. 6·10


Exact continuum results
$\frac{M_0^- - 2m}{g}$
10
1
10^{-1}
10^{-2}
$\sqrt{2/\pi}$
(b)
$0.642\left(\frac{m}{g}\right)^{-1/3}$
(a)
10^{-2}
10^{-1}
1
10
100
$\frac{m}{g}$

(i)


Exact continuum results
$\frac{M_1^+ - 2m}{g}$
10
1
10^{-1}
10^{-2}
(b)
$\sqrt{2/\pi}$
(a)
(b)
(c)
$1.473\left(\frac{m}{g}\right)^{-1/3}$
10^{-2}
10^{-1}
1
10
100
$\frac{m}{g}$

(ii)

Fig. 6·11

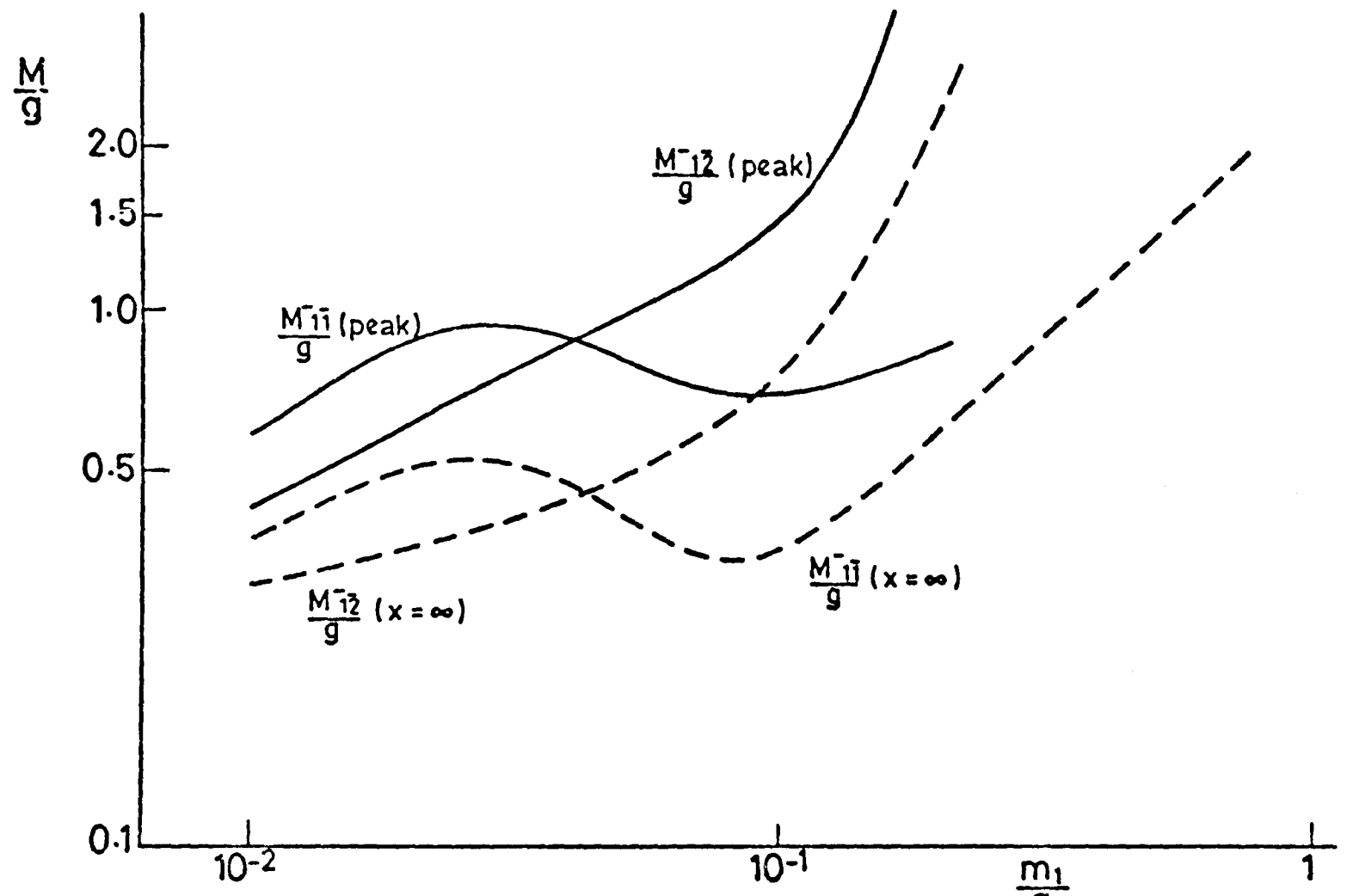


Fig. 6·12